



**ADVERTIMENT.** L'accés als continguts d'aquesta tesi queda condicionat a l'acceptació de les condicions d'ús establertes per la següent llicència Creative Commons:  <https://creativecommons.org/licenses/?lang=ca>

**ADVERTENCIA.** El acceso a los contenidos de esta tesis queda condicionado a la aceptación de las condiciones de uso establecidas por la siguiente licencia Creative Commons:  <https://creativecommons.org/licenses/?lang=es>

**WARNING.** The access to the contents of this doctoral thesis it is limited to the acceptance of the use conditions set by the following Creative Commons license:  <https://creativecommons.org/licenses/?lang=en>



Escola d'Enginyeria

Departament d'Enginyeria Química, Biològica i Ambiental

Programa de Doctorat en Biotecnologia

**Purification, formulation, and  
functionalization of HIV-1-based virus-like  
particles for vaccine and therapeutic  
applications**

**Elianet Lorenzo Romero**

**Advisors**

Dr Francesc Gòdia Casablanca

Dr Laura Cervera Gràcia

**Title:** Purification, formulation, and functionalization of HIV-1-based virus-like particles for vaccine and therapeutic applications

**Keywords** HEK 293, virus-like particles, downstream process, formulation, functionalization, T22 peptide

**Author** Elianet Lorenzo Romero

**Advisors** Dr Francesc Gòdia Casablanca  
Dr Laura Cervera Gràcia

PhD Program in Biotechnology

Departament d'Enginyeria Química, Biològica i Ambiental

Escola d'Enginyeria

Universitat Autònoma de Barcelona

July 2024

El Dr. Francesc Gòdia Casablanças, Catedràtic d'Enginyeria, i la Dra. Laura Cervera Gràcia, Professora Serra Hunter, del Departament d'Enginyeria Química, Biològica i Ambiental de la Universitat Autònoma de Barcelona

**Certifiquem:**

Que la graduada en Bioquímica i Biologia Molecular Elianet Lorenzo Romero ha dut a terme al Departament d'Enginyeria Química, Biològica i Ambiental de la Universitat Autònoma de Barcelona i amb la nostra direcció, la tesi doctoral titulada **"Purification, formulation, and functionalization of HIV-1-based virus-like particles for vaccine and therapeutic applications"**. La mateixa, es presenta en aquesta memòria i constitueix el manuscrit per optar al Grau de Doctor en Biotecnologia per la Universitat Autònoma de Barcelona.

I per tal que se'n prengui coneixement i consti als efectes oportuns, signem aquest certificat a Bellaterra, a juliol de 2024.

Elianet Lorenzo Romero

(Autor)

Laura Cervera Gràcia

(co-directora)

Francesc Gòdia Casablanças

(co-director)

***A mi sol eterno***

**TABLE OF CONTENTS**

<b>Resum</b>	7
<b>Resumen</b>	10
<b>Summary</b>	13
<b>Introduction</b>	16
<b>Objectives</b>	56
<b>Results</b>	58
 <b>Chapter One-</b> Downstream process design for Gag HIV-1 based virus-like particles.....	59
 <b>Chapter Two-</b> Optimizing lyophilization formulations for HIV-1 Gag VLPs: Enhancing quality and stability for biopharmaceutical applications.....	92
 <b>Chapter Three-</b> Development of a scalable production bioprocess for HIV-1 virus-like particles coupling continuous upstream with end-to-end downstream processing.....	120
 <b>Chapter Four-</b> Engineering of a CXCR4-targeted HIV-1 Gag VLP by T22 peptide functionalization via copper-free click chemistry.....	147
 <b>General Discussion</b>	174
<b>Conclusions</b>	192

## ABBREVIATIONS

**AC** - Affinity Chromatography

**AF4-MALS** - Asymmetric Flow Field-Flow Fractionation coupled with Multiple-Angle Light Scattering

**AFM** - Atomic Force Microscopy

**ATF** - Alternating Tangential Flow

**CHO** - Chinese Hamster Ovary

**Cryo-TEM** - Cryogenic Transmission Electron Microscopy

**DC** - Dendritic Cells

**DLS** - Dynamic Light Scattering

**DOX** - Doxorubicin

**DSP** - Downstream Processing

**ELISA** - Enzyme-Linked Immunosorbent Assay

**EVs** - Extracellular Vesicles

**FDA** - Food and Drug Administration

**GFP** - Green Fluorescent Protein

**HBP** - Hepatitis B Virus

**HCP** - Host Cell Protein

**HEK 293** - Human Embryonic Kidney 293

**HIC** - Hydrophobic Interaction Chromatography

**HIV-1** - Human Immunodeficiency Virus Type 1

**HPLC** - High Pressure Liquid Chromatography

**HPV** - Human Papilloma Virus

**IEC** - Ion Exchange Chromatography

**MHC** - Major Histocompatibility Complex

**NHS** - N-Hydroxysuccinimide

**NTA** - Nanoparticle Tracking Analysis

**PEI** - Polyethylenimine

**PTM** - Post-Translational Modifications

**RP-HPLC** - Reverse-Phase High Pressure Liquid Chromatography

**RSV** - Respiratory Syncytial Virus

**SDS-PAGE** - Sodium Dodecyl Sulphate Polyacrylamide Gel Electrophoresis

**SEC** - Size-Exclusion Chromatography

**SE-HPLC** - Size Exclusion High Pressure Liquid Chromatography

**SGE** - Stable Gene Expression

**TGE** - Transient Gene Expression

**USP** - Upstream Processing

**VLPs** - Virus Like Particles

## **RESUM**

---



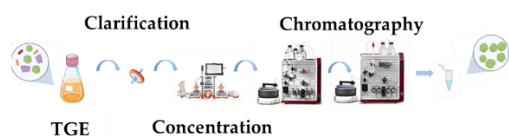
## RESUM

L'interès creixent en l'ús de partícules similivíriques (VLPs) com a candidats vacunals, vectors per a teràpia gènica i càncer, i nanotransportadors per a l'administració de fàrmacs ha incrementat la demanda de plataformes de biomanufactura eficients i escalables. La seva similitud estructural amb els virus, sense els components virals infecciosos, els converteix en candidats excel·lents per a aquestes aplicacions. Tanmateix, la seva fabricació implica processos complexos, incloent la producció mitjançant cultiu cel·lular, purificació i formulació per complir amb els estàndards clínics. Aquesta tesi aborda els desafiaments crítics en el bioprocessament de VLPs en quatre capítols, centrant-se en la purificació, formulació i funcionalització de les VLPs de VIH. La purificació de les VLPs és una fase crucial en el bioprocés per a l'eliminació de contaminants com ara vesícules extracel·lulars, proteïnes de les cèl·lules hoste i ADN. Al **Capítol Ú**, es comparen diverses tecnologies per optimitzar la purificació de les VLPs. El procés de purificació proposat inclou quatre passos clau: clarificació mitjançant filtració en profunditat i filtració estàndard, concentració i purificació intermèdia a través de filtració de flux tangencial o cromatografia multimodal, captura utilitzant cromatografia d'intercanvi iònic, cromatografia d'interacció hidrofòbica i afinitat per heparina, i poliment amb cromatografia d'exclusió per mida. L'estudi avalua cada pas en base al rendiment, la puresa i l'eficiència en l'eliminació de contaminants. Es defineix un procés de purificació integral basat en els millors resultats obtinguts en cada pas. Aquest procés aconsegueix un rendiment global del 38% i una puresa del 64%, complint amb els estàndards reguladors per a contaminants d'ADN i proteïnes. El **Capítol Dos** es centra en l'optimització de les formulacions de liofilització per a les VLPs de VIH mitjançant Disseny d'Experiments. S'avaluen diversos excipients, incloent crio-lío protectors, agents de càrrega, tampons, modificadors de tonicitat i surfactants, pel seu impacte en la mida, concentració i qualitat de les VLPs. La formulació optimitzada composta per sacarosa, arginina, TrisHCl, clorur de sodi i polisorbat 80 preserva amb èxit la integritat de les VLPs. Els estudis de termoestabilitat demostren que les característiques d'integritat estructural es mantenen a 4°C durant 4 setmanes, tant en forma liofilitzada com reconstituïda. Al **Capítol Tres**, els avenços en purificació i formulació s'apliquen per desenvolupar un procés biotecnològic complet, incloent una producció en perfusió seguida per un procés de purificació en tres passos. La producció en perfusió millora 2.4 vegades la productivitat volumètrica de les VLPs en comparació amb resultats anteriors.

Els processos de purificació que segueixen, incloent l'aclariment secundari i la cromatografia d'intercanvi aniónic mostren valors aproximats de puresa del 60%. El pas final de liofilització manté la integritat de les VLPs. La funcionalització de les VLPs per a l'administració dirigida de fàrmacs representa una alternativa en la teràpia contra el càncer. Al **Capítol Quatre** s'explora l'ús de les VLPs de VIH funcionalitzades amb el pèptid T22, un conegut antagonista del receptor CXCR4 associat a diversos càncers. Les VLPs produïdes en cèl·lules HEK293 i purificades mitjançant el procés de purificació proposat al capítol ú es funcionalitzen mitjançant reaccions químiques. Els estudis *in vitro* demostren que les VLPs funcionalitzades amb T22 es dirigeixen i penetren en cèl·lules positives per CXCR4 de forma específica, amb un augment notable en la fluorescència intracel·lular en comparació amb les VLPs no funcionalitzades. Aquesta especificitat ressalta el potencial de les VLPs com a nanotransportadors per a l'administració selectiva de fàrmacs. En general, aquesta tesi proporciona una exploració integral de la purificació, formulació i funcionalització de les VLPs de VIH-1, abordant desafiaments clau i obrint el camí per a la seva aplicació clínica com a vacunes i teràpies dirigides contra el càncer.

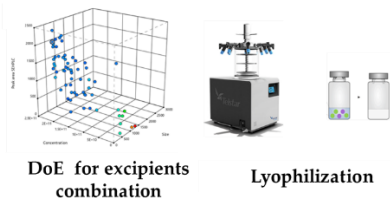
#### CHAPTER ONE

Downstream process design for Gag HIV-1 based VLPs



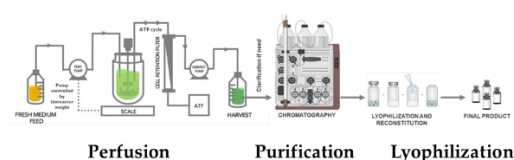
#### CHAPTER TWO

Optimizing lyophilization formulations for HIV-1 Gag VLPs



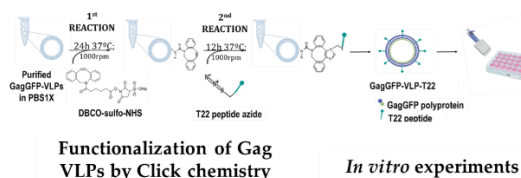
#### CHAPTER THREE

Development of a complete bioprocess for HIV-1 Gag VLPs



#### CHAPTER FOUR

Engineering of a CXCR4-targeted HIV-1 Gag VLP by T22 peptide functionalization



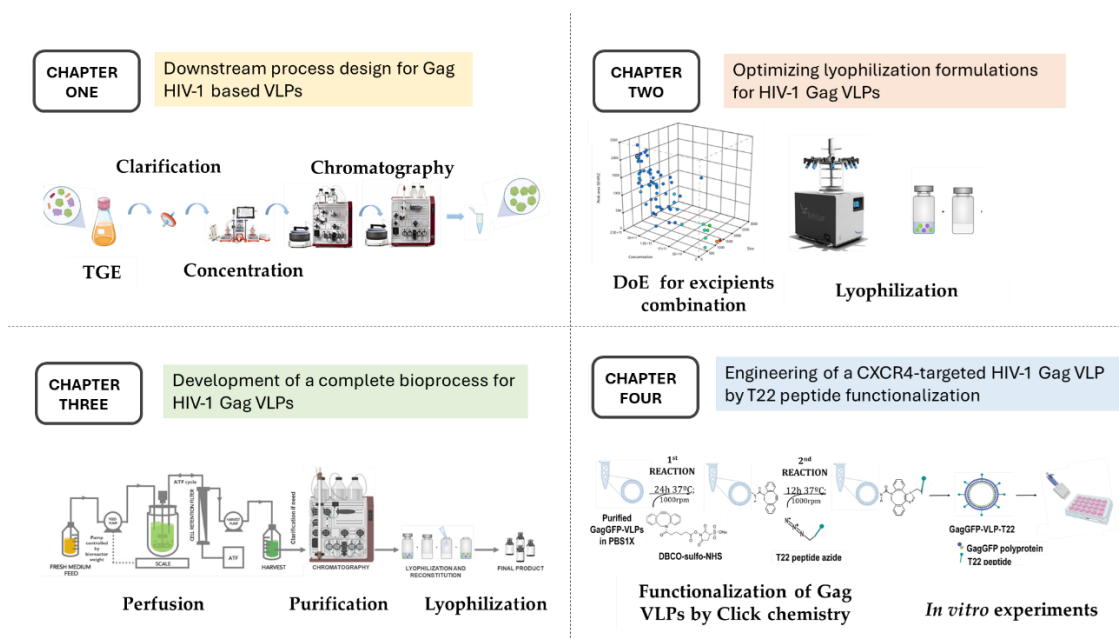
## **RESUMEN**

---

## RESUMEN

El creciente interés en el uso de partículas similares a virus (VLP) como candidatos vacunales, vectores para terapias génicas y oncológicas y nanoportadores para la administración de fármacos ha generado una mayor demanda de plataformas de biofabricación eficientes y escalables. Su similitud estructural con los virus los convierte en excelentes candidatos. Sin embargo, su fabricación implica procesos complejos, incluida la producción mediante cultivo celular, purificación y formulación para cumplir con los estándares clínicos. Esta tesis aborda los desafíos críticos en el bioprocesamiento de las VLPs a través de cuatro capítulos, centrándose en la purificación, formulación y funcionalización de las VLPs basadas en la poliproteína Gag del VIH-1. La purificación de las VLPs es una fase crucial en el bioproceso de estas nanopartículas. El **Capítulo Uno** profundiza en la comparación de tecnologías para optimizar la purificación de las Gag VLPs. El proceso de purificación propuesto abarca cuatro pasos: clarificación mediante filtración profunda y filtración estándar, concentración y purificación intermedia mediante filtración de flujo tangencial o cromatografía multimodal, captura mediante cromatografía de intercambio iónico, interacción hidrofóbica y afinidad por heparina, y pulido con cromatografía de exclusión por tamaño. Se evalúa cada paso según el rendimiento, la pureza y la eliminación de contaminantes. Se ha definido un proceso de purificación integral en base a los mejores resultados obtenidos en cada paso. Este proceso produjo una recuperación general del 38 % y una pureza del 64 %. Los niveles de ADN y proteínas contaminantes cumplieron con los estándares regulatorios. El **Capítulo Dos** se centra en la optimización de formulaciones de liofilización para las Gag VLPs mediante un enfoque de Diseño de Experimentos. Se evalúan varios excipientes, incluidos crio-lío protectores, agentes de carga, tampones, modificadores de tonicidad y tensioactivos, para determinar su impacto en el tamaño, la concentración y la calidad de las VLPs. La formulación optimizada compuesta por sacarosa, arginina, TrisHCl, cloruro de sodio y polisorbato 80 preserva con éxito la integridad de las VLPs. Los estudios de termoestabilidad muestran que las características de integridad estructural se mantienen a 4°C durante 4 semanas, tanto en forma liofilizada como reconstituida. En el **Capítulo Tres** se aplican los avances en purificación y formulación para desarrollar un bioproceso completo. Esto incluye una producción previa basada en perfusión seguida de un proceso de purificación. El enfoque basado en perfusión produce una mejora 2.4 veces en la productividad volumétrica de las VLPs en comparación con

resultados anteriores. El proceso de purificación que incluyó la clarificación secundaria y la cromatografía de intercambio aniónico, muestran valores aproximados de pureza del 60%. El paso final de liofilización mantuvo la integridad de las VLPs. La funcionalización de las VLPs para la administración dirigida de fármacos representa una alternativa importante en la terapia del cáncer. En el **Capítulo Cuatro** se analiza el uso de las Gag VLPs funcionalizadas con el péptido T22, conocido antagonista del receptor CXCR4 el cual está asociado a varios cánceres. Las VLPs producidas en células HEK293 y purificadas mediante el proceso propuesto en el capítulo uno se han funcionalizado mediante reacciones químicas. Los estudios *in vitro* han demostrado que las VLPs funcionalizadas se dirigen específicamente y penetran en las células CXCR4 positivas, con un aumento notable de la fluorescencia intracelular en comparación con las VLPs no funcionalizadas. Esta especificidad resalta el potencial de las VLPs como nanoportadores para la administración selectiva de fármacos. En general, esta tesis proporciona una exploración integral de la purificación, formulación y funcionalización de las Gag VLP del VIH-1, abordando desafíos claves y allanando el camino para su aplicación clínica como vacunas y terapias dirigidas contra el cáncer.



## **SUMMARY**

---

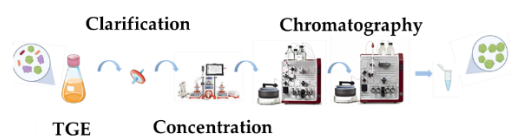
## SUMMARY

The increasing interest in using virus-like particles (VLPs) as vaccine candidates, vectors for gene and cancer therapy, and nanocarriers for drug delivery has led to a higher demand for efficient and scalable biomanufacturing platforms. Their structural similarity to viruses, without containing the infectious viral components, makes them excellent candidates for these applications. However, their manufacturing involves complex processes, including production by cell culture, purification, and formulation to meet clinical standards. This thesis addresses the critical challenges in VLP bioprocessing through four chapters, focusing on purification, formulation and functionalization of HIV-1 Gag VLPs. Purification of VLPs is a crucial phase in the bioprocess of these nanoparticles, which ensures the removal of contaminants such as extracellular vesicles, host cell proteins, and DNA. **Chapter One** delves into the comparison of various downstream processing technologies to optimize the purification of HIV-1 Gag VLPs. The purification process proposed encompasses four key steps: clarification through depth filtration and standard filtration, concentration and intermediate purification via tangential flow filtration or multimodal chromatography, capture using ion exchange, hydrophobic interaction and heparin affinity chromatography, and polishing with size exclusion chromatography. The study evaluates each step based on yield, purity, and contaminant removal efficiency. A comprehensive purification process has been defined based on the best results obtained in each step. This process yielded an overall recovery of 38% and purity of 64% after the polishing step. The levels of DNA and protein contaminants met regulatory standards. **Chapter Two** focuses on the optimization of lyophilization formulations for HIV-1 Gag VLPs using a Design of Experiments approach. Various excipients, including cryo-lyo protectants, bulking agents, buffers, tonicity modifiers, and surfactants, are evaluated for their impact on VLP size, concentration, and quality. The optimized formulation composed by sucrose, arginine, TrisHCl, sodium chloride and polysorbate 80 successfully preserves the integrity of the VLPs. The thermostability studies show that structural integrity characteristics is maintained at 4°C for 4 weeks, in both lyophilized and reconstituted form. In **Chapter Three**, the advances in purification and formulation are applied to develop a complete bioprocess for HIV-1 Gag VLPs. This includes a perfusion-based upstream production followed by a three-step downstream purification process. The perfusion-based approach yields a 2.4-fold improvement in VLP volumetric productivity compared to

previous results. The subsequent downstream processes, including secondary clarification and anion exchange chromatography show around a 60% purity of VLPs. The final lyophilization step maintained VLP integrity. The functionalization of VLPs for targeted drug delivery represents a significant alternative in cancer therapy. In **Chapter Four** the use of HIV-1 Gag VLPs functionalized with the T22 peptide, a known antagonist of the CXCR4 receptor associated to various cancers. VLPs produced in HEK293 cells and purified through the DSP proposed in chapter one have been functionalized via click chemistry. *In vitro* studies have demonstrated that the T22-functionalized VLPs specifically target and penetrate CXCR4-positive cells, with a notable increase in intracellular fluorescence compared to non-functionalized VLPs. This specificity highlights the potential of VLPs as nanocarriers for selective drug delivery. Overall, this thesis provides a comprehensive exploration of the purification, formulation, and functionalization of HIV-1 Gag VLPs, addressing key challenges and paving the way for their clinical application as vaccines and targeted cancer therapies.

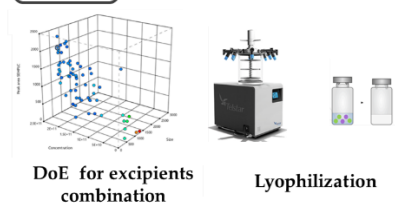
#### CHAPTER ONE

Downstream process design for Gag HIV-1 based VLPs



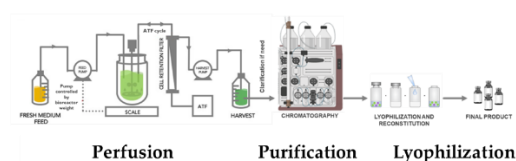
#### CHAPTER TWO

Optimizing lyophilization formulations for HIV-1 Gag VLPs



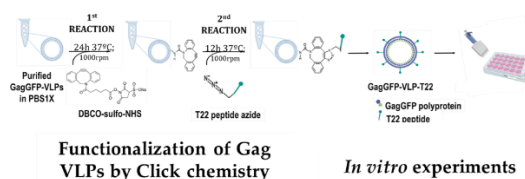
#### CHAPTER THREE

Development of a complete bioprocess for HIV-1 Gag VLPs



#### CHAPTER FOUR

Engineering of a CXCR4-targeted HIV-1 Gag VLP by T22 peptide functionalization





# **INTRODUCTION**

---

## 1. Virus-based biopharmaceutical products

For over three centuries, virus-based products have significantly contributed to promoting human health by preventing infectious diseases [1]. The concept of vaccination was first introduced by Edward Jenner in the late 18th century, who utilized the animal pox virus to combat smallpox [2]. Since then, there has been an increasing interest in virus-based products, accompanied by advancements in related technologies and manufacturing capabilities. Nowadays, in addition to recombinant vaccines [3], [4], virus-based products are providing innovative applications in gene therapy [5], cancer immunotherapies [6], and drug delivery [7] [8] (**Figure 1**).

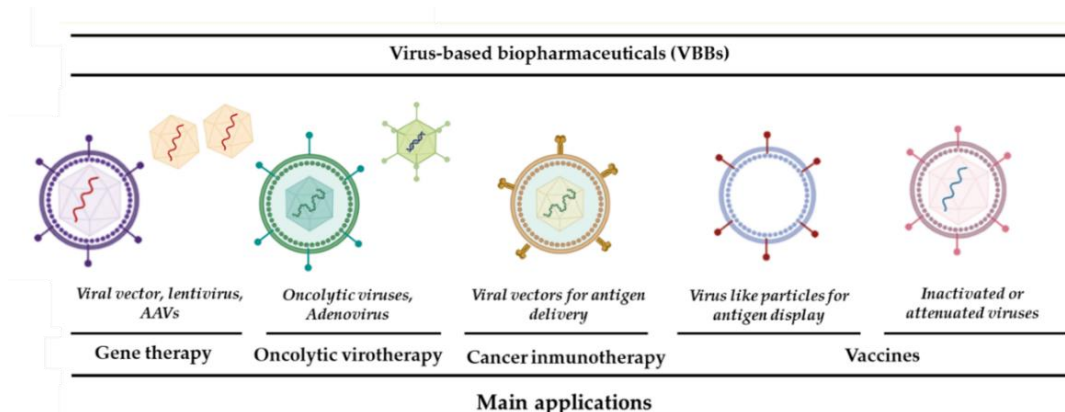


**Figure 1:** Virus-based products and their applications (adapted from [9]).

## 2. Vaccines

In the field of vaccination, a primary strategy to prevent viral infections involves using vaccines containing either an attenuated (weakened) or inactivated (killed) virus. These vaccines are administered to individuals to elicit a protective immune response [4]. Typically, these conventional vaccines are highly effective and usually do not require a second dose or the addition of adjuvants to boost their efficacy. However, there are certain risks associated with attenuated vaccines, particularly in their production and application stages, as they have the potential to revert to a virulent form [2], [10]. To enhance safety, newer generations of vaccines have been developed that exclude the use of whole viruses. Instead, these vaccines utilize alternative approaches such as protein subunits, DNA, virus like particles (VLPs) or RNA [1], [11] (**Figure 2**).

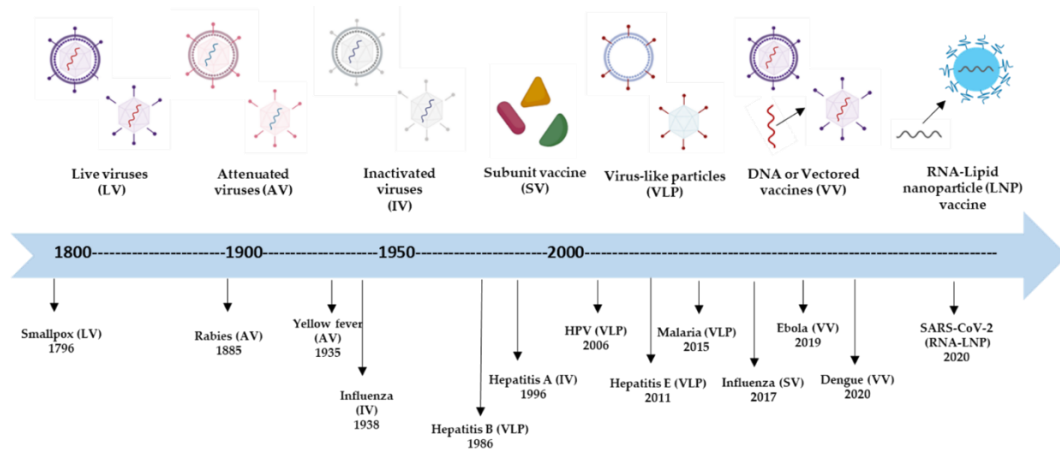


**Figure 2:** Schematic overview over the evolution of vaccine design with the advancements in technology (adapted from [1], [11]).

Subunit vaccines consist either of recombinant viral proteins or proteins purified from the virus in its wild type. These proteins serve as antigens, and when administered, they provoke an immune response without the presence of live virus [12]. Another innovative approach involves the direct administration of plasmid DNA that encodes for an antigenic protein. Once administered, this DNA is taken up by the recipient's cells, which then produce the antigenic protein internally, triggering an immune response [13].

VLPs are distinguished from other subunit vaccines by their potent immunogenicity, which results from presenting repetitive antigenic epitopes in a configuration that closely resembles the natural form to the immune system. They are comparable to viral vector-based vaccines in developing protective, effective, and efficient vaccines against severe infectious diseases [3].

On the other hand, mRNA technology has emerged as a novel platform for vaccine development. mRNA-based vaccines hold several attractive advantages. For example, mRNA triggers rapid and immediate antigen expression in the cytoplasm without the need for crossing the nuclear membrane. In addition, there is no potential risk of infection or insertional mutagenesis [11]. Moreover, mRNA vaccines demonstrated exceptional speed and flexibility in their development and production, enabling rapid responses to emerging diseases. Their success during the COVID-19 pandemic has established mRNA

technology as a pivotal tool in the fight against infectious diseases, showcasing its potential for future vaccine development against various pathogens [14].

### 3. Virus like particles (VLPs)

VLPs are non-infectious multiprotein structures that resemble native viruses but lack the disease-causing viral genome [15], [16], [17]. Due to their optimal size (20–200 nm), they can effectively display any epitope in a multivalent format, ensuring a robust humoral and cell-mediated immune response in the host [18], [19], [20]. The versatility of VLPs is reflected in the vast range of structural configurations they can adopt, incorporating one or multiple viral proteins. These configurations might include single, double, or triple layered structures, with some possessing an additional membrane derived from the host cell [22]. VLPs are categorized broadly into two types: enveloped and non-enveloped [21] (**Figure 3A**). Non-enveloped VLPs consist solely of viral proteins, whereas enveloped VLPs (eVLPs) also incorporate a membrane derived from the host cell. VLPs have been effectively produced using a variety of expression systems, with the most prominent being bacteria, yeast, mammalian and insect cells, and recombinant plants [15], [23]. At the initial stages of development, choosing the optimal expression system heavily depends on the structural complexity of the VLP, the necessary post-translational modifications, and the specific conditions required for protein folding. These aspects are essential considerations in ensuring proper protein conformation. Additionally, the robustness of the manufacturing process and cost efficiency, become critical considerations to reach the market scale [24] (**Figure 3B**).

These nanoparticles can be engineered to display different molecules in their surface by two main methods: molecular fusion by genetic engineering or chemical conjugation [25] [26]. This adaptability allows VLPs to carry a diverse range of antigens, turning them into hybrid platforms capable of presenting new immunological epitopes. These engineered hybrids are versatile in combining various viral proteins and presenting important epitopes from different viruses, multiple strains of the same virus and/or specifically the virus on which the VLP is based enhancing the breadth of immune responses elicited [27], [28], [29], [30], [31]. Moreover, VLPs are being developed not only for vaccine candidate but also as delivery vehicles for nucleic acids [32] and heterologous proteins [33], [34] (**Figure 3C**).

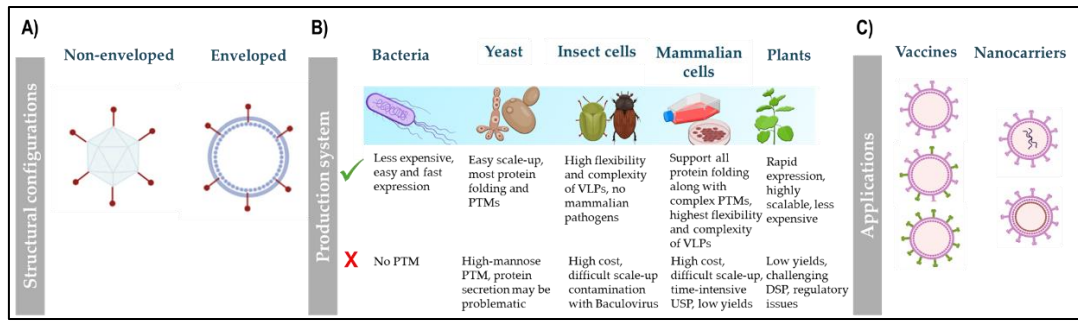


**Figure 3:** VLPs general characteristics. **A)** VLPs can be classified in non-enveloped and enveloped structures depending on the nature of the wild-type virus. For both types single or multilayered protein can be found [23]. **B)** Production systems: bacteria, yeast, insect cells, mammalian cells and plants are used to produce different VLP candidates. Summary of the main advantages and disadvantages is presented in this figure [15]. **C)** Some of the principal applications of VLPs. By the addition of chimeric antigens, multimeric vaccines or pseudotyping of different VLP scaffolds are proposed. Furthermore, surface modification and cell-specific targeting molecules are also described in the literature for the controlled release of nucleic acids, peptides or proteins, increase their immune response [33], [35]. *PTM*: post-translational modifications; *USP*: Upstream process; *DSP*: Downstream process.

### 3.1. VLPs-based vaccines against infectious diseases

VLPs-based vaccines have been used for the prevention of various infectious diseases. The first VLP vaccine was based on the hepatitis B virus surface antigen (HBsAg) in 1979 [36]. To date, 110 viral proteins from 35 viral families have been shown to be capable of assembly in the VLPs. From these studies, several VLP-based vaccines targeting different viruses including Norwalk Virus, HIV, Ebola Virus, SARS-CoV-2 Virus, Respiratory Syncytial Virus (RSV) and Influenza Virus are already in the market demonstrates their positive impact [37], [38], [39], [40], [41] (**Table 1**).

However, there are ongoing technical challenges in developing vaccines based on VLPs. These challenges include issues related to their design, production, processing, and storage, with the biggest one focused on the purification process [42]. For VLP-based vaccines to be effective, it is crucial that the viral surface antigens are correctly folded and glycosylated. These processes are vital for ensuring stability, facilitating immune recognition, and influencing pathogenicity [41].

**Table 1** Examples of FDA approved or clinical trial stage VLP-based vaccines against infectious diseases (adapted from [41]).

Trade name	Infectious agent	Target disease	Expression system
<b>Gardasil®</b>	Human Papilloma Virus (HPV)	Human papillomavirus, Types 6, 11, 16, 18, 31, 33, 45, 52, and 58	Yeast
<b>Cervarix®</b>	Human Papilloma Virus (HPV)	Human papillomavirus (Types 16 and 18)	Insect cells
<b>Sci-B-Vac™</b>	Hepatitis B Virus	Hepatitis B	Chinese hamster ovary (CHO) cells
<b>Mosquirix™</b>	Plasmodium falciparum	Malaria	Yeast
<b>NanoFlu™</b>	Influenza Virus	Seasonal Influenza	Insect cells
<b>Hecolin®</b>	Hepatitis E Virus	Hepatitis E	Escherichia coli
<b>Covifenz*</b>	SARS-CoV-2	COVID-19	Plant

\*VLP-based vaccine against COVID-19, developed by Medicago Inc. and approved only in Canada [43].

### 3.2. VLPs-based vaccines in cancer therapy

VLPs were originally designed as a vaccine platform for viral infections, but their application in cancer therapy has become increasingly important recently. [44]. This is largely due to their optimal size, which allows them to freely travel to lymph nodes and interact with dendritic cells (DC) for effective antigen presentation. More in details, VLPs effectively engage with DCs, which are the most powerful antigen-presenting cells, resulting in the display of viral antigens on MHC class I and MHC class II molecules. Once activated, DCs travel to lymph nodes to stimulate antigen-specific CD4<sup>+</sup> helper T cells and CD8<sup>+</sup> cytotoxic T cells. Specifically, the activation of CD8<sup>+</sup> T cells enable them to perform their cytotoxic function against chronically infected cells that present the peptide-MHC-I complex (**Figure 4**). CD4<sup>+</sup> helper T cells differentiate into two main subtypes, Th2 and Th1, steering adaptive immunity towards either a humoral or cellular immune response, respectively. Consequently, VLPs trigger both humoral and cellular responses, making them a potent vaccine strategy for both preventive and therapeutic purposes [45].

In this context, the positive outcomes achieved by preventive VLP-based vaccines against cancers caused by infectious diseases, such as hepatitis B virus (HBV) and human papilloma virus (HPV), have been approved for human use by international regulatory bodies. Notably, Cervarix, Gardasil, and Gardasil 9 offer protection against HPV, while Heplisav-B prevents liver cancer resulting from HBV

infection [46]. Furthermore, numerous efforts are underway to develop VLP-based vaccines targeting various non-infection-related cancers. Various VLP-based therapeutic cancer vaccines have been tested in preclinical and clinical trials for different cancers, including melanoma, breast cancer, colorectal cancer, pancreatic cancer, and breast cancer [44], [47], [48]. Some of these promising preclinical and clinical studies are detailed in **Table 2**

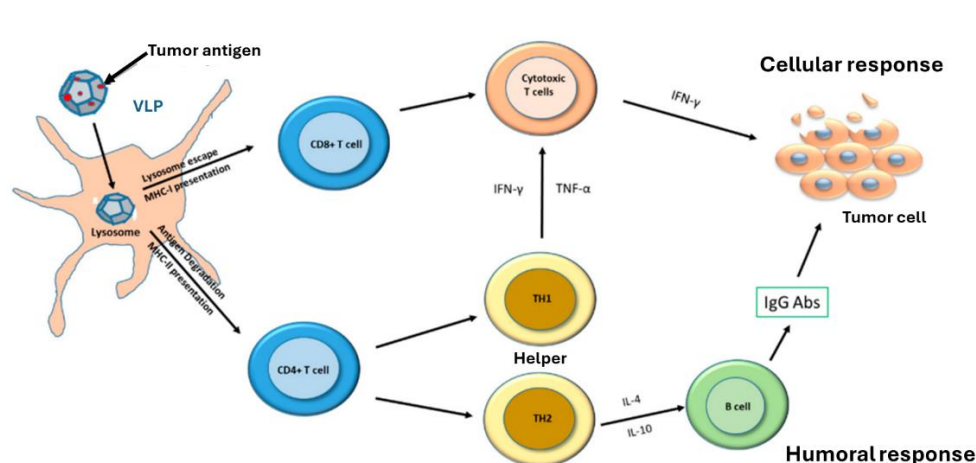


**Figure 4:** VLP-based vaccine: mechanism of action against tumor cells. VLPs are phagocytized and processed by dendritic cells (DCs), which then present the tumor antigens on MHC-I and MHC-II molecules for detection by CD8+ and CD4+ T cells. CD4+ T cells differentiate into TH2 and TH1 cells, which are involved in the inflammatory response and supporting the activity of CD8+ T cells (cytotoxic T cells), respectively. CD8+ T cells perform cytotoxic functions on tumor cells. (adapted from [45]).

**Table 2** List of preclinical studies and clinical trials using VLPs as a vaccine in different types of solid tumors (adapted from [6]).

VLPs	Cancer type	Study phase
Polyomavirus	Melanoma	Preclinical
Bacteriophage Q $\beta$	Melanoma Stage II/IV	Clinical Phase IIa
Chimeric HPV16-VLPs	Cervical intraepithelial neoplasia (CIN 2/3)	Clinical Phase I
RHDV	Colorectal cancer	Preclinical
IBDV	Cervical cancer	Preclinical

HPV: human papilloma virus; RHDV: rabbit haemorrhagic disease virus; IBDV: infectious bursal disease virus.

### 3.3. VLPs as nanocarriers in drug delivery

While VLPs are widely known for their immunogenic properties, their potential in other applications, such as targeted drug delivery, particularly in cancer treatment, has begun to gain attention [8] [49].

Prominent examples of this include the use of Rotavirus-VLPs and Cucumber mosaic-VLPs in directed

tumor therapy [50], [51]. The ability to modify the surfaces of VLPs allows for the specific targeting of certain cells, enhancing both the precision and efficacy of VLP-based therapies. Beyond merely displaying peptides, proteins, or other active molecules on their surface, VLPs can also encapsulate proteins, nucleic acids, or small molecules. This capability enables the targeted delivery of these substances to designated cells, tissues, or organs, expanding their therapeutic potential [41]. Furthermore, VLPs are highly suitable for drug delivery purposes due to their ability to escape endosomes before lysosomal degradation [49].

Certain VLPs inherently exhibit a preference for specific tissues, a trait inherited from the viruses from which they are derived. For example, VLPs derived from the Hepatitis B Virus, which naturally infects the liver, tend to target liver cells. Similarly, rotaviruses primarily affect the intestines, and this characteristic is exploited in their derived VLPs for targeted drug delivery to intestinal tissues. Enhanced targeting is often achieved by displaying receptor-binding domains on the surface of VLPs. These domains, whether chemically or genetically attached to the VLP surface, enable the selective binding of VLPs to cancer cells that express specific receptors, thereby enhancing the drug's therapeutic impact.

In this regard, successful transfer of VLPs packaged with anticancer agents was described for bleomycin (BLM) and doxorubicin (DOX). Both conjugates were chemically coupled to VLPs (BLM to adenoviral VLPs and DOX to Rotavirus VLPs) and have demonstrated improved drug bioavailability and growth inhibition of targeted cancer cells [50].

VLPs can also be used to deliver nucleic acids. For example, one study showed that systematic delivery of miR-146a, a known gene silencer, via bacteriophage MS2 -derived VLPs, is an effective treatment for reducing inflammatory cytokines in mice susceptible to systemic lupus erythematosus

On the other hand, protein delivery by VLPs has been described for heterologous antigens, antibodies, cytokines, enzymes, and reporter proteins such as green fluorescent protein (GFP) or maltose binding protein (MBP) [52]. Successful examples of VLP applications in drug delivery are detailed in **Table 3** [52].



**Table 3:** Some examples of application of VLPs as drug delivery (adapted from [41]).

VLPs	Cargo	Application
<b>Adenovirus (AdV)</b>	Bleomycin (BLM) Paclitaxel (PTX) mRNA cap analog	Tumor therapy
<b>Bacteriophage MS2</b>	Doxorubicin, Cisplatin, 5-fluorouracil siRNA Ricin toxin A-chain (RTA)	Tumor therapy
<b>Bacteriophage Q<math>\beta</math></b>	Azithromycin/clarithromycin	Antimicrobial drug
<b>Polyomavirus</b>	Methotrexate (MTX)	Tumor therapy

#### 4. HIV-1-derived VLPs

First identified in 1981, the human immunodeficiency virus-1 (HIV-1) is the causative agent of AIDS and since then has posed a significant global challenge in the development of a protective vaccine [53]. HIV-1 virions are complex spherical particle with an average size 120-200 nm in diameter formed by an internal protein core surrounded by a lipid bilayer derived from the host cell membrane [54]. The conical capsid contains the HIV-1 genome composed by two single-stranded RNA (ssRNA) molecules, encompassing nine open reading frames (ORFs). The genome includes three primary structural genes—*gag*, *pol*, and *env*—along with two regulatory proteins (*tat* and *rev*) and four accessory genes (*nef*, *vif*, *vpr*, and *vpu*) [55] (**Figure 5A**). From the three main genes, *gag* codes for the structural polyprotein Gag, encompassing the nucleocapsid (NC), capsid (CA) and matrix (MA), while *pol* and *env* encode for the main enzymes (PR (Protease), RT (Retrotranscriptase) and IN (Integrase)) and the receptor binding protein Env (gp120 and gp41), respectively (**Figure 5B**). After translation, the Gag polyprotein is synthesized in the cytoplasm and subsequently transported to the plasma membrane of the host cell [56]. During the cytosolic transport, the Gag proteins start to self-assemble into intermediate structures and accumulate at the cytosolic side of the plasma membrane in dense patches [57]. The formation of Gag protein complexes leads to a plasma membrane protuberance that leads to the release of matured VLPs by budding [58], [59]. This process is triggered by the mere presence of Gag polyprotein, independently of the rest of the viral proteome. This led to the expression of Gag by recombinant DNA technology in different cell lines to produce Gag VLPs as platform for vaccine and drug delivery therapies. Gag VLPs typically contain about 2200 to 3200 Gag monomers

and have the same size of the HIV-1 mature virions (approximately 100 to 200 nm) depending on the production platform employed [60]. Also, they do not contain viral genetic material, being non-infectious like all recombinant vaccines, as mentioned above. Additionally, is important to mention, that Gag VLPs lack the proteolytic maturation of Gag polyprotein, forming a shell underneath the cell membrane conforming the protein core [60] (**Figure 5C**).

Due to the flexible assembly process of Gag VLPs, fluorescently tagged Gag virions with the expected morphology can be efficiently generated by expressing Gag as a fusion construct with the green fluorescent protein (GFP) [61], [62], [63]. Gag::GFP forms VLPs with an efficiency equivalent to that of Gag alone [64], a beneficial feature that our laboratory has exploited [60], [65], [66] in developing bioprocessing strategies for VLPs. These fluorescently tagged VLPs facilitate easy detection and quantification [67] [68]. While retaining the fluorescent tag is not desirable in the final VLP product, its use during product development is invaluable for swiftly and simply evaluating various process alternatives. Additionally, using Gag VLPs as nanocarriers for reporter genes enables targeted cell identification and functional VLP quantitation [66] [69].

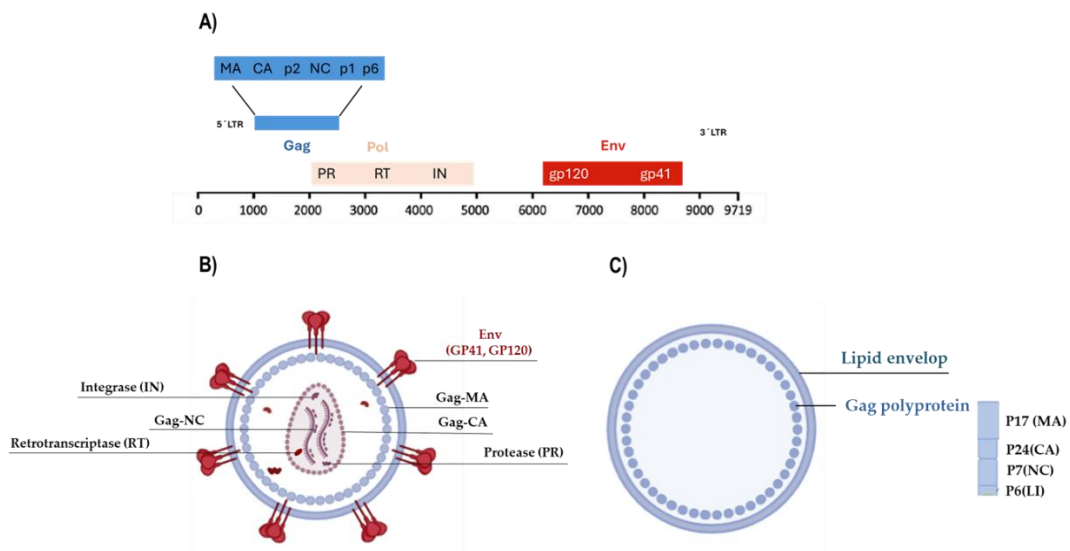


**Figure 5:** Structure of HIV-1 Gag VLP. **A)** Schematic representation of HIV-1 genome. In short, the genome is composed of 3 structural genes (*gag*, *pol* and *env*). *Gag* is further processed into 6 protein domains known as matrix (MA or p17), capsid (CA or p24), spacer peptide 1 (SP1 or p2), nucleocapsid (NC or p7), spacer peptide 2 (SP2 or p1) and p6. **B)** Morphological structure of wild type Gag HIV-1 virions composed by the cleavage products of the three major viral polyproteins: Gag, Pol and Env. **C)** Morphological structure of the recombinant Gag VLPs. The sole expression of Gag polyprotein gives rise to the generation of Gag VLPs, which are basically immature HIV-1 particles carrying uncleaved Gag capsids surrounded by a host cell lipid layer, (adapted from [60] and [70]). *gp*: glycoprotein; *MA*: matrix; *CA*: capsid; *NC*: nucleocapsid; *P6*: peptide 6 linker.

#### **4.1. The Use of HIV-1 Gag VLPs**

Initially, these Gag VLPs were used to develop HIV-1 vaccine candidates by displaying the native Env glycoprotein on their surface. However, this method proved to be highly inefficient, leading researchers to shift their focus towards employing recombinant-truncated and conserved fragments of Env [70], [71]. Beyond their application in HIV-1 vaccines, Gag VLPs have also been explored for their potential in creating chimeric VLPs as a platform aimed at combating various diseases or as part of novel delivery strategies [72], [73]. Several researchers have utilized the Gag polyprotein to present antigens from various pathogens, including influenza, dengue, West Nile virus, HPV, equine herpes virus, pseudorabies and recently SARS-CoV-2 [70], [74], [75], [76], [77], [78]. Furthermore, the Gag sequence has been genetically modified to deliver nucleic acids, enzymes, and drugs [79], [80], [81].

In the field of cancer research, the immunogenic properties of these VLPs have been examined [82], [83]. Notably, Gag VLPs functionalized for therapeutic purposes have been proposed as vaccine candidates for treating pancreatic cancer [84].

#### **5. Production of HIV-1 Gag VLPs.**

The optimal production process of HIV-1 VLPs should be cost-effective, highly productive, scalable and provide VLPs with the correct structure and immunogenicity [70]. As HIV-1 VLPs are enveloped particles the choice of the production platform is crucial, since the envelope of the VLP is derived from the producer cell during the budding process into the culture supernatant, as detailed in the previous section. HIV-1 Gag VLPs are produced through recombinant protein expression in biotechnological processes. The manufacturing process is divided into upstream processing (USP), where protein building blocks are produced during fermentation, and downstream processing (DSP), where the molecule or particle of interest is purified using various separation techniques to obtain the purified product [42]. HIV-1 Gag VLP production has been achieved in several cellular platforms, but most research is conducted with animal cell culture [85].

Despite mammalian cells typically generating lower yields of the desired protein compared to other systems, they have the capacity to perform more complex and accurate post-translational modifications

[86] [87]. This capability makes them particularly promising for producing intricate eVLPs composed of multiple structural proteins. In the case of HIV-1 Gag VLPs, the human embryonic kidney (HEK 293) cell line is considered as a reference for its production, since they are easily transfected and can be cultured in suspension, resulting in good scalability [65], [88], [89]. HEK 293 cells has been also tested for the production of other VLPs such as influenza or rabies [90], [91]. Additionally, HEK 293 cells are preferred to other cells when human-specific post-translational modifications are advantageous for the final product [92].

The production of virus-like particles (VLPs) in animal cell cultures can be achieved through two primary methods: stable gene expression (SGE) and transient gene expression (TGE). SGE involves integrating the protein-coding gene into the cellular genome, making it a preferred method for well-established and thoroughly characterized bioprocesses [93]. This method also eliminates the need for generating large amounts of DNA during scale-up, thereby reducing the costs associated with transfection reagents and minimizing the risk of contamination during transfection procedures [94]. Conversely, TGE is a rapid and straightforward approach where multiple copies of the gene of interest (GOI) are delivered into the cell using physical or chemical methods, resulting in high protein yields [95]. Table 4 summarizes the main advantages and disadvantages of both strategies.

**Table 4:** Advantages and drawbacks of stable and transient gene expression approaches

	Stable gene expression (SGE)	Transient gene expression (TGE)
<b>Generation time</b>	Up to 12 months (the first time)	Weeks
<b>Difficulty</b>	Laborious	Easy
<b>Economic cost</b>	High the first time, then low	Medium (repeated)
<b>Expression</b>	Chromosome integrated	Episomal: lost over time
<b>Homogeneity</b>	Clonal: well-defined and characterized homogenous cell line and product	Heterologous: different GOI copies and presence of non-producer cells
<b>Cell density</b>	No limitations	Limited to transfection procedure: cell density effect
<b>Scalability</b>	No limitations	Small to medium scale
<b>Common applications</b>	Industrial and large-scale production	Research and small-scale or pre-clinical recombinant protein or viral vector production

### 5.1. PEI-mediated Gag VLPs production

Several physical and chemical methods are found in the literature for TGE purpose [96]. However, in industrial biotechnology, transfection reagents such as calcium phosphate and, to a greater extent, the cationic polymer polyethylenimine (PEI) are predominantly used [95]. For over thirty years, PEI has been a prominent tool for gene delivery in both *in vitro* and *in vivo* settings [97]. PEI is noted for its simplicity, effectiveness with suspension cells, compatibility with serum-free media, and cost efficiency. Since Boussif et al (1995) [98] first reported its use as a transfection reagent, various polymer lengths and configurations, including linear and branched PEI, have been explored for DNA delivery [99], [100]. The amine groups in PEI interact with the negatively charged phosphate groups of nucleic acids, forming positively charged complexes known as polyplexes. This interaction condenses the DNA sequences and protects them from nuclease degradation. **Figure 6** illustrates the PEI-mediated transient gene expression (TGE) used for producing HIV-1 Gag VLPs.

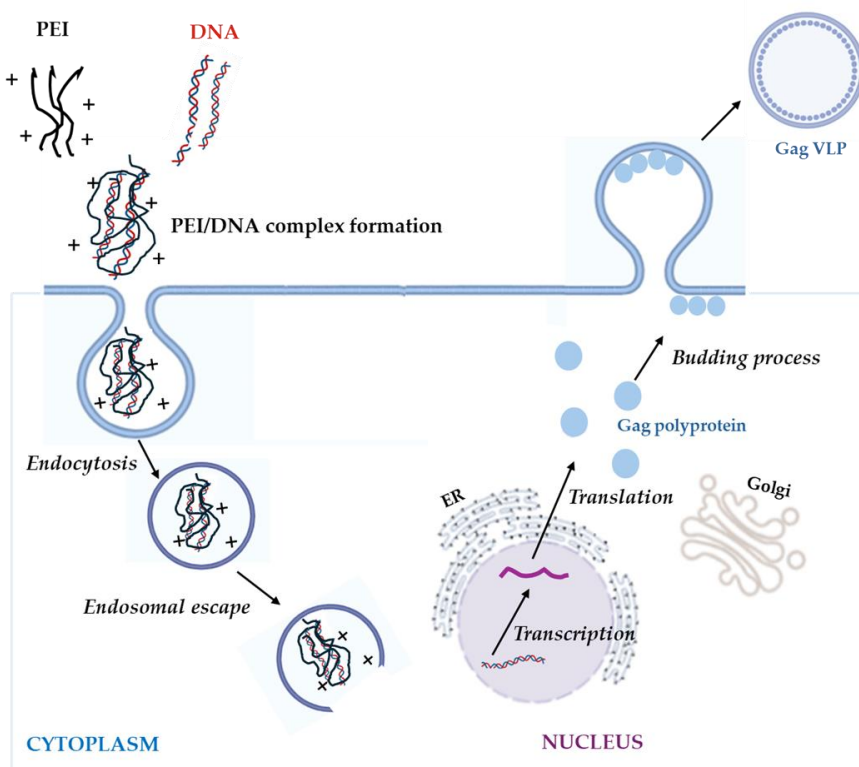


**Figure 6:** PEI-mediated TGE for the production of HIV-1 Gag VLPs (figure adapted from [101]).ER: endoplasmic reticulum.

Cell culture media for mammalian cells has evolved towards serum-free, animal-component free and chemically defined media, driven by regulatory and quality criteria, but also enabling a much reproducible process performance, highly relevant at manufacturing scale. The production of HIV-1 Gag VLPs has been achieved in chemically defined cell culture media, with supplementation strategies targeting cell growth and production yields [65]. On the other hand, the yields of viable cell densities and VLP production can be significantly improved using perfusion instead of batch mode in bioreactors [102]. Perfusion is a specific type of continuous operational mode where fresh media is constantly fed into the culture system while spent media is continuously removed, while retaining the cells within the culture system using a cell retention device [103]. Thus, cell growth and VLP production can be maintained for longer periods under optimal conditions while the product is harvested.

The production of HIV-1 Gag VLPs by transient transfection using HEK293 cells and PEI as transfection agent has been studied in batch processes, achieving production levels up to  $2.7 \cdot 10^9$  VLPs/mL [65]. This process has been optimised by prolonging the production through repeated transfection of the suspension cell culture combined with repeated medium exchange, generating a novel methodology named extended gene expression (EGE) with a total production of  $9.2 \cdot 10^{11}$  VLPs in 120 mL, a 12-fold increase compared to the standard batch transient transfection protocol [104]. However, a common limitation observed in transfection efficiency is the cell density effect, where transfection efficiency decreases substantially at higher cell densities [105], [106]. EGE has been successfully transferred to bioreactor scale maintaining the same production titres using an hollow fiber alternating tangential flow filtration (ATF) as a cell retention device to perform perfusion [107], [108]. Process intensification towards continuous manufacturing, and the optimization of process parameters could further enhance the final production in Gag VLPs-based products [109].

## **6. Purification of HIV-1 Gag VLPs**

The goal of downstream processing is to produce a purified, biologically active, and quality-consistent product by removing host-cell impurities and culture media components [110]. One significant challenge in producing Gag VLPs in mammalian cells is the concomitant secretion of extracellular vesicles (EVs),

such as microvesicles and exosomes, alongside the desired VLPs [89]. This complicates the purification process, as both enveloped VLPs and EVs share the same host cell-derived membrane, making them very similar in their physicochemical properties. Their similar sizes and densities add further difficulty in separation and analysis [111], [112]. An optimal purification process should achieve a high purification and concentration factor and yield, in a cost-effective manner. The required product quantities and purification levels vary depending on the product's final application (*in vitro*, preclinical, or clinical testing), necessitating different technologies. Regulatory agencies have set a limit of 10 ng of dsDNA of less than 200 bp and 100 ppm of Host-Cell Protein (HCP) per dose for clinical use [113], [114]. However, some proteins may be inherently incorporated into viral structures, making the limit product-dependent [115], [116]. For VLPs in clinical tests and approved products, 15 to 60 µg of antigen per 0.5 mL dose has been reported. The route of administration, adjuvant composition, and dosage number will influence the final antigen amount required [3].

Due to the similarity between enveloped VLPs and host cell-derived EVs, a sequence of separation steps is necessary to purify and concentrate HIV-1 Gag VLPs (and generally, enveloped viruses) to achieve high purity level [117], [118]. Conventional methods mostly used at laboratory scale like centrifugation and ultracentrifugation are time-consuming, labor-intensive, and non-scalable [42]. In recent years, significant efforts have been made to establish scalable techniques, such as chromatographic and membrane-based methods, for purifying HIV-1-based particles for clinical purposes [66], [77], [119], [120]. Advances in gene therapy using lentiviral vectors, which share similar physicochemical properties with HIV-1 VLPs, have greatly contributed to developing these new scalable purification techniques [121]. **Figure 7** provides an overview of typical purification steps targeted to remove specific impurities and potential techniques achieve them [118].

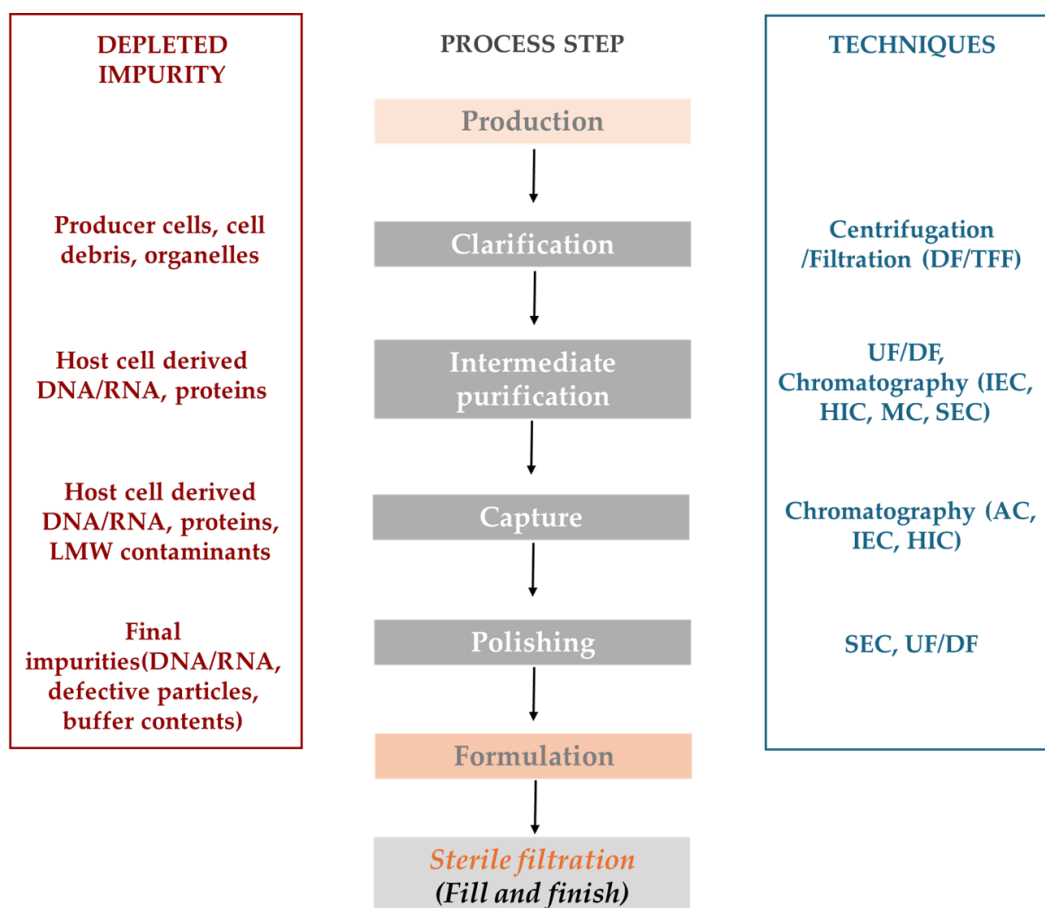


**Figure 7:** Process diagram of typical DSP for HIV-1 Gag VLPs. After the initial production and clarification, the typical three stage purification strategy is used. The process starts with a clarification step to separate cells and debris from the VLPs that have been released to the supernatant by budding. Then, to remove the host cell DNA/RNA and proteins an intermediate purification or concentration step is often performed. A capture step follows, in which most of the process-related impurities (host cell DNA/RNA and proteins, monomeric HIV-1 Gag proteins, baculovirus, etc.) are removed. Next, a polishing step would be required to remove the product-related impurities and formulate the product in the most suitable buffer. Finally, a sterile filtration step is performed. The potential purification techniques and the depleted impurities are shown for each step. *DF*: depth filtration; *TFF*: tangential flow filtration; *UF/DF*: ultrafiltration / diafiltration; *AC*: affinity chromatography; *IEC*: ion exchange chromatography; *HIC*, hydrophobic interaction chromatography; *MC*, multimodal chromatography; *SEC*, size-exclusion chromatography; *LMW*: low molecular weight

By combining purification steps based on different techniques, it is often possible to achieve a high degree of VLPs purity combined with high concentrations [122]. Various examples of recent purification processes have been published, but no universal purification process exists for these complex particles [66], [72], [77], [123], [124], [125]. Simplifying the purification train is beneficial, as an increase in the number of unit operations negatively impacts the purification yield and associated costs [110]. To delve deeper into each step of the HIV-1 VLPs purification process, it is essential to understand the rationale behind the selection of specific techniques and their role in removing impurities. The following sections will examine each purification step in more detail, highlighting the most commonly used methods.



### **6.1. Clarification**

During the budding process, the Gag VLPs are released from the cells and accumulate in the culture supernatant. This secretion into the extracellular medium simplifies their collection, as the Gag VLPs are already present outside the cells, avoiding the need for cell lysis procedures and making the subsequent clarification process more efficient [126]. Clarification, widely used as the first step in downstream processing, can be performed with centrifugation and/or depth filtration [127] to remove cells, cell debris, large particles, and aggregates [101]. However, in perfusion process, since VLPs are continuously harvested through a filter that removes cells [108], the clarification step is effectively integrated into this initial phase of upstream processing, presenting a clear advantage for the subsequent DSP operations.

Filtration techniques, using either dead-end and depth filters or membrane devices have been incorporated into the manufacturing processes of viral particles [128]. Depth filters use multiple porous layers with decreasing pore size to retain particles throughout the medium, rather than just on the surface, unlike with microfiltration (pore size from 0.1 to 10  $\mu\text{m}$ ) or ultrafiltration (pore size from 0.01 to 0.1  $\mu\text{m}$ ). This means that VLPs are sieved through a size-dependent separation factor [42]. However, non-inert materials may bind efficiently not only cellular debris or aggregates but also the VLPs being sieved, hence a careful selection of the depth filter material is crucial. For large-scale processes, long-term storage at  $-80^{\circ}\text{C}$  is frequently necessary. This can cause the presence of aggregates and precipitates after the sample is thawed. In these cases, a second clarification step is sometimes needed in DSP strategies. Turbidity is an important parameter that should be monitored during the clarification process and can serve as an indication of its efficiency. Also, the turbidity breakthrough is an indication of filter capacity [77].

### **6.2. Concentration / Intermediate purification**

Following clarification, a concentration or intermediate purification step is commonly included in the DSP. Ultrafiltration by tangential flow filtration (TFF) and multimodal chromatography (MC) are widely used. Concentration is a critical step, ubiquitous for the DSP of VLPs. The stream volume should be

reduced as early as possible in order to reduce the upfront investment in the downstream equipment and overall consumables and buffers. T-Series cassettes with omega polyethersulfone (PES) membrane, and molecular weight cut-off of 300 kDa, has been satisfactorily reported in VLPs purification [120], [129]. On the other hand, MC is based on a combination of different binding mechanisms. A relevant example of MC is the Capto™ Core 700 and Capto™ Core 400 resins. These resins feature a ligand-activated core and an inactive shell, providing both size exclusion and binding properties. They are ideal for flow-through mode chromatography, effectively binding impurities while allowing the target particles to pass through and be collected in the flow-through. This technology has been employed in various purification processes for viral particles and extracellular vesicles [117], [119], [130].

### 6.3. Capture

Chromatography have been recognized as a method which can meet the challenges regarding VLPs preparation purity. It has proved to be very efficient for VLPs- based pharmaceuticals and has an advantage of easy scale up from laboratory to the preparative scale. When chromatography is operated as a capture step, good concentration factors and high purity levels can be achieved upon elution if the capacity of the chosen matrix is significant for the VLP in question [42] [127]. Ion-exchange chromatography (IEC) is one of the most widely used chromatographic techniques for purification of large particles which exploits the differences in particle's charge [127]. Anion or cation exchange chromatography techniques can be applied depending on the net charge of the particle to be purified. The net charge at neutral pH will depend on the particle surface composition which differs from each viral particle. Most of the viral particles have an isoelectric point below 7.4, being negatively charged at physiological pH. Given that HIV-1 Gag VLPs possess an overall negative net charge [112], they have been efficiently purified using anion exchange chromatography. Examples of successful applications include the Monolith QA, Mustang® Q XT, and Capto™ Q ImpRes columns [131]. In the QA Monolithic column, a quaternary amine group is bound to a highly cross-linked, porous monolithic polymer with a well-defined channel size distribution. The large channels allow high-capacity convection flow separation of nanoparticles [111], [112], [132]. Mustang® Q XT has 16 layers of membrane PES-based,

with 0.8  $\mu\text{m}$  pore size, and a cross-linked polymeric coating of quaternary amine functional groups. This membrane adsorber enables the handling of higher flows and scalability [66], [133], [134]. The Capto™ Q ImpRes column, featuring a quaternary amine group attached to a high-flow agarose base matrix modified with a dextran surface extender, has demonstrated high recovery rates. This type of resin is highly effective for purifying HIV-1 Gag VLPs and other negatively charged particles like AAVs and influenza virus [124], [135], [136].

Hydrophobic-interaction chromatography (HIC) offers an alternative approach for the capture step in virus purification. This technique leverages the hydrophobic regions on protein surfaces by utilizing hydrophobic resins and kosmotropic salts to adjust the polarity and surface tension of the mobile phase [137]. Despite its potential, HIC has been less frequently used for virus and viral particle purification. The primary reasons are the high salt concentrations required, which can compromise virus integrity or cause precipitation, and the complexity involved in selecting optimal operating conditions [138], [139]. Additionally, the absence of predictive models needs extensive screening studies for process optimization [140]. However, high yields have been achieved employing polymethacrylate base material bonded with polypropylene glycol [136] and hydroxyl-groups [111].

Affinity chromatography (AC) is an extremely powerful chromatography technique, as it exploits the highly selective interaction between the ligand and solute in the mobile phase. Originally it was developed as a pure antibody-antigen, lectin-glycoprotein or enzyme-substrate interaction (biospecific ligands). By now, the term affinity also refers to interactions due to the binding to specific groups on the protein or particle of interest (pseudo-specific ligands) [141], [142], [143]. The biggest advantage of affinity ligands is their selectivity for their target structure. Usually, AC is used as capture step, where only target molecules bind to the column and all impurities not carrying the binding site for the ligand pass the column without any interaction, leading to a high purity of the eluate. It has been shown that viruses and VLPs can be purified efficiently using heparin affinity chromatography, as alternative method for VLP and EV separation [117], [144]. Drawbacks of this technique are the high cost for the resin, as expensive binding site screening needs to be performed, or a specific tag has to be introduced and later cleaved and separated from the product [145].

#### 6.4. Polishing

The last steps in biotherapeutic particles purification usually include an important polishing step that can be associated with the final particles' formulation. This purification step is critical since purity and quality/ potency of the final product should be as high as possible. The remaining impurities are usually related to the product and more difficult to remove and should be eliminated in this step. Size-exclusion chromatography (SEC) or diafiltration, both being scalable techniques, are the most commonly used techniques [42], [120], [122]. SEC separates the molecules according to their size because the smaller ones are trapped in the pores of the resin, whereas larger molecules cannot enter and pass by, eluting faster. The polished and reformulated VLPs in the final buffer are obtained in the void volume (VV) of the gel filtration column. Examples of implemented SEC are those based on Sephadex G-25 resin and Sepharose 4 Fast Flow resin. The Sephadex G-25 resin has a cross-linked dextran matrix with epichlorohydrin under alkaline conditions. Conversely, the Sepharose 4 Fast Flow resin consists of a cross-linked 4% agarose matrix [146] [147]. However, SEC main drawbacks are low capacity (4-20% of CV) and dilution effects ( $\sim 1.1 - 1.2$ ). Another drawback is the limited pressure resistance of the resins, which results in low process velocities and reduces overall productivity. Despite these limitations, SEC is frequently used as a final purification and polishing step in bioseparation. In the later stages of the purification process, the product is typically in a small volume and high concentrated, making SEC an effective choice [118], [146], [148].

#### 7. Formulation and storage of HIV-1 Gag VLPs

Formulation development has traditionally focused on ensuring that the marketed therapeutic products are efficacious, safe to administer and remain stable during shipping and storage [23]. This final preparation must ensure not only that potency and stability are maintained during storage, but also should be designed to be conveniently administered to patients, since concentration or volume will vary depending on the administration route. The diversity of formulation components, VLP vaccine preparation states and routes of administration is outlined in **Figure 8** [149], [150].

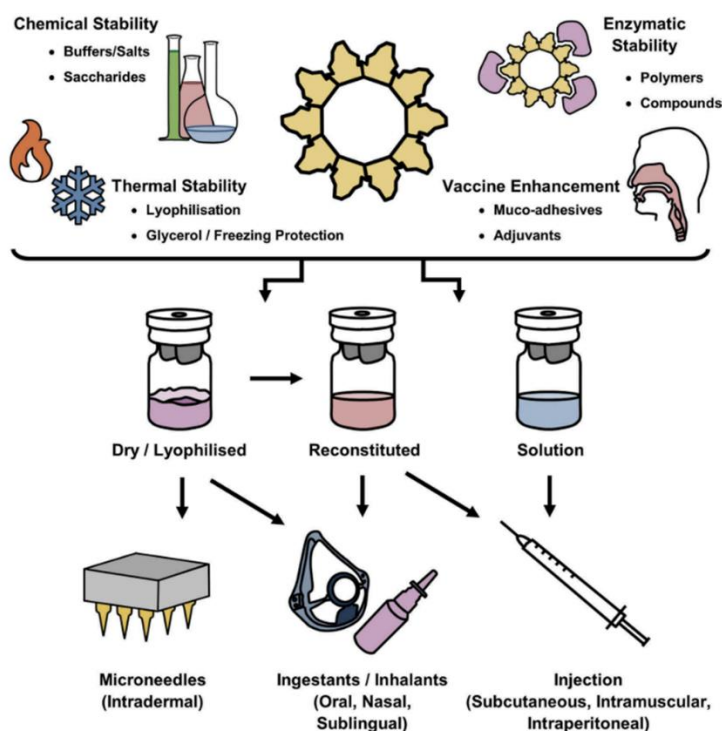


**Figure 8:** Formulation in VLP vaccines manufacture includes the chemical composition of buffers, preservatives, additives, and other stabilizing compounds for maintaining VLPs intact. This includes protecting VLPs from chemical or physical instability, and enzymatic degradation. Formulations can also include targeted delivery compounds, such as muco-adhesives, and immunogenic components such as adjuvants. Storage and distribution of VLP vaccines, and the subsequent route of administration are also important considerations in formulation, and are critical in determining the efficiency and immunogenicity of the vaccine (adapted from [149]).

The majority of VLP vaccines currently in the market and under clinical evaluation are liquid suspensions, ready for administration by intramuscular injection (**Table 5**). This places strict limitations on VLP vaccine storage and distribution for safe and compliant administration. As a consequence of this, commercial Hepatitis B vaccines and HPV VLP vaccines must be stored at 2-8 °C presenting a good shelf life of 3-4 years [150]. Nonetheless, keeping these temperatures is not always feasible; the breakage of the cold-chain due to handling errors occurs frequently, even in developed countries [151]. This cold-chain instability could be caused by several types of water-mediated destabilization and degradation pathways. Maintenance of the cold chain is challenging, especially in developing countries, where vaccines are needed the most. The cold chain also contributes to the financial burden of vaccination programs. According to the World Health Organization, approximately half of supplied vaccines are wasted due to cold chain disruption, which has a detrimental effect on vaccination programs [152]. Thus, alternative frozen and powder formulations have been developed to overcome this issue and extend the lifespan of viral vectors [153].

**Table 5:** Compositions of VLP-based vaccines in the market (adapted from [23] [150] [149]).

Commercial vaccine	Administration route	Antigen	Adjuvant	Excipient
<b>Engerix®-B hepatitis B vaccine (1 mL/dose)</b>	Liquid (IM)	HBsAg (20 µg)	Aluminum hydroxide (500 µg)	2-phenoxyethanol (5 mg)
<b>Recombivax HB® hepatitis B vaccine (1 mL/dose)</b>	Liquid (IM)	HBsAg (10 µg)	Aluminum hydroxyphosphate (500 µg)	NaCl (9 mg), Sodium borate (70 µg)
<b>Gardasil® human papillomavirus vaccine (0.5 mL/dose)</b>	Liquid (IM)	HPV 6 L1 (20 µg) HPV 11 L1 (40 µg) HPV 16 L1 (40 µg) HPV 18 L1 (20 µg)	Aluminum hydroxyphosphate sulfate (225 µg)	NaCl (9.56 mg), L-histidine (0.78 mg), Polysorbate 80 (50 µg), Sodium borate (35 µg)
<b>Cervarix® human papillomavirus vaccine (0.5 mL/dose)</b>	Liquid (IM)	HPV 16 L1 (20 µg) HPV 18 L1 (20 µg)	AS04 adjuvant system (50 µg of 3-O-desacyl-4' monophosphoryl lipid A, 500 µg aluminum hydroxyphosphate)	NaCl (4.4 mg), NaH <sub>2</sub> PO <sub>4</sub> - (0.624 mg)
<b>Hecolin® hepatitis E vaccine (0.5 mL/dose)</b>	Liquid (IM)	HE antigen (30 µg)	Aluminum hydroxide (800 µg)	Buffered saline
<b>Mosquirix™ malaria vaccine (0.5mL/dose)</b>	Liquid and Lyo (IM)	Portion of P. falciparum circumsporozoite protein fused with HBsAg (25 µg)	AS01E (Quillaja saponaria Molina, fraction 21 (QS-21) (25 µg) and 3-O-desacyl-4'-monophosphoryl lipid A (MPL) (25 µg)	Liquid: Dioleoyl phosphatidylcholine, cholesterol, NaCl, Na <sub>2</sub> HPO <sub>4</sub> · 2H <sub>2</sub> O, KH <sub>2</sub> PO <sub>4</sub> , water for injections Lyo: Sucrose, polysorbate 80, Na <sub>2</sub> HPO <sub>4</sub> · 2H <sub>2</sub> O, NaH <sub>2</sub> PO <sub>4</sub> · 2H <sub>2</sub> O.

The use of freeze-drying also referred as lyophilization [66], [151] and spray-drying [154] offer great promise in this regard. Freeze-drying involves freezing of a liquid solution followed by removal of water by sublimation of ice and thereafter by desorption of remaining water at low pressure and higher temperature. This results in a dried cake in the final container and requires reconstitution before administration [155]. The first evidence of freeze-drying process to preserve food came from the Incas, who stored their potatoes and other food crops in the mountain heights above Machu Picchu. The cold mountain temperatures froze the food, and, under the low air pressure of the high altitudes, water inside slowly vaporized. However, as part of science and technology, freeze-drying is only a matter of a century. Some key milestones in the history of freeze-drying (excluding food products) are described in **Figure 9**. Nowadays, the freeze-drying process has taken more importance in the parenteral industry and is considered an essential tool for the pharmaceutical industry [156]. Live-attenuated vaccines,

such as Varicella, Zoster or Rotavirus, inactivated vaccines against Rabies and Japanese Encephalitis are some examples of lyophilized viral-based products [150].

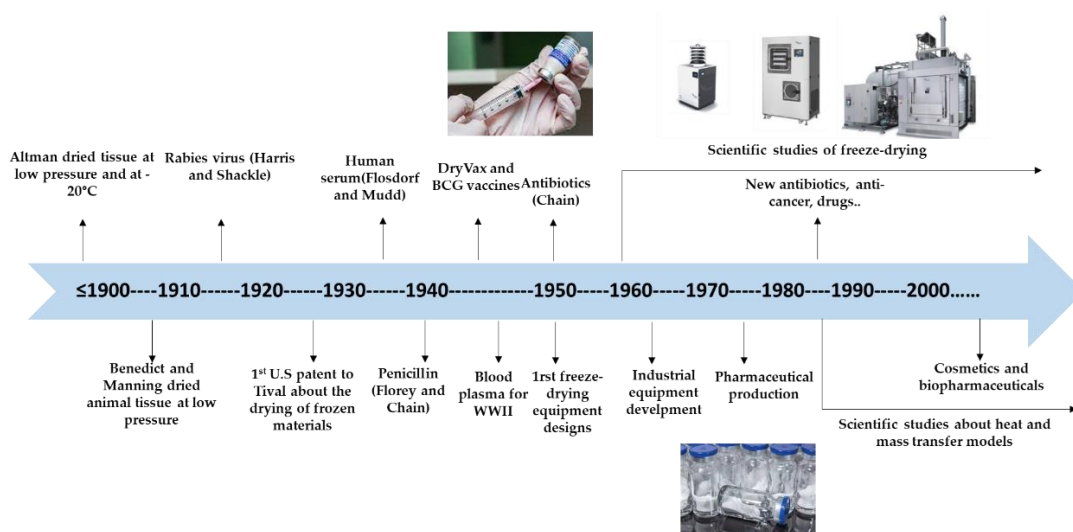


**Figure 9:** Timeline diagram of the key milestones in the history of freeze-drying. Sourced from [156]

Despite advances, the freeze-drying process for viral vaccines, particularly for enveloped viruses, continues to pose significant challenges. Issues such as membrane damage, pH or osmolarity changes, and aggregation frequently lead to a loss of vaccine potency. To mitigate these adverse effects, optimizing formulations and methodologies is crucial. This involves identifying the ideal combination of freeze-dried excipients that can preserve viral activity during both lyophilization and storage [157], [158]. Excipients are substances that have undergone rigorous safety evaluations and are intentionally included in drug delivery systems. Typically, excipients constitute a high percentage of any formulation and serve various functions [159]. Selecting the appropriate excipients is vital to ensure a safe, effective, and high-quality pharmaceutical product [160]. In lyophilization processes, excipients are generally categorized into five groups: CryoLyo-protectants, bulking agents, buffers, tonicity modifiers, and surfactants. CryoLyo-protectants stabilize the product during freeze-drying and subsequent storage. Bulking agents improve the product's appearance and provide mechanical support. Buffers control and stabilize the solution's pH. Tonicity modifiers ensure the isotonicity of the reconstituted solution at the point of use. Surfactants reduce denaturation during freezing, prevent protein loss, and help refold structurally altered forms preventing aggregation [161]. Each category includes a wide range of

compounds that can be used at varying concentrations, leading to numerous possible combinations [158], as shown in **Figure 10**.

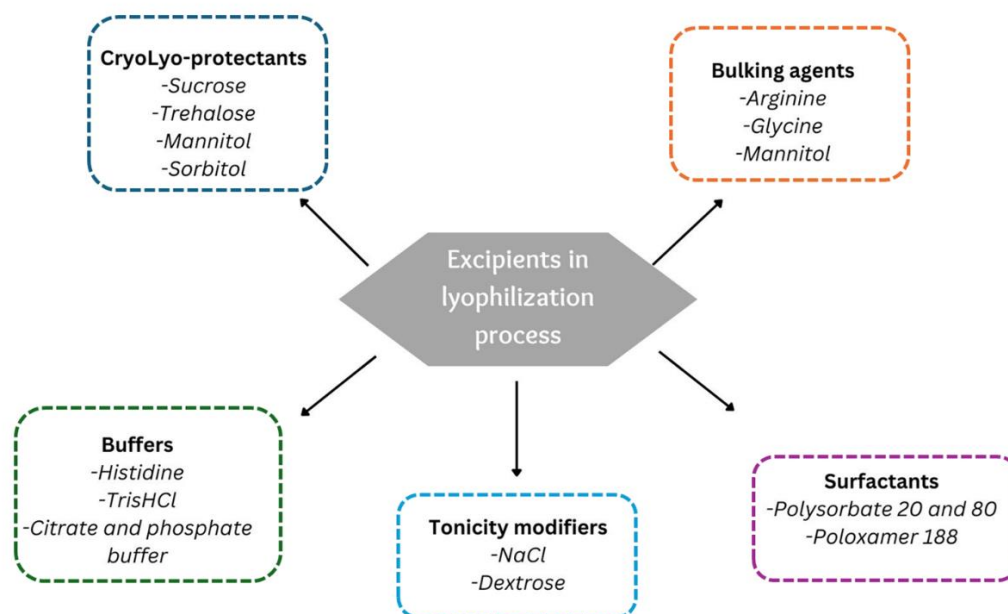


**Figure 10:** Types of excipients used in formulations for lyophilization (adapted from [158])

Traditionally, viral-based product formulations have been designed through trial and error, testing various combinations of excipients, process conditions, and particle concentrations. A deeper understanding of the physicochemical properties affected during storage would greatly benefit the development of more rational-based formulation approaches. Therefore, utilizing Design of Experiments (DoE) strategies could significantly enhance the design of new formulations, making the process more efficient and systematic [153], [162].

## 8. Functionalization of HIV-1 Gag VLPs

The surfaces of VLPs can be modified with various ligands to enhance their therapeutic efficacy, bioavailability, and cellular interactions. As explained above, there are two main approaches to modify the surface of VLPs: genetic fusion and chemical crosslinking [163]. The chosen method significantly influences the quality of the immune response, as it affects both the density of antigen molecules on the particle and the overall stability of the VLP. **Figure 11** provides an illustration of this classification,



as well as examples of potential ligands used for VLP functionalization [164]. In the first approach, foreign peptides are genetically inserted into the coding sequence of a viral structural protein. When expressed in an appropriate host, the protein self-assembles into a VLP with the peptide displayed on its surface. Although the most commonly used VLP platforms for genetic peptide display are based on the woodchuck hepatitis virus (WHBV) and several RNA bacteriophages [44], there are also reports of HIV-1 Gag VLPs engineered to enhance the display of antigens on the VLP surface [72], [73]. Additionally, through genetic co-expression, various epitopes or viral proteins have been displayed on the membrane of Gag VLPs for disease targeting and therapeutic purposes [128] [165] [166] [167]. This functionalization method relies on gene transfection, enabling the expression of peptides or proteins on the surface of VLPs. However, this approach is time-consuming and can present challenges such as transfection efficiency and recombinant protein expression [168]. Consequently, the entire process must be repeated and optimized for each specific peptide or protein.

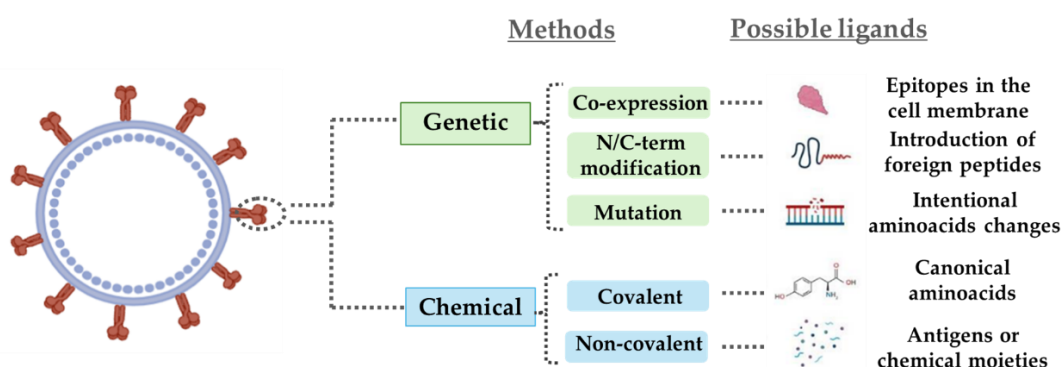


**Figure 11:** Methods, classification, and possible ligands to functionalize VLPs (adapted from [169])

In recent years, chemical conjugation has emerged as another approach to functionalize VLPs, garnering significant interest for its advantages over other existing methods and its substantial potential in biomedical applications [7], [170]. In the covalent approach, canonical amino acids (i.e., aspartic acid, cysteine, glutamic acid, lysine, and tyrosine) are incorporated to act as reactive side chain moieties able to form biocompatible bonds with the VLP surface [8], [171]. In the case of noncovalent methods, electrostatic interactions include antigens and adaptors to decorate the surfaces of VLPs, however, these approaches might lead to unstable VLPs during storage [169]. With the rapid advancement of the so called click chemistry, a simple and efficient method, proteins and nucleic acids can be conjugated

to azide or alkyne groups, and then directly linked to the VLP surface using either copper-catalyzed or copper-free click chemistry reactions [172], [173]. In this approach, the VLP, the epitope, and the linker are synthesized separately and combined later in the cross-linking reaction to produce the vaccine or nanocarrier to specific targeting therapy [174]. The chemical cross-linking process increases the cost of production but avoids potential protein folding/self-assembly issues that sometimes occur due to genetic fusion. The chemical approach also sometimes allows for higher antigen densities on the VLP surface [44].

Specifically, copper-free click chemistry reactions involve two steps (**Figure 12**) [175]. In the first step, the free lysine residues on the surface of VLPs, the most commonly used amino acid for modification, react with N-hydroxysuccinimide (NHS) esters, resulting in a stable amide bond. In the second step, azide-containing molecules react with the formed dibenzocyclooctyne, forming a triazole linkage. Triazole linkages are highly water-soluble and have similar properties to amide bonds, but with different hydrolysis reactions, making them very stable under biological conditions. Additionally, their lack of flexibility hinders aggregation [22], [172], [176]. This mode of chemical attachment has been used to functionalized exosomes [177], [178], which share similar membrane characteristics with Gag VLPs, as mentioned above, in previous sections.

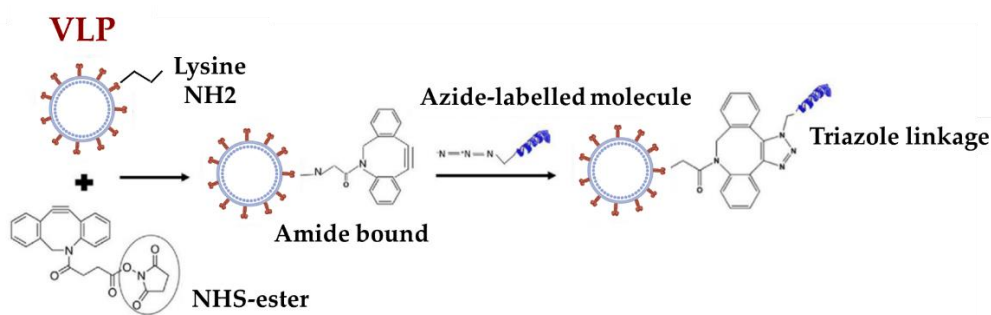


**Figure 12:** Example of Copper-free click chemistry using dibenzocyclooctyne-NHS ester (DBCO) linker which reacts with Lys residues on VLPs and incorporates cyclooctyne moiety. The formed dibenzocyclooctyne reacts with azide-labelled molecule forming a stable triazole linkage without Cu catalyst (adapted from [22])

## 9. Characterization and quantification of HIV-1 Gag VLPs

Analytical tools are critical in process development and play a crucial role in up and downstream process monitoring, being also fundamental to ensure the final product characterization regarding its quality and

safety. This characterization is usually obtained through the combination of different analytical methods [127]. Compared to simple protein-based bioproducts, the study of critical quality attributes in the production of VLPs becomes more difficult, since not only protein composition but also their three-dimensional structure should be ensured. Biochemical, biological and biophysical methods have been used in VLP characterization [23], [68]. Examples of various analytical tools used for characterization of VLPs are shown in **Figure 13**.

Biochemical	Technics	Properties
	<ul style="list-style-type: none"> <li>• SDS-PAGE and WB</li> <li>• MS</li> <li>• RP-HPLC</li> </ul>	<ul style="list-style-type: none"> <li>Purity and molecular weight</li> <li>Amino acid composition and molecular weight</li> <li>Purity</li> </ul>
Biophysical	Technics	Properties
	<ul style="list-style-type: none"> <li>• TEM</li> <li>• AFM</li> <li>• CryoTEM</li> <li>• DLS</li> <li>• AF4-MALS</li> <li>• NTA</li> <li>• SE-HPLC</li> <li>• Flow virometry</li> </ul>	<ul style="list-style-type: none"> <li>Visualization and size</li> <li>Visualization and size</li> <li>Visualization and size</li> <li>Size and polydispersity</li> <li>Size and polydispersity</li> <li>Size, polydispersity and concentration</li> <li>Size, fragments and aggregates</li> <li>Size, polydispersity and concentration</li> </ul>
Biological	Technics	Properties
	<ul style="list-style-type: none"> <li>• ELISA and immunoblot</li> <li>• SPR</li> </ul>	<ul style="list-style-type: none"> <li>Antibody binding</li> <li>Antibody binding</li> </ul>
	Technics	Properties
	<ul style="list-style-type: none"> <li>• Density gradient</li> </ul>	<ul style="list-style-type: none"> <li>Density</li> </ul>

**Figure 13:** Analytical tools for VLP characterization. A range of analytical tools is available for VLP characterization based on their biochemical, biophysical, and biological properties. *AF4-MALS*: Asymmetric Flow Field-Flow Fractionation coupled with Multiple-Angle Light Scattering; *AFM*: Atomic Force Microscopy; *Cryo-TEM*: cryogenic Transmission Electron Microscopy; *DLS*: Dynamic Light Scattering; *ELISA*: Enzyme-Linked Immunosorbent Assay; *HPLC*: High Pressure Liquid Chromatography; *MS*: Mass Spectrometry; *NTA*: nanoparticle tracking analysis; *SDS-PAGE*: Sodium Dodecyl Sulphate Polyacrylamide Gel Electrophoresis; *RP-HPLC*: Reverse-Phase HPLC; *SE-HPLC*: Size exclusion HPLC; *SEM*: Scanning Electron Microscopy; *SPR*: Surface Plasmon Resonance; *TEM*: Transmission Electron Microscopy; (Adapted from [41] and [23]).

For final product characterization, also the quantification of residual DNA and proteins from the producing cell line is always required for clinical lot release due to the stringent guidelines for this impurities [66] [179]. Among the different methods used for host cell DNA quantification PicoGreen® assay, hybridization, Threshold™ technology, and qPCR, are the most used. HCP are an impurity that must be reduced during the manufacturing process to low levels to ensure clinical safety [180]. Quantification of HCP is commonly performed by ELISA technique, using either commercially available or customized assays [110].

The specific detection and quantification of HIV-1 Gag VLPs presents several challenges. These nanoparticles need to be distinguished from other similar nanovesicles, such as EVs, including exosomes and microvesicles [181]. To counteract this limitation, in previous studies, a fluorescence-based assay was created utilizing the GFP tag fused to the Gag polyprotein [60], [69]. In this study, HIV-1 Gag VLPs is fused with GFP (HIV-1 Gag::GFP VLPs), what is very useful to selectively quantify Gag-containing particles among total nanoparticles through fluorescence-based particle counting methods, such as Nanoparticle tracking analysis (NTA) or flow virometry.

**REFERENCES**

- [1] V. P. Kodali and R. Sen, "Viral vaccines and their manufacturing cell substrates: New trends and designs in modern vaccinology," *Biotechnol. J.*, vol. 10, pp. 1329–1344, 2015, doi: 10.1002/biot.201500387.
- [2] S. Plotkin, "History of vaccination," *Proc. Natl. Acad. Sci. U. S. A.*, vol. 111, no. 34, pp. 12283–12287, 2014, doi: 10.1073/pnas.1400472111.
- [3] A. Roldão, M. C. M. Mellado, L. R. Castilho, M. J. T. Carrondo, and P. M. Alves, "Virus-like particles in vaccine development," *Expert Review of Vaccines*, vol. 9, no. 10, pp. 1149–1176, Oct. 2010, doi: 10.1586/erv.10.115.
- [4] J. B. Ulmer, U. Valley, and R. Rappuoli, "Vaccine manufacturing: Challenges and solutions," *Nat. Biotechnol.*, vol. 24, no. 11, pp. 1377–1383, 2006, doi: 10.1038/nbt1261.
- [5] T. Wirth, N. Parker, and S. Ylä-Herttuala, "History of gene therapy," *Gene*, vol. 525, no. 2, pp. 162–169, 2013, doi: 10.1016/j.gene.2013.03.137.
- [6] M. O. Mohsen, D. E. Speiser, A. Knuth, and M. F. Bachmann, "Virus-like particles for vaccination against cancer," *Wiley Interdiscip. Rev. Nanomedicine Nanobiotechnology*, vol. 12, no. 1, 2020, doi: 10.1002/wnan.1579.
- [7] J. He *et al.*, "Virus-like Particles as Nanocarriers for Intracellular Delivery of Biomolecules and Compounds," 2022.
- [8] M. J. Rohovie, M. Nagasawa, and J. R. Swartz, "Virus-like particles: Next-generation nanoparticles for targeted therapeutic delivery," *Bioeng. Transl. Med.*, vol. 2, no. 1, pp. 43–57, 2017, doi: 10.1002/btm2.10049.
- [9] A. F. Rodrigues, M. J. T. Carrondo, P. M. Alves, and A. S. Coroadinha, "Cellular targets for improved manufacturing of virus-based biopharmaceuticals in animal cells," *Trends Biotechnol.*, vol. 32, no. 12, pp. 602–607, 2014, doi: 10.1016/j.tibtech.2014.09.010.
- [10] P. H. Mäkelä, "Vaccines, coming of age after 200 years," *FEMS Microbiol. Rev.*, vol. 24, no. 1, pp. 9–20, 2000, doi: 10.1016/S0168-6445(99)00025-X.
- [11] T. Ye, Z. Zhong, A. García-Sastre, M. Schotsaert, and B. G. De Geest, "Current Status of COVID-19 (Pre)Clinical Vaccine Development," *Angew. Chemie - Int. Ed.*, vol. 59, no. 43, pp. 18885–18897, 2020, doi: 10.1002/anie.202008319.
- [12] J. T. Schiller and D. R. Lowy, "Raising expectations for subunit vaccine," *J. Infect. Dis.*, vol. 211, no. 9, pp. 1373–1375, 2015, doi: 10.1093/infdis/jiu648.
- [13] M. A. Liu, "DNA vaccines: A review," *J. Intern. Med.*, vol. 253, no. 4, pp. 402–410, 2003, doi: 10.1046/j.1365-2796.2003.01140.x.
- [14] S. Jain, A. Venkataraman, M. E. Wechsler, and N. A. Peppas, "Messenger RNA-based vaccines: Past, present, and future directions in the context of the COVID-19 pandemic," *Adv. Drug Deliv. Rev.*, vol. 179, 2021, doi: <https://doi.org/10.1016/j.addr.2021.114000>.
- [15] J. Fuenmayor, F. Gòdia, and L. Cervera, "Production of virus-like particles for vaccines," *New Biotechnology*, vol. 39, Elsevier B.V., pp. 174–180, Oct. 25, 2017, doi: 10.1016/j.nbt.2017.07.010.
- [16] J. M. Galarza, T. Latham, and A. Cupo, "Virus-like particle vaccine conferred complete protection against a lethal influenza virus challenge," *Viral Immunol.*, vol. 18, no. 2, pp. 365–372, 2005, doi: 10.1089/vim.2005.18.365.
- [17] B. Chackerian, "Virus-like particles: Flexible platforms for vaccine development," *Expert Rev. Vaccines*, vol. 6, no. 3, pp. 381–390, 2007, doi: 10.1586/14760584.6.3.381.

- [18] H. Tariq, S. Batool, S. Asif, M. Ali, and B. H. Abbasi, "Virus-Like Particles: Revolutionary Platforms for Developing Vaccines Against Emerging Infectious Diseases," *Front. Microbiol.*, vol. 12, no. January, 2022, doi: 10.3389/fmicb.2021.790121.
- [19] Y. T. Lee *et al.*, "Intranasal vaccination with M2e5x virus-like particles induces humoral and cellular immune responses conferring cross-protection against heterosubtypic influenza viruses," *PLoS One*, vol. 13, no. 1, pp. 1–15, 2018, doi: 10.1371/journal.pone.0190868.
- [20] C. Wang, X. Zheng, W. Gai, G. Wong, and H. Wang, "Novel chimeric virus-like particles vaccine displaying MERS-CoV receptor-binding domain induce specific humoral and cellular immune response in mice," vol. 140, pp. 55–61, 2017, doi: <http://dx.doi.org/10.1016/j.antiviral.2016.12.019>.
- [21] H. Jeong and B. L. Seong, "Exploiting virus-like particles as innovative vaccines against emerging viral infections," *J. Microbiol.*, vol. 55, no. 3, pp. 220–230, 2017, doi: 10.1007/s12275-017-7058-3.
- [22] M. O. Mohsen, L. Zha, G. Cabral-Miranda, and M. F. Bachmann, "Major findings and recent advances in virus-like particle (VLP)-based vaccines," *Semin. Immunol.*, vol. 34, no. August, pp. 123–132, 2017, doi: 10.1016/j.smim.2017.08.014.
- [23] L. H. L. Lua, N. K. Connors, F. Sainsbury, Y. P. Chuan, N. Wibowo, and A. P. J. Middelberg, "Bioengineering Virus-Like Particles as Vaccines," *Biotechnol. Bioeng.*, vol. 111, pp. 425–440, 2014, doi: 10.1002/bit.25159/abstract.
- [24] R. Gupta *et al.*, "Platforms, advances, and technical challenges in virus-like particles-based vaccines," *Front. Immunol.*, vol. 14, no. February, pp. 1–21, 2023, doi: 10.3389/fimmu.2023.1123805.
- [25] G. T. Jennings and M. F. Bachmann, "The coming of age of virus-like particle vaccines," *Biol. Chem.*, vol. 389, no. 5, pp. 521–536, 2008, doi: 10.1515/BC.2008.064.
- [26] M. Peacey, S. Wilson, and V. K. Baird, Margaret A. Ward, "Versatile RHDV Virus-Like Particles: Incorporation of Antigens by Genetic Modification and Chemical Conjugation," *Biotechnol. Bioeng.*, vol. 98, pp. 968–977, 2007, doi: 10.1002/bit.
- [27] L. W. McGinnes *et al.*, "Assembly and Immunological Properties of Newcastle Disease Virus-Like Particles Containing the Respiratory Syncytial Virus F and G Proteins," *J. Virol.*, vol. 85, no. 1, pp. 366–377, 2011, doi: 10.1128/jvi.01861-10.
- [28] P. Pushko *et al.*, "Influenza virus-like particle can accommodate multiple subtypes of hemagglutinin and protect from multiple influenza types and subtypes," *Vaccine*, vol. 29, no. 35, pp. 5911–5918, 2011, doi: 10.1016/j.vaccine.2011.06.068.
- [29] and S.-M. K. Fu-Shi Quan, Gangadhara Sailaja, Ioanna Skountzou, Chunzi Huang, Andrei Vzorov, Richard W. Compans, "Immunogenicity of virus-like particles containing modified human immunodeficiency virus envelope proteins," *Vaccine*, vol. 25, no. 19, pp. 3841–3850, 2007.
- [30] H. D. Foley, J. P. McGettigan, C. A. Siler, B. Dietzschold, and M. J. Schnell, "A recombinant rabies virus expressing vesicular stomatitis virus glycoprotein fails to protect against rabies virus infection," *Proc. Natl. Acad. Sci. U. S. A.*, vol. 97, no. 26, pp. 14680–14685, 2000, doi: 10.1073/pnas.011510698.
- [31] S. Wang *et al.*, "Viral vectored vaccines: design, development, preventive and therapeutic applications in human diseases," *Signal Transduct. Target. Ther.*, vol. 8, no. 1, 2023, doi: 10.1038/s41392-023-01408-5.
- [32] R. K. Keswani, I. M. Pozdol, and D. W. Pack, "Design of Hybrid Lipid/Retroviral-Like Particle Gene Delivery Vectors," *Mol. Pharm.*, vol. 10, no. 5, pp. 1725–1735, 2013, doi: 10.1021/mp300561y.
- [33] Y. H. Chung, H. Cai, and N. F. Steinmetz, "Viral nanoparticles for drug delivery, imaging, immunotherapy, and theranostic applications," *Adv. Drug Deliv. Rev.*, vol. 156, pp. 214–235, 2020,

doi: 10.1016/j.addr.2020.06.024.

- [34] S. M. DePorter and B. R. McNaughton, "Engineered M13 Bacteriophage Nanocarriers for Intracellular Delivery of Exogenous Proteins to Human Prostate Cancer Cells," *Bioconjug. Chem.*, vol. 25, no. 9, pp. 1620–1625, 2014, doi: 10.1021/bc500339k.
- [35] H. K. Charlton Hume, J. Vidigal, M. J. T. Carrondo, A. P. J. Middelberg, A. Roldão, and L. H. L. Lua, "Synthetic biology for bioengineering virus-like particle vaccines," *Biotechnol. Bioeng.*, vol. 116, no. 4, pp. 919–935, 2019, doi: 10.1002/bit.26890.
- [36] C. J. Burrell, P. Mackay, P. J. Greenaway, P. H. Hofschneider, and K. Murray, "Expression in *Escherichia coli* of hepatitis B virus DNA sequences cloned in plasmid pBR322," *Nature*, vol. 279, no. 5708, pp. 43–47, 1979, doi: 10.1038/279043a0.
- [37] A. Monie, C. F. Hung, R. Roden, and T. C. Wu, "Cervarix™: A vaccine for the prevention of HPV 16, 18-associated cervical cancer," *Biol. Targets Ther.*, vol. 2, no. 1, pp. 107–113, 2008, doi: 10.2147/btt.s1877.
- [38] J. Atsmon *et al.*, "Rapid and high seroprotection rates achieved with a tri-antigenic Hepatitis B vaccine in healthy young adults: Results from a Phase IV study," *Vaccine*, vol. 39, no. 8, pp. 1328–1332, 2021, doi: 10.1016/j.vaccine.2020.12.050.
- [39] Manon M.J. Cox, Peter A. Patriarca, and John Treanor, "FluBlok, a recombinant hemagglutinin influenza vaccine," *Influenza Other Respi. Viruses*, vol. 2, no. 6, pp. 211–219, Nov. 2008, doi: 10.1111/j.1750-2659.2008.00055.x.
- [40] M. Dhawan, A. A. Saied, and M. Sharma, "Virus-like particles (VLPs)-based vaccines against COVID-19: Where do we stand amid the ongoing evolution of SARS-CoV-2?," *Heal. Sci. Rev.*, vol. 9, no. October, p. 100127, 2023, doi: 10.1016/j.hsr.2023.100127.
- [41] S. Nooraei *et al.*, "Virus-like particles: preparation, immunogenicity and their roles as nanovaccines and drug nanocarriers," *J. Nanobiotechnology*, vol. 19, no. 1, pp. 1–27, 2021, doi: 10.1186/s12951-021-00806-7.
- [42] T. Vicente, A. Roldão, C. Peixoto, M. J. T. Carrondo, and P. M. Alves, "Large-scale production and purification of VLP-based vaccines," *Journal of Invertebrate Pathology*, vol. 107, no. SUPPL. Jul. 2011, doi: 10.1016/j.jip.2011.05.004.
- [43] A. A. Zasada *et al.*, "COVID-19 Vaccines over Three Years after the Outbreak of the COVID-19 Epidemic," *Viruses*, vol. 15, no. 9, 2023, doi: 10.3390/v15091786.
- [44] F. P. and F. C. Jerri C. Caldeira, Michael Perrine, "Virus-Like Particles as an Immunogenic Platform for Cancer Vaccines," *Viruses*, vol. 12, p. 488, 2020, doi: 10.3390/v12050488.
- [45] A. L. Tornesello, M. Tagliamonte, F. M. Buonaguro, M. L. Tornesello, and L. Buonaguro, "Virus-Like Particles as Preventive and Therapeutic Cancer Vaccines," *Vaccines*, vol. 10, no. 2, pp. 1–20, 2022, doi: 10.3390/vaccines10020227.
- [46] M. Stanley, "Tumour virus vaccines: Hepatitis B virus and human papillomavirus," *Philos. Trans. R. Soc. B Biol. Sci.*, vol. 372, no. 1732, 2017, doi: 10.1098/rstb.2016.0268.
- [47] B. Donaldson, F. Al-Barwani, S. J. Pelham, K. Young, V. K. Ward, and S. L. Young, "Multi-target chimaeric VLP as a therapeutic vaccine in a model of colorectal cancer," *J. Immunother. Cancer*, vol. 5, no. 1, pp. 1–13, 2017, doi: 10.1186/s40425-017-0270-1.
- [48] K. Campbell *et al.*, "Delivering two tumour antigens survivin and mucin-1 on virus-like particles enhances anti-tumour immune responses," *Vaccines*, vol. 9, no. 5, pp. 1–14, 2021, doi: 10.3390/vaccines9050463.
- [49] M. Zdanowicz and J. Chroboczek, "Virus-like particles as drug delivery vectors," *Acta Biochim. Pol.*, vol. 63, no. 3, pp. 469–473, 2016, doi: 10.18388/abp.2016\_1275.

- [50] Q. Zhao, W. Chen, Y. Chen, L. Zhang, J. Zhang, and Z. Zhang, "Self-assembled virus-like particles from rotavirus structural protein VP6 for targeted drug delivery," *Bioconjug. Chem.*, vol. 22, no. 3, pp. 346–352, 2011, doi: 10.1021/bc1002532.
- [51] Q. Zeng *et al.*, "Cucumber mosaic virus as drug delivery vehicle for doxorubicin," *Biomaterials*, vol. 34, no. 19, pp. 4632–4642, 2013, doi: 10.1016/j.biomaterials.2013.03.017.
- [52] A. Naskalska and K. Pyrc, "Virus like particles as immunogens and universal nanocarriers."
- [53] P. M. Sharp and B. H. Hahn, "Origins of HIV and the AIDS pandemic," *Cold Spring Harb. Perspect. Med.*, vol. 1, no. 1, pp. 1–22, 2011, doi: 10.1101/cshperspect.a006841.
- [54] J. A. G. Briggs, T. Wilk, R. Welker, H. G. Kräusslich, and S. D. Fuller, "Structural organization of authentic, mature HIV-1 virions and cores," *EMBO J.*, vol. 22, no. 7, pp. 1707–1715, 2003, doi: 10.1093/emboj/cdg143.
- [55] K. R. Young, S. P. McBurney, L. U. Karkhanis, and T. M. Ross, "Virus-like particles: Designing an effective AIDS vaccine," *Methods*, vol. 40, no. 1, pp. 98–117, 2006, doi: 10.1016/j.ymeth.2006.05.024.
- [56] M. Delchambre *et al.*, "The GAG precursor of simian immunodeficiency virus assembles into virus-like particles," *EMBO J.*, vol. 8, no. 9, pp. 2653–2660, 1989, doi: 10.1002/j.1460-2075.1989.tb08405.x.
- [57] K. Mergener, M. Fäcke, R. Welker, V. Brinkmann, H. R. Gelderblom, and H. G. Krüsslich, "Analysis of HIV particle formation using transient expression of subviral constructs in mammalian cells," *Virology*, vol. 186, no. 1, pp. 25–39, 1992, doi: 10.1016/0042-6822(92)90058-W.
- [58] B. Meng and A. M. L. Lever, "Wrapping up the bad news - HIV assembly and release," *Retrovirology*, vol. 10, no. 1, pp. 1–12, 2013, doi: 10.1186/1742-4690-10-5.
- [59] U. K. Von Schwedler *et al.*, "The protein network of HIV budding," *Cell*, vol. 114, no. 6, pp. 701–713, 2003, doi: 10.1016/S0092-8674(03)00714-1.
- [60] J. Lavado-García, I. Jorge, A. Boix-Besora, J. Vázquez, F. Gòdia, and L. Cervera, "Characterization of HIV-1 virus-like particles and determination of Gag stoichiometry for different production platforms," *Biotechnol. Bioeng.*, vol. 118, no. 7, pp. 2660–2675, 2021, doi: 10.1002/bit.27786.
- [61] N. M. Sherer *et al.*, "Visualization of retroviral replication in living cells reveals budding into multivesicular bodies," *Traffic*, vol. 4, no. 11, pp. 785–801, 2003, doi: 10.1034/j.1600-0854.2003.00135.x.
- [62] B. Müller, J. Daেকে, O. T. Fackler, M. T. Dittmar, H. Zentgraf, and H.-G. Kräusslich, "Construction and Characterization of a Fluorescently Labeled Infectious Human Immunodeficiency Virus Type 1 Derivative," *J. Virol.*, vol. 78, no. 19, pp. 10803–10813, 2004, doi: 10.1128/jvi.78.19.10803-10813.2004.
- [63] M. Lampe *et al.*, "Double-labelled HIV-1 particles for study of virus-cell interaction," *Virology*, vol. 360, no. 1, pp. 92–104, 2007, doi: 10.1016/j.virol.2006.10.005.
- [64] L. Hermida-Matsumoto and M. D. Resh, "Localization of Human Immunodeficiency Virus Type 1 Gag and Env at the Plasma Membrane by Confocal Imaging," *J. Virol.*, vol. 74, no. 18, pp. 8670–8679, 2000, doi: 10.1128/jvi.74.18.8670-8679.2000.
- [65] L. Cervera, S. Gutiérrez-Granados, M. Martínez, J. Blanco, F. Gòdia, and M. M. Segura, "Generation of HIV-1 Gag VLPs by transient transfection of HEK 293 suspension cell cultures using an optimized animal-derived component free medium," *J. Biotechnol.*, vol. 166, no. 4, pp. 152–165, Jul. 2013, doi: 10.1016/j.jbiotec.2013.05.001.
- [66] I. González-Domínguez, E. Lorenzo, A. Bernier, L. Cervera, F. Gòdia, and A. Kamen, "A four-step purification process for gag vlps: From culture supernatant to high-purity lyophilized particles,"



- Vaccines*, vol. 9, no. 10, pp. 1–19, 2021, doi: 10.3390/vaccines9101154.
- [67] J. Hermle, M. Anders, A. M. Heuser, and B. Müller, “A simple fluorescence based assay for quantification of human immunodeficiency virus particle release,” *BMC Biotechnol.*, vol. 10, 2010, doi: 10.1186/1472-6750-10-32.
  - [68] I. González-Domínguez, E. Puente-Massaguer, L. Cervera, and F. Gòdia, “Quality assessment of virus-like particles at single particle level: A comparative study,” *Viruses*, vol. 12, no. 2, pp. 1–24, 2020, doi: 10.3390/v12020223.
  - [69] S. Gutiérrez-Granados, L. Cervera, F. Gòdia, J. Carrillo, and M. M. Segura, “Development and validation of a quantitation assay for fluorescently tagged HIV-1 virus-like particles,” *J. Virol. Methods*, vol. 193, no. 1, pp. 85–95, 2013, doi: 10.1016/j.jviromet.2013.05.010.
  - [70] L. Cervera *et al.*, “Production of HIV-1-based virus-like particles for vaccination: achievements and limits,” *Appl. Microbiol. Biotechnol.*, vol. 103, no. 18, pp. 7367–7384, 2019, doi: 10.1007/s00253-019-10038-3.
  - [71] L. X. Doan, M. Li, C. Chen, and Q. Yao, “Virus-like particles as HIV-1 vaccines,” *Rev. Med. Virol.*, vol. 15, no. 2, pp. 75–88, 2005, doi: 10.1002/rmv.449.
  - [72] F. Tarrés-Freixas *et al.*, “An engineered HIV-1 Gag-based VLP displaying high antigen density induces strong antibody-dependent functional immune responses,” *npj Vaccines*, vol. 8, no. 1, 2023, doi: 10.1038/s41541-023-00648-4.
  - [73] R. Ortiz *et al.*, “Exploring FeLV-Gag-Based VLPs as a New Vaccine Platform—Analysis of Production and Immunogenicity,” *Int. J. Mol. Sci.*, vol. 24, no. 10, 2023, doi: 10.3390/ijms24109025.
  - [74] A. Venereo-Sanchez *et al.*, “Hemagglutinin and neuraminidase containing virus-like particles produced in HEK-293 suspension culture: An effective influenza vaccine candidate,” *Vaccine*, vol. 34, no. 29, pp. 3371–3380, Jun. 2016, doi: 10.1016/j.vaccine.2016.04.089.
  - [75] A. J. Chua *et al.*, “A novel platform for virus-like particle-display of flaviviral envelope domain III: Induction of Dengue and West Nile virus neutralizing antibodies,” *Virol. J.*, vol. 10, pp. 1–18, 2013, doi: 10.1186/1743-422X-10-129.
  - [76] L. Garnier *et al.*, “Incorporation of pseudorabies virus gD into human immunodeficiency virus type 1 Gag particles produced in baculovirus-infected cells,” *J. Virol.*, vol. 69, no. 7, pp. 4060–4068, 1995, doi: 10.1128/jvi.69.7.4060-4068.1995.
  - [77] A. Boix-Besora, E. Lorenzo, J. Lavado-García, F. Gòdia, and L. Cervera, “Optimization, Production, Purification and Characterization of HIV-1 GAG-Based Virus-like Particles Functionalized with SARS-CoV-2,” *Vaccines*, vol. 10, no. 2, pp. 1–18, 2022, doi: 10.3390/vaccines10020250.
  - [78] A. B. Gashti *et al.*, “Production, purification and immunogenicity of Gag virus-like particles carrying SARS-CoV-2 components,” *Vaccine*, vol. 42, no. 1, pp. 40–52, 2024, doi: 10.1016/j.vaccine.2023.11.048.
  - [79] I. Voráčková, P. Ulbrich, W. E. Diehl, and T. Ruml, “Engineered retroviral virus-like particles for receptor targeting,” *Arch. Virol.*, vol. 159, no. 4, pp. 677–688, 2014, doi: 10.1007/s00705-013-1873-6.
  - [80] S. J. Kaczmarczyk, K. Sitaraman, H. A. Young, S. H. Hughes, and D. K. Chatterjee, “Protein delivery using engineered virus-like particles,” 2011, doi: 10.1073/pnas.1101874108/-/DCSupplemental.www.pnas.org/cgi/doi/10.1073/pnas.1101874108.
  - [81] X. Wu *et al.*, “Targeting foreign proteins to human immunodeficiency virus particles via fusion with Vpr and Vpx,” *J. Virol.*, vol. 69, no. 6, pp. 3389–3398, 1995, doi: 10.1128/jvi.69.6.3389-3398.1995.
  - [82] P. Di Bonito *et al.*, “Anti-tumor CD8+ T cell immunity elicited by HIV-1-based virus-like particles incorporating HPV-16 E7 protein,” *Virology*, vol. 395, no. 1, pp. 45–55, 2009, doi:

- 10.1016/j.virol.2009.09.012.
- [83] H. K. Ong, W. S. Tan, and K. L. Ho, "Virus like particles as a platform for cancer vaccine development," *PeerJ*, vol. 2017, no. 11, pp. 1–31, 2017, doi: 10.7717/peerj.4053.
  - [84] S. Zhang, L. K. Yong, D. Li, R. Cubas, C. Chen, and Q. Yao, "Mesothelin Virus-Like Particle Immunization Controls Pancreatic Cancer Growth through CD8+ T Cell Induction and Reduction in the Frequency of CD4+foxp3+ICOS- Regulatory T Cells," *PLoS One*, vol. 8, no. 7, 2013, doi: 10.1371/journal.pone.0068303.
  - [85] N. Kushnir, S. J. Streatfield, and V. Yusibov, "Virus-like particles as a highly efficient vaccine platform: Diversity of targets and production systems and advances in clinical development," *Vaccine*, vol. 31, pp. 58–83, 2012, doi: <http://dx.doi.org/10.1016/j.vaccine.2012.10.083>.
  - [86] J. Zhu, "Mammalian cell protein expression for biopharmaceutical production," *Biotechnol. Adv.*, vol. 30, no. 5, pp. 1158–1170, 2012, doi: 10.1016/j.biotechadv.2011.08.022.
  - [87] J. Lavado-García, T. Zhang, L. Cervera, F. Gòdia, and M. Wuhler, "Differential N- and O-glycosylation signatures of HIV-1 Gag virus-like particles and coproduced extracellular vesicles," *Biotechnol. Bioeng.*, vol. 119, no. 5, pp. 1207–1221, 2022, doi: 10.1002/bit.28051.
  - [88] L. J. Ausubel *et al.*, "Production of CGMP-Grade Lentiviral Vectors," *Bioprocess Int*, vol. 10, no. 2, pp. 32–43, 2012, [Online]. Available: doi:10.1080/15332985.2011.628602.
  - [89] J. Lavado-García, I. González-Domínguez, L. Cervera, I. Jorge, J. Vázquez, and F. Gòdia, "Molecular Characterization of the Coproduced Extracellular Vesicles in HEK293 during Virus-Like Particle Production," *J. Proteome Res.*, vol. 19, no. 11, pp. 4516–4532, 2020, doi: 10.1021/acs.jproteome.0c00581.
  - [90] D. Fontana, R. Kratje, M. Etcheverrigaray, and C. Prieto, "Immunogenic virus-like particles continuously expressed in mammalian cells as a veterinary rabies vaccine candidate," *Vaccine*, vol. 33, no. 35, pp. 4238–4246, 2015, doi: 10.1016/j.vaccine.2015.03.088.
  - [91] A. Venereo-Sánchez *et al.*, "Characterization of influenza H1N1 Gag virus-like particles and extracellular vesicles co-produced in HEK-293SF," *Vaccine*, vol. 37, no. 47, 2019, doi: 10.1016/j.vaccine.2019.07.057.
  - [92] S. Dietmair, M. P. Hodson, L. E. Quek, N. E. Timmins, P. Gray, and L. K. Nielsen, "A multi-omics analysis of recombinant protein production in Hek293 cells," *PLoS One*, vol. 7, no. 8, 2012, doi: 10.1371/journal.pone.0043394.
  - [93] K. Büsow, "Stable mammalian producer cell lines for structural biology," *Curr. Opin. Struct. Biol.*, vol. 32, no. Table 1, pp. 81–90, 2015, doi: 10.1016/j.sbi.2015.03.002.
  - [94] D. L. Hacker and S. Balasubramanian, "Recombinant protein production from stable mammalian cell lines and pools," *Curr. Opin. Struct. Biol.*, vol. 38, no. Figure 1, pp. 129–136, 2016, doi: 10.1016/j.sbi.2016.06.005.
  - [95] S. Gutiérrez-Granados, L. Cervera, A. A. Kamen, and F. Gòdia, "Advancements in mammalian cell transient gene expression (TGE) technology for accelerated production of biologics," *Critical Reviews in Biotechnology*, vol. 38, no. 6. Taylor and Francis Ltd, pp. 918–940, Aug. 18, 2018, doi: 10.1080/07388551.2017.1419459.
  - [96] N. Bono, F. Ponti, D. Mantovani, and G. Candiani, "Non-viral in vitro gene delivery: It is now time to set the bar!," *Pharmaceutics*, vol. 12, no. 2, 2020, doi: 10.3390/pharmaceutics12020183.
  - [97] B. Shi *et al.*, "Challenges in DNA Delivery and Recent Advances in Multifunctional Polymeric DNA Delivery Systems," *Biomacromolecules*, vol. 18, no. 8, pp. 2231–2246, 2017, doi: 10.1021/acs.biomac.7b00803.
  - [98] O. BOUSSIF *et al.*, "A versatile vector for gene and oligonucleotide transfer into cells in culture and

- in vivo: Polyethylenimine,” *Biochemistry*, vol. 92, no. August, pp. 7297–7301, 1995, doi: 10.4043/2822-ms.
- [99] Y. Yue and C. Wu, “Progress and perspectives in developing polymeric vectors for in vitro gene delivery,” *Biomater. Sci.*, vol. 1, no. 2, pp. 152–170, 2013, doi: 10.1039/c2bm00030j.
- [100] K. Xiu, J. Zhang, J. Xu, Y. E. Chen, and P. X. Ma, “Recent progress in polymeric gene vectors: Delivery mechanisms, molecular designs, and applications,” *Biophys. Rev.*, vol. 4, no. 1, pp. 1–11, 2023, doi: 10.1063/5.0123664.
- [101] L. Cervera, I. Gonz Alez-Dom Inguez, M. Ia, M. Segura, and F. G. Odia, “Intracellular Characterization of Gag VLP Production by Transient Transfection of HEK 293 Cells,” doi: 10.1002/bit.26367/abstract.
- [102] M. Butler, “Animal cell cultures: Recent achievements and perspectives in the production of biopharmaceuticals,” *Appl. Microbiol. Biotechnol.*, vol. 68, no. 3, pp. 283–291, 2005, doi: 10.1007/s00253-005-1980-8.
- [103] M. D. Hein, A. Chawla, M. Cattaneo, S. Y. Kupke, Y. Genzel, and U. Reichl, “Cell culture–based production of defective interfering influenza A virus particles in perfusion mode using an alternating tangential flow filtration system,” *Appl. Microbiol. Biotechnol.*, vol. 105, no. 19, pp. 7251–7264, 2021, doi: 10.1007/s00253-021-11561-y.
- [104] L. Cervera, S. Gutiérrez-Granados, N. S. Berrow, M. M. Segura, and F. Gòdia, “Extended gene expression by medium exchange and repeated transient transfection for recombinant protein production enhancement,” *Biotechnol. Bioeng.*, vol. 112, no. 5, pp. 934–946, 2015, doi: 10.1002/bit.25503.
- [105] E. Carpentier, S. Paris, A. A. Kamen, and Y. Durocher, “Limiting factors governing protein expression following polyethylenimine-mediated gene transfer in HEK293-EBNA1 cells,” *J. Biotechnol.*, vol. 128, no. 2, pp. 268–280, 2007, doi: 10.1016/j.jbiotec.2006.10.014.
- [106] J. Lavado-García, P. Pérez-Rubio, L. Cervera, and F. Gòdia, “The cell density effect in animal cell-based bioprocessing: Questions, insights and perspectives,” *Biotechnol. Adv.*, vol. 60, no. May, 2022, doi: 10.1016/j.biotechadv.2022.108017.
- [107] J. Fuenmayor, L. Cervera, F. Gòdia, and A. Kamen, “Extended gene expression for Gag VLP production achieved at bioreactor scale,” *J. Chem. Technol. Biotechnol.*, vol. 94, no. 1, pp. 302–308, Jan. 2019, doi: 10.1002/jctb.5777.
- [108] J. Lavado-García, L. Cervera, and F. Gòdia, “An Alternative Perfusion Approach for the Intensification of Virus-Like Particle Production in HEK293 Cultures,” *Front. Bioeng. Biotechnol.*, vol. 8, no. June, pp. 1–16, 2020, doi: 10.3389/fbioe.2020.00617.
- [109] S. Gutiérrez-Granados, F. Gòdia, and L. Cervera, “Continuous manufacturing of viral particles,” *Curr. Opin. Chem. Eng.*, vol. 22, pp. 107–114, 2018, doi: 10.1016/j.coche.2018.09.009.
- [110] M. G. Moleirinho, R. J. S. Silva, P. M. Alves, M. J. T. Carrondo, and C. Peixoto, “Current challenges in biotherapeutic particles manufacturing,” *Expert Opin. Biol. Ther.*, vol. 00, no. 00, pp. 1–15, 2019, doi: 10.1080/14712598.2020.1693541.
- [111] P. Steppert *et al.*, “Separation of HIV-1 gag virus-like particles from vesicular particles impurities by hydroxyl-functionalized monoliths,” *J. Sep. Sci.*, vol. 40, no. 4, pp. 979–990, 2017, doi: 10.1002/jssc.201600765.
- [112] P. Steppert *et al.*, “Purification of HIV-1 gag virus-like particles and separation of other extracellular particles,” *J. Chromatogr. A*, vol. 1455, pp. 93–101, Jul. 2016, doi: 10.1016/j.chroma.2016.05.053.
- [113] L. C. Eaton, “Host cell contaminant protein assay development for recombinant biopharmaceuticals,” *J. Chromatogr. A*, vol. 705, no. 1, pp. 105–114, 1995, doi: 10.1016/0021-

9673(94)01249-E.

- [114] I. Knezevic, G. Stacey, and J. Petricciani, "WHO Study Group on cell substrates for production of biologicals, Geneva, Switzerland, 11-12 June 2007," *Biologicals*, vol. 36, no. 3, pp. 203–211, 2008, doi: 10.1016/j.biologicals.2007.11.005.
- [115] T. P. Pato *et al.*, "Development of a membrane adsorber based capture step for the purification of yellow fever virus," *Vaccine*, vol. 32, no. 24, pp. 2789–2793, 2014, doi: 10.1016/j.vaccine.2014.02.036.
- [116] D. Sviben, D. Forcic, J. Ivancic-Jelecki, B. Halassy, and M. Brgles, "Recovery of infective virus particles in ion-exchange and hydrophobic interaction monolith chromatography is influenced by particle charge and total-to-infective particle ratio," *J. Chromatogr. B Anal. Technol. Biomed. Life Sci.*, vol. 1054, no. January, pp. 10–19, 2017, doi: 10.1016/j.jchromb.2017.04.015.
- [117] K. Reiter, P. P. Aguilar, V. Wetter, P. Steppert, A. Tover, and A. Jungbauer, "Separation of virus-like particles and extracellular vesicles by flow-through and heparin affinity chromatography," *J. Chromatogr. A*, vol. 1588, pp. 77–84, Mar. 2019, doi: 10.1016/j.chroma.2018.12.035.
- [118] C. L. Effio and J. Hubbuch, "Next generation vaccines and vectors: Designing downstream processes for recombinant protein-based virus-like particles," *Biotechnology Journal*, vol. 10, no. 5. Wiley-VCH Verlag, pp. 715–727, May 01, 2015, doi: 10.1002/biot.201400392.
- [119] T. M. Lima, M. O. Souza, and L. R. Castilho, "Purification of flavivirus VLPs by a two-step chromatographic process," *Vaccine*, vol. 37, no. 47, pp. 7061–7069, 2019, doi: 10.1016/j.vaccine.2019.05.066.
- [120] S. B. Carvalho *et al.*, "Membrane-Based Approach for the Downstream Processing of Influenza Virus-Like Particles," *Biotechnol. J.*, vol. 14, no. 8, Aug. 2019, doi: 10.1002/biot.201800570.
- [121] A. S. Moreira, D. G. Cavaco, T. Q. Faria, P. M. Alves, M. J. T. Carrondo, and C. Peixoto, "Advances in Lentivirus Purification," *Biotechnol. J.*, vol. 16, no. 1, 2021, doi: 10.1002/biot.202000019.
- [122] R. Morenweiser, "Downstream processing of viral vectors and vaccines," *Gene Ther.*, vol. 12, pp. S103–S110, 2005, doi: 10.1038/sj.gt.3302624.
- [123] V. Bandeira *et al.*, "Downstream processing of lentiviral vectors: Releasing bottlenecks," *Hum. Gene Ther. Methods*, vol. 23, no. 4, pp. 255–263, Aug. 2012, doi: 10.1089/hgtb.2012.059.
- [124] M. G. Moleirinho *et al.*, "Clinical-Grade Oncolytic Adenovirus Purification Using Polysorbate 20 as an Alternative for Cell Lysis," *Curr. Gene Ther.*, vol. 18, no. 6, pp. 366–374, 2018, doi: 10.2174/1566523218666181109141257.
- [125] T. Weigel, T. Solomaier, A. Peuker, T. Pathapati, M. W. Wolff, and U. Reichl, "A flow-through chromatography process for influenza A and B virus purification," *J. Virol. Methods*, vol. 207, pp. 45–53, 2014, doi: 10.1016/j.jviromet.2014.06.019.
- [126] L. Besnard *et al.*, "Clarification of vaccines: An overview of filter based technology trends and best practices," *Biotechnol. Adv.*, vol. 34, no. 1, pp. 1–13, Jan. 2016, doi: 10.1016/j.biotechadv.2015.11.005.
- [127] P. Kramberger, L. Urbas, and A. Štrancar, "Downstream processing and chromatography based analytical methods for production of vaccines, gene therapy vectors, and bacteriophages," *Hum. Vaccines Immunother.*, vol. 11, no. 4, pp. 1010–1021, 2015, doi: 10.1080/21645515.2015.1009817.
- [128] A. Venereo-Sanchez *et al.*, "Process intensification for high yield production of influenza H1N1 Gag virus-like particles using an inducible HEK-293 stable cell line," *Vaccine*, vol. 35, no. 33, pp. 4220–4228, Jul. 2017, doi: 10.1016/j.vaccine.2017.06.024.
- [129] S. Y. Lin, H. Y. Chiu, B. L. Chiang, and Y. C. Hu, "Development of EV71 virus-like particle purification processes," *Vaccine*, vol. 33, no. 44, pp. 5966–5973, 2015, doi: 10.1016/j.vaccine.2015.04.077.

- [130] M. Zaveckas, K. Goda, D. Ziogiene, and A. Gedvilaite, "Purification of recombinant trichodysplasia spinulosa-associated polyomavirus VP1-derived virus-like particles using chromatographic techniques," *J. Chromatogr. B Anal. Technol. Biomed. Life Sci.*, vol. 1090, no. May, pp. 7–13, 2018, doi: 10.1016/j.jchromb.2018.05.007.
- [131] J. S. Fritz, "Ion Chromatography," vol. 59, no. 4, 1987.
- [132] P. Pereira Aguilar *et al.*, "Capture and purification of Human Immunodeficiency Virus-1 virus-like particles: Convective media vs porous beads," *J. Chromatogr. A*, vol. 1627, pp. 1–11, 2020, doi: 10.1016/j.chroma.2020.461378.
- [133] D. J. McNally, D. Darling, F. Farzaneh, P. R. Levison, and N. K. H. Slater, "Optimised concentration and purification of retroviruses using membrane chromatography," *J. Chromatogr. A*, vol. 1340, pp. 24–32, 2014, doi: 10.1016/j.chroma.2014.03.023.
- [134] A. J. Valkama *et al.*, "Development of Large-Scale Downstream Processing for Lentiviral Vectors," *Mol. Ther. Methods Clin. Dev.*, vol. 17, no. June, pp. 717–730, 2020, doi: 10.1016/j.omtm.2020.03.025.
- [135] É. Szabó, L. Z. Baranyai, Z. Sütő, A. Salgó, and S. Gergely, "Attenuated total reflection fourier transform infrared spectroscopy based methods for identification of chromatography media formulations used in downstream processes," *J. Pharm. Biomed. Anal.*, vol. 180, 2020, doi: 10.1016/j.jpba.2019.113060.
- [136] T. Weigel, R. Soliman, M. W. Wolff, and U. Reichl, "Hydrophobic-interaction chromatography for purification of influenza A and B virus," *J. Chromatogr. B Anal. Technol. Biomed. Life Sci.*, vol. 1117, pp. 103–117, 2019, doi: 10.1016/j.jchromb.2019.03.037.
- [137] R. M. Kennedy, "Hydrophobic-Interaction Chromatography," *Curr. Protoc. Protein Sci.*, vol. 00, no. 1, pp. 1–21, 1995, doi: 10.1002/0471140864.ps0804s00.
- [138] P. Gagnon, E. Grund, and T. Lindbäck, "Large Scale Process Development for Hydrophobic Interaction Chromatography, Part 1: Gel Selection and Development of Binding Conditions," no. 541, pp. 1–9, 1995.
- [139] Y. Lu, B. Williamson, and R. Gillespie, "Recent Advancement in Application of Hydrophobic Interaction Chromatography for Aggregate Removal in Industrial Purification Process," *Curr. Pharm. Biotechnol.*, vol. 10, no. 4, pp. 427–433, 2009, doi: 10.2174/138920109788488897.
- [140] J. T. McCue, *Chapter 25 Theory and Use of Hydrophobic Interaction Chromatography in Protein Purification Applications*, 1st ed., vol. 463, no. C. Elsevier Inc., 2009.
- [141] L. Opitz, S. Lehmann, U. Reichl, and M. W. Wolff, "Sulfated membrane adsorbers for economic pseudo-affinity capture of influenza virus particles," *Biotechnol. Bioeng.*, vol. 103, no. 6, pp. 1144–1154, 2009, doi: 10.1002/bit.22345.
- [142] G. Carta and A. Jungbauer, *Protein Chromatography*. 2010.
- [143] M. Zhao, M. Vandersluis, J. Stout, U. Haupts, M. Sanders, and R. Jacquemart, "Affinity chromatography for vaccines manufacturing: Finally ready for prime time?," *Vaccine*, vol. 37, no. 36, pp. 5491–5503, 2019, doi: 10.1016/j.vaccine.2018.02.090.
- [144] M. M. Segura, A. Garnier, Y. Durocher, H. Coelho, and A. Kamen, "Production of lentiviral vectors by large-scale transient transfection of suspension cultures and affinity chromatography purification," *Biotechnol. Bioeng.*, vol. 98, no. 4, pp. 789–799, 2007, doi: 10.1002/bit.21467.
- [145] M. M. Segura, M. Mangion, B. Gaillet, and A. Garnier, "New developments in lentiviral vector design, production and purification," *Expert Opin. Biol. Ther.*, vol. 13, no. 7, pp. 987–1011, 2013, doi: 10.1517/14712598.2013.779249.
- [146] P. Nestola, C. Peixoto, R. R. J. S. Silva, P. M. Alves, J. P. B. Mota, and M. J. T. Carrondo, "Improved

- virus purification processes for vaccines and gene therapy," *Biotechnol. Bioeng.*, vol. 112, no. 5, pp. 843–857, 2015, doi: 10.1002/bit.25545.
- [147] M. C. Nweke, R. G. McCartney, and D. G. Bracewell, "Mechanical characterisation of agarose-based chromatography resins for biopharmaceutical manufacture," *J. Chromatogr. A*, vol. 1530, pp. 129–137, 2017, doi: 10.1016/j.chroma.2017.11.038.
  - [148] M. W. Wolf and U. Reichl, "Downstream processing of cell culture-derived virus particles," *Expert Rev. Vaccines*, vol. 10, no. 10, pp. 1451–1475, 2011, doi: 10.1586/erv.11.111.
  - [149] B. Donaldson, Z. Lateef, G. F. Walker, S. L. Young, and V. K. Ward, "Virus-like particle vaccines: immunology and formulation for clinical translation," *Expert Rev. Vaccines*, vol. 17, no. 9, pp. 833–849, 2018, doi: 10.1080/14760584.2018.1516552.
  - [150] O. S. Kumru, S. B. Joshi, D. E. Smith, C. R. Middaugh, T. Prusik, and D. B. Volkin, "Vaccine instability in the cold chain: Mechanisms, analysis and formulation strategies," *Biologicals*, vol. 42, no. 5, pp. 237–259, 2014, doi: 10.1016/j.biologicals.2014.05.007.
  - [151] L. J. J. Hansen, R. Daoussi, C. Vervaet, J. P. Remon, and T. R. M. De Beer, "Freeze-drying of live virus vaccines: A review," *Vaccine*, vol. 33, no. 42, pp. 5507–5519, 2015, doi: 10.1016/j.vaccine.2015.08.085.
  - [152] WHO, "United Nations Environment Programme," *Why optimized cold-chains could save a billion COVID vaccines*, 2020. <https://www.unep.org/news-and-stories/story/why-optimized-cold-chains-could-save-billion-covid-vaccines>.
  - [153] N. K. Jain, N. Sahni, O. S. Kumru, S. B. Joshi, D. B. Volkin, and C. Russell Middaugh, "Formulation and stabilization of recombinant protein based virus-like particle vaccines," *Advanced Drug Delivery Reviews*, vol. 93, Elsevier, pp. 42–55, Oct. 01, 2015, doi: 10.1016/j.addr.2014.10.023.
  - [154] G. Kanojia, R. ten Have, P. C. Soema, H. Frijlink, J. P. Amorij, and G. Kersten, "Developments in the formulation and delivery of spray dried vaccines," *Hum. Vaccines Immunother.*, vol. 13, no. 10, pp. 2364–2378, 2017, doi: 10.1080/21645515.2017.1356952.
  - [155] G. Adams, "The principles of freeze-drying," *Methods Mol. Biol.*, vol. 368, no. 2, pp. 15–38, 2007, doi: 10.1007/978-1-59745-362-2\_2.
  - [156] W. J. Kessler, P. Sharma, and M. Mujat, "Lyophilized Biologics and Vaccines," *Lyophilized Biol. Vaccines*, 2015, doi: 10.1007/978-1-4939-2383-0.
  - [157] Y. Liu *et al.*, "Screening and Stability Evaluation of Freeze-Dried Protective Agents for a Live Recombinant Pseudorabies Virus Vaccine," vol. 12(1), p. 65, 2024, doi: 10.3390/vaccines12010065.
  - [158] M. Bjelošević, A. Zvonar Pobirk, O. Planinšek, and P. Ahlin Grabnar, "Excipients in freeze-dried biopharmaceuticals: Contributions toward formulation stability and lyophilisation cycle optimisation," *Int. J. Pharm.*, vol. 576, p. 119029, 2020, doi: 10.1016/j.ijpharm.2020.119029.
  - [159] S. Pramanick, D. Singodia, and V. Chandel, "Excipient selection in parenteral formulation development," *Pharma Times*, vol. 45, no. 3, pp. 65–77, 2013, doi: 10.1080/03639045.2018.1483392.
  - [160] E. Trenkenschuh and W. Friess, "Freeze-drying of nanoparticles: How to overcome colloidal instability by formulation and process optimization," *Eur. J. Pharm. Biopharm.*, vol. 165, no. May, pp. 345–360, 2021, doi: 10.1016/j.ejpb.2021.05.024.
  - [161] R. L. Remmele, S. Krishnan, and W. J. Callahan, "Development of Stable Lyophilized Protein Drug Products," *Curr. Pharm. Biotechnol.*, vol. 13, no. 3, pp. 471–496, 2012, doi: 10.2174/138920112799361990.
  - [162] S. Saboo *et al.*, "Optimized Formulation of a Thermostable Spray-Dried Virus-Like Particle Vaccine against Human Papillomavirus," *Mol. Pharm.*, vol. 13, no. 5, pp. 1646–1655, 2016, doi:

- 10.1021/acs.molpharmaceut.6b00072.
- [163] D. I. Setyo Utomo, H. Suhaimi, N. A. Muhammad Azami, F. Azmi, M. C. I. Mohd Amin, and J. Xu, "An Overview of Recent Developments in the Application of Antigen Displaying Vaccine Platforms: Hints for Future SARS-CoV-2 VLP Vaccines," *Vaccines*, vol. 11, no. 9, pp. 1–14, 2023, doi: 10.3390/vaccines11091506.
  - [164] M. O. Mohsen, A. C. Gomes, M. Vogel, and M. F. Bachmann, "Interaction of viral capsid-derived virus-like particles (VLPs) with the innate immune system," *Vaccines*, vol. 6, no. 3, pp. 1–12, 2018, doi: 10.3390/vaccines6030037.
  - [165] A. Boix-Besora, F. Gòdia, and L. Cervera, "Gag Virus-like Particles Functionalized with SARS-CoV-2 Variants: Generation, Characterization and Recognition by COVID-19 Convalescent Patients' Sera," *Vaccines*, vol. 11, no. 11, 2023, doi: 10.3390/vaccines11111641.
  - [166] D. Fontana, E. Garay, L. Cervera, R. Kratje, C. Prieto, and F. Gòdia, "Chimeric vlps based on hiv-1 gag and a fusion rabies glycoprotein induce specific antibodies against rabies and foot-and-mouth disease virus," *Vaccines*, vol. 9, no. 3, 2021, doi: 10.3390/vaccines9030251.
  - [167] R. Chapman *et al.*, "Immunogenicity of HIV-1 vaccines expressing chimeric envelope glycoproteins on the surface of Pr55 gag virus-like particles," *Vaccines*, vol. 8, no. 1, pp. 1–17, 2020, doi: 10.3390/vaccines8010054.
  - [168] T. K. Kim and J. H. Eberwine, "Mammalian cell transfection: The present and the future," *Anal. Bioanal. Chem.*, vol. 397, no. 8, pp. 3173–3178, 2010, doi: 10.1007/s00216-010-3821-6.
  - [169] J. L. Mejía-Méndez, R. Vazquez-Duhalt, L. R. Hernández, E. Sánchez-Arreola, and H. Bach, "Virus-like Particles: Fundamentals and Biomedical Applications," *Int. J. Mol. Sci.*, vol. 23, no. 15, 2022, doi: 10.3390/ijms23158579.
  - [170] M. T. Smith, A. K. Hawes, and B. C. Bundy, "Reengineering viruses and virus-like particles through chemical functionalization strategies," *Curr. Opin. Biotechnol.*, vol. 24, no. 4, pp. 620–626, 2013, doi: 10.1016/j.copbio.2013.01.011.
  - [171] D. T. Le and K. M. Müller, "In vitro assembly of virus-like particles and their applications," *Life*, vol. 11, no. 4, 2021, doi: 10.3390/life11040334.
  - [172] D. D. Hein, Christopher. Liu, Xin-Ming. Wang, "Click Chemistry, a Powerful Tool for Pharmaceutical Sciences," *Natl. Inst. Heal. J.*, vol. 25, no. 10, pp. 1–7, 2008, doi: 10.1007/s11095-008-9616-1.Click.
  - [173] "Recent trends in click chemistry as a promising technology for virus-related research," no. January, 2020.
  - [174] T. Ramqvist, K. Andreasson, and T. Dalianis, "Vaccination, immune and gene therapy based on virus-like particles against viral infections and cancer," *Expert Opin. Biol. Ther.*, vol. 7, no. 7, pp. 997–1007, 2007, doi: 10.1517/14712598.7.7.997.
  - [175] J. C. Jewett, E. M. Sletten, and C. R. Bertozzi, "Rapid Cu-free click chemistry with readily synthesized biarylazacyclooctynones," *J. Am. Chem. Soc.*, vol. 132, no. 11, pp. 3688–3690, 2010, doi: 10.1021/ja100014q.
  - [176] H. C., K. and K., and B. Sharpless, "The growing impact of click chemistry on drug discovery," vol. 8, no. 24, pp. 401–422, 2003, doi: 10.1016/s1936-7961(08)00219-4.
  - [177] T. Tian *et al.*, "Surface functionalized exosomes as targeted drug delivery vehicles for cerebral ischemia therapy," *Biomaterials*, vol. 150, pp. 137–149, 2018, doi: 10.1016/j.biomaterials.2017.10.012.
  - [178] H. Zhu *et al.*, "An efficient and safe MUC1-dendritic cell-derived exosome conjugate vaccine elicits potent cellular and humoral immunity and tumor inhibition in vivo," *Acta Biomater.*, vol. 138, pp. 491–504, 2022, doi: 10.1016/j.actbio.2021.10.041.

- [179] X. Wang, D. M. Morgan, G. Wang, and N. M. Mozier, "Residual DNA analysis in biologics development: Review of measurement and quantitation technologies and future directions," *Biotechnol. Bioeng.*, vol. 109, no. 2, pp. 307–317, 2012, doi: 10.1002/bit.23343.
- [180] K. Reiter, M. Suzuki, L. R. Olano, and D. L. Narum, "Host cell protein quantification of an optimized purification method by mass spectrometry," *J. Pharm. Biomed. Anal.*, vol. 174, pp. 650–654, 2019, doi: 10.1016/j.jpba.2019.06.038.
- [181] J. C. Akers, D. Gonda, B. Ryan Kim, B. S. Carter, and C. C. Chen, "Biogenesis of extracellular vesicles (EV): exosomes, microvesicles, retrovirus-like vesicles, and apoptotic bodies," *J. Neurooncol.*, vol. 113, no. 1, pp. 1–11, 2013, doi: 10.1007/s11060-013-1084-8.Biogenesis.



## **OBJECTIVES**

---

## OBJECTIVES

This work aims to address current challenges in the field of VLP-based biomanufacturing and provides strategies to enhance the purification, formulation, and functionalization of HIV-1 Gag::eGFP VLPs for their use as drug delivery systems. In more detail, the following specific objectives are defined:

1. Design a purification process for HIV-1 Gag::eGFP VLPs.
  - a. Evaluate different unit operations for each step of the downstream (DSP) process, including clarification, concentration/intermediate purification, capture chromatography, and polishing.
  - b. Conduct and analyse a complete purification process using the selected optimal equipment, materials and methods for each step.
2. Enhance the stability and shelf life of purified HIV-1 Gag::eGFP VLPs.
  - a. Optimize the lyophilization formulation buffer using a Design of Experiments approach.
  - b. Study of VLPs thermostability in the optimized formulation.
3. Develop a scalable bioprocess for HIV-1 Gag VLPs that combines a continuous perfusion-based upstream system with a robust DSP sequence, followed by a formulation and lyophilization step
4. Explore the potential of HIV-1 Gag::eGFP VLPs as nanocarriers for targeted drug delivery.
  - a. Functionalize the VLPs with the T22 peptide using strain-promoted alkyne-azide cycloaddition copper-free click chemistry approach.
  - b. Validate the targeted recognition and up-take of T22-functionalized Gag::eGFP VLPs into CXCR4 positive cells.

## **RESULTS**

---

# CHAPTER ONE

Downstream process design for Gag HIV-1 based virus-like particles

---

Published in *Biotechnology and Bioengineering*. vol. 120, no. 9, pp. 2672–2684, 2023.

DOI: 10.1002/bit.28419.

## **ABSTRACT**

Virus-like particles-based vaccines have been gaining interest in recent years. The manufacturing of these particles includes their production by cell culture followed by their purification to meet the requirements of its final use. The presence of host cell extracellular vesicles represents a challenge for better virus-like particles purification, because both share similar characteristics which hinders their separation. The present study aims to compare some of the most used downstream processing technologies for capture and purification of virus-like particles, specifically HIV-1 Gag virus-like particles. Four steps of the purification process were studied, including a clarification step by depth filtration and standard filtration, a concentration / intermediate step by tangential flow filtration and multimodal chromatography, a capture step by ion exchange, hydrophobic interaction and heparin affinity chromatography and finally, a polishing step by size exclusion chromatography. In each step, the yields were evaluated by percentage of recovery of the particles of interest, purity, and elimination of main contaminants. Finally, a complete purification train was implemented using the best results obtained in each step. An overall recovery of 38% and a purity of 64% after the polishing step was achieved, with host cell DNA and protein levels complying with regulatory standards. This work has resulted in the development of a purification process for HIV-1 Gag virus-like particles suitable for scale-up.

## **ABBREVIATIONS**

**AC:** Affinity Chromatography, **DLS:** Dynamic Light Scattering, **DSP:** Downstream Processing, **dsDNA:** Double-Stranded DNA, **EVs:** Extracellular Vesicles, **GFP:** Green Fluorescent Protein, **HEK293:** Human Embryonic Kidney 293, **HIV-1:** Human Immunodeficiency Virus Type 1, **IEC:** Ion Exchange Chromatography, **MC:** Multimodal Chromatography, **MHD:** Mean Hydrodynamic Diameter, **MWCO:** Molecular Weight Cut-Off, **NTA:** Nanoparticle Tracking Analysis, **PDI:** Polydispersity Index, **PBS:** Phosphate Buffered Saline, **PEI:** Polyethylenimine, **QA:** Quaternary Amine, **RFU:** Relative Fluorescence Unit, **SDS-PAGE:** Sodium Dodecyl Sulfate Polyacrylamide Gel Electrophoresis, **SEC:** Size-Exclusion Chromatography, **TEM:** Transmission Electron Microscopy, **TFF:** Tangential Flow Filtration, **VLPs:** Virus-Like Particles.

## INTRODUCTION

Vaccines stimulate the immune system allowing the individual itself to develop defense mechanisms against a specific agent. Among the different types, virus-like particles (VLPs)-based vaccines have been gaining interest in recent years as they can trigger both humoral and cellular immune responses [1], [2]. The manufacturing of these particles includes their production by cell culture followed by their purification to meet the requirements of its final use [3], [4]. Downstream processing (DSP) of nanoparticles is still a challenge. Although filtration and centrifugation techniques are scalable to a certain extent and often used in industrial scale for vaccine and gene therapy products manufacturing, they are labour-intensive and requiring expensive equipment (in the case of centrifugation) [5]. Consequently, in the past few years, the focus has been moving to chromatography and membrane-based separation techniques [6]. Despite the efforts made in this field, it is known that even purified VLP preparations are contaminated with some extracellular vesicles (EVs) [7]. They share very similar properties that make difficult to obtain final VLP formulations with high purity levels [8].

Here, we propose the study of a purification process, specifically for enveloped HIV-1 Gag VLPs fused to the Green Fluorescent Protein (GFP). Based on the process reported by González-Domínguez et al (2021) [7], we focused on the evaluation of different unit operations in each step of the DSP strategy, with the aim of improving the results previously obtained. This DSP proposal includes the study of the following steps: clarification, concentration / intermediate purification, capture chromatography and polishing [7], [9], [10]. The best alternatives were determined considering the yield obtained in terms of recovery of Gag VLPs, the purity with respect to the total nanoparticles, including EVs, and the reduction of contaminating proteins and dsDNA. After selecting the best options in the different steps of the proposed DSP, a complete run was performed and characterized in order to demonstrate the output of the overall process.

During the budding process, the Gag VLPs are released from the cells and accumulate in the culture supernatant. This secretion into the extracellular medium simplifies their harvest, avoiding the need for cell lysis procedures. Therefore, the DSP process is considered to start from supernatant with a clarification step, which is necessary to remove cell debris, large particles, and aggregates [4]. Dead-end disposable

depth-filters are used in this step and have shown a high yield of the product of interest with a high impurity removal capacity [7], [11]. Long-term storage at -80°C ensuing clarification is frequently necessary for large-scale processes, thus, a secondary clarification is sometimes required in DSP strategies to remove the precipitates and/or aggregates resulted from thawed material. Following clarification, a concentration or intermediate purification step is commonly included in the DSP train. Ultrafiltration by tangential flow filtration (TFF) and multimodal chromatography (MC) are widely used [10], [12], [13]. Even when there is a bind-elution step afterwards, the concentration step is beneficial for reducing loading times in chromatographic columns while increasing the concentration of loaded material [10]. The advantages of including a MC as intermediate purification step is the elimination of impurities that could interact with the resins/membranes, favouring a good capture of the molecule of interest in the following bind-elution steps [12], [14], [15].

Different chromatographic modes can be applied for capture and purification of these particles. Ion exchange chromatography (IEC) is commonly used to capture and concentrate VLPs. Anion exchange resins like CIMmultus QA Monolith, Mustang Q, and Capto Q ImpRes have been the most used for the purification of these nanoparticles with good yields and purity [10], [13], [16]. Moreover, a combination of different binding mechanisms, for example, hydroxyl-functionalized polymethacrylate monoliths is a type of chromatography that has been used in the purification of HIV-1 Gag VLPs [17]. Affinity chromatography (AC) has recently gained higher importance in biotherapeutics manufacturing field due to unique selectivity capacity [9], [18], [19]. It has been shown that viruses and VLPs can be purified efficiently using heparin affinity chromatography [19], [20]. However, after this capture step, usually, it is necessary to perform a polishing step. Size exclusion chromatography (SEC) and ultrafiltration/diafiltration are the most used alternatives at this stage [3], [10], [21].

## **MATERIALS AND METHODS**

All reagents were acquired from Sigma Aldrich (Saint Louis, MO, USA), unless otherwise mentioned.

### **Cell culture conditions**

HEK293SF-3F6 cells, kindly provided by Dr. Amine Kamen from McGill University (Montreal, QC, Canada), were cultured in HyCell TransFx-HTM (Hyclone, Road Logan, UT, USA) medium supplemented with 2%

GlutaMAX<sup>TM</sup> (Gibco, Thermo Fisher Scientific, Waltham, MA, USA) and 0.1% Pluronic<sup>TM</sup> (Gibco, Life Technologies, Thermo Fisher Scientific). Cells were routinely maintained in disposable polycarbonate Erlenmeyer flasks (Corning, Steuben, NY, USA), and incubated at 37°C, 5% of CO<sub>2</sub>, 85% relative humidity, and 130 rpm. Cell quantification and viability were determined with the automated cell counter NucleoCounter<sup>®</sup> NC-3000<sup>TM</sup> (Chemometec, Allerød, Denmark).

### **VLP production by transient transfection**

HEK293SF-3F6 cells were transfected at  $1.8\text{--}2\cdot 10^6$  cells/mL, and viability greater than 90% as previously described [22]. In essence, the DNA at a final concentration of 1 µg/mL was added into fresh culture medium and vortexed for 10 seconds. The transfection reagent PEIpro<sup>®</sup> (Polyplus-transfection SA, Illkirch-Graffenstaden, France) at a DNA:PEI ratio of 1:2 w/w was then added. The mix was vortexed three times for three seconds and incubated for 15 minutes at room temperature. Lastly, formed complexes were added into the cell culture. Medium was also supplemented with 3.36 mM valproic acid and 5.04 mM caffeine four hours post-transfection (hpt) to increase cell productivity upon transient gene expression [23]. Culture was stopped at 72 hpt to maximize VLP yields. The plasmid used in the transfection, encoded the HIV-1 Gag polyprotein linked in-frame with the eGFP under the same CMV enhancer and CMV promoter, hereafter noted as Gag::eGFP VLPs. More details were described by A. Venereo-Sanchez et al (2016) [24]. To measure the transfection efficiency, the percentage of GFP-positive cells was assessed using a BD FACS Canto II flow cytometer (BD Biosciences, San Jose, CA, USA).

### **Clarification**

Filtration experiments were performed using an automated Spectrum<sup>®</sup> KrosFlo<sup>®</sup> Research 2i TFF System (Repligen, Rancho Dominguez, CA, USA).

Cell culture was sedimented by two hours and bulk clarification of the supernatant (the fraction where the VLPs are found) was directly performed from the shake flask [7]. Each filter was preequilibrated with Phosphate Buffered Saline (PBS) 1X (Hyclone, Road Logan, UT, USA) prior to filtration. For primary clarification, MilliStak<sup>®</sup>+ D0HC µpod <sup>®</sup>+ depth filter (Merck, Kenilworth, NJ, USA), and Supracap<sup>™</sup> 50V100 <sup>™</sup> depth filter capsules (Pall Corporation, New York, NY, USA) were compared. The supernatant after cell



sedimentation (volume =1L) was loaded to each filter tested. MasterFlex® 96410-13 silicon tubes (Cole-Parmer, Vernon Hills, IL, USA) were connected to the filter inlet and outlet; and a pressure sensor (Cole-Parmer, Vernon Hills, IL, USA) connected to the filter inlet. The filtration flux was set to 5 mL·min<sup>-1</sup> for the MilliStak®+ D0HC µpod ®+ depth filter and 4 mL·min<sup>-1</sup> for the Supracap™ 50V100 depth filter capsules. After selection of the primary clarification filter, 500mL clarified bulk was used as secondary clarification feed. For secondary clarification, the used filters were Sartopore® SartoScale 25 PP3 ® (Sartorius AG, Göttingen, Germany) and Supor® EAV - Mini Kleenpak™ 20 ® filter capsules (Pall Corporation, New York, NY, USA). Their filtration flux was set to 5 mL·min<sup>-1</sup> and the same experimental setup was used. After filtration, the filters were emptied with air to recover all the product. The turbidity of the supernatant and clarified material was measured using a portable turbidimeter (Thermo Fisher Scientific, Waltham, MA, USA).

### **Tangential flow filtration**

The ultrafiltration step was performed using a Centramate Cassette with a 300 kDa molecular weight cut-off (MWCO) membrane (Pall Corporation, New York, NY, USA). The omega PES membrane had an effective filtration area of 0.02 m<sup>2</sup>. Before starting, the membrane was sanitized with 1M sodium hydroxide (NaOH), neutralized with ultrapure water, and pre-conditioned with PBS 1X. A factor of concentration of ten times starting with a volume of 2L of clarified cell culture supernatant and a flux of 35 mL·min<sup>-1</sup> were selected. Transmembrane pressure was maintained at 0.6 bar approximately. After filtration, the membrane was sanitized with 0.5M NaOH overnight and neutralized with ultrapure water.

### **Chromatographic system**

Chromatographic runs were performed using an Äkta Pure 25M2 system (Cytiva, GE Healthcare Live Sciences, Uppsala, Sweden) with a S9 sample pump and a F9-C fraction collector, equipped with a 1.4 mL mixer chamber. System control, data acquisition, and analyses were performed using the Unicorn 6.4.1 software (Cytiva, GE Healthcare Live Sciences, Uppsala, Sweden). UV absorbance (280, 260, and 488 nm wavelengths), pressure, pH, and conductivity were continuously monitored.

## Chromatography media and mobile phases

All preparative chromatographic experiments for Multimodal and Ion Exchange were performed using 50mM HEPES, pH 7.2 as mobile phase A and 50mM HEPES, 2M NaCl, pH 7.2 as mobile phase B. In case of Hydrophobic interaction, it was also used 50mM HEPES, pH 7.2 as mobile phase A, but 50mM HEPES, 1.5M  $(\text{NH}_4)_2\text{SO}_4$ , pH 7.2 as mobile phase B. The Capto Heparin was performed with 0.1M Tris, 0.01M Citric Acid, 0.23M NaCl, pH 7.4 as mobile phase A and 0.1M Tris, 0.01M Citric Acid, 2M NaCl, pH 7.4 as mobile phase B. For POROS Heparin was used 50mM Tris-HCL, pH 7.5 as mobile phase A and 50mM Tris-HCL, 2M NaCl, pH 7.5 as mobile phase B. Different concentrations of the modifier (NaCl or  $(\text{NH}_4)_2\text{SO}_4$ ) were obtained by mixing mobile phases A and B using the chromatography system. For SEC experiments a formulation buffer composed by 20mM  $\text{NaH}_2\text{PO}_4$ , 50mM NaCl, 2mM  $\text{MgCl}_2$ , 2% Sucrose, pH 7.5 was used as mobile phase. If not further stated, cleaning in place was performed using 1M NaOH solution in MC, IEC and HIC, 0.1M NaOH in AC and 0.5M in SEC. The chromatography media tested are summarized in **Table 1**. All materials were used for a single cycle.

**Table 1:** Chromatography media used for preparative chromatography

Type of Chromatography		Type of column and name	Manufacturer	Column volume (mL)
Multimodal	Agarose based core beads	HiScreen Capto Core 700	Cytiva., Uppsala, Sweden	4.7
Ion exchange	Poly-methacrylate based monolithic column	CIMmultus Monolith QA	Sartorius AG Göttingen, Germany	1
	Polypropylene based membrane	Mustang QXT Acrodisc	Pall Corporation, NY, USA	0.86
	High flow agarose-based beads	HiScreen Capto Q ImpRes	Cytiva., Uppsala, Sweden	4.7
Hydrophobic interaction	Poly-methacrylate based monolithic column	CIMmultus Monolith OH-	Sartorius AG, Göttingen, Germany	1
Affinity (Heparin)	Agarose based beads	HiTrap Capto Heparin	Cytiva., Uppsala, Sweden	1
	Cross-linked poly(styrene-divinylbenzene)	XK 16/20 POROS Heparin	Thermo Fisher Scientific, Massachusetts, USA	5.6
Size exclusion	Cross-linked dextran-based beads	HiTrap Sephadex G-25	Cytiva., Uppsala, Sweden	5
	Highly cross-linked 4% agarose-based beads	XK 16/40 Sepharose 4 Fast Flow	Cytiva., Uppsala, Sweden	48

### Intermediate purification, capture and polishing of Gag::eGFP VLPs

For the intermediate purification and capture of Gag::eGFP VLPs, clarified supernatant from different produced batches was directly loaded onto the pre-packed columns/membranes HiScreen Capto Core 700, CIMmultus Monolith QA, Mustang QXT Acrodisc, HiScreen Capto Q ImpRes, HiTrap Capto Heparin and manually packed XK16/20 POROS Heparin. The clarified material loaded into CIMmultus Monolith OH<sup>-</sup> was previously diluted 1:2 with 50mM HEPES, 3M (NH<sub>4</sub>)<sub>2</sub>SO<sub>4</sub>, pH 7.2. Polishing after capture step was performed with two desalting columns. The eluted fraction of interest resulted from capture step was directly loaded into a pre-packed HiTrap Sephadex G-25 (SG-25) and a manual packed XK 16/40 Sepharose 4 fast flow (S4FF) columns. In the cases of manual packed columns, the packing protocol was performed following the instructions suggested by the manufacturer (**Table 2**).

**Table 2:** Parameters used in the chromatography experiments

Type of Chromatography	Flow rate (mL/min)	Column Volume (mL)	Residence time (min)	*Loaded material	Loaded volume (mL)	Equilibration and wash	Step gradient elution
MC Capto Core 700 [14][25]	1.2	4.7	3.92	$8.53 \cdot 10^{11}$	70.5	6% B in 5CV	100% B in 10CV
IEC Monolith QA [26][16]	1	1	1.00	$4.44 \cdot 10^{12}$	120	5% B in 5CV	15%, 35%, 45%, and 65% B in 20CV
IEC Mustang Q [7][27]	0.8	0.86	1.08	$3.6 \cdot 10^{12}$	240	5% B in 5CV	15%, 35%, 45%, and 65% B in 20CV
IEC Capto Q ImpRes [10][28]	1.2	4.7	3.92	$7.0 \cdot 10^{11}$	70.5	6% B in 5CV	15%, 35%, 45%, and 65% B in 20CV
HIC Monolith OH <sup>-</sup> [17]	1	1	1.00	$5.7 \cdot 10^{11}$	77	100% B in 5CV	100%, 65%, 0% B in 20CV
AC Capto Heparin [26][29]	1	1	1.00	$8.1 \cdot 10^{11}$	45	5% B in 8CV	12%, 25%, 50% B in 10CV
AC POROS Heparin [19]	2	5.6	2.80	$1.4 \cdot 10^{12}$	100	5% B in 5CV	15%, 35%, 45%, and 65% B in 20CV
SEC Sephadex G-25	1	5	5.00	$9.20 \cdot 10^{10}$	0.5	FB in 5CV	100% FB in 2CV
SEC Sepharose 4 FF [7][30]	1	48	48.00	$1.78 \cdot 10^{12}$	5	FB in 5CV	100% FB in 2CV

\*Load material is referred to total nanoparticles (including Gag::eGFP VLPs and Extracellular Vesicles) quantify by NTA. The numbers of the first column indicate the references: MC, Multimodal Chromatography; IEC, Ion Exchange Chromatography; HIC, Hydrophobic Interaction Chromatography; AC, Affinity Chromatography; SEC, Size Exclusion Chromatography; CV, Column Volume; B, Buffer corresponding to mobile phase B; FB, Formulation Buffer.

In all cases, the flow rates used were those recommended by the manufacturers. In all chromatographic experiments, equilibration of the stationary phase was performed before loading using the corresponding equilibration buffer. After loading, columns were washed with equilibration buffer to ensure the removal of unbound material from the column. In multimodal chromatography, elution was achieved by a 100% buffer B. In capture experiments, elution was achieved by salt step gradients. In SEC step, Gag::eGFP VLPs were eluted with the formulation buffer in the void volume (VV). After the elution phase, columns were regenerated using 100% B buffer. Fractions were collected and pooled according to the chromatograms, considering the UV absorbance signals of 280, 260 and 488 nm.

### **Western blot and SDS-PAGE**

40  $\mu$ L of sample were mixed with 20  $\mu$ L of 4x LDS Sample Buffer and 7  $\mu$ L of 2M DTT, followed by 20 minutes incubation at 96°C. The prepared samples were stored at 4°C until applied. 20  $\mu$ L of each sample were loaded onto precast NuPAGE Bis/Tris gels 4–12% (Invitrogen, Carlsbad, CA, USA). 5  $\mu$ L of SeeBlue® Plus2 Pre-stained Protein Standard (Invitrogen, Carlsbad, CA, USA) was used as molecular weight control. Gels were run at 200V, 400mA, 45 minutes, in MES-SDS running buffer. For SDS-PAGE gels, proteins were stained with Coomassie Brilliant Blue G-250 based EZBlue™ Gel Staining Reagent (Sigma Aldrich, St. Louis, MO, USA). For Western blot analysis, proteins were transferred onto 0,2  $\mu$ m nitrocellulose membranes using the Trans-Blot® turbo system (Bio-Rad Laboratories, Hercules, CA, USA). Membranes were blocked with PBS 5% (w/v) non-fat dry milk for 30 minutes, washed with PBS 0.1% (w/v) Tween 20, and then incubated overnight at 4°C with the primary mouse monoclonal antibody anti-HIV-1 p24 (dilution 1:2000 in PBS1X) (A2-851-500 Icosagen AS, Tartumaa, Estonia). After washing, product immunodetection was performed with an anti-mouse IgG antibody conjugated with an alkaline phosphatase (dilution 1:5000 in PBS 1X) (A3562, Merck, Kenilworth, NJ, USA), incubated 2 hours at room temperature, and washed with PBS 0,1% (w/v) Tween 20. For protein bands visualization, the membranes were incubated with NBT-BCIP solution (#1706432, Bio-Rad Laboratories, Hercules, CA, USA) for 2-3 minutes. The enzymatic reaction was stopped with ultrapure water.

### **Nanoparticle tracking analysis**

Nanoparticle tracking analysis (NTA) was used to determine particle size distribution and particle concentration with the NanoSight® NS300 device (Malvern Panalytical, Malvern, United Kingdom) equipped with a blue laser module (488 nm) to quantify HIV-1 Gag::eGFP VLPs, and a neutral density filter for total particle quantification by light scattering. Samples were serially diluted in particle-free water to achieve a concentration of 20-80 particles per video frame (the instrument's linear range). For the injected samples, 3 replicates of each dilution were measured at 22°C, with a viscosity of 0,9 cP, and 3 videos of 60 seconds length were acquired. Capture settings were recorded with an sCMOS camera, setting the screen gain to 1, manually adjusting the camera level before each measurement (eight for samples containing Gag::eGFP VLPs and 11 for controls), and setting a detection threshold of 4. The remaining analysis parameters were automatically selected by the software and kept constants for all samples. Data were acquired and processed with the NanoSight NTA software version 3.2. The data obtained from these analyses were also used to calculate the percentage of Gag::eGFP VLPs relative to the total nanoparticles in the measured samples.

### **Fluorescence intensity measurements**

The fluorescence intensity was measured in a Cary Eclipse Fluorescence Spectrophotometer (Agilent Technologies, Santa Clara, CA, USA) to determine the concentration of Gag::eGFP VLPs. The settings were  $\lambda_{excitation} = 488$  nm (slit = 5 nm) and  $\lambda_{emission} = 510$  nm (slit = 10 nm). The relative fluorescence unit (RFU) values were calculated by subtracting the obtained fluorescence intensity (FU) values from the non-transfected negative control samples. An in-house developed and validated quantification assay was used to convert RFU values to Gag::eGFP concentration values [22].

### **Total protein and dsDNA quantification**

Host cell protein concentration was determined using the Micro BCA protein assay kit (#23225, Thermo Fisher Scientific, Waltham, MA, USA), according to the manufacturer's instructions. Briefly, serial PBS-buffer dilutions (between 2-256-fold) of standard and samples were dispensed into the wells. After adding 150µL of the Micro BCA working reagent into each well, plates were incubated for one hour at 37°C. The bovine

serum standard curve ranged from 1,5 to 200 µg/mL, and the absorbance was measured at 562 nm in the Victor 3 reader (Perkin Elmer, MA, USA). Protein concentration of the samples was determined using the standard curve.

Host cell DNA concentration was determined using the Quant-it™ Picogreen dsDNA assay kit (#P11496, Thermo Fisher Scientific, Waltham, MA, USA), according to the manufacturer's instructions. Briefly, serial TE 1X- buffer dilutions (between 2-256-fold) of standard and the samples were dispensed into 96-well microplates. After adding 100µL of the Quant-it™ PicoGreen® reagent (dilution 1:1000) into each well, plates were incubated for 5 minutes at room temperature. The dsDNA standard curve ranged from 1,5 to 500 µg/mL, and the absorbance was measured on the Victor 3 (Perkin Elmer, MA, USA), prior and later to the Quant-it™ PicoGreen® reagent addition since HIV-1 Gag::eGFPVLPs emit at the same range. The settings were  $\lambda_{excitation} = 480 \text{ nm}$  and  $\lambda_{emission} = 520 \text{ nm}$ . DNA concentration of the samples was determined using the standard curve and subtracting the native fluorescence.

### **Flow virometry analysis**

Concentration of Gag::eGFP fluorescent events was quantified using a CytoFLEX LX (Beckman Coulter, Brea, CA, USA), equipped with a 405 nm filter. The threshold of the trigger signal (VSSC) was manually adjusted to 1500, and gains were set as 9, 95, and 115 for VSSC, FSC, and B525-FITC lasers, respectively. Samples were diluted with PBS 1X until an abort rate value below 2% was achieved. A total of 300,000 events were analysed at a flow rate of 10 µL/min per sample. VSSC-H vs B525-FITC density plots were used to gate the different particle populations. Gating was adjusted manually for each channel. Events after 50 s were taken for analysis. The results were analyzed with CytExpert v.2.3 software (Beckman Coulter, Brea, CA, USA).

### **Dynamic light scattering**

The dynamic light scattering technique was used to determine the size of HIV-1 Gag::eGFP VLPs. The measurements were carried out at 25°C in a Zetasizer Nano ZS instrument (Malvern Instruments, Malvern, UK), equipped with a He/Ne 633 nm laser at 173°. 100 µL of the sample were placed in disposable plastic cuvettes. Three consecutive measurements of each sample with 10-15 scans of ten seconds were

performed for each independent measurement. The hydrodynamic diameter (MHD), particle size distribution, derived count rate, and polydispersity index (PDI) average results were automatically obtained.

## **RESULTS AND DISCUSSION**

The proposed DSP process for HIV-1 Gag::eGFP VLPs was tested and characterized. A purification train consisting of clarification, concentration / intermediate purification, capture and polishing steps was developed. The evaluation of the different unit operations tested at each step was conducted by analysing the following parameters: recovery of the Gag::eGFP VLPs, purity concerning the total nanoparticles, enrichment of purity relative to the previous purification step, and reduction of principal contaminants (total proteins and dsDNA). Additionally, a characterization of the VLPs was performed in terms of their size. A schematic representation of the general experimental approach performed is presented in **Figure 1**.

### **Gag::eGFP VLPs production and clarification step**

To produce enough Gag nanoparticles for evaluating the various steps in the DSP strategies, multiple batches of HEK 293 cells were transfected following the aforementioned transfection protocol. Parameters such as cell viability, cell density, supernatant GFP-associate fluoresce, and transfection efficiency were monitored every 24h. In all cases, the RFU values and the number of GFP-positive cells showed an expected increase in fluorescence intensity following transfection, indicating the presence of Gag::eGFP. At 72hpt, which was determined to be the optimal harvest time [31], the transfection efficiency was approximately 80%, with RFU values reaching around 50. Also, although a reduction in cell viability was observed after transfection, it remained above 85%. These results indicate the successful production of Gag::eGFP VLPs in the supernatant of the HEK293 cells, confirming the effectiveness of the transfection protocol for this purpose. Similar results regarding the transient transfection under these conditions to produce Gag::eGFP VLPs have been reported by J. Lavado-García et al (2021) [32], [33].

After removal of cells by sedimentation, the DSP process began with clarification of the supernatant, a critical step to improve the subsequent purification steps. For this stage, two depth filters were evaluated based on the parameters mentioned above. **Table 3** shows the results of the evaluation of the two filters regarding the characteristics of the loaded material.

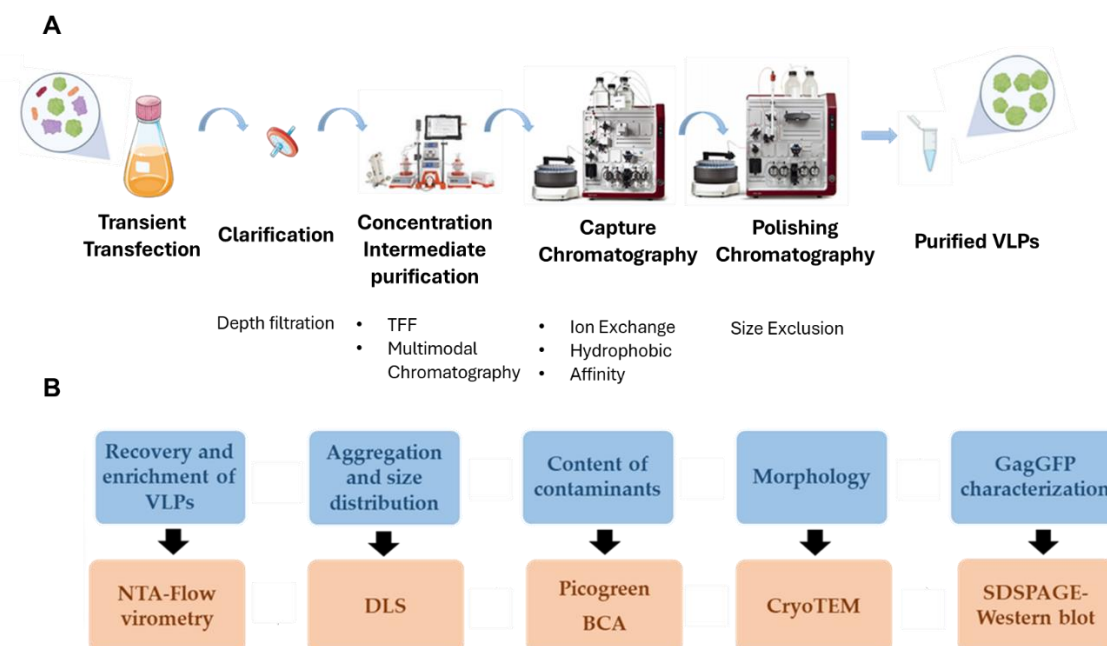


**Figure 1:** Overview of the experimental workflow. **(A)** Process for purifying Gag::eGFP VLPs starting with transient transfection. The steps included clarification using depth filtration and filtration, followed by concentration / intermediate purification through tangential flow filtration (TFF) and multimodal chromatography. Capture chromatography involved ion exchange, hydrophobic interactions, and affinity chromatography. Finally, polishing step included the use of size exclusion chromatography. **(B)** Parameters evaluated and analytical techniques developed for the characterization of each step of the DSP.

**Table 3:** Mass balance of Gag::eGFP VLPs and contaminants reduction in clarification step using MilliStak®+ D0HC µpod®+ and Supracap™ 50V100™ depth filters.

Sample	Volume (mL)	Total Protein and dsDNA Contaminant Reduction				Gag::eGFP VLPs recovery and Purity			
		Total Protein (ug/mL)	Step Reduction (%)	dsDNA (ng/mL)	Step Reduction (%)	Total Gag::eGFP VLPs	Step Recovery (%)	Purity (%)	VLPs enrichment (%)
Load 1	1000	732	-	2430	-	$1.66 \cdot 10^{13}$	100	30	-
CL1	1000	608	16	2391	2	$1.27 \cdot 10^{13}$	77	40	10
Load 2	1000	255.6	-	613.12	-	$7.74 \cdot 10^{12}$	100	27	-
CL2	1000	228.9	10	218	65	$7.11 \cdot 10^{12}$	92	56	29

*Load 1* and *Load 2*: Load samples using for test MilliStak®+ D0HC µpod depth filter and Supracap™ 50V100 depth filter respectively; *CL1* and *CL2*, clarified materials corresponding to MilliStak®+ D0HC µpod depth filter and Supracap™ 50V100 depth filter, respectively.

Higher recovery and purity were achieved with the Supracap™ 50V100 depth filter. One possible explanation is the difference in nominal retention rating. The Supracap™ 50V100 depth filter has a nominal filter retention range between 2 - 4 µm; and the MilliStak®+ D0HC µpod depth filter has a nominal filter retention between 0.5 - 10 µm approximately [34]. This implies that more heterogenous particles in size can pass through the MilliStak®+ D0HC µpod depth filter and they can also retain VLPs. However, higher



recoveries of Gag VLPs were achieved in previous studies using the MilliStak®+ D0HC µpod depth filter [7], [27] and a possible cause could be that in both reported cases a lower amount of Gag VLPs was loaded compared to the amount loaded here. Another remarkable result using the Supracap™ 50V100 depth filter was the high reduction in contaminating dsDNA, an important characteristic that make this filter a very promising alternative for the clarification step. Additionally, previous studies have shown that clarification using nominal filtration processes achieves satisfactory recovery yields of around 80%, aligning well with our findings [35].

The DLS profile followed the same trend in both cases, although the peak was slightly higher for the Supracap™ 50V100 depth filter since there was a lower loss of Gag::eGFP VLPs (**Figure 2A**). The smaller peak of the supernatant seen on the right may be due to cell debris or aggregates, which was diminished by the clarification. Electrophoresis confirmed the presence of a band greater than 75 kDa (the molecular weight of Gag::eGFP is approximately 88 kDa), confirmed to be Gag::eGFP, either free monomer or forming part of VLPs, by Western blot (**Figure 2B**).

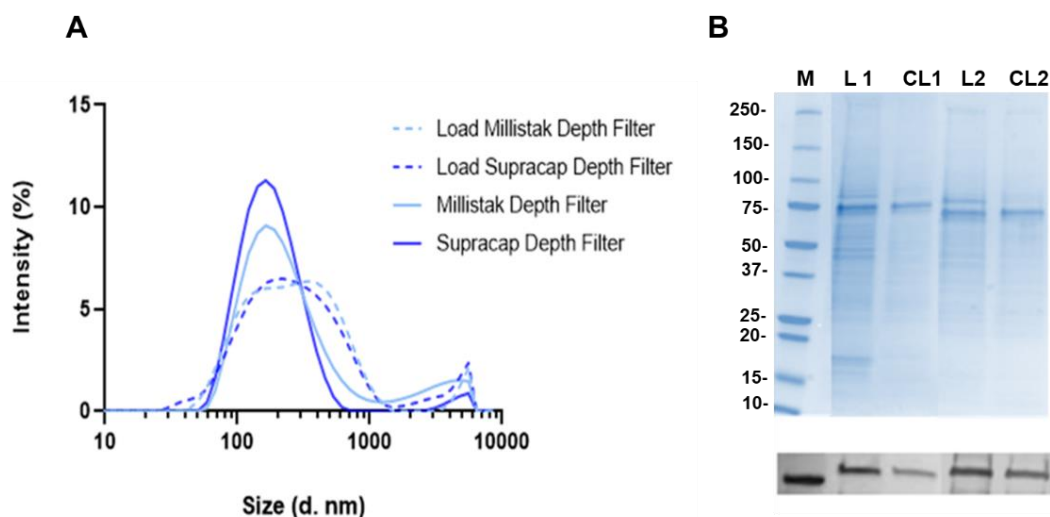


**Figure 2:** Primary clarification of Gag::eGFP VLPs supernatant. **(A)** Dynamic light scattering (DLS) analysis of the MilliStak®+ D0HC µpod depth filter loaded material (PDI =0.439, MHD=223.8), MilliStak®+ D0HC µpod depth filter clarified material PDI =0.387, MHD=195.6), Supracap™ 50V100 depth filter loaded material (PDI =0.457, MHD=242.3), Supracap™ 50V100 depth filter clarified material (PDI =0.239, MHD=161.2). **(B)** SDS-PAGE and p24 Western blot of the depth filtration runs. PDI, polydispersity index; MHD, mean hydrodynamic diameter; M, molecular weight standard; L1 and L2, Loaded material using for test MilliStak®+ D0HC µpod depth filter and Supracap™ 50V100 depth filter respectively; CL1 and CL2, clarified material corresponding to MilliStak®+ D0HC µpod depth filter and Supracap™ 50V100 depth filter, respectively.

It should also be considered that a secondary clarification in DSP strategies is sometimes required. An additional clarification step is added in case that a previously frozen sample was to be used and precipitates and/or aggregates appear during its thawing. The turbidity of the sample is an indication of how necessary it is to clarify again before continuing with the subsequent chromatography steps. For that reason, two different filters were evaluated (Sartopore® SartoScale 25 PP3 and Supor® EAV - Mini Kleenpak™ 20 filters) in case this step needs to be included in the purification process. The same parameters analysed in the case of primary clarification were also considered in these experiments. **Table 4** shows the results of the evaluation of the two filters regarding the characteristics of the loaded material.

**Table 4:** Mass balance of Gag::eGFP VLPs and contaminants reduction in secondary clarification step using Sartopore® SartoScale 25 PP3 and Supor® EAV - Mini Kleenpak™ 20 filters.

Sample	Volume (mL)	Total Protein and dsDNA Contaminant Reduction				Gag::eGFP VLPs recovery and Purity			
		Total Protein (ug/mL)	Step Reduction (%)	dsDNA (ng/mL)	Step Reduction (%)	Total Gag::eGFPVLPs	Step Recovery (%)	Purity (%)	VLPs enrichment (%)
CL2	500	228.9	100	218	100	$3.2 \cdot 10^{12}$	100	56	-
CL2.1	500	225.4	2	175.3	20	$2.0 \cdot 10^{12}$	56	56	0
CL2.2	500	191.6	15	146.2	44	$3.0 \cdot 10^{12}$	88	54	0

CL2, Loaded material using for test both filters; CL2.1 and CL2.2, clarified material corresponding to Sartopore® SartoScale 25 PP3 filter and a Supor® EAV - Mini Kleenpak™ 20 filters, respectively

The null enrichment of Gag::eGFP VLPs in the secondary clarification could be because conventional filtration does not serve to enrich the preparation with Gag::eGFP VLPs in respect to the total nanoparticles, since the large particles have already been removed by depth filtration. Moreover, although both filters reduced the amount of dsDNA respect to the load, it appears that the Supor® EAV - Mini Kleenpak™ 20 filter had some selectivity for dsDNA and certain proteins since the observed reduction was higher compared to Sartopore® SartoScale 25 PP3 filter. Although the Gag::eGFP VLPs did not increase with respect to total particles, it was possible to remove part of the contaminants, obtaining an optimal sample characteristics that allows a better performance of the column for the next chromatographic step [11].

Regarding the size distribution characterization, **figure 3A** showed the DLS results of both clarified materials, where a similar profile was observed. The presence of Gag::eGFP was also confirmed by SDS-PAGE and Western blot at the expected molecular size (**Figure 3B**).

Overall, the best results in primary clarification were obtained with the Supracap™ 50V100 depth filter. Regarding secondary clarification, the Supor® EAV - Mini Kleenpak™ 20 filter was selected as the best option, if required. The selected method offers a robust approach for the clarification of Gag::eGFP VLPs. Similar results were reported for the clarification of influenza VLPs produced in insect cells [34].

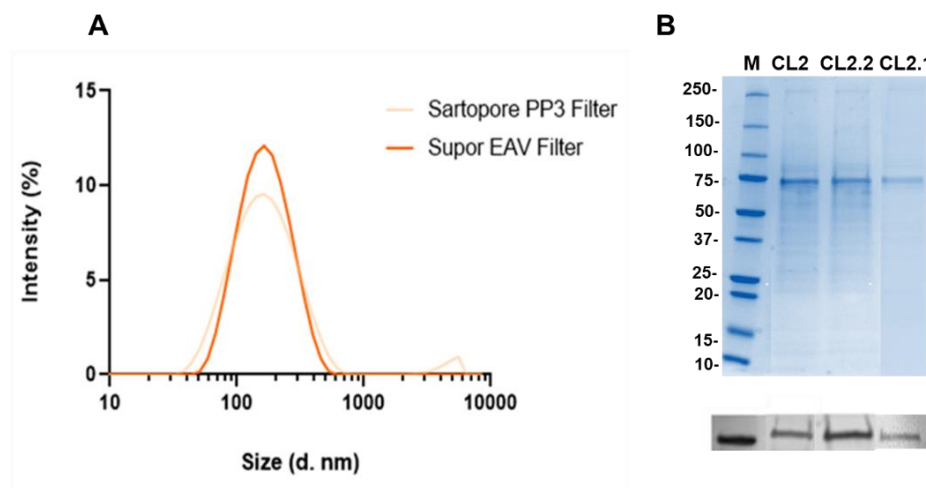


**Figure 3:** Secondary clarification of Gag::eGFP VLPs. **(A)** Dynamic light scattering (DLS) analysis of the Sartopore® SartoScale 25 PP3 filter clarified (PDI =0.329, MHD= 137.8), Supor® EAV - Mini Kleenpak™ 20 filter clarified (PDI =0.321, MHD=143.3). **(B)** SDS-PAGE and p24 Western blot of the filtration runs, using a Sartopore® SartoScale 25 PP3 and a Supor® EAV - Mini Kleenpak™ 20 filters. *PDI*, polydispersity index; *MHD*, mean hydrodynamic diameter; *M*, molecular weight standard, *CL2*, Loaded material using for test both filters; *CL2.1* and *CL2.2*, clarified material corresponding to Sartopore® SartoScale 25 PP3 filter and a Supor® EAV - Mini Kleenpak™ 20 filters, respectively.

### Concentration / Intermediate purification step

Following clarification, a concentration step is often included in a purification process. It is very useful when the volume of the starting material is high, and it is also a step that allows the removal of contaminants [3], [10]. For that reason, in this work, we evaluated the capacity of TFF, specifically using T-Series cassettes with omega polyethersulfone (PES) membrane of 300 kDa, to concentrate Gag::eGFP VLPs. In this case, the operation was also characterized considering all the parameters evaluated in the previous steps. **Table 5** presents the results of the TFF evaluation, focusing on the retentate fraction and its characteristics in relation to the loaded material.

All Gag::eGFP VLPs have been recovered and concentrated ten-fold, with presence of some aggregates and a shift in the particle size as shown by the DLS profile (**Figure 4A**). However, when the retentate material was diluted and then analysed by NTA, although the presence of aggregates was also observed, the particle size obtained for the Gag::eGFP VLPs was 146nm (data not shown), which corresponds to the expected

results for these nanoparticles. In the electrophoresis, a band greater than 75 kDa could be seen in the retentate, which did not appear in the permeate (data not shown). It was confirmed that this band corresponds to Gag::eGFP by Western blot (**Figure 4B**). T-Series cassettes with PES membrane, and molecular weight cut-off of 1000 and 300 kDa, have been reported for VLPs concentration enabling a removal of >80% of proteins while recovering approximately 60-80% of VLPs [24], [30]. In this case, ultrafiltration/diafiltration using TFF mode to concentrate Gag::eGFP VLPs, as well as to successfully remove contaminating dsDNA and proteins, is proposed as an intermediate step in DSP train with better results than previously reported [2], [24].

Another alternative to follow in this intermediate purification step is the use of a multimodal chromatography (MC). In this work the HiScreen Capto Core 700 column was evaluated considering the parameters described above. This MC has size exclusion and binding properties. The beads have a nonfunctionalized outer layer, in which the size exclusion limit is 70kDa, and a functionalized core with an attached ligand (octylamine) where most contaminants are retained, therefore, the product of interest is collected in the flow-through (FT) fraction [12]. In **Table 5** is observed the results of the MC evaluation, focusing on the FT fraction and its characteristics in relation to the loaded material. The mass balance results indicate that most of the contaminating proteins in the evaluated fraction have a high molecular weight. Consequently, only 11% of these contaminant proteins were removed, leaving 88% in the FT along with the Gag::eGFP VLPs [20]. A narrower profile was observed by DLS (**Figure 4A**), with a lower PDI and MHD, which indicated the presence of less aggregates in the FT fraction, which was then later confirmed to be Gag::eGFP by Western blot (**Figure 4B**).

**Table 5:** Mass balance of Gag::eGFP VLPs and contaminants reduction in concentration step using Tangential flow filtration (TFF) with 300kDa PES membrane and intermediate purification using Multimodal Chromatography (MC) with Capto Core 700 column

Total Protein and dsDNA Contaminant Reduction						Gag::eGFP VLPs recovery and Purity					
	Sample	Volume (mL)	Total Protein (ug/mL)	Step Reduction (%)	dsDNA (ng/mL)	Step Reduction (%)	Total Gag::eGFP VLPs	Step Recovery (%)	Purity (%)	VLPs enrichment (%)	Concentration factor
TFF	Load	2000	414.2	100	557	100	$7.34 \cdot 10^{12}$	100	37	-	-
	Retentate	200	568	76	201	96	$7.7 \cdot 10^{12}$	105	42	5	10
MC	Load	70.5	512	100	200.1	100	$3.05 \cdot 10^{11}$	100	23	-	-
	Flow-Through	70.5	455.4	11	60.3	68	$2.21 \cdot 10^{11}$	72	36	13	-

In previous reports, a yield of 90.9% has been reported in the purification of Zika VLPs [12], 89.7% for yellow fever VLPs [12] and 89% for influenza VLPs [25]. However, it must be considered that for HIV-1 Gag VLPs a maximum of 73.1% recovery has been reported [20], close to the results obtained here. In respect to other studies, although similar residence times and loading volumes were evaluated, the total number of nanoparticles loaded to the column was lower [12], [20], [25]. Possibly this could be the cause of the low recovery percentages and reduction of contaminating proteins observed.

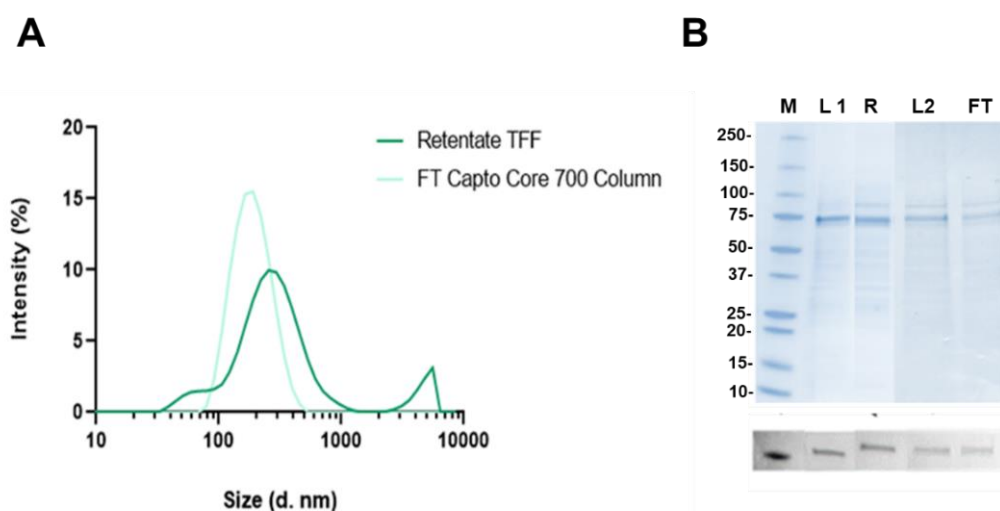


**Figure 4:** Tangential flow filtration and multimodal chromatography experiments for concentration and intermediate purification of Gag::eGFP VLPs. **(A)** Dynamic light scattering (DLS) analysis of the TFF retentate fraction (PDI =0.501, MHD=241.8), Capto Core 700 column FT fraction (PDI =0.166, MHD=165.2); **(B)** SDS-PAGE and p24 Western blot of the filtration run with a 300 kDa PES membrane by TFF, and a chromatographic run with a Capto Core 700 column. *PDI*, polydispersity index; *MHD*, mean hydrodynamic diameter; *M*, molecular weight standard; *L* loaded material used in TFF and MC; *R*, retentate fraction resulted from TFF; *FT* flow through fraction obtain in MC.

### Capture step

The evaluation of the capture step included six different chromatography methodologies: three based on ion exchange, one based on hydrophobic interactions and two based on heparin affinity. The characteristics of the samples loaded in the six chromatographies are summarized in **Table 6**. All runs were analysed considering the parameters described above for the other steps. The mass balance analysis of these chromatographies is shown in **Table 7**.

Among several chromatographic techniques, ion exchange chromatography has been already used to purify VLPs. Here, three IEC were tested: Monolith QA, Mustang Q, and Capto Q ImpRes. In all the cases, the fractions obtained during the runs were analysed from the corresponding chromatogram. The second step in the elution phase fraction (named P2) was considered the main product fraction due to the higher

Gag::eGFP VLPs concentration and simultaneous lower total protein and dsDNA content (**Supplementary Material S1**). The P2 fraction, corresponds to conductivity values of 45-55 mS/cm. Similar elution conditions for VLPs have been reported [16], [36]. Therefore, the subsequent comparative analyses were performed focusing on the P2 fraction in relation to the loaded material.

**Table 6:** Summary of the characteristics of the initial material loaded in each chromatography experiment

	Loaded Material									
	Volume (mL)	Gag::eGFP VLPs (VLPs)		Gag::eGFP VLPs and other nanoparticles (NP)		Purity	Total Protein		Total dsDNA	
		VLP/mL	Total VLPs	NP/mL	Total NP	VLPs/NP (%)	µg Prot/mL	mg Prot	ng dsDNA/mL	ng dsDNA
IEC Monolith QA	120	$1.10 \cdot 10^{10}$	$1.32 \cdot 10^{12}$	$3.70 \cdot 10^{10}$	$4.44 \cdot 10^{12}$	30	847	101.64	341.6	40992
IEC Mustang Q	240	$3.90 \cdot 10^9$	$9.36 \cdot 10^{11}$	$1.50 \cdot 10^{10}$	$3.6 \cdot 10^{12}$	26	655.6	157.34	141.6	33984
IEC Capto Q ImpRes	70.5	$3.15 \cdot 10^9$	$2.22 \cdot 10^{11}$	$9.90 \cdot 10^9$	$7.0 \cdot 10^{11}$	32	297.2	20.95	145.6	10264.8
HIC Monolith OH <sup>-</sup>	77	$5.00 \cdot 10^9$	$3.85 \cdot 10^{11}$	$7.40 \cdot 10^9$	$5.7 \cdot 10^{11}$	68	78	6.00	60.4	4650.8
AC Capto Heparin	45	$1.24 \cdot 10^{10}$	$5.58 \cdot 10^{11}$	$1.80 \cdot 10^{10}$	$8.1 \cdot 10^{11}$	69	267	12.01	340	15300
AC POROS Heparin	100	$9.70 \cdot 10^9$	$9.70 \cdot 10^{11}$	$1.40 \cdot 10^{10}$	$1.4 \cdot 10^{12}$	69	266.3	26.63	62.4	6240

Regarding the Monolith QA chromatographic run, this method effectively separates the main impurities, including host cell proteins and dsDNA. The recovery of Gag::eGFP VLPs in the main elution fraction P2 is less than 50%; however, these results are consistent with previously reported data [13], [16].

For the Mustang Q, an improvement in yield compared to previously reported results was obtained in this work [7] [27]. A possible explanation for this could be that, in this case, the loaded sample had been previously clarified using both filters, Supracap™ 50V100 and Supor® EAV - Mini Kleenpak, which allows a better performance of the membrane reducing as many precipitates as possible in the sample and avoiding system overpressure. In addition, the concentration of loaded material in this case was lower than in the previously reports, which has also allowed better results in yield.

Highest recovery was achieved using Capto Q ImpRes which allowed not only the separation of Gag::eGFP VLPs from host cell protein and dsDNA but also the enrichment respect to total nanoparticles. The yield

obtained was similar when using the same resin for adenoviruses (~80%), according to previous reports [10]. These data support the use of strong quaternary amine ion exchangers to concentrate and purify HIV-1 Gag VLPs.

**Table 7:** Mass balance of Gag::eGFP VLPs and contaminants reduction in capture step using Monolith QA, Mustang Q, Capto Q ImpRes, Monolith OH, Capto Heparin, and POROS Heparin

Total Protein and dsDNA Contaminant Reduction							Gag::eGFP VLPs recovery and Purity				
	Sample	Volume (mL)	Total Protein (ug/mL)	Step Reduction (%)	dsDNA (ng/mL)	Step Reduction (%)	dsDNA/dose (ng/10 <sup>9</sup> VLPs)	Total Gag::eGFP VLPs	Step Recovery (%)	Purity (%)	VLPs enrichment (%)
<b>Monolith QA</b>	Load	120	847	100	341.6	100	-	1.32·10 <sup>12</sup>	100	29	-
	P2	4	289	99	880	81	6.24	5.60·10 <sup>11</sup>	42	42	13
<b>Mustang Q</b>	Load	240	655.6	100	141.6	100	-	9.4·10 <sup>11</sup>	100	29	-
	P2	6	96.7	99	111.3	98	1.3	5.3·10 <sup>11</sup>	56	48	19
<b>Capto Q ImpRes</b>	Load	70.5	297.2	100	145.6	100	-	2.2·10 <sup>11</sup>	100	32	-
	P2	6	79.3	98	226.4	87	8.6	1.6·10 <sup>11</sup>	72	69	37
<b>Monolith OH.</b>	Load	77	300	100	60.4	100	-	3.85·10 <sup>11</sup>	100	68	-
	P3	4	50.3	99	14.3	99	0.17	8.4·10 <sup>10</sup>	22	53	0
<b>Capto Heparin</b>	Load	45	267	100	340	100	-	5.58·10 <sup>11</sup>	100	69	-
	W	2	68	99	241	97	1.9	1.30·10 <sup>11</sup>	23	72	3
<b>POROS Heparin</b>	Load	100	266.3	100	62.4	100	-	9.70·10 <sup>11</sup>	100	69	-
	P1	4	58.7	99	49.6	97	0.5	4.04·10 <sup>11</sup>	42	80	11

The use of hydroxyl-functionalized polymethacrylate monolith was also tested in the capture step. The fraction corresponding to elution step 3 (P3) showed the highest content of Gag::eGFP VLPs (22%). In this case the elution buffers used were different than in IEC experiments and the major Gag::eGFP VLP concentration fraction presents conductivity values approximately of 20 mS/cm (**Supplementary Material S2**). Similar results were reported regarding the recovery of Gag VLPs in two main elution peaks using this column [17].

Regarding the enrichment of VLPs, no increase was observed, however, an almost total elimination of contaminating host cell proteins and DNA was observed. The overall advantages for macroporous polymethacrylate monoliths are well established [37]. From the two types of functionalized monoliths tested, the best results were obtained with the Monolith QA, which suggests that the ion exchange principle provided by the QA ligand allows a better recovery of the Gag VLPs, compared to the hydrophobic exchanges provided by the OH ligand.

Several studies have shown the potential of heparin affinity chromatography for the purification of VLPs allowing its separation from other nanoparticles populations [20]. Different chromatography media have been used to couple the heparin ligand [19]. Here, Capto Heparin and POROS Heparin columns were tested. In both cases it was observed a similar chromatographic profile where the fraction with higher amount of Gag::eGFP VLPs elute at 20-25 mS/cm values of conductivity with high reduction of protein and dsDNA contaminants (**Supplementary Material S3**). Despite these similarities, POROS Heparin was superior in its ability to capture the Gag::eGFP VLPs. The results obtained show the effectiveness of this resin to separate the Gag::eGFP VLPs from other nanoparticles present in the material.

Furthermore, as shown in **Table 7**, data related to the amount of contaminating dsDNA per dose of Gag::eGFP VLPs, assuming a possible vaccine dose consists of  $1 \cdot 10^9$  VLPs [38], were included to characterize this capture step. This consideration is crucial, as regulatory agencies have established a limit of 10 ng of dsDNA per dose in the final biological product for clinical use [39], [40]. In all chromatographies evaluated, the values obtained for this parameter were within the established range.

The PDI and MHD analysed by DLS were very similar in all capture chromatography evaluated (**Figure 5A**). Also, it was observed in all the cases a band with the expected size by SDS-PAGE, confirmed to be Gag::eGFP by Western blot (**Figure 5B**).

Considering that the initial samples used for the tests were different, the main criteria of evaluation were based on the recovery of Gag VLPs, considering the total Gag VLPs/mL of column/membrane loaded and eluted in each case. According to the obtained results, the Capto Q ImpRes column offers a better recovery of the product of interest, enriching its presence with respect to the rest of the nanoparticles, and at the same time maintaining low amounts of contaminants. These parameters, together with the molecular characterization of the Gag VLPs, make this column the optimal option for the capture and purification of the Gag VLPs.



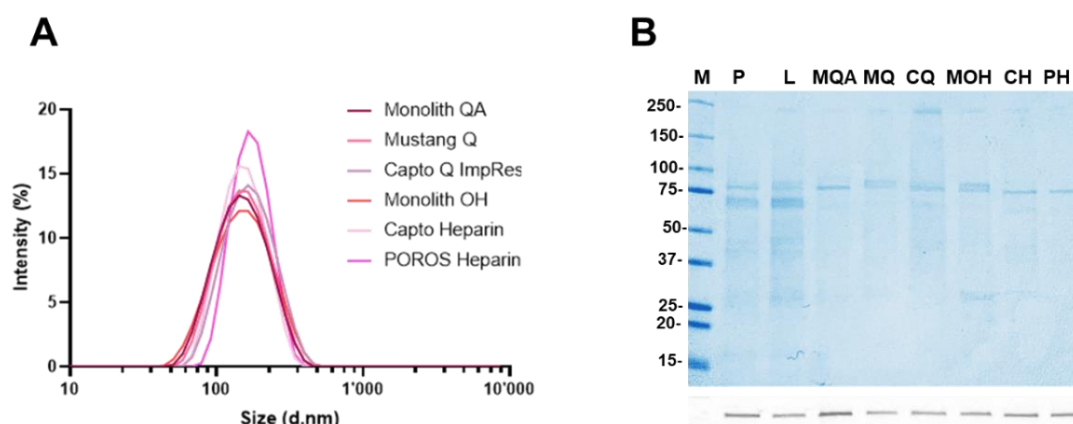


**Figure 5:** Purification of Gag::eGFP VLPs by an ion exchange, hydrophobic interaction, and affinity chromatography. **(A)** Dynamic light scattering (DLS) analysis of the P2 fraction of the Monolith QA column (PDI=0.190, MHD=137.9), Mustang Q column (PDI=0.176, MHD=135.5) and Capto Q ImpRes column (PDI=0.151, MHD=152.0), P3 fraction of the Monolith OH column (PDI=0.18, MHD=132), W fraction of the Capto Heparin column (PDI=0.13, MHD=140) and P1 of the POROS Heparin column (PDI=0.1, MHD=162.8). **(B)** SDS-PAGE and p24 Western blot of the production, load material and the Gag::eGFP VLPs main fraction of each chromatographic run: P1, P2 and P3 elution peaks from respective step gradient; W, fraction corresponding to wash step; PDI, polydispersity index; MHD, mean hydrodynamic diameter; M, molecular weight standard, P, Supernatant production sample; L, load sample; MQA, MQ, CQ, MOH, CH, PH, main fraction corresponding to Monolith QA, Mustang Q, Capto Q ImpRes Monolith OH, Capto Heparin and POROS heparin columns, respectively.

### Polishing step

Polishing is a critical step to achieve a final clinical grade material. After capture step we evaluated size exclusion chromatography (SEC) as a polishing step with two different columns, HiTrap® Sephadex G-25 column, and a XK 16/40 Sepharose 4FF column. The characteristics of the samples loaded in the two chromatographies are summarized in **Table 8**. The same parameters as in the previous steps were used for characterization. In SEC, Gag VLPs elute in the void volume (VV) (**Supplementary Material S4**). The mass balance results of both runs are summarized in **Table 9**. The PDI and MHD were very similar. Also, a band greater than 75 kDa was observed by electrophoresis and Western blot (**Figure 6**).

**Table 8:** Summary of the characteristics of the initial samples loaded in each chromatography experiment

	Loaded Material									
	Volume (mL)	Gag::eGFP VLPs (VLPs)		Gag::eGFP VLPs + other nanoparticles (NP)		Purity	Total Protein		Total dsDNA	
		VLP/mL	Total VLPs	NP/mL	Total NP	VLPs/NP (%)	µg Prot/mL	mg Prot	ng dsDNA/mL	ng dsDNA
SEC Sephadex G25	0.5	$8.70 \cdot 10^{10}$	$4.35 \cdot 10^{10}$	$1.84 \cdot 10^{11}$	$9.20 \cdot 10^{10}$	47%	96.7	0.05	111.3	55.65
SEC Sepharose 4 FF	5	$1.17 \cdot 10^{11}$	$5.85 \cdot 10^{11}$	$3.55 \cdot 10^{11}$	$1.78 \cdot 10^{12}$	33%	540	2.7	1610	8050

**Table 9:** Mass balance of Gag::eGFP VLPs and contaminants reduction using HiTrap Sephadex G-25 (SG-25) and XK Sepharose 4FF 16/40 (S4FF).

	Sample	Volume (mL)	Total Protein and dsDNA Contaminant Reduction				Gag::eGFP VLPs recovery and Purity				
			Total Protein (ug/mL)	Step Reduction (%)	dsDNA (ng/mL)	Step Reduction (%)	dsDNA/dose (ng/10 <sup>9</sup> VLPs)	Total Gag::eGFP VLPs	Step Recovery (%)	Purity (%)	VLPs enrichment (%)
<b>SG-25</b>	*Load	0.5	96.7	100	111.3	100	-	4.40·10 <sup>10</sup>	100	47	-
	VV	1	22.6	53	26.5	52	0.12	1.70·10 <sup>10</sup>	39	40	0
<b>S4FF</b>	Load	5	540.9	100	1610	100		5.85·10 <sup>11</sup>	100	33	-
	VV	10	33	88	26	97	0.6	4.33·10 <sup>11</sup>	74	56	23

\*This Run was performed 12 times until process 6mL of sample.

VV: void volume fraction

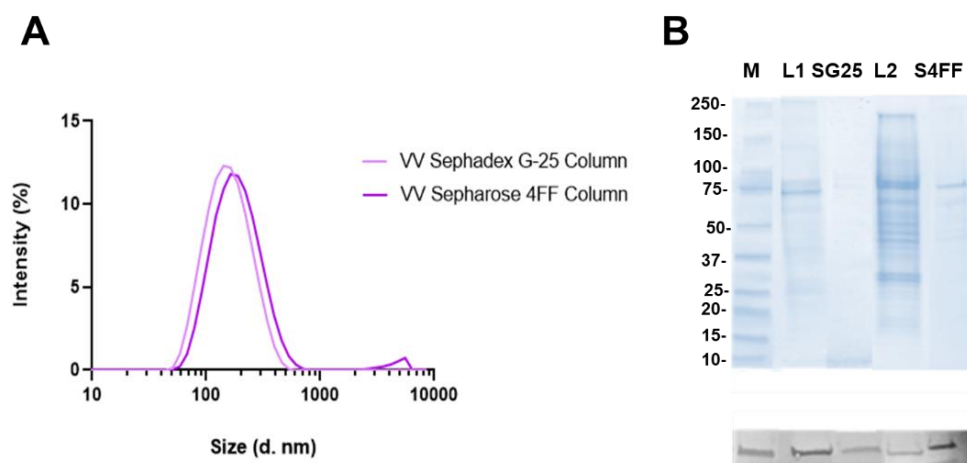


**Figure 6:** Purification of Gag::eGFP VLPs by size exclusion chromatography. **(A)** Dynamic light scattering (DLS) analysis of the VV fraction of the Sephadex G-25 column (PDI=0.174, MHD=139.9), and Sepharose 4FF column (PDI=0.217, MHD=172.8). **(B)** SDS-PAGE and p24 Western blot of the chromatographic runs using a Sephadex G-25 column and a Sepharose 4FF column. VV, void volume; PDI, polydispersity index; MHD, mean hydrodynamic diameter; M, molecular weight standard; SG25, VV from Sephadex G-25 column; S4FF, VV from Sepharose 4FF column, L1 and L2, loaded sample in SG25 and S4FF, respectively.

The Sepharose 4 FF gave better results compared to the Sephadex G-25 column. A possible explanation could be the use of different resins, the difference in the column dimensions, or both [7]. Even so, in this step, it was still possible to eliminate more dsDNA and total protein for both cases. This polishing step also has the advantage of enabling the exchange of the process buffer for a formulation or storage buffer which is an advantage for their subsequent lyophilization [10], [41].

## Evaluation of the optimized purification process

To finally validate the process, a 100mL harvest material from a production batch was treated through the complete purification train, using the techniques showing a better performance at each step. First, clarification was performed using the Supracap™ 50V100 depth filter. Secondary clarification was not necessary, since the turbidity values were acceptable after the first filtration, which ruled out the presence of large aggregates and precipitates. The next step was capture with the IEC with the HiScreen Capto Q ImpRes column. The TFF step was not included since in this case it was not necessary to concentrate the sample before chromatography. In general terms, it is suggested to consider the TFF step in the DSP train when it is necessary to concentrate the sample. After IEC, desalting was performed with XK 16/40 Sepharose 4FF column. The mass balance of this complete validation run is summarized in **Table 10**.

**Table 10:** Mass balance of Gag::eGFP VLPs and contaminants removal obtained from final DSP validation run.

Sample	Volume (mL)	Total Protein and dsDNA Contaminant Reduction					Gag::eGFP VLPs Recovery and Purity				Gag::eGFP protein Recovery and Purity	
		Total Protein (ug/mL)	Step Reduction (%)	dsDNA (ng/mL)	Step Reduction (%)	dsDNA/dose (ng/10 <sup>9</sup> VLPs)	Total Gag::eGFP VLPs	VLP Recovery (%)	Purity (%)	VLPs enrichment (%)	Gag::eGFP protein (ug/mL)	Gag::eGFP/Total protein (%)
SN	100	560.9	-	613	-	69.6	$8.8 \cdot 10^{11}$	100	38		15.1	3
CL	100	550	2	217	65	27.4	$7.9 \cdot 10^{11}$	90	43	5	10.2	2
IEC	2	542	98	488.4	96	1.6	$6.04 \cdot 10^{11}$	76	60	17	175	32
SEC	6	30.0	83	5.8	96	0.4	$8.4 \cdot 10^{10}$	55**	64	4	21	70
<b>Overall***</b>			<b>100</b>		<b>100</b>			<b>38</b>				

\*\* This percentage was calculated taking into account that the sample loaded in SEC was diluted 4 times.

\*\*\* Final recovery/reduction of the entire process with respect to the initial sample (crude supernatant of the production step).

SN: supernatant; CL: Clarified material; IEC: Peak 2 fraction from elution step in Ion Exchange Chromatography using Capto Q ImpRes column; SEC: Peak of void volume from Size Exclusion Chromatography using Sepharose 4 fast flow column.

The results demonstrate an overall improvement in the process performance and product purity compared to previously reported VLP purification processes [7], [16], [17], [27]. On the other hand, **Figure 7** shows a molecular characterization of Gag::eGFP VLPs obtained in each step. Final concentrated and purified Gag::eGFP VLPs were clearly observed in cryo-TEM micrographs (**Figure 7A**). The Gag VLPs were detected as spherical electrodense nanoparticles surrounded by a lipid membrane. On the other hand, as observed in the SDS-PAGE, as the process progresses, the sample corresponding to Gag::eGFP was concentrated and other contaminating proteins were eliminated. Furthermore, in all steps the presence of Gag::eGFP was confirmed by Western blot (**Figure 7B**). The DLS allowed to characterize the nanoparticles

in each step of the process. As the sample underwent purification, the peak narrowed compared to the initial crude supernatant, as shown in **Figure 7C**. This behaviour is indicative of a homogeneous material.

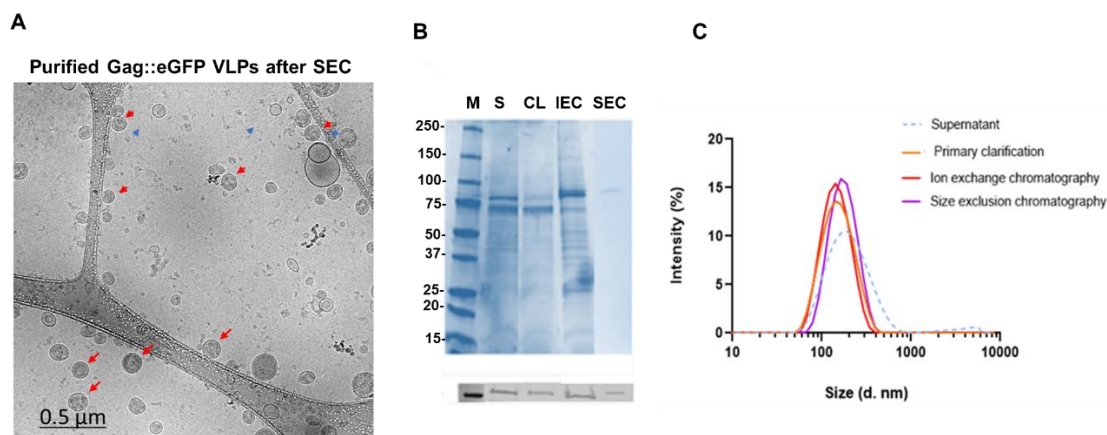


**Figure 7:** Molecular and biophysical characterization of Gag::eGFP VLPs obtained in all steps of the final DSP run (**A**) Cryo-TEM micrographs of purified material; (**B**) SDS-PAGE, p24 Western blot, (**C**) Dynamic light scattering (DLS). *M*, molecular weight standard; *S*, supernatant; *C*, clarified; *IEC*, elution peak 2 from Capto Q ImpRes and *SEC*, void volume from Sepharose 4FF. Red and blue narrows indicate Gag::eGFP VLPs and other nanoparticles, respectively.

## CONCLUSIONS

HIV-1 Gag VLPs present a highly promising platform for vaccine development strategies. The design of HIV-1 Gag::eGFP VLPs purification process, comparing different unit operations in each step has been achieved in this work. In the primary clarification, it was possible to separate most of the cell aggregates and debris from the HIV-1 Gag::eGFP VLPs of the supernatant by means of depth filtration, without involving a significant loss of VLPs. This was refined by secondary clarification by filtration, resulting in a significant reduction in the contaminating dsDNA content. Tangential flow filtration enabled further concentration, and more than 85% of dsDNA and total protein content removal. Capto Q ImpRes IEC showed the best results among all chromatography tested in capturing and purifying VLPs. Last, it was possible to achieve a higher purity, as well as a desalting and buffer exchange with the S4FF SEC. The process has shown a total recovery of 38% of Gag::eGFP VLPs with a total protein, and dsDNA removal of almost 100% from the crude supernatant. Along with a robust purification platform, efficient process monitoring tools are critical for process development and robust characterization to meet regulatory demands. Analytical methods such as DLS, NTA, flow virometry, electrophoresis, and Western blot, performed in this study, have been widely applied to monitor multiple quality attributes of VLPs [7], [13], [20]. Overall, the DSP unit operations and the

analytical tools studied here are suitable for large-scale manufacturing, supporting the use of the developed DSP bioprocess as platform for HIV-1 Gag VLPs purification. A more detailed discussion of the results presented in this chapter can be found in the general discussion section of this thesis.

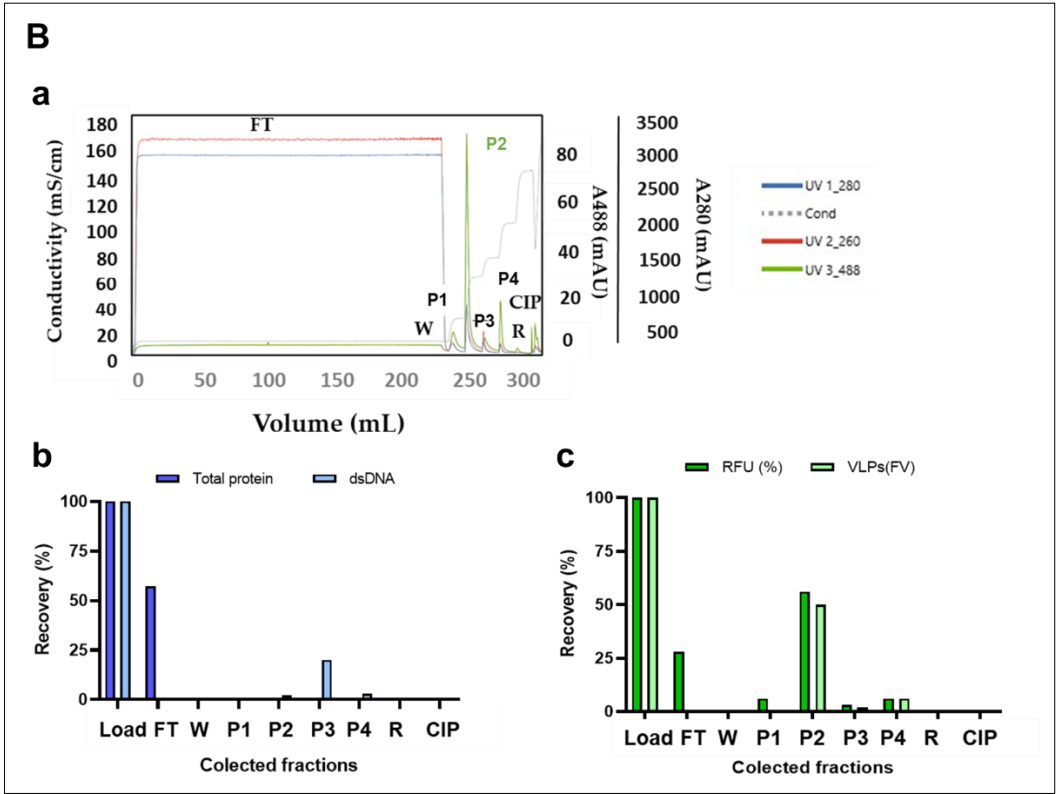
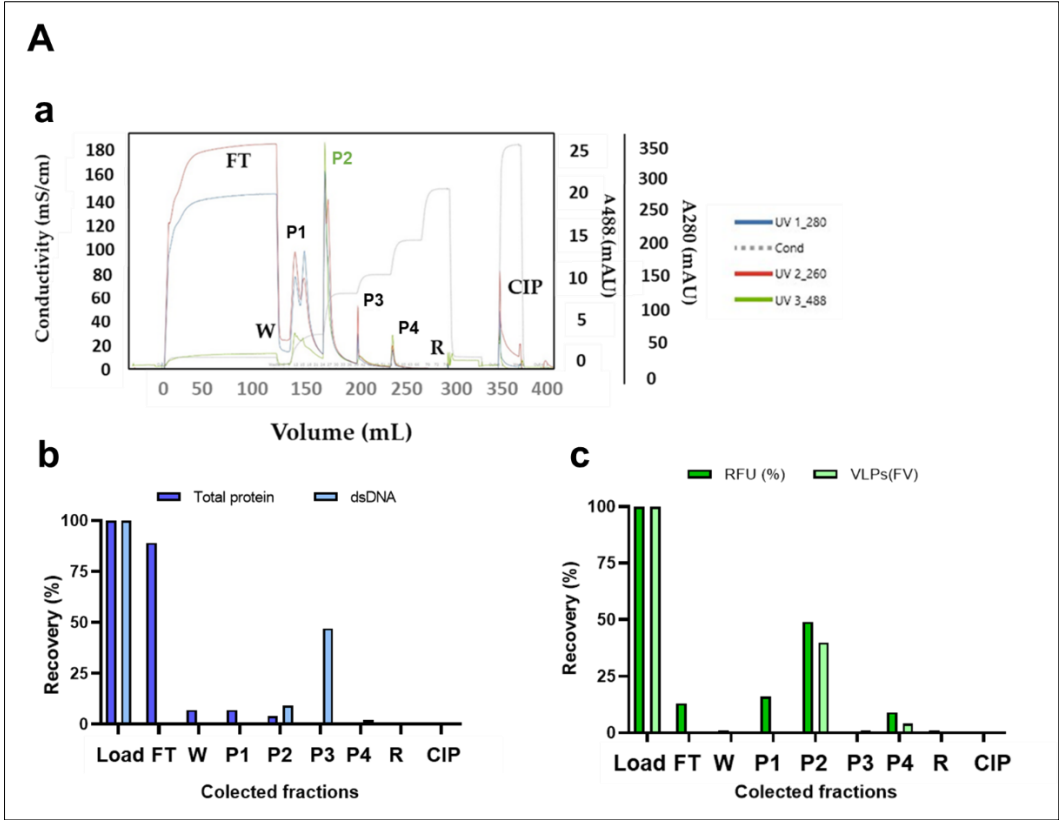
## REFERENCES

- [1] J. Fuenmayor, F. Gòdia, and L. Cervera, "Production of virus-like particles for vaccines," *New Biotechnology*, vol. 39, Elsevier B.V., pp. 174–180, Oct. 25, 2017, doi: 10.1016/j.nbt.2017.07.010.
- [2] S. Nooraei *et al.*, "Virus-like particles: preparation, immunogenicity and their roles as nanovaccines and drug nanocarriers," *J. Nanobiotechnology*, vol. 19, no. 1, pp. 1–27, 2021, doi: 10.1186/s12951-021-00806-7.
- [3] T. Vicente, A. Roldão, C. Peixoto, M. J. T. Carrondo, and P. M. Alves, "Large-scale production and purification of VLP-based vaccines," *Journal of Invertebrate Pathology*, vol. 107, no. SUPPL. Jul. 2011, doi: 10.1016/j.jip.2011.05.004.
- [4] M. Mittal, M. Banerjee, L. H. L. Lua, and A. S. Rathore, "Current status and future challenges in transitioning to continuous bioprocessing of virus-like particles," *J. Chem. Technol. Biotechnol.*, vol. 97, no. 9, pp. 2376–2385, 2022, doi: 10.1002/jctb.6821.
- [5] M. G. Moleirinho, R. J. S. Silva, P. M. Alves, M. J. T. Carrondo, and C. Peixoto, "Current challenges in biotherapeutic particles manufacturing," *Expert Opin. Biol. Ther.*, vol. 20, no. 5, pp. 451–465, 2019, doi: 10.1080/14712598.2020.1693541.
- [6] P. Kramberger, L. Urbas, and A. Štrancar, "Downstream processing and chromatography based analytical methods for production of vaccines, gene therapy vectors, and bacteriophages," *Hum. Vaccines Immunother.*, vol. 11, no. 4, pp. 1010–1021, 2015, doi: 10.1080/21645515.2015.1009817.
- [7] I. González-Domínguez, E. Lorenzo, A. Bernier, L. Cervera, F. Gòdia, and A. Kamen, "A four-step purification process for gag vlps: From culture supernatant to high-purity lyophilized particles," *Vaccines*, vol. 9, no. 10, pp. 1–19, 2021, doi: 10.3390/vaccines9101154.
- [8] J. Lavado-García, I. Jorge, L. Cervera, J. Vázquez, and F. Gòdia, "Multiplexed Quantitative Proteomic Analysis of HEK293 Provides Insights into Molecular Changes Associated with the Cell Density Effect, Transient Transfection, and Virus-Like Particle Production," *J. Proteome Res.*, vol. 19, no. 3, pp. 1085–1099, 2020, doi: 10.1021/acs.jproteome.9b00601.
- [9] V. Bandeira *et al.*, "Downstream processing of lentiviral vectors: Releasing bottlenecks," *Hum. Gene Ther. Methods*, vol. 23, no. 4, pp. 255–263, 2012, doi: 10.1089/hgtb.2012.059.
- [10] M. G. Moleirinho *et al.*, "Clinical-Grade Oncolytic Adenovirus Purification Using Polysorbate 20 as an Alternative for Cell Lysis," *Curr. Gene Ther.*, vol. 18, no. 6, pp. 366–374, 2018, doi: 10.2174/1566523218666181109141257.
- [11] L. Besnard *et al.*, "Clarification of vaccines: An overview of filter based technology trends and best practices," *Biotechnol. Adv.*, vol. 34, no. 1, pp. 1–13, Jan. 2016, doi: 10.1016/j.biotechadv.2015.11.005.
- [12] T. M. Lima, M. O. Souza, and L. R. Castilho, "Purification of flavivirus VLPs by a two-step chromatographic process," *Vaccine*, vol. 37, no. 47, pp. 7061–7069, 2019, doi: 10.1016/j.vaccine.2019.05.066.
- [13] P. Pereira Aguilar *et al.*, "Capture and purification of Human Immunodeficiency Virus-1 virus-like particles: Convective media vs porous beads," *J. Chromatogr. A*, vol. 1627, p. 461378, 2020, doi:

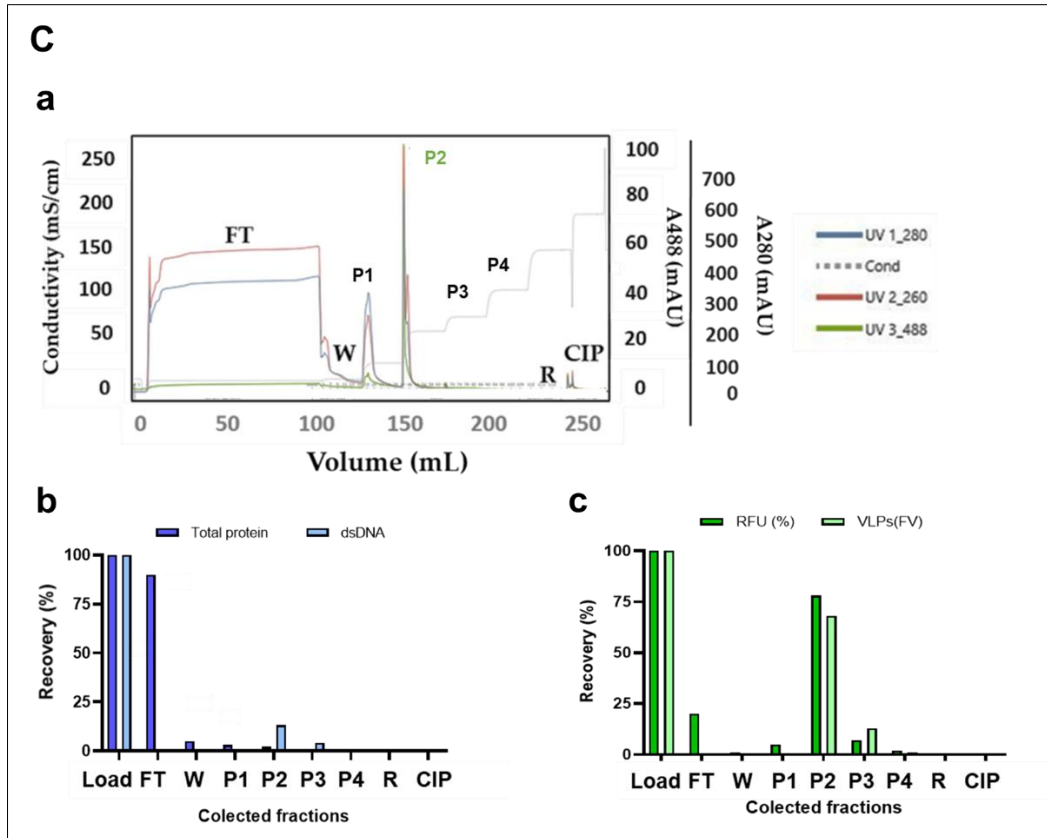
- 10.1016/j.chroma.2020.461378.
- [14] K. Reiter, P. Pereira Aguilar, D. Grammelhofer, J. Joseph, P. Steppert, and A. Jungbauer, "Separation of influenza virus-like particles from baculovirus by polymer-grafted anion exchanger," *J. Sep. Sci.*, vol. 43, no. 12, pp. 2270–2278, 2020, doi: 10.1002/jssc.201901215.
  - [15] M. Zaveckas, K. Goda, D. Ziogiene, and A. Gedvilaite, "Purification of recombinant trichodysplasia spinulosa-associated polyomavirus VP1-derived virus-like particles using chromatographic techniques," *J. Chromatogr. B Anal. Technol. Biomed. Life Sci.*, vol. 1090, no. May, pp. 7–13, 2018, doi: 10.1016/j.jchromb.2018.05.007.
  - [16] P. Steppert *et al.*, "Purification of HIV-1 gag virus-like particles and separation of other extracellular particles," *J. Chromatogr. A*, vol. 1455, pp. 93–101, Jul. 2016, doi: 10.1016/j.chroma.2016.05.053.
  - [17] P. Steppert *et al.*, "Separation of HIV-1 gag virus-like particles from vesicular particles impurities by hydroxyl-functionalized monoliths," *J. Sep. Sci.*, vol. 40, no. 4, 2017, doi: 10.1002/jssc.201600765.
  - [18] M. M. Segura, M. Mangion, B. Gaillet, and A. Garnier, "New developments in lentiviral vector design, production and purification," *Expert Opin. Biol. Ther.*, vol. 13, no. 7, pp. 987–1011, 2013, doi: 10.1517/14712598.2013.779249.
  - [19] M. Zhao, M. Vandersluis, J. Stout, U. Haupts, M. Sanders, and R. Jacquemart, "Affinity chromatography for vaccines manufacturing: Finally ready for prime time?," *Vaccine*, vol. 37, no. 36, pp. 5491–5503, 2019, doi: 10.1016/j.vaccine.2018.02.090.
  - [20] K. Reiter, P. P. Aguilar, V. Wetter, P. Steppert, A. Tover, and A. Jungbauer, "Separation of virus-like particles and extracellular vesicles by flow-through and heparin affinity chromatography," *J. Chromatogr. A*, vol. 1588, 2019, doi: 10.1016/j.chroma.2018.12.035.
  - [21] M. C. Nweke, R. G. McCartney, and D. G. Bracewell, "Mechanical characterisation of agarose-based chromatography resins for biopharmaceutical manufacture," *J. Chromatogr. A*, vol. 1530, pp. 129–137, 2017, doi: 10.1016/j.chroma.2017.11.038.
  - [22] L. Cervera, S. Gutiérrez-Granados, M. Martínez, J. Blanco, F. Gòdia, and M. M. Segura, "Generation of HIV-1 Gag VLPs by transient transfection of HEK 293 suspension cell cultures using an optimized animal-derived component free medium," *J. Biotechnol.*, vol. 166, no. 4, pp. 152–165, Jul. 2013, doi: 10.1016/j.jbiotec.2013.05.001.
  - [23] L. Cervera, J. Fuenmayor, I. González-Domínguez, S. Gutiérrez-Granados, M. M. Segura, and F. Gòdia, "Selection and optimization of transfection enhancer additives for increased virus-like particle production in HEK293 suspension cell cultures," *Appl. Microbiol. Biotechnol.*, vol. 99, no. 23, pp. 9935–9949, Dec. 2015, doi: 10.1007/s00253-015-6842-4.
  - [24] A. Venereo-Sanchez *et al.*, "Hemagglutinin and neuraminidase containing virus-like particles produced in HEK-293 suspension culture: An effective influenza vaccine candidate," *Vaccine*, vol. 34, no. 29, pp. 3371–3380, Jun. 2016, doi: 10.1016/j.vaccine.2016.04.089.
  - [25] P. Lagoutte *et al.*, "Scalable chromatography-based purification of virus-like particle carrier for epitope based influenza A vaccine produced in *Escherichia coli*," *J. Virol. Methods*, vol. 232, pp. 8–11, 2016, doi: 10.1016/j.jviromet.2016.02.011.
  - [26] P. Pereira Aguilar *et al.*, "Capture and purification of Human Immunodeficiency Virus-1 virus-like particles: Convective media vs porous beads," *J. Chromatogr. A*, vol. 1627, pp. 1–11, 2020, doi: 10.1016/j.chroma.2020.461378.
  - [27] A. Boix-Besora, E. Lorenzo, J. Lavado-García, F. Gòdia, and L. Cervera, "Optimization, Production, Purification and Characterization of HIV-1 GAG-Based Virus-like Particles Functionalized with SARS-CoV-2," *Vaccines*, vol. 10, no. 2, pp. 1–18, 2022, doi: 10.3390/vaccines10020250.
  - [28] M. G. Moleirinho, R. J. S. Silva, P. M. Alves, M. J. T. Carrondo, and C. Peixoto, "Current challenges

- in biotherapeutic particles manufacturing,” *Expert Opinion on Biological Therapy*. 2019, doi: 10.1080/14712598.2020.1693541.
- [29] K. Reiter, P. P. Aguilar, V. Wetter, P. Steppert, A. Tover, and A. Jungbauer, “Separation of virus-like particles and extracellular vesicles by flow-through and heparin affinity chromatography,” *J. Chromatogr. A*, vol. 1588, pp. 77–84, 2019, doi: 10.1016/j.chroma.2018.12.035.
- [30] S. Y. Lin, H. Y. Chiu, B. L. Chiang, and Y. C. Hu, “Development of EV71 virus-like particle purification processes,” *Vaccine*, vol. 33, no. 44, pp. 5966–5973, 2015, doi: 10.1016/j.vaccine.2015.04.077.
- [31] L. Cervera, I. Gonz Alez-Dom Inguez, M. Ia, M. Segura, and F. G. Odia, “Intracellular Characterization of Gag VLP Production by Transient Transfection of HEK 293 Cells,” doi: 10.1002/bit.26367/abstract.
- [32] J. Lavado-García, A. Díaz-Maneh, N. Canal-Paulí, P. Pérez-Rubio, F. Gòdia, and L. Cervera, “Metabolic engineering of HEK293 cells to improve transient transfection and cell budding of HIV-1 virus-like particles,” *Biotechnol. Bioeng.*, vol. 118, no. 4, pp. 1649–1663, 2021, doi: 10.1002/bit.27679.
- [33] J. Lavado-García, I. Jorge, A. Boix-Besora, J. Vázquez, F. Gòdia, and L. Cervera, “Characterization of HIV-1 virus-like particles and determination of Gag stoichiometry for different production platforms,” *Biotechnol. Bioeng.*, vol. 118, no. 7, pp. 2660–2675, 2021, doi: 10.1002/bit.27786.
- [34] S. B. Carvalho *et al.*, “Efficient filtration strategies for the clarification of influenza virus-like particles derived from insect cells,” *Sep. Purif. Technol.*, vol. 218, no. February, pp. 81–88, 2019, doi: 10.1016/j.seppur.2019.02.040.
- [35] S. B. Carvalho *et al.*, “Membrane-Based Approach for the Downstream Processing of Influenza Virus-Like Particles,” *Biotechnol. J.*, vol. 14, no. 8, Aug. 2019, doi: 10.1002/biot.201800570.
- [36] P. Pereira Aguilar *et al.*, “Polymer-grafted chromatography media for the purification of enveloped virus-like particles, exemplified with HIV-1 gag VLP,” *Vaccine*, vol. 37, no. 47, pp. 7070–7080, 2019, doi: 10.1016/j.vaccine.2019.07.001.
- [37] A. Jungbauer and R. Hahn, “Monoliths for fast bioseparation and bioconversion and their applications in biotechnology,” *J. Sep. Sci.*, vol. 27, no. 10–11, pp. 767–778, 2004, doi: 10.1002/jssc.200401812.
- [38] A. J. Valkama *et al.*, “Development of Large-Scale Downstream Processing for Lentiviral Vectors,” *Mol. Ther. Methods Clin. Dev.*, vol. 17, no. June, pp. 717–730, 2020, doi: 10.1016/j.omtm.2020.03.025.
- [39] I. Knezevic, G. Stacey, and J. Petricciani, “WHO Study Group on cell substrates for production of biologicals, Geneva, Switzerland, 11-12 June 2007,” *Biologicals*, vol. 36, no. 3, pp. 203–211, 2008, doi: 10.1016/j.biologicals.2007.11.005.
- [40] C. Ladd Effio, L. Wenger, O. Ötes, S. A. Oelmeier, R. Kneusel, and J. Hubbuch, “Downstream processing of virus-like particles: Single-stage and multi-stage aqueous two-phase extraction,” *J. Chromatogr. A*, vol. 1383, pp. 35–46, 2015, doi: 10.1016/j.chroma.2015.01.007.
- [41] C. Peixoto, M. F. Q. Sousa, A. C. Silva, M. J. T. Carrondo, and P. M. Alves, “Downstream processing of triple layered rotavirus like particles,” *J. Biotechnol.*, vol. 127, no. 3, pp. 452–461, 2007, doi: 10.1016/j.jbiotec.2006.08.002.

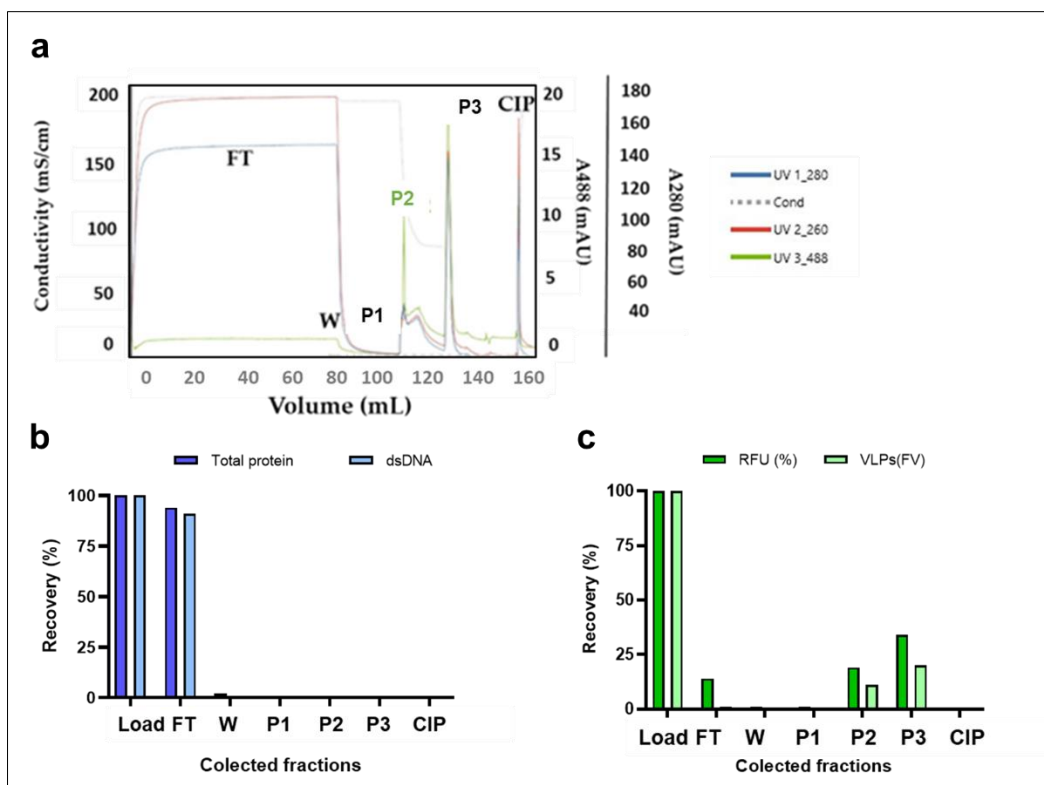
SUPPLEMENTARY MATERIALS



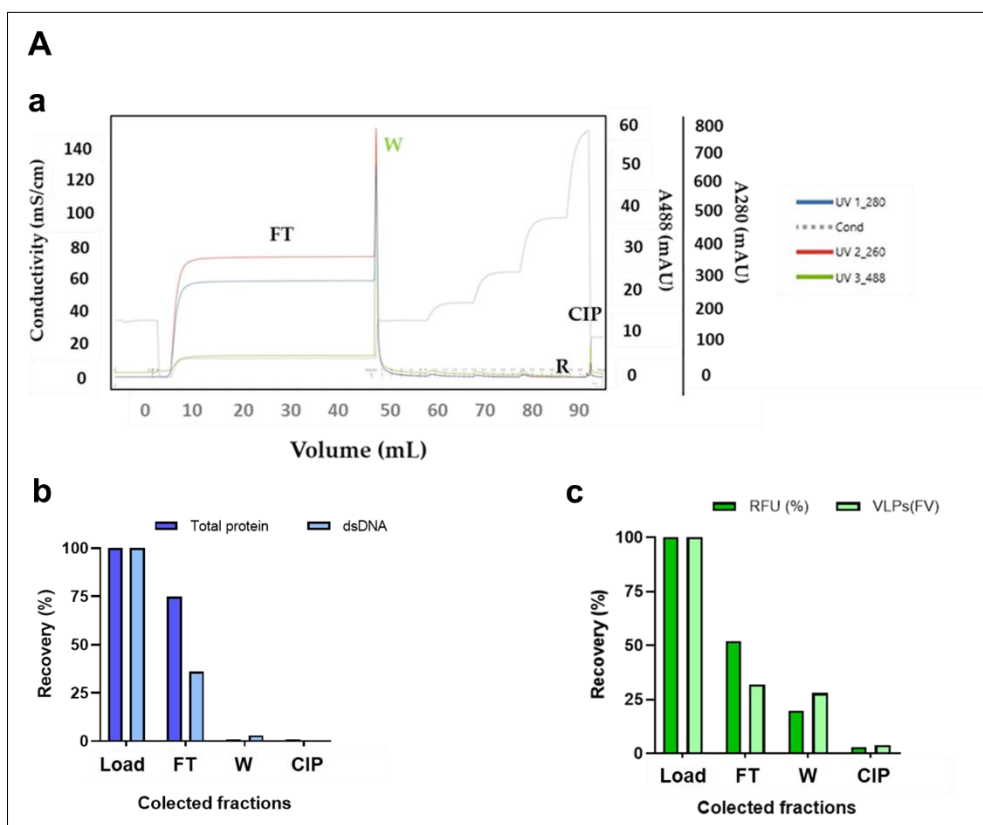


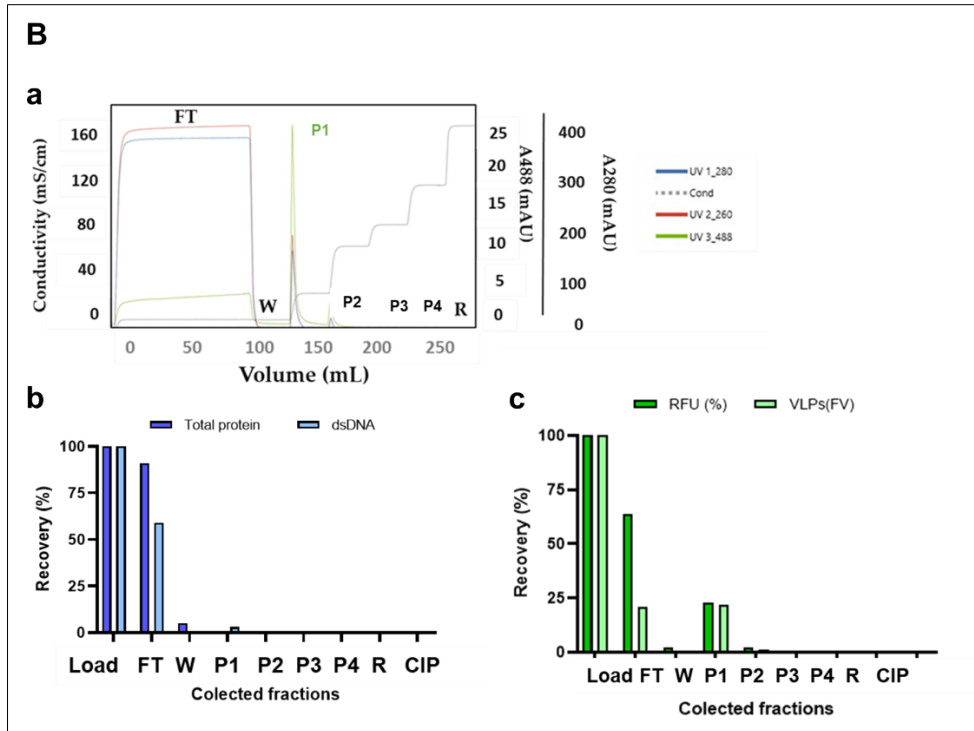


**Supplementary Material S1.** Purification of Gag::eGFP VLPs by ion exchange chromatography. **(A)** Monolith QA; **(B)** Mustang Q; **(C)** Capto Q ImpRes. **(a)** Chromatogram of the step-gradient (15%, 35%, 45%, and 65%) purification of Gag::eGFP VLP clarified supernatant; **(b)** Total protein and dsDNA content measured by BCA and picogreen respectively; **(c)** Recovery of Gag::eGFP VLP nanoparticle measured by flow virometry (VLPs) and fluorimetry (RFU). *FT*: flowthrough; *W*: wash; *P1-P4*: pooled fractions for elution peaks 1–4; *R*: Column Regeneration; *CIP*: cleaning in place; *RFU*: relative fluorescent units

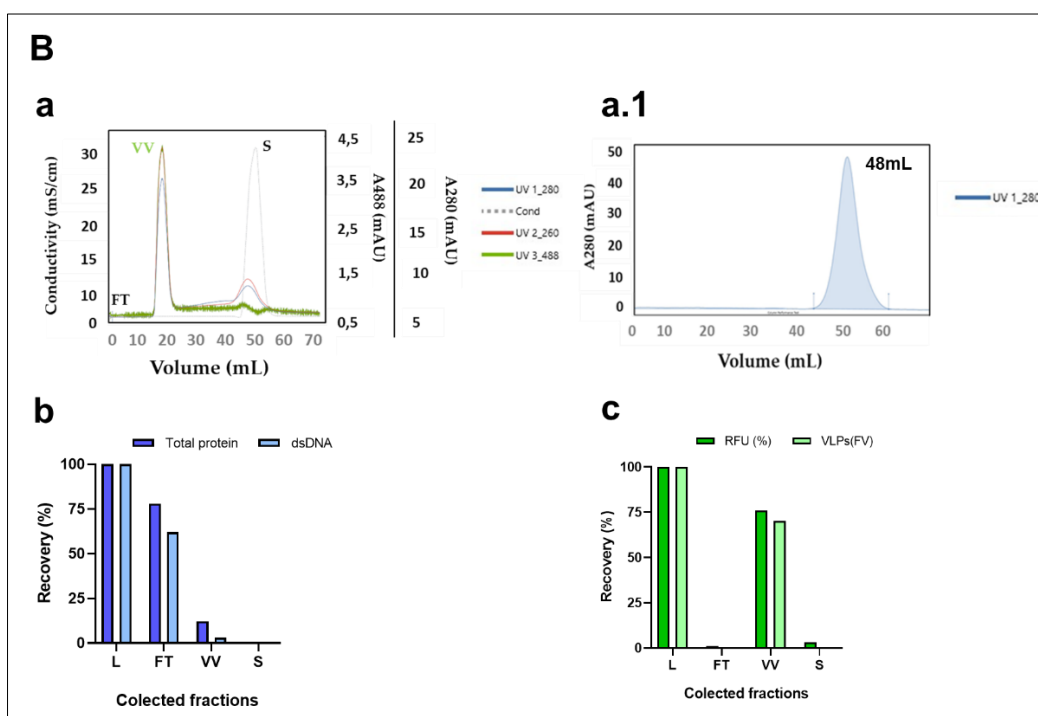
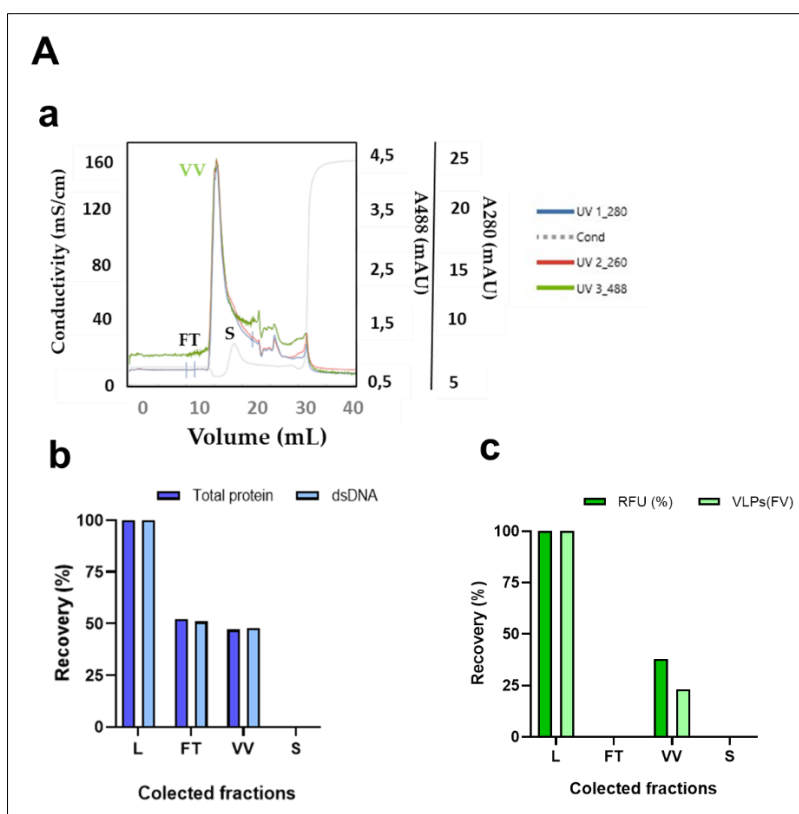


**Supplementary Material S2:** Purification of Gag::eGFP VLPs by hydrophobic interaction chromatography using Monolith OH column. **(a)** Chromatogram of the step-gradient (50%, 32.5% and 0%) purification of Gag::eGFP VLP clarified supernatant diluted 2X with 50 mM HEPES; 3M  $(\text{NH}_4)_2\text{SO}_4$ ; pH 7.2; **(b)** Total protein and dsDNA content measured by BCA and picogreen respectively; **(c)** Recovery of Gag::eGFP VLP nanoparticle measured by flow virometry (VLPs) and fluorimetry (RFU). *FT*: flowthrough; *W*: wash; *P1-P3*: pooled fractions for peaks 1–3; *CIP*: cleaning in place; *RFU*: relative fluorescent units.





**Supplementary Material S3:** Purification of Gag::eGFP VLPs by affinity chromatography using (A) Capto heparin column (B) POROS heparin. (a) Chromatogram of the step-gradient ((A):12%, 25% and 50%, (B) 15%, 35%, 45%, and 65%) purification of Gag::eGFP VLP clarified supernatant; (b) Total protein and dsDNA content measured by BCA and picogreen respectively (VLPs) and relative fluorescent units (RFU) measured by fluorimetry; (c) Recovery of Gag::eGFP VLP nanoparticle measured by flow virometry (VLPs) and fluorimetry (RFU). FT: flowthrough; W: wash; P1-P4: pooled fractions for peaks 1–4; CIP: cleaning in place; RFU: relative fluorescent units.



**Supplementary Material S4:** Purification of Gag::eGFP VLPs by size exclusion chromatography. **(A)** HiTrap® Sephadex G-25 **(B):** XK 16/40 Sepharose 4FF column. **(a)** Chromatogram of SEC from the peak 2 obtained in IEC using Mustang Q; **(b)** total protein and dsDNA content measured by BCA and picogreen respectively; **(c)** recovery of Gag::eGFP VLP nanoparticle concentration measured by flow virometry (VLPs) and fluorimetry (RFU); **(a.1)** Chromatogram of Column performance test using acetone 1%, corresponding to XK 16/40 Sepharose 4FF manual packing column FT: flowthrough; VV: void volume fraction S: Salt peak, RFU: relative fluorescent units.

## **CHAPTER TWO**

Optimizing lyophilization formulations for HIV-1 Gag VLPs: Enhancing quality and  
stability for biopharmaceutical applications

---

Submitted to *International Journal of Pharmaceutics*: Under review

## ABSTRACT

Virus-like particles (VLPs) have good potential for novel vaccine development. Particularly, HIV-1 Gag VLPs, present a robust platform for vaccine production. However, successful translation from the laboratory to biomanufacturing requires focus on formulation, with lyophilization playing a pivotal role in enhancing stability and facilitating distribution. The challenge lies in the potential damage inflicted during the lyophilization, impacting product integrity and stability. To address this, optimization of formulations and methodologies are imperative. Formulation excipients, play an important role, with cryo-lyo protectants, bulking agents, buffers, tonicity modifiers, and surfactants being commonly utilized. This work focuses on optimizing lyophilization formulation for Gag::eGFP VLPs, employing a Design of Experiments approach. The impact of five main excipients is studied, using size, concentration, and quality of the Gag::eGFP VLPs as attributes to characterize. Moreover, the impact of specific storage conditions after lyophilization is also evaluated. The lyophilized Gag::eGFP VLPs, formulated with the optimized formulation, exhibited characteristics akin to those observed in the non-lyophilized Gag::eGFP VLPs. The stability studies revealed the Gag::eGFP VLPs stored at 4°C for 4 weeks, in lyophilized or reconstituted form maintain their integrity. This investigation contributes to the stability and preservation insights of Gag::eGFP VLPs, crucial for their potential application as vaccines.

## ABBREVIATIONS

**AEC:** Anion exchange chromatography, **DLS:** Dynamic light scattering, **DoE:** Design of experiments, **EV:** Extracellular vesicle, **FV:** Flow virometry, **GFP:** Green fluorescent protein, **HEK293:** Human embryonic kidney 293, **HIV-1:** Human immunodeficiency virus I, **MWCO:** Molecular weight cutoff, **NaCl:** Sodium chloride, **NTA:** Nanoparticle tracking analysis, **PBS:** Phosphate-buffered saline, **Pdl:** Polydispersity index, **PEI:** Polyethyleneimine, **P20:** Polysorbate 20, **P80:** Polysorbate 80, **RFU:** Relative fluorescent units, **SDS-PAGE:** Sodium dodecyl sulfate polyacrylamide gel electrophoresis, **SE-HPLC:** Size exclusion-high pressure liquid chromatography, **TGE:** Transient gene expression, **TEM:** Transmission electron microscopy, **TrisHCl,** Tris hydrochloride, **TPs,** Total particles, **VLP:** Virus-like particle.

## INTRODUCTION

Virus-like particles (VLPs) have been gaining interest in the development of vaccines due to their inherent safety, high immunogenicity, and ability to mimic viral structures without containing genetic material. HIV-1 Gag VLPs, present a promising platform for vaccine production [1], [2]. However, the successful translation of VLP-based vaccines from the laboratory to biomanufacturing demands a profound attention to the formulation and stability of these complex biological entities [3], [4].

Ensuring access to vaccines worldwide is vital for effectively addressing public health challenges. However, the need for ultra-low temperature storage, as observed with the mRNA vaccine against SARS-CoV-2, which requires storage at -80°C, presents significant logistical challenges, especially in areas with scarce resources. This requirement for stringent cold chain maintenance creates obstacles to distribution, impeding equitable vaccine access [5]. Lyophilization or freeze-drying is an interesting alternative as it improves the stability, shelf life, storage, and facilitates transportation and distribution of vaccines, offering a promising solution for reaching underserved communities in underdeveloped regions, where the challenges of maintaining a cold chain are particularly acute [6], [7].

The freeze-drying process remains a challenge in viral vaccines, especially for enveloped viruses. Damage in the membranes of the nanoparticles, changes in pH or osmolarity or aggregation are some of the reported drawbacks often associated with the loss of vaccine potency [8], [9]. To minimize the negative effects of the process, it is essential to use optimized formulations and methodologies. Optimization of the formulation involves determining the optimal combination of freeze-dried excipients to preserve the viral activity during lyophilization and storage [10], [11].

Excipients are defined as substances that have been adequately evaluated for safety and are intentionally included in a drug delivery system. In general, excipients represent the majority of any formulation composition and have different functions [12], [13]. To provide a safe, efficient and high-quality pharmaceutical product, the choice of appropriate excipients is essential [14]. The most commonly used excipients in lyophilization processes can be organized in five categories, as listed in **Table 1**: cryo-lyo protectants which stabilize the product during freeze-drying and subsequent storage; bulking agents, which

enhance the product's appearance and provide adequate mechanical support; buffers, which control and stabilize the solution's pH; tonicity modifiers, which ensure the isotonicity of the reconstituted solution at the point of use; and surfactants, which reduce denaturation during freezing, prevent protein loss, and contribute to the refolding of structurally altered forms to prevent aggregation [12], [15]. Each of these classes encompasses a wide range of compounds that can be utilized at different concentrations, as described in the literature [16], resulting in numerous possible combinations. Consequently, testing all combinations for every type of excipient simultaneously poses a significant challenge.

The use of fractional factorial design of experiments allows to test a large number of factors (independent variables) simultaneously using a reduced number of experiments [17], [18], [19], [20]. In a factorial design, a predetermined series of experiments is established to combine the compounds of independent variables and analyse their impact on the dependent variables of interest through models derived from multiple linear regression. These models allow the construction of response surface graphs to describe the behaviour of the system all over the experimental domain. This is, therefore, an excellent approach to reduce the number of experiments and still obtain accurate results [21].

When dealing with VLPs, the attributes that deserve the most attention in formulation include: nanoparticles size, concentration, and presence of fragments or aggregates [22], [23], [24]. Therefore, it is essential to define an adequate analytical setup to properly analyze these characteristics. Due to the specific properties of Gag VLPs, such as its large size, complex composition and non-infectivity, the choice of applicable analytical methods remains challenging [2]. Dynamic light scattering (DLS) is commonly used as an analytical tool to investigate aggregated species in VLPs preparations [25]. On the other hand, size exclusion-high pressure liquid chromatography (SE-HPLC) is the standard analytical tool for detecting fragmentation products [26], [27], [28]. The flow virometry method, coupled to fluorescence has facilitated the specific quantification of Gag VLPs fused to GFP, among other nanoparticles, such as extracellular vesicles, present in the samples [25], [29], [30].

Hence, this work proposes the optimization of lyophilization formulation buffer for purified Gag VLPs, using a Design of Experiments (DoE) approach. Specifically, a fractional factorial design was applied to study the effect of different combinations of the five excipients mentioned above on size, concentration, and quality of



the VLPs of interest. The work presented expands the knowledge on the VLPs lyophilization process and establishes techniques for the routine evaluation of VLP quality. This comprehensive investigation aims to provide insights into the stability and preservation of Gag VLPs, crucial for their potential application in vaccine development.

## **MATERIALS AND METHODS**

### **Cell line and culture conditions**

HEK293SF-3F6 cells, kindly provided by Dr. Amine Kamen from National Research Council (NRC) (Montreal, QC, Canada), were cultured in HyCell TransFx-H™ (Hyclone, Road Logan, UT, USA) medium supplemented with 2% GlutaMAX™ (Gibco, Thermo Fisher Scientific, Waltham, MA, USA) and 0.1% Pluronic™ (Gibco, Life Technologies, Thermo Fisher Scientific). Cells were routinely maintained in disposable polycarbonate Erlenmeyer flasks (Corning, Steuben, NY, USA), and incubated at 37°C, 5% of CO<sub>2</sub>, 85% relative humidity, and 130 rpm in a Kuhner shaker LT-X (Kuhner, Birsfelden, Switzerland). Cell quantification and viability were determined by the automated cell counter NucleoCounter® NC-3000™ (Chemometec, Allerød, Denmark).

### **VLP production by transient transfection**

HEK293SF-3F6 cells were transfected at  $1.8\text{--}2\cdot 10^6$  cells/mL, and viability greater than 90% as previously described [31]. In essence, the DNA at a final concentration of 1 µg/mL was added into fresh culture medium and vortexed for 10 seconds. The transfection reagent PEIpro® (Polyplus-transfection SA, Illkirch-Graffenstaden, France) at a DNA:PEI ratio of 1:2 w/w was then added. The mix was vortexed three times for three seconds and incubated for 15 minutes at room temperature. Lastly, formed complexes were added into the cell culture. Culture was stopped at 72 hpt to maximize VLP yields. The plasmid used in the transfection, encoded the HIV-1 Gag polyprotein linked in-frame with the eGFP under the same CMV enhancer and CMV promoter, hereafter noted as Gag::eGFP VLPs. More details were described by A. Venereo-Sanchez et al (2016) [32]. To measure the transfection efficiency, the percentage of GFP-positive cells was assessed using a BD FACS Canto II flow cytometer (BD Biosciences, San Jose, CA, USA).

### **Gag::eGFP VLP purification process**

Cell culture supernatant (1250mL) was clarified with Supracap™ 50V100™ depth filter capsules (Pall Corporation, New York, NY, USA). The filter was preequilibrated with phosphate-buffered saline (PBS) 1X at pH 7.5 before filtration. Then, the clarified supernatant was loaded into a 4.7mL prepacked HiScreen™ Capto Q™ ImpRes (Cytiva, Uppsala, Sweden) automatically operated in an AKTA Pure system (Cytiva, Uppsala, Sweden). The purification protocol was deeply described in chapter one [30].

### **Optimization of lyophilization formulation buffer using DoE**

Lyophilization formulation buffer was optimized to achieve Gag::eGFP VLPs with the desired characteristics post-lyophilization. A methodology based on Design of Experiments (DoE) was applied. The optimization experiments for the formulation buffer were conducted using a comparative fractional factorial approach to examine the impact of five key factors (independent variables, refer to the five types of excipients) involving various compounds on three dependent variables (considered the responses in the DoE): size, concentration, and quality. The concentration was quantified as the recovery percentage, while the quality was assessed based on the similarity percentage of the SE-HPLC profile of the Gag::eGFP VLPs following a lyophilization process, relative to purified Gag::eGFP VLP material. The similarity percentage of the SE-HPLC profile is determined by comparing the retention times and peak areas of the analysed profiles. Details of all formulation factors, with their corresponding compounds and final concentration used are shown in **Table 1**. The selected compounds of each factor were defined from data available in the literature. In short, the fractional factorial experiment with resolution IV, comprising 64 combinations as outlined in **Table 2**, was generated from a full factorial experiment consisting of 128 combinations by choosing an alias structure. The alias structure determines which effects are confounded with others [33]. The design was constructed using R software (R Development Core Team, Vienna, Austria).

### **Sample preparation and lyophilization process**

Sample preparation and lyophilization process for fractional factorial optimization, validation and stability studies were carried out as detailed here. A volume of 100uL of purified Gag::eGFP VLPs was aliquoted in 1 mL glass vials (Scharlau, Sentmenat, Barcelona, Spain) for their lyophilization. The purified Gag::eGFP

VLPs were previously buffer exchanged into designated lyophilization formulation using Zebaspin columns MWCO 7K, 0.5 ml (Life Technologies S.A, Thermo Fisher Scientific). Aliquots were frozen at -80°C and subsequently lyophilized at -60°C at 100  $\mu$ bar [24] for 48h in a Coolvacuum, Lyomicron (Granollers, Barcelona, Spain). Lyophilized samples were reconstituted in PBS 1X prior to analysis. Particle size, concentration, and quality were assessed using DLS, flow virometry, and SE-HPLC, respectively.

**Table 1:** List of the 5 factors with the corresponding compounds tested during the experiment

Independent variables		Final concentration		References	Functions
Factors	Compounds	% (w/v)	mM		
<b>Cryo-Lyo protectants</b>	Sucrose		500	Sigma, St. Louis, MO, USA [34]	Stabilize the product during the freeze-drying and storage processes
	Mannitol	4.4		Sigma, St. Louis, MO, USA [26]	
	Sorbitol	40		Sigma, St. Louis, MO, USA [23], [35]	
	Trehalose	15		Sigma, St. Louis, MO, USA [36]	
<b>Bulking agents</b>	Arginine	5		PanReac AppliChem, Barcelona, Spain [16], [37], [38]	Enhance the appearance of the product and provide adequate mechanical support
	Glycine	5		Sigma, St. Louis, MO, USA [22]	
<b>Buffers</b>	Sodium citrate		100	Sigma, St. Louis, MO, USA [39]	Control and stabilize the pH of the solution
	Sodium phosphate		20	Sigma, St. Louis, MO, USA [26]	
	TrisHCl		10	Invitrogen, Carlsbad, USA [40], [41]	
	Histidine		10	Thermo Scientific Waltham, MA, USA [37], [42]	
<b>Tonicity modifiers</b>	NaCl		75	Sigma, St. Louis, MO, USA [42]	Ensure the isotonicity of the reconstituted solution at the point of use
	Dextrose	5		Thermo Scientific Waltham, MA, USA [22]	
<b>Surfactants</b>	P 20	0.05		Thermo Scientific Waltham, MA, USA [23], [35]	Reduce denaturation during freezing. Prevent protein loss. Aid in refolding of structurally altered forms preventing aggregation
	P80	0.02		Sigma, St. Louis, MO, USA [37]	

The ingredients of each formulation were dissolved in PBS 1X (pH 7.20–7.5); *NaCl*: Sodium chloride, *TrisHCl*: Tris hydrochloride; *P20*: Polysorbate 20; *P80*: Polysorbate 80

### Storage stability studies

After the lyophilization process, dried samples were stored at 4°C, 25°C, and 37°C. Additionally, reconstituted samples were preserved at 4°C, 25°C, and -80°C for a duration of up to 8 weeks. The subsequent analyses were conducted at two distinct time points, 4- and 8-weeks post-storage. The evaluation of Gag::eGFP VLPs encompassed different analytical techniques. DLS for size determination, flow virometry to ascertain concentration, and SE-HPLC profile for evaluating quality. The measurement of each characteristic was quantified as a percentage relative to the purified Gag::eGFP VLP material.

**Table 2:** Matrix of the 64 different combinations tested during the DoE experiment. The first column corresponds to the number of the combinations tested, then the next 5 columns correspond to the 5 factors (independent variables with their respective compounds and the last 3 columns correspond to the 3 dependent variables studied.

Independent Variables					Dependent Variables (Responses)			
FB	CryoLyoprotectant	Bulking	Buffer	Tonicity	Surfactant	Size	Conc.	Quality
<b>SM</b>		<b>Purified Gag::eGFP VLPs in PBS1X</b>				<b>156.4</b>	<b>100</b>	<b>100</b>
1	Sorbitol	Arginine	Sodium citrate	NaCl	P20	143.6	71.84	56.36
2	Trehalose	Arginine	Sodium citrate	NaCl	P20	138.3	61.17	71.72
3	Sucrose	Glycine	Sodium citrate	NaCl	P20	388.8	1.63	9.04
4	Sorbitol	Glycine	Sodium citrate	NaCl	P20	1039	1.40	6.42
5	Mannitol	Arginine	Sodium phosphate	NaCl	P20	137.3	50.51	72.46
6	Trehalose	Arginine	Sodium phosphate	NaCl	P20	142.6	47.70	71.85
7	Sucrose	Glycine	Sodium phosphate	NaCl	P20	136.8	80.16	71.33
8	Trehalose	Glycine	Sodium phosphate	NaCl	P20	155	65.26	59.53
9	Sucrose	Arginine	TrisHCl	NaCl	P20	155.8	69.66	92.53
10	Sorbitol	Arginine	TrisHCl	NaCl	P20	237.1	32.87	60.54
11	Sucrose	Glycine	TrisHCl	NaCl	P20	166.7	70.69	82.08
12	Mannitol	Glycine	TrisHCl	NaCl	P20	140.9	58.62	88.78
13	Trehalose	Arginine	Histidine	NaCl	P20	158.9	70.39	72.83
14	Mannitol	Glycine	Histidine	NaCl	P20	169.2	75.75	90.54
15	Sorbitol	Glycine	Histidine	NaCl	P20	144.4	69.01	72.03
16	Trehalose	Glycine	Histidine	NaCl	P20	147.3	95.55	81.65
17	Mannitol	Arginine	Sodium citrate	Dextrose	P20	148.2	54.91	98.32
18	Sorbitol	Arginine	Sodium citrate	Dextrose	P20	122.4	39.92	75.44
19	Sucrose	Glycine	Sodium citrate	Dextrose	P20	388.8	1.20	9.72
20	Mannitol	Glycine	Sodium citrate	Dextrose	P20	1189	0.37	4.23
21	Sucrose	Arginine	Sodium phosphate	Dextrose	P20	176.4	38.04	98.07
22	Mannitol	Arginine	Sodium phosphate	Dextrose	P20	204.6	43.73	107.21
23	Sorbitol	Glycine	Sodium phosphate	Dextrose	P20	144.1	32.54	76.49
24	Trehalose	Glycine	Sodium phosphate	Dextrose	P20	241.7	44.59	84.06
25	Sucrose	Arginine	TrisHCl	Dextrose	P20	149	79.21	92.76
26	Mannitol	Arginine	TrisHCl	Dextrose	P20	220.6	100.00	99.55
27	Trehalose	Arginine	TrisHCl	Dextrose	P20	227.4	51.40	86.79
28	Trehalose	Glycine	TrisHCl	Dextrose	P20	170.4	83.23	89.75
29	Sucrose	Arginine	Histidine	Dextrose	P20	131.5	70.71	92.96
30	Sorbitol	Arginine	Histidine	Dextrose	P20	150.4	72.05	71.01
31	Mannitol	Glycine	Histidine	Dextrose	P20	213.9	100.00	88.76
32	Sorbitol	Glycine	Histidine	Dextrose	P20	114.1	75.04	67.03
33	Sucrose	Arginine	Sodium citrate	NaCl	P80	148.4	86.96	87.33
34	Trehalose	Arginine	Sodium citrate	NaCl	P80	160.6	84.98	90.66
35	Sucrose	Glycine	Sodium citrate	NaCl	P80	347.4	3.46	7.79
36	Mannitol	Glycine	Sodium citrate	NaCl	P80	490.4	1.00	9.58
37	Mannitol	Arginine	Sodium phosphate	NaCl	P80	149.3	79.27	94.76
38	Trehalose	Arginine	Sodium phosphate	NaCl	P80	160.5	100.00	97.98
39	Sucrose	Glycine	Sodium phosphate	NaCl	P80	127.6	82.78	82.07
40	Sorbitol	Glycine	Sodium phosphate	NaCl	P80	213.6	71.74	70.24
41	Mannitol	Arginine	TrisHCl	NaCl	P80	121.4	93.16	108.30
42	Sorbitol	Arginine	TrisHCl	NaCl	P80	175.1	100.00	88.41
43	Sorbitol	Glycine	TrisHCl	NaCl	P80	142.5	66.49	77.63
44	Trehalose	Glycine	TrisHCl	NaCl	P80	148.7	100.00	90.48

45	Sucrose	Arginine	Histidine	NaCl	P80	131.2	93.59	70.67
46	Sorbitol	Arginine	Histidine	NaCl	P80	185	100.00	87.62
47	Trehalose	Arginine	Histidine	NaCl	P80	125.4	46.84	96.91
48	Mannitol	Glycine	Histidine	NaCl	P80	164.1	75.24	82.03
49	Sorbitol	Arginine	Sodium citrate	Dextrose	P80	233.2	85.32	80.60
50	Trehalose	Arginine	Sodium citrate	Dextrose	P80	184.8	100.00	92.94
51	Mannitol	Glycine	Sodium citrate	Dextrose	P80	408	3.40	6.76
52	Trehalose	Glycine	Sodium citrate	Dextrose	P80	611.7	1.36	9.48
53	Sucrose	Arginine	Sodium phosphate	Dextrose	P80	131.5	77.65	92.85
54	Sorbitol	Arginine	Sodium phosphate	Dextrose	P80	160.1	88.39	67.01
55	Mannitol	Glycine	Sodium phosphate	Dextrose	P80	151.8	1.66	85.80
56	Sorbitol	Glycine	Sodium phosphate	Dextrose	P80	145.7	45.45	65.67
57	Mannitol	Arginine	TrisHCl	Dextrose	P80	132.6	61.72	97.22
58	Sucrose	Glycine	TrisHCl	Dextrose	P80	162.4	100.00	85.92
59	Sorbitol	Glycine	TrisHCl	Dextrose	P80	138.2	49.96	63.42
60	Trehalose	Glycine	TrisHCl	Dextrose	P80	141.6	100.00	59.33
61	Sucrose	Arginine	Histidine	Dextrose	P80	168.3	79.67	94.01
62	Mannitol	Arginine	Histidine	Dextrose	P80	149.1	89.86	95.55
63	Sucrose	Glycine	Histidine	Dextrose	P80	128.8	92.48	84.06
64	Trehalose	Glycine	Histidine	Dextrose	P80	2629	94.91	86.45

FB: formulation buffers, Size: diameter (nm), Conc: Recovery (%) of VLP concentration, Quality: SE-HPLC profile similarity (%), SM: Starting material; NaCl: Sodium chloride; TrisHCl: Tris hydrochloride; P20: Polysorbate 20; P80: Polysorbate 80

#### Gag::eGFP VLP quantification – Fluorimetry

The fluorescence intensity was measured in a Cary Eclipse Fluorescence Spectrophotometer (Agilent Technologies, Santa Clara, CA, USA) to determine the concentration of Gag::eGFP VLPs. The settings were:  $\lambda_{excitation}$  = 488 nm (slit = 5 nm) and  $\lambda_{emission}$  = 510 nm (slit = 10 nm). The relative fluorescence unit (RFU) values were calculated by subtracting the obtained fluorescence intensity (FU) values from the non-transfected negative control samples. An in-house developed and validated quantification assay was used to convert RFU values to Gag::eGFP concentration values [31], [43].

#### Gag::eGFP VLP quantification – Flow Virometry (FV)

Concentration of Gag::eGFP fluorescent events was quantified using a CytoFLEX LX (Beckman Coulter, Brea, CA, USA), equipped with a 405 nm filter. The VLPs were detected based on violet side scatter (V-SSC) and FITC fluorescence signals. Laser gains were optimized with values set to 72 for forward scatter (FSC), 135 for side scatter (SSC), 9 for V-SSC, and 500 for FITC. Samples were diluted with PBS 1X until an abort rate value below 2% was achieved. A total of 300,000 events were analysed at a flow rate of 10  $\mu$ L/min per sample. VSSC-H vs B525-FITC density plots were used to gate the different particle populations.

Gating was adjusted manually for each channel. Events after 50 s were taken for analysis. The results were normalized employing an internal control. The results were analysed with CytExpert v.2.3 software (Beckman Coulter, Brea, CA, USA).

#### **Gag::eGFP VLP and Extracellular Vesicle (EV) quantification – Nanoparticle Tracking Analysis (NTA)**

Nanoparticle tracking analysis (NTA) was used to determine particle size distribution and particle concentration. NanoSight® NS300 device (Malvern Panalytical, Malvern, United Kingdom) equipped with a blue laser module (488 nm) to quantify HIV-1 Gag::eGFP VLPs, and a neutral density filter for total particle quantification by light scattering. Samples were serially diluted in particle-free water to achieve a concentration of 20-80 particles per video frame (corresponding to the instrument's linear range). For the injected samples, 3 replicates of each dilution were measured at 22°C, with a viscosity of 0,9 cP, and 3 videos of 60 seconds length were acquired. Capture settings were recorded with an sCMOS camera, setting the screen gain to 1, manually adjusting the camera level before each measurement (eight for samples containing Gag::eGFP VLPs and 11 for controls), and setting a detection threshold of 4. The remaining analysis parameters were automatically selected by the software and kept constants for all samples. Data was acquired and processed with the NanoSight NTA software version 3.2. The data obtained from these analyses were also used to calculate the percentage of Gag::eGFP VLPs relative to the total nanoparticles in the measured samples

#### **Western Blot and SDS-PAGE**

40 µL of sample were mixed with 20 µL of 4x LDS Sample Buffer and 7 µL of 2M DTT, followed by 20 minutes incubation at 96°C. The prepared samples were stored at 4°C until applied. 20 µL of each sample were loaded onto precast NuPAGE Bis/Tris gels 4–12% (Invitrogen, Carlsbad, CA, USA). 5 µL of SeeBlue® Plus2 Pre-stained Protein Standard (Invitrogen, Carlsbad, CA, USA) was used as low molecular weight control. Gels were run at 200V, 400mA for 45 minutes in MES-SDS running buffer. For SDS-PAGE gels, proteins were stained with Coomassie Brilliant Blue G-250 based EZBlue™ Gel Staining Reagent (Sigma Aldrich, St. Louis, MO, USA). For Western blot analysis, proteins were transferred onto 0,2 µm nitrocellulose membranes using the Trans-Blot® turbo system (Bio-Rad Laboratories, Hercules, CA, USA). Membranes

were blocked with PBS 5% (w/v) non-fat dry milk for 30 minutes, washed with PBS 0.1% (w/v) Tween-20, and then incubated overnight at 4°C with the primary monoclonal antibody against HIV-1 p24 (dilution 1:2000 in PBS) (A2-851-500 Icosagen AS, Tartumaa, Estonia). After washing, product immunodetection was performed with an anti-mouse IgG antibody conjugated with a horseradish peroxidase (dilution 1:5000 in PBS 1X) (#1706516 Bio-Rad Laboratories, Hercules, CA, USA), incubated 2 hours at room temperature, and washed with PBS 0.1% (w/v) Tween-20. Protein bands were visualized by incubating the membranes with a Clarity™ Western ECL Substrate solutions for 2–3 minutes and scans were taken in a ChemiDoc MP (Bio-Rad Laboratories, Hercules, CA, USA).

### **Dynamic Light Scattering**

The dynamic light scattering (DLS) technique was used to determine the size of Gag::eGFP VLPs. The measurements were carried out at 25°C in a Zetasizer Nano ZS instrument (Malvern Instruments, Malvern, UK), equipped with a He/Ne 633 nm laser at 173°. 100 µL of the sample diluted 1:200 was placed in disposable plastic cuvettes. Three consecutive measurements of each sample with 10-15 scans of 10 seconds were performed for each independent measurement. The hydrodynamic diameter (MHD), particle size distribution in volume, derived count rate, and polydispersity index (PDI) average results were automatically obtained.

### **SE-HPLC analysis**

High-pressure liquid chromatography (HPLC) analyses were conducted with an Agilent 1100 Series HPLC System (Agilent Technologies, Santa Clara, CA, USA) equipped with a SEC 300A 2.7µm (7.8x50mm) Guard and a SEC 300A 2.7µm (7.8x300mm) columns (Agilent Technologies) at Servei d'Anàlisi Química (SAQ, UAB, Barcelona, Spain). The mobile phase was composed of 150 mM sodium phosphate (pH 7.0). The analytics were performed at a flow rate of 1 mL/min with UV detection at 220 nm. Samples were directly plunged (25µL) provided column equilibration. Recorded signal from PBS and elution buffer as blanks were taken.

### **Gag::eGFP VLPs visualization by Cryo-TEM**

The morphology and electron density of Gag::eGFP VLPs were investigated under cryogenic conditions. Samples were rapidly frozen by plunging them into liquid ethane at a temperature of -180°C. Approximately 2 µL of sample were then applied to holey carbon grids that had been pre-treated with glow discharge using a PELCO easiGlow discharger unit. The cryo-frozen samples were transferred to a Leica EM GP cryo workstation and subsequently examined using a JEM-2011 electron microscope (JEOL Ltd., Tokyo, Japan) operating at an acceleration voltage of 200kV. Throughout the imaging process, the temperature was maintained at -180°C by the continuous addition of liquid ethane. Images were captured using a CCD-multiscan camera (Gatan Inc., Pleasanton, CA, USA) for further analysis and characterization.

### **Statistical analysis of the DoE**

Analysis of variance (ANOVA) was used to test the model significance by means of F tests. Model was considered significant if the obtained mean square was statistically greater than the residual mean squares, indicating that the variation in the dependent variable was indeed caused by the variations of the independent variables [18], [44]. Response scatterplot graphs were built to describe the behaviour of the responses over the experimental domain. The half-normal plot of the effects was used [21] to select the significant factors that influence on the size, concentration, and quality of Gag::eGFP VLPs. Design Expert software (StatEase, Minneapolis) v 13 was used to analyse the data and build the graphs.

## **RESULTS AND DISCUSSION**

### **Purification process of Gag::eGFP VLPs**

The Gag::eGFP VLP material used in the formulation's optimization experiments for the lyophilization process was obtained from a batch production of 1254 mL by transient transfection and its subsequent purification. First, clarification of the supernatant produced was performed. After two hours of sedimentation, the harvested media was subjected to primary clarification using Supracap™ 50V100 depth filter for the removal of cell debris, intact cells, aggregates, impurities, and other contaminating particulate materials from the harvested product. This process resulted in a 75% recovery of Gag::eGFP VLPs and a 33% enrichment in respect to the total nanoparticles presents in the clarified material (**Table 3**). It has been previously



demonstrated that clarification of VLPs based on nominal filtration processes can reach recovery yields of around 80%, which is consistent with the obtained results [30], [45].

The next step was capture with the HiScreen Capto Q ImpRes column. The capture step consisted of an anion exchange chromatography (AEC) to separate molecules based on their net surface charge, concentrating the desired VLPs while decreasing the contaminants' content. As the ion concentration was changed in different steps, the expected elution peaks were observed in the chromatograms at 488 nm absorbance (**Figure 1A**). Absorbance at 488 nm is caused by Gag::eGFP proteins, which allow monitoring Gag::eGFP VLPs presence at the different stages of the process. The fractions obtained during the process were collected and analyzed. The second step in the elution phase fraction (named P2) was considered the main product fraction due to the higher Gag::eGFP VLP concentration according to flow virometry and fluorimetry results (**Figure 1B**). Biochemical analyses confirmed Gag::eGFP polyprotein presence in all collected fractions (~87 kDa) by means of SDS-PAGE and Western blot anti-p24 (**Figure 1C**). To evaluate the purity and the recovery percentage, fraction P2 was analyzed by NTA. According to the results, P2 fraction contained  $2.53 \times 10^{11}$  Gag::eGFP VLPs/mL, which represents almost 30 % of recovery respect to the clarified sample with a purity of 60% (**Table 3**). This represents a VLP concentration of 26-fold and volume reduction of 125-fold compared to crude supernatants.

**Table 3:** Data collection for the purification of Gag::eGFP VLPs for the lyophilization experiments

Gag::eGFP VLPs Recovery and Purity					
Sample	Volume (mL)	Gag::eGFP VLPs/mL (by NTA)	Step Recovery (%)	Purity (%) (VLPs/Total Particle)	Enrichment (%) (VLPs/Total Particle)
Harvest	1254	$9.74 \cdot 10^9$	100	25	-
Clarified	1200	$7.29 \cdot 10^9$	75	58	33
P2	10	$2.53 \cdot 10^{11}$	29	60	2

P2: Gag::eGFP VLPs from elution peak 2 of Capto Q chromatography

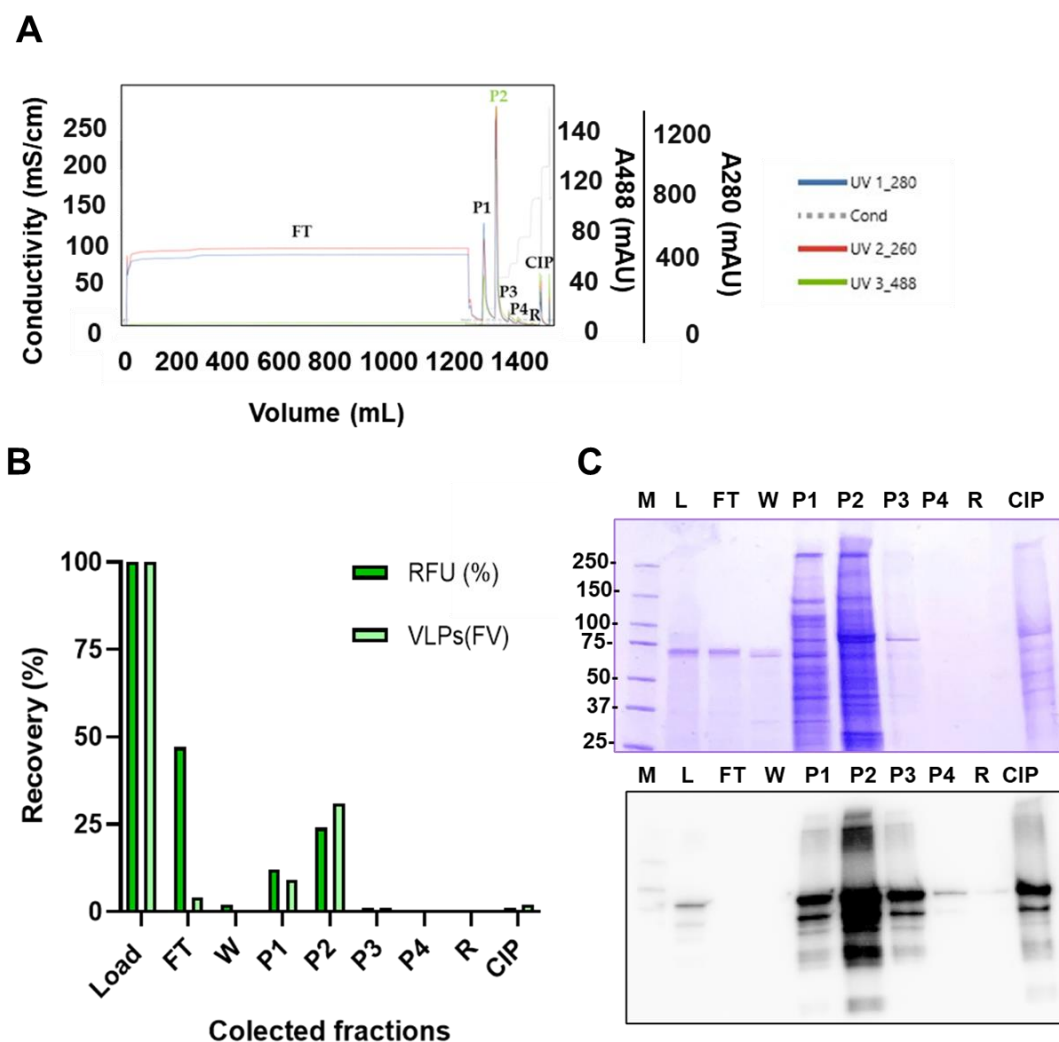


**Figure 1.** Purification data corresponding to Gag::eGFP VLPs. **A)** Chromatogram of the step-gradient (15%, 35%, 45%, and 65%) purification of Gag::eGFP VLPs clarified supernatant by Capto Q ImpRes column; **B)** Gag::eGFP VLPs quantified through flow virometry (VLP) and relative fluorescent units (RFU), recovery percentages (%). **C)** SDS-PAGE and p24 Western blot of purification run. SDS-PAGE, sodium dodecyl sulfate polyacrylamide gel electrophoresis; FV, flow virometry; M, molecular weight standard; L, sample loaded into the column (clarified material); FT: flowthrough; W: wash; P1-P4: pooled fractions for elution peaks 1–4; R: Column Regeneration and CIP: cleaning in place.

### Characterization of purified Gag::eGFP VLPs

Molecular, biophysical, and biological characterization of purified VLPs plays an essential role in the development of VLP-based vaccines allowing for the assessment of functionality, quality and stability of the product [3]. In this context, the concentrated and purified Gag::eGFP-VLPs from the P2 fraction were further processed by exchanging the buffer to PBS1X using Zebaspin columns, resulting in the material designated as P2.1 with a concentration of  $2.01 \times 10^{11}$  Gag::eGFP-VLPs/mL. The resulting nanoparticles were stored at  $-80^{\circ}\text{C}$  until further analysis to determine size, SE-HPLC profile, and shape.

DLS is recognized as the standard analytical technique for determining size and aggregation pattern of VLPs [2], [28]. Analysis of the particle size distribution (PSD) of the P2.1 material revealed a mean hydrodynamic diameter of  $156.4 \pm 0.98$  nm, with a low polydispersity index (Pdl) of 0.26 (**Figure 2A**). The obtained profile indicates a homogeneous sample free of aggregates. These results are consistent with the expected profile for purified Gag::eGFP VLPs [24], [30], [46].

SE-HPLC provide a simple, rapid, and versatile alternative method for quality control of VLPs-based vaccines [27]. This technique plays a significant role in monitoring the stability and degradation pattern of biopharmaceuticals [26], [28]. The SE-HPLC profile of P2.1 material, along with a PBS1X blank, and an elution buffer blank, are presented in **Figure 2B**. The chromatogram corresponding to the P2.1 material displays several peaks. Each peak corresponds to a specific retention time, indicating that the components interact differently with the chromatography column due to variations in molecular size, shape, or surface properties. Monitoring changes in the number and area of these peaks can serve as a measure for quality control, indicating that retention times and peak areas are critical for characterizing sample quality. The presence of these peaks could represent various components of the P2.1 material, each contributing to a comprehensive understanding of the material's composition. The retention time of peak 9 in P2.1 material aligns with the singular peak observed in the elution buffer blank sample. This suggests that this peak may be attributed to buffer components such as salts and HEPES, which may persist in the P2 material after the buffer exchange step. As expected, the PBS1X buffer does not give any signal.

On the other hand, fundamental insights in VLP morphology and shape are acquired through standard laboratory techniques including transmission electron microscopy (TEM). Although relatively simple, TEM sample preparation can cause VLP deformation. Alternative visualization techniques, such as Cryo-TEM, are less likely to cause structural deformation due to rapid freezing during sample processing [47]. This technique has been applied for the characterization of Gag VLPs produced in different production platforms [25], [43], [48]. **Figure 2C** shows a cryo-TEM micrograph of P2.1 where abundant Gag::eGFP VLPs can be observed as spherical electron-dense nanoparticles surrounded by a lipid membrane. Similar results have been previously obtained for purified Gag::eGFP VLPs samples [30]. For subsequent analyses of

lyophilization experiments, purified Gag::eGFP VLPs from P2.1 will serve as the non-lyophilized reference sample, hereafter referred to as starting material.

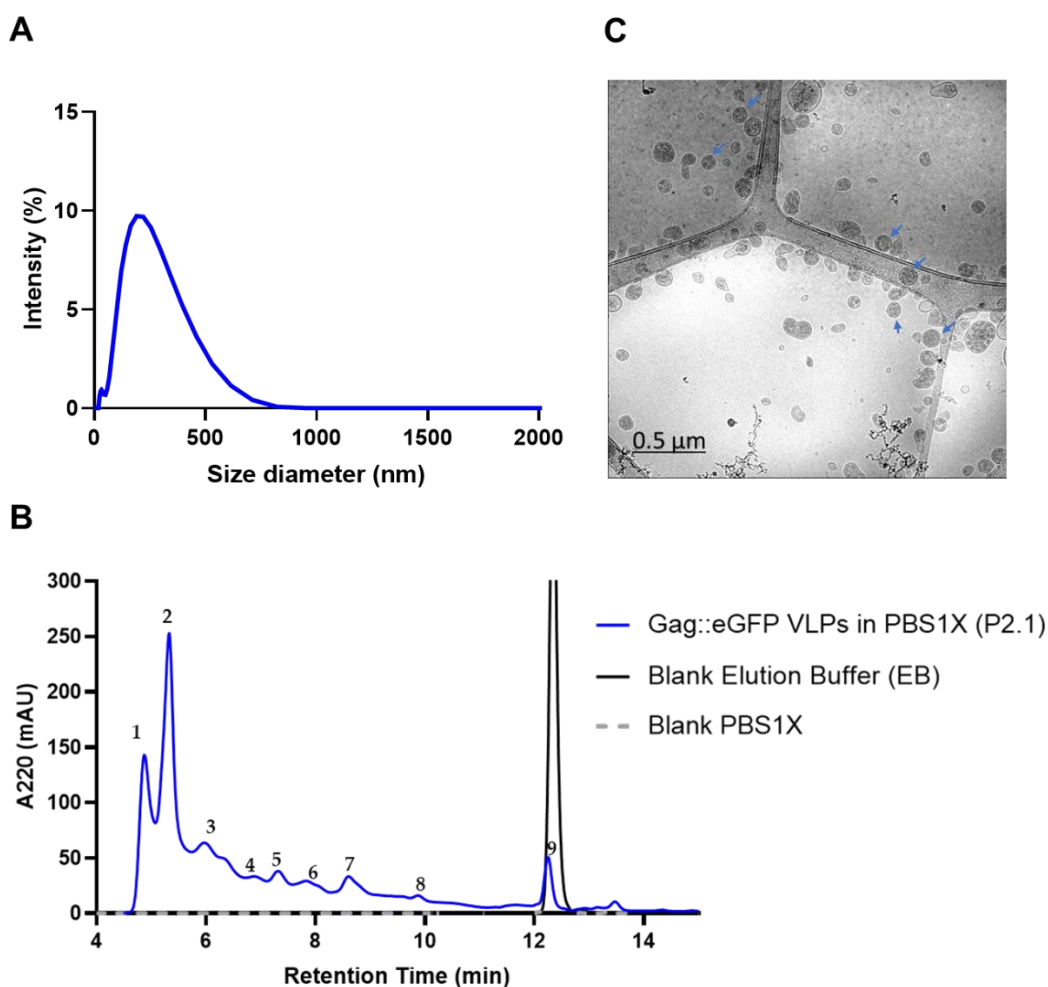


**Figure 2.** Molecular and biophysical characterization of purified Gag::eGFP VLPs obtained in PBS1X after the buffer exchange step. **A)** Particle size distribution analysis by DLS ( $MHD=156.4$  and  $PdI=0.267$ ). **B)** SE-HPLC profile. Main elution peaks of P2.1 material are indicated numerically. **C)** Cryo-TEM micrograph. Blue narrows indicate Gag::eGFP VLPs. *DLS*, Dynamic Light Scattering; *PdI*, polydispersity index; *MHD*, mean hydrodynamic diameter; *SE-HPLC*, Size Exclusion-High pressure liquid chromatography; *Cryo-TEM*, Cryo-Transmission Electron Microscopy.

### Gag::eGFP VLPs formulation optimization using DoE

Effective formulations of biopharmaceuticals should provide stability and quality maintenance not only in solution but also during critical processes like freeze-drying and storage [22], [23], [26], [39]. The role of excipients in formulations is very broad and selection of the optimal ones remains challenging, especially in the context of VLP lyophilization [49]. As mentioned, this challenge is addressed here by a Design of Experiments (DoE) approach, specifically a fractional factorial design. A schematic representation of the experimental procedure is presented in **Figure 3**.

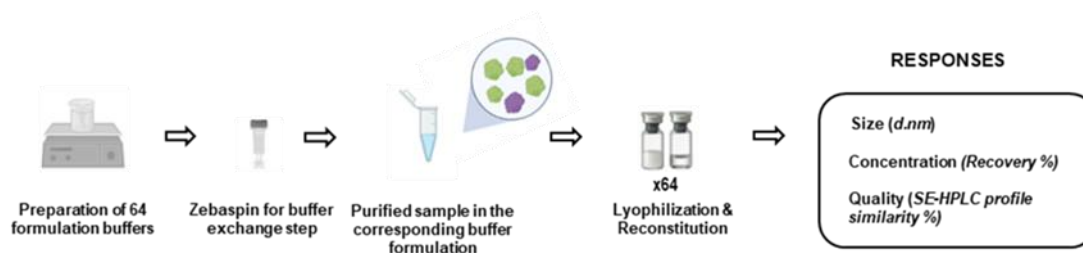


**Figure 3:** Overview of the experimental workflow. Initial step involves the preparation of 64 distinct formulations, followed by the generation of Gag::eGFP VLPs samples using a zebaspin type column for buffer exchange. Subsequently, all conditions undergo lyophilization and were reconstituted in PBS 1X for analysis. The effect of the different formulations (independent variables) was studied on size, concentration, and quality of the Gag::eGFP VLPs (responses).

Briefly, 64 formulations buffers were prepared according to the fractional factorial design (**Tables 1 and 2**) and Gag::eGFP VLP aliquotes from the starting material were transferred to each of the formulation buffers using Zebaspin columns. Then, VLPs in the different formulation buffers were lyophilized. Following the lyophilization process, the samples were reconstituted in PBS1X. Subsequently, their size, concentration, and quality were assessed to identify an optimal condition exhibiting comparable characteristics to the starting material. The experimental design matrix and responses are shown in **Table 2**. Experimental data were represented on three scatterplot graphs providing a visual overview of the results (**Figure 4**).

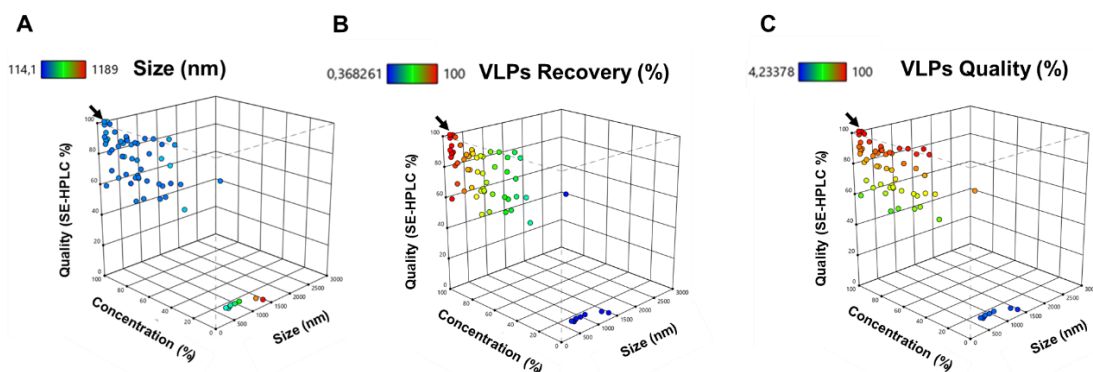


**Figure 4:** Scatterplot representation of the results of Gag::eGFP VLPs formulation optimization through a fractional factorial design experiment. Each data point reflects the outcome under specific parameter combinations, providing a visual overview of the experimental space (**A**) VLPs Size (d.nm), **B**) VLPs Concentration (Recovery %), **C**) VLPs Quality (SE-HPLC profile similarity %). The black arrow indicates the point corresponding to the initial sample, before lyophilization, used as a positive reference control for the analysis of the rest of the samples

According to the results obtained, 19 of the formulations buffers tested exhibited characteristics significantly similar to the starting material, with particle sizes ranging between 140 and 200 nm, and both recovery rate and percentage of SE-HPLC profile similarity exceeding 70%. (**Table 2**). The remaining formulations did not demonstrate these values of similarity across the three characteristics analyzed. **Figure 5** illustrates the

DLS and SE-HPLC profiles of two representative formulations, one showing high similarity and the other showing low similarity to the starting material.

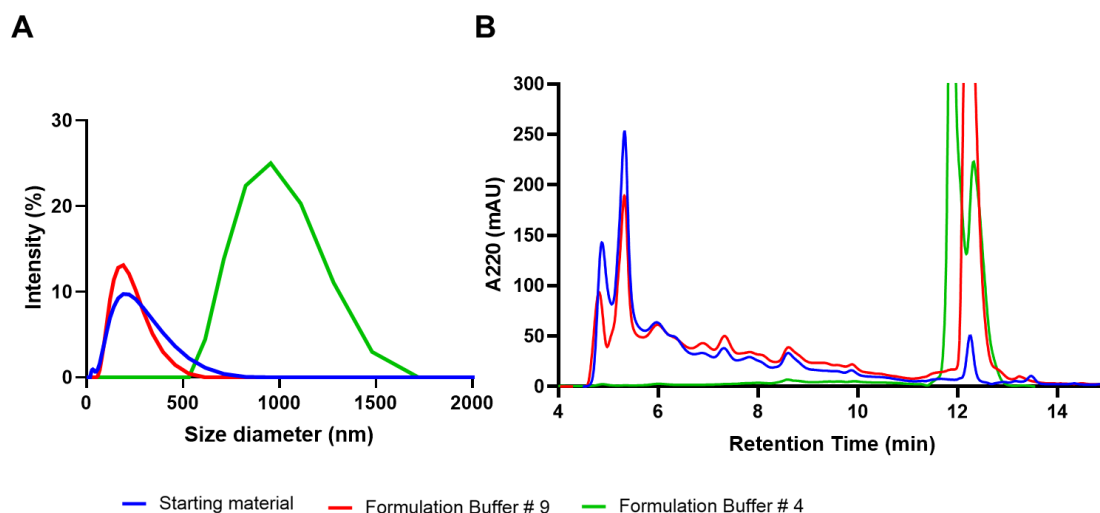


**Figure 5:** Characteristic profiles of two formulations buffers, #9, exhibit high similarity and #4 displays low similarity to the starting material **A)** DLS and **B)** SE-HPLC. DLS, Dynamic Light Scattering; SE-HPLC, Size Exclusion-High pressure liquid chromatography.

Based on the acquired results the model was used to assess the influence of the different excipients of the tested formulations buffers on the three responses and generate an optimal combination resulting in a high-quality lyophilized and reconstituted sample. **Figure 6** shows the factors influencing size, concentration, and quality in Gag::eGFP VLP samples after the lyophilization process. The significant effects are those that deviate from the straight line centered in zero. In the three cases significant binary interactions are identified, highlighting the appropriateness of the use of DoE approach to study this topic. The analysis of variance of the model containing the significant coefficients is presented in **Supplementary Material S1, S2 and S3**. The F value considering the regression mean square and the residual mean square, was also calculated for each dependent variable, indicating that the model is significant in all cases.

The optimal combination found using the model contained the following excipients: sucrose, arginine, tris-HCL, sodium chloride and polysorbate 80. With this formulation, the model predicts the following responses intervals: Size diameter: [107.93 – 218.34 nm]; Concentration: [67.7 – 169.0 % of recovery]; and Quality [75.72 – 114.39 SE-HPLC % of profile similarity]. To corroborate the model generated optimum, a validation experiment was performed at the optimal condition (n=2). A size diameter of  $151.25 \pm 8.83$  nm, a recovery percentage of  $98.57 \pm 5.32$  and a SE-HPLC profile similarity percentage of  $84.7 \pm 10.37$  were obtained after

the lyophilization and reconstitution process, corroborating the predictability of the model and setting the conditions of lyophilization to maximize the obtention of the Gag::eGFP VLPs with appropriate characteristics regarding size, concentration, and quality.

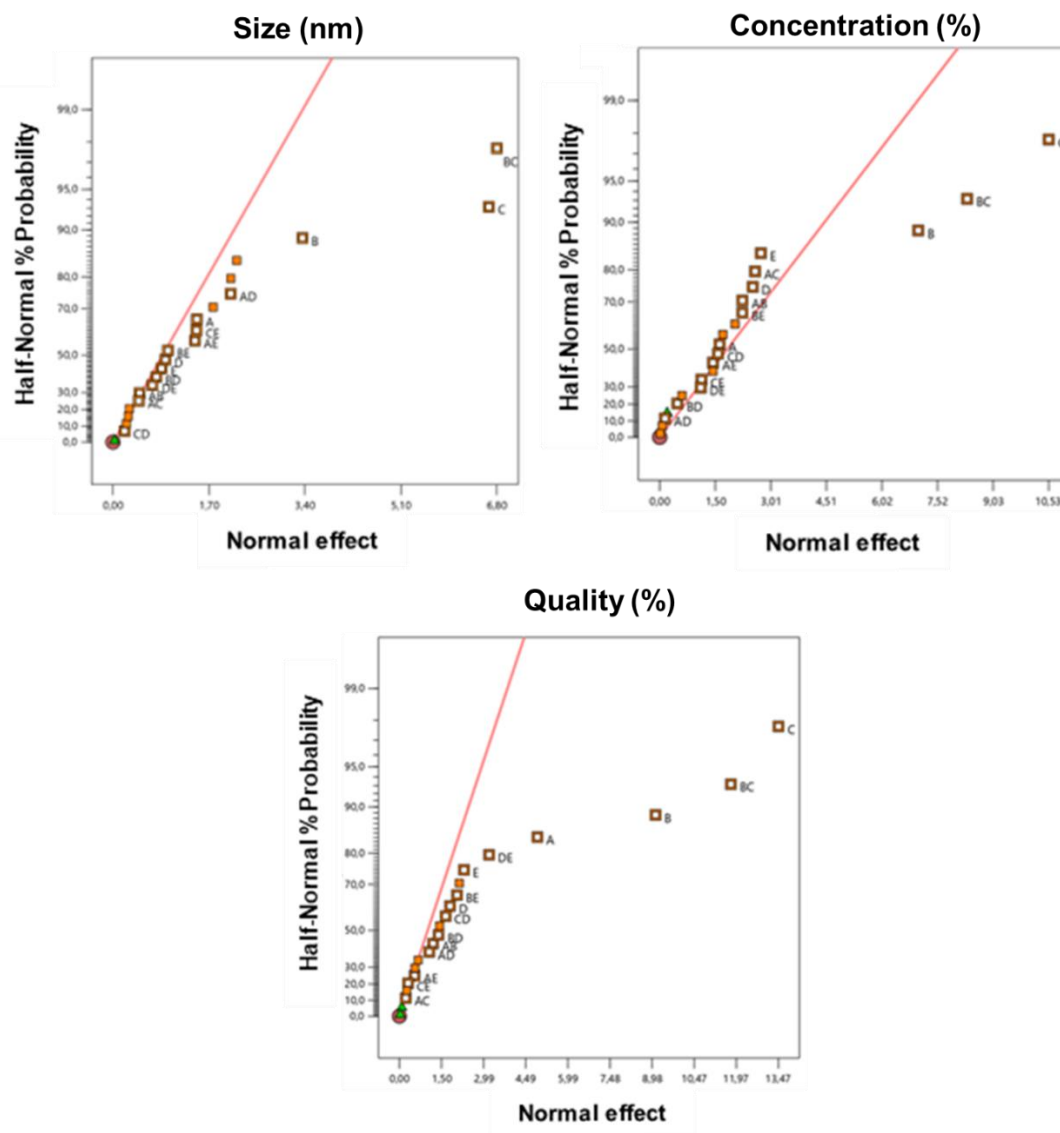


**Figure 6:** Half-normal plot of the standardized effects of the different formulations assayed on Size (d.nm), Concentration (Recovery %) and Quality (SE-HPLC profile similarity %) of the purified Gag::eGFP VLPs. A, CryoLioprotectants; B, Bulking; C, Buffers; D, Tonicity; E, Surfactants; DLS, Dynamic Light Scattering; SE-HPLC, Size Exclusion-High pressure liquid chromatography.

Although each excipient within a formulation has a specific function and influence, according to the obtained results, bulking agents, buffers, and the interaction between them are the factors exerting the most significant influence on the three characteristics under investigation. It is well known that the selection of buffers, and bulking agents are important for stabilizing the product during the freeze-drying process as well

as during storage [11]. Bulking agents are a group of excipients that are designed to provide the appropriate structure to the lyophilized cake and that can affect the efficiency of the lyophilization process [16]. Here we proposed the use of arginine as bulking agent. The use of this amino acid has received increasing interest in recent years, particularly for highly concentrated protein formulations for subcutaneous administration. The mechanism behind arginine-stabilizing effects is based on its weak binding to the protein surface, which can thus prevent protein–protein interactions and aggregation, while showing amorphous behavior during and after lyophilization. Arginine hydrochloride reduces the viscosity of formulations and contributes to protein solubility [16], [42]. On the other hand buffers are used to adjust and stabilize the pH, in addition to optimizing the solubility and stability of the product [11], [49]. Like histidine, the pH of TrisHCl buffer increases by one pH unit from 7.4 to 8.5 upon freezing to  $-30^{\circ}\text{C}$ . However, studies on pH indicators have demonstrated no pH change for 10 mM Tris buffer pH 7.4 up to  $-40^{\circ}\text{C}$  [11], [41], making it a promising alternative.

#### Storage stability study of lyophilized Gag::eGFP VLP formulations

To study the Gag::eGFP VLP preservation after lyophilization process, the influence of various combinations of temperature, time, and preservation forms (lyophilized or reconstituted) was investigated and compared with the starting material (**Table 7**).

**Table 7:** Lyophilized Gag::eGFP VLPs storage stability study

Sample	Temperature	4 weeks			8 weeks		
		Size	% Recovery	Quality	Size	% Recovery	Quality
<i>Lyophilized</i>	$4^{\circ}\text{C}$	$184.7\pm 11.0$	$100.0\pm 5.3$	100.00	$681.3\pm 39.2$	$13.46\pm 1.14$	17.6
	$25^{\circ}\text{C}$	$249.5\pm 23.9$	$90.1\pm 1.1$	51.33	$317.4\pm 55.7$	$34.5\pm 1.51$	22.16
	$37^{\circ}\text{C}$	$271.5\pm 14.3$	$94.8\pm 3.5$	53.92	$614.1\pm 35.4$	$27.64\pm 1.46$	66.43
<i>Reconstituted</i>	$4^{\circ}\text{C}$	$188.5\pm 26.5$	$100.0\pm 5.1$	100	$396.1\pm 25.6$	$28.57\pm 1.03$	90.66
	$25^{\circ}\text{C}$	$852.5\pm 57.3$	$53.4\pm 5.5$	69.74	$1794.0\pm 36.7$	$16.72\pm 0.74$	57.81
	$-80^{\circ}\text{C}$	$148.2\pm 24.8$	$83.4\pm 2.8$	100	$187.5\pm 37.5$	$40.43\pm 0.94$	37.13

The influence of the conditions on the Gag::eGFP VLPs' size was investigated through the analysis of the particle size distribution whose variations could indicate fragmentation or aggregation of VLPs. Flow virometry was used to calculate the Gag::eGFP VLPs sample's concentration. The analyses by SE-HPLC



facilitated the evaluation of sample quality based on the percentage of similarity with the profile of the starting material [50], whose fluctuation might suggest damage on Gag::eGFP VLPs samples.

Regarding the impact of storage conditions on the diameter of Gag::eGFP VLPs, **Figure 7A** demonstrates that Gag::eGFP VLPs stored at 25 °C for 4 weeks, whether in lyophilized or reconstituted form, as well as those stored at 37 °C for the same duration, exhibited an increase in diameter compared to the starting material. This increase indicates a general aggregation of the VLPs over the storage period.[24]. The size diameter of the VLPs was not affected by the remaining conditions, staying within the specified range acceptable for Gag VLPs (140-200 nm) [25], [46], [51]. After 8 weeks, all conditions exhibited an increase in size diameter except for samples that were reconstituted and stored at -80°C. González-Domínguez et.al [24] reported similar findings for Gag VLPs lyophilization and storage at 25°C for 8 weeks.

In **Figure 7B**, flow virometry measurements revealed that after 4 weeks, the Gag::eGFP VLPs samples stored in different conditions maintained VLPs concentration similar to the starting material. However, the exception was the reconstituted sample stored at 25°C, indicating that this preservation method affected the integrity of the Gag::eGFP VLPs. These results suggest that for lyophilized form of preservation and short storage time, i.e., 4 weeks, the concentration of Gag::eGFP VLPs remained comparable to starting material (over 90% of recovery), regardless of the storage temperature employed. On the contrary, for reconstituted samples, the storage at 25°C was the most detrimental, resulting in lower Gag::eGFP VLPs after 4 weeks (53% of recovery) (**Table 7**). For reconstituted samples stored at 4°C and -80°C, 100% and 83% recoveries were obtained, respectively.

The SE-HPLC assay (**Figure 7C**) confirmed the flow virometry results. For Gag::eGFP VLPs stored in both lyophilized and reconstituted form at 4 °C for 4 weeks, the profile similarity percentage resulted in 100% to the starting material. The main issues arose in the storage conditions of 25 °C and 37 °C for the lyophilized samples and 25 °C for the reconstituted samples, in which the profile similarity percentage diminish below 70%. The low similarity could be the consequence of damages in Gag::eGFP-VLPs hence the release of their fragments or aggregates [24]. The sample reconstituted and stored at -80°C for 4 weeks also presents excellent quality (100% similarity in the SE-HPLC profile).

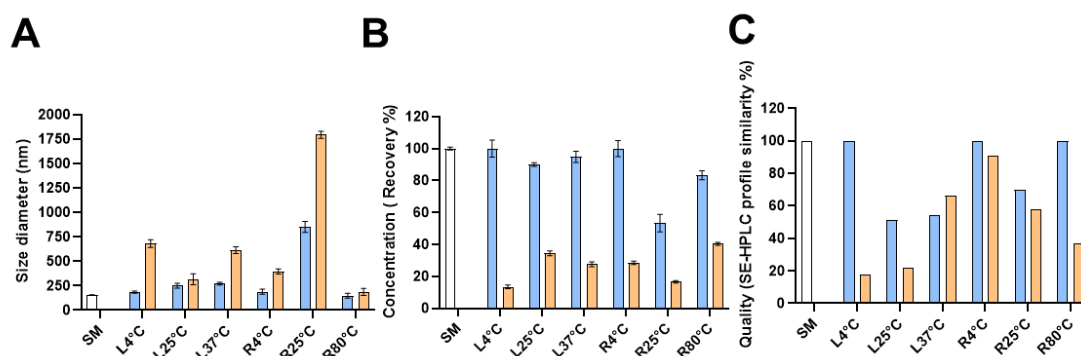


**Figure 7. (A)** Size diameter by DLS, **(B)** concentration by flow virometry, and **(C)** quality analysis by SE-HPLC, results of Gag::eGFP VLPs sample stored at different temperatures after 4 weeks (blue bars), and 8 weeks (orange bars). Flow virometry and SE-HPLC analysis data were represented as a percentage of the starting material (white bar). Graphs were plotted as mean of analytical replicates  $\pm$  SE. Abbreviations: SM, Starting material; L4°C, L25°C, L37°C, lyophilized material at corresponding temperature, respectively; R4°C, R25°C, R-80°C, reconstituted material at corresponding temperature, respectively; DLS, Dynamic Light Scattering; SE-HPLC, Size Exclusion-High pressure liquid chromatography.

Upon analyzing the recovery and the SE-HPLC profiles at 8 weeks, a general trend was observed, with a decrease in percentage values, relative not only to the starting material but also to the results obtained at 4 weeks. This decreases hints at a potential deterioration or alteration in the composition or structural integrity of the Gag::eGFP VLP over time, potentially affecting the samples' overall quality and stability.

In summary, based on our results, the optimal method for preserving Gag::eGFP VLPs after lyophilization for a period of up to 4 weeks, whether in lyophilized or reconstituted form, is at a temperature of 4°C. The freezing rate, among other lyophilization parameters, has been deemed critical in preventing ice formation during lyophilization and minimizing nanoparticle membrane damage and aggregation. Therefore, additional optimization of process parameters may improve these results.

## CONCLUSIONS

In this study, a formulation for a lyophilization process of HIV-1 Gag::eGFP VLPs, composed by sucrose, arginine, TrisHCl, sodium chloride and polysorbate 80, has been optimized and validated. The VLPs obtained after the lyophilization process presented characteristics of size, concentration, and quality remarkably akin to the non-lyophilized VLPs. Additionally, VLP storage at 4°C for 4 weeks, either in freeze-dried or reconstituted form, preserves their integrity and stability. Also, the selection of analytical methods for characterizing the VLPs was crucial for obtaining comprehensive insights into their structural properties.

The choice of these analytical techniques contributed to the overall reliability of the results. All in all, this work presents an exploration of formulation optimization for lyophilization of Gag::eGFP VLPs. From purification and characterization to systematic formulation and stability studies, each stage contributes to the understanding of the complexities involved in the use of VLPs for vaccine development. The results obtained contribute to future advances in VLP-based vaccines, making evident the relevance of exhaustive formulation design to facilitate manufacturing of VLPs with enhanced properties facilitating their transportation, distribution and access as vaccines. A more detailed discussion of the results presented in this chapter can be found in the general discussion section of this thesis.

## REFERENCES

- [1] J. Fuenmayor, F. Gòdia, and L. Cervera, "Production of virus-like particles for vaccines," *New Biotechnology*, vol. 39. Elsevier B.V., pp. 174–180, Oct. 25, 2017, doi: 10.1016/j.nbt.2017.07.010.
- [2] L. H. L. Lua, N. K. Connors, F. Sainsbury, Y. P. Chuan, N. Wibowo, and A. P. J. Middelberg, "Bioengineering Virus-Like Particles as Vaccines," *Biotechnol. Bioeng*, vol. 111, pp. 425–440, 2014, doi: 10.1002/bit.25159/abstract.
- [3] S. Nooraei *et al.*, "Virus-like particles: preparation, immunogenicity and their roles as nanovaccines and drug nanocarriers," *J. Nanobiotechnology*, vol. 19, no. 1, pp. 1–27, 2021, doi: 10.1186/s12951-021-00806-7.
- [4] B. Donaldson, Z. Lateef, G. F. Walker, S. L. Young, and V. K. Ward, "Virus-like particle vaccines: immunology and formulation for clinical translation," *Expert Rev. Vaccines*, vol. 17, no. 9, pp. 833–849, 2018, doi: 10.1080/14760584.2018.1516552.
- [5] M. L. Fahrni *et al.*, "Management of COVID-19 vaccines cold chain logistics: a scoping review," *J. Pharm. Policy Pract.*, vol. 15, no. 1, 2022, doi: 10.1186/s40545-022-00411-5.
- [6] X. C. Tang and M. J. Pikal, "Design of Freeze-Drying Processes for Pharmaceuticals: Practical Advice," *Pharm. Res.*, vol. 21, no. 2, pp. 191–200, 2004, doi: 10.1023/b:pham.0000016234.73023.75.
- [7] F. Emami, A. Vatanara, E. J. Park, and D. H. Na, "Drying technologies for the stability and bioavailability of biopharmaceuticals," *Pharmaceutics*, vol. 10, no. 3, pp. 1–22, 2018, doi: 10.3390/pharmaceutics10030131.
- [8] L. J. J. Hansen, R. Daoussi, C. Vervaet, J. P. Remon, and T. R. M. De Beer, "Freeze-drying of live virus vaccines: A review," *Vaccine*, vol. 33, no. 42. Elsevier Ltd, pp. 5507–5519, Oct. 13, 2015, doi: 10.1016/j.vaccine.2015.08.085.
- [9] Y. Liu *et al.*, "Screening and Stability Evaluation of Freeze-Dried Protective Agents for a Live Recombinant Pseudorabies Virus Vaccine," vol. 12(1), p. 65, 2024, doi: 10.3390/vaccines12010065.
- [10] B. S. Bhatnagar, R. H. Bogner, and M. J. Pikal, "Protein stability during freezing: Separation of stresses and mechanisms of protein stabilization," *Pharm. Dev. Technol.*, vol. 12, no. 5, pp. 505–523, 2007, doi: 10.1080/10837450701481157.
- [11] C. Wu, S. Shamblin, D. Varshney, and E. Shalaev, "Advance Understanding of Buffer Behavior during Lyophilization," *Lyophilized Biol. Vaccines*, pp. 25–41, 2015, doi: 10.1007/978-1-4939-2383-

- 0.
- [12] S. Pramanick, D. Singodia, and V. Chandel, "Excipient selection in parenteral formulation development," *Pharma Times*, vol. 45, no. 3, pp. 65–77, 2013, doi: 10.1080/03639045.2018.1483392.
  - [13] A. Baheti, L. Kumar, and A. K. Bansal, "Excipients used in lyophilization of small molecules," *J. Excipients Food Chem.*, vol. 1, no. 1, pp. 41–54, 2010.
  - [14] J. J. Schwegman, L. M. Hardwick, and M. J. Akers, "Practical formulation and process development of freeze-dried products," *Pharm. Dev. Technol.*, vol. 10, no. 2, pp. 151–173, 2005, doi: 10.1081/PDT-200056308.
  - [15] R. L. Remmele, S. Krishnan, and W. J. Callahan, "Development of Stable Lyophilized Protein Drug Products," *Curr. Pharm. Biotechnol.*, vol. 13, no. 3, pp. 471–496, 2012, doi: 10.2174/138920112799361990.
  - [16] M. Bjelošević, A. Zvonar Pobirk, O. Planinšek, and P. Ahlin Grabnar, "Excipients in freeze-dried biopharmaceuticals: Contributions toward formulation stability and lyophilisation cycle optimisation," *Int. J. Pharm.*, vol. 576, p. 119029, 2020, doi: 10.1016/j.ijpharm.2020.119029.
  - [17] J. N. Gardeur, N. Mathis, A. Kobilinsky, and J. Brun-Bellut, "Simultaneous effects of nutritional and environmental factors on growth and flesh quality of *Perca fluviatilis* using a fractional factorial design study," *Aquaculture*, vol. 273, no. 1, pp. 50–63, 2007, doi: 10.1016/j.aquaculture.2007.09.024.
  - [18] S. Pillay, A. Meyers, A. L. Williamson, and E. P. Rybicki, "Optimization of chimeric HIV-1 virus-like particle production in a baculovirus-insect cell expression system," *Biotechnol. Prog.*, vol. 25, no. 4, pp. 1153–1160, 2009, doi: 10.1002/btpr.187.
  - [19] A. Trabelsi, J. N. Gardeur, F. Teletchea, and P. Fontaine, "Effects of 12 factors on burbot *Lota lota* (L., 1758) weaning performances using fractional factorial design experiment," *Aquaculture*, vol. 316, no. 1–4, pp. 104–110, 2011, doi: 10.1016/j.aquaculture.2011.03.027.
  - [20] S. Saboo *et al.*, "Optimized Formulation of a Thermostable Spray-Dried Virus-Like Particle Vaccine against Human Papillomavirus," *Mol. Pharm.*, vol. 13, no. 5, pp. 1646–1655, 2016, doi: 10.1021/acs.molpharmaceut.6b00072.
  - [21] C. A. Rezende, B. W. Atta, M. C. Breitzkreitz, R. Simister, L. D. Gomez, and S. J. McQueen-Mason, "Optimization of biomass pretreatments using fractional factorial experimental design," *Biotechnol. Biofuels*, vol. 11, no. 1, pp. 1–15, 2018, doi: 10.1186/s13068-018-1200-2.
  - [22] F. Susa *et al.*, "Comparative Studies of Different Preservation Methods and Relative Freeze-Drying Formulations for Extracellular Vesicle Pharmaceutical Applications," *ACS Biomater. Sci. Eng.*, vol. 9, no. 10, pp. 5871–5885, 2023, doi: 10.1021/acsbiomaterials.3c00678.
  - [23] J. Mohr, Y. P. Chuan, Y. Wu, L. H. L. Lua, and A. P. J. Middelberg, "Virus-like particle formulation optimization by miniaturized high-throughput screening," *Methods*, vol. 60, no. 3, pp. 248–256, 2013, doi: 10.1016/j.ymeth.2013.04.019.
  - [24] I. González-Domínguez, E. Lorenzo, A. Bernier, L. Cervera, F. Gòdia, and A. Kamen, "A four-step purification process for gag vlps: From culture supernatant to high-purity lyophilized particles," *Vaccines*, vol. 9, no. 10, pp. 1–19, 2021, doi: 10.3390/vaccines9101154.
  - [25] I. González-Domínguez, E. Puente-Massaguer, L. Cervera, and F. Gòdia, "Quality assessment of virus-like particles at single particle level: A comparative study," *Viruses*, vol. 12, no. 2, pp. 1–24, 2020, doi: 10.3390/v12020223.
  - [26] R. Lang, G. Winter, L. Vogt, A. Zürcher, B. Dorigo, and B. Schimmele, "Rational design of a stable, freeze-dried virus-like particle-based vaccine formulation," *Drug Dev. Ind. Pharm.*, vol. 35, no. 1, pp.

- 83–97, 2009, doi: 10.1080/03639040802192806.
- [27] Y. Yang *et al.*, “Size-exclusion HPLC provides a simple, rapid, and versatile alternative method for quality control of vaccines by characterizing the assembly of antigens,” *Vaccine*, vol. 33, no. 9, pp. 1143–1150, 2015, doi: 10.1016/j.vaccine.2015.01.031.
  - [28] M. A. Al-ghobashy, M. M. Mostafa, H. S. Abed, F. A. Fathalla, and M. Y. Salem, “Correlation between Dynamic Light Scattering and Size Exclusion High Performance Liquid Chromatography for Monitoring the Effect of pH on Stability of Biopharmaceuticals Correspondence : Aggregate formation is a major problem affecting both safety and eff,” *J. Chromatogr. B*, vol. 1060, pp. 1–9, 2017, doi: 10.1016/j.jchromb.2017.05.029.
  - [29] S. Gutiérrez-Granados, L. Cervera, F. Gòdia, J. Carrillo, and M. M. Segura, “Development and validation of a quantitation assay for fluorescently tagged HIV-1 virus-like particles,” *J. Virol. Methods*, vol. 193, no. 1, pp. 85–95, 2013, doi: 10.1016/j.jviromet.2013.05.010.
  - [30] E. Lorenzo, L. Miranda, F. Gòdia, and L. Cervera, “Downstream process design for Gag HIV - 1 based virus - like particles,” *Biotechnol. Bioeng.*, vol. 120, no. 9, pp. 2672–2684, 2023, doi: 10.1002/bit.28419.
  - [31] L. Cervera, S. Gutiérrez-Granados, M. Martínez, J. Blanco, F. Gòdia, and M. M. Segura, “Generation of HIV-1 Gag VLPs by transient transfection of HEK 293 suspension cell cultures using an optimized animal-derived component free medium,” *J. Biotechnol.*, vol. 166, no. 4, pp. 152–165, Jul. 2013, doi: 10.1016/j.jbiotec.2013.05.001.
  - [32] A. Venereo-Sanchez *et al.*, “Hemagglutinin and neuraminidase containing virus-like particles produced in HEK-293 suspension culture: An effective influenza vaccine candidate,” *Vaccine*, vol. 34, no. 29, pp. 3371–3380, Jun. 2016, doi: 10.1016/j.vaccine.2016.04.089.
  - [33] J. Lawson, *Design and analysis of experiments with R*. New York, 2015.
  - [34] M. Czyz *et al.*, “Freeze-drying of plant tissue containing HBV surface antigen for the oral vaccine against hepatitis B,” *Biomed Res. Int.*, vol. 2014, p. 10, 2014, doi: 10.1155/2014/485689.
  - [35] A. Seth *et al.*, “Modular virus-like particles for sublingual vaccination against group A streptococcus,” *Vaccine*, vol. 34, no. 51, pp. 6472–6480, 2016, doi: 10.1016/j.vaccine.2016.11.008.
  - [36] A. Lynch, A. E. Meyers, A. L. Williamson, and E. P. Rybicki, “Stability studies of HIV-1 Pr55gag virus-like particles made in insect cells after storage in various formulation media,” *Virol. J.*, vol. 9, pp. 1–5, 2012, doi: 10.1186/1743-422X-9-210.
  - [37] J. Horn, E. Tolardo, D. Fissore, and W. Friess, “Crystallizing amino acids as bulking agents in freeze-drying,” *Eur. J. Pharm. Biopharm.*, vol. 132, pp. 70–82, 2018, doi: 10.1016/j.ejpb.2018.09.004.
  - [38] P. Stärtzel, “Arginine as an Excipient for Protein Freeze-Drying: A Mini Review,” *J. Pharm. Sci.*, vol. 107, no. 4, pp. 960–967, 2018, doi: 10.1016/j.xphs.2017.11.015.
  - [39] R. M. Kramer *et al.*, “Development of a Stable Virus-Like Particle Vaccine Formulation against Chikungunya Virus and Investigation of the Effects of Polyanions,” *J. Pharm. Sci.*, vol. 102(12), pp. 4305–4314, 2013, doi: 10.1002/jps.23749.
  - [40] W. Zheng and S. Zhang, “Formulations of adenovirus for gene therapy. US Patent,” 6,689,600 B1, 2011.
  - [41] M. A. Croyle, B. J. Roessler, B. L. Davidson, J. M. Hilfinger, and G. L. Amidon, “Factors that influence stability of recombinant adenoviral preparations for human gene therapy,” *Pharm. Dev. Technol.*, vol. 3, no. 3, pp. 373–383, 1998, doi: 10.3109/10837459809009865.
  - [42] R. K. Evans *et al.*, “Development of Stable Liquid Formulations for Adenovirus-Based Vaccines,” vol. 93, no. 10, pp. 2458–2475, 2004, doi: 10.1002/jps.20157.

- 
- [43] J. Lavado-García, I. Jorge, A. Boix-Besora, J. Vázquez, F. Gòdia, and L. Cervera, "Characterization of HIV-1 virus-like particles and determination of Gag stoichiometry for different production platforms," *Biotechnol. Bioeng.*, vol. 118, no. 7, pp. 2660–2675, 2021, doi: 10.1002/bit.27786.
- [44] R.E. Bruns, I.S. Scarminio, B. de Barros Neto, "CHAPTER 4 When there are many variables," in *Data Handling in Science and Technology*, Volumen 25., Elsevier, 2005, pp. 147–198.
- [45] S. B. Carvalho *et al.*, "Membrane-Based Approach for the Downstream Processing of Influenza Virus-Like Particles," *Biotechnol. J.*, vol. 14, no. 8, Aug. 2019, doi: 10.1002/biot.201800570.
- [46] P. Steppert *et al.*, "Separation of HIV-1 gag virus-like particles from vesicular particles impurities by hydroxyl-functionalized monoliths," *J. Sep. Sci.*, vol. 40, no. 4, pp. 979–990, 2017, doi: 10.1002/jssc.201600765.
- [47] M. Adrian, J. Dubochet, J. Lepault, and A. W. McDowell, "Cryo-electron microscopy of viruses," *Nature*, vol. 308, no. 5954, pp. 32–36, 1984, doi: 10.1038/308032a0.
- [48] J. A. G. Briggs and H. G. Kräusslich, "The molecular architecture of HIV," *J. Mol. Biol.*, vol. 410, no. 4, pp. 491–500, 2011, doi: 10.1016/j.jmb.2011.04.021.
- [49] B. Donaldson, Z. Lateef, G. F. Walker, S. L. Young, and V. K. Ward, "Virus-like particle vaccines: immunology and formulation for clinical translation," *Expert Rev. Vaccines*, vol. 17, no. 9, pp. 833–849, 2018, doi: 10.1080/14760584.2018.1516552.
- [50] N. T. Lan *et al.*, "Stability of virus-like particles of red-spotted grouper nervous necrosis virus in the aqueous state, and the vaccine potential of lyophilized particles," *Biologicals*, vol. 51, no. October, pp. 25–31, 2018, doi: 10.1016/j.biologicals.2017.11.002.
- [51] P. Steppert, D. Burgstaller, M. Klausberger, A. Tover, E. Berger, and A. Jungbauer, "Quantification and characterization of virus-like particles by size-exclusion chromatography and nanoparticle tracking analysis," *J. Chromatogr. A*, vol. 1487, pp. 89–99, 2017, doi: 10.1016/j.chroma.2016.12.085.

## SUPPLEMENTARY MATERIALS

**Supplementary Material S1:** ANOVA analysis of the investigated formulations' ability to influence size of the Gag::eGFP VLPs.

Factors/Factor Interactions Tested	Sum of Squares	Degrees of freedom	Mean Square	F-value	p-value
<b>Model</b>	<b>0.0002</b>	<b>39</b>	<b>4.811E-06</b>	<b>5.11</b>	<b>&lt; 0.0001</b>
A-Cryoprotectant	6.258E-06	3	2.086E-06	2.22	0.1136
B-Bulking agent	9.084E-06	1	9.084E-06	9.65	0.0050
C-Buffer	0.0000	3	0.0000	16.85	< 0.0001
D-Tonicity Modifier	6.633E-07	1	6.633E-07	0.7044	0.4099
E-Surfactant	9.271E-07	1	9.271E-07	0.9845	0.3314
AB	1.602E-06	3	5.339E-07	0.5669	0.6424
AC	6.503E-06	9	7.226E-07	0.7674	0.6469
AD	7.992E-06	3	2.664E-06	2.83	0.0609
AE	5.063E-06	3	1.688E-06	1.79	0.1768
BC	0.0001	3	0.0000	18.06	< 0.0001
BD	5.587E-07	1	5.587E-07	0.5933	0.4490
BE	8.955E-07	1	8.955E-07	0.9510	0.3396
CD	8.035E-07	3	2.678E-07	0.2844	0.8361
CE	5.177E-06	3	1.726E-06	1.83	0.1694
DE	4.595E-07	1	4.595E-07	0.4879	0.4919
<b>Residual</b>	<b>0.0000</b>	<b>23</b>	<b>9.417E-07</b>		
<b>Cor Total</b>	<b>0.0002</b>	<b>62</b>			

The Model F-value of 5.11 implies the model is significant. There is only a 0.01% chance that an F-value this large could occur due to noise. P-values less than 0.0500 indicate model terms are significant. In this case B, C, BC correspond to significant model terms. Values greater than 0.1000 indicate the model terms are not significant.

**Supplementary Material S2:** ANOVA analysis of the investigated formulations' ability to influence concentration of the Gag::eGFP VLPs

Factors/Factor Interactions Tested	Sum of Squares	Degrees of freedom	Mean Square	F-value	p-value
<b>Model</b>	<b>459.81</b>	<b>39</b>	<b>11.79</b>	<b>11.50</b>	<b>&lt; 0.0001</b>
A-CryoLioprotectant	6.72	3	2.24	2.19	0.1171
B-Bulking agent	49.98	1	49.98	48.76	< 0.0001
C-Buffer	134.91	3	44.97	43.87	< 0.0001
D-Tonicity Modifier	8.54	1	8.54	8.33	0.0083
E-Surfactant	8.63	1	8.63	8.42	0.0080
AB	9.56	3	3.19	3.11	0.0462
AC	22.25	9	2.47	2.41	0.0428
AD	0.6586	3	0.2195	0.2142	0.8856
AE	5.46	3	1.82	1.78	0.1799
BC	79.85	3	26.62	25.97	< 0.0001
BD	0.2354	1	0.2354	0.2296	0.6363
BE	5.12	1	5.12	5.00	0.0353
CD	6.09	3	2.03	1.98	0.1450
CE	4.13	3	1.38	1.34	0.2848
DE	1.27	1	1.27	1.24	0.2779
<b>Residual</b>	<b>23.58</b>	<b>23</b>	<b>1.03</b>		
<b>Cor Total</b>	<b>483.39</b>	<b>62</b>			

The Model F-value of 11.50 implies the model is significant. There is only a 0.01% chance that an F-value this large could occur due to noise. P-values less than 0.0500 indicate model terms are significant. In this case B, C, D, E, AB, AC, BC, BE correspond to significant model terms. Values greater than 0.1000 indicate the model terms are not significant.

**Supplementary Material S3:** ANOVA analysis of the investigated formulations' ability to influence quality of the Gag::eGFP VLPs.

Factors/Factor Interactions Tested	Sum of Squares	Degrees of freedom	Mean Square	F-value	p-value
<b>Model</b>	45605.64	39	1169.38	17.55	< 0.0001
A-CryoLioprotectant	2100.21	3	700.07	10.51	0.0002
B-Bulking agent	4784.90	1	4784.90	71.81	< 0.0001
C-Buffer	14399.10	3	4799.70	72.03	< 0.0001
D-Tonicity Modifier	190.87	1	190.87	2.86	0.1041
E-Surfactant	400.05	1	400.05	6.00	0.0223
AB	286.08	3	95.36	1.43	0.2594
AC	344.11	9	38.23	0.5738	0.8045
AD	251.09	3	83.70	1.26	0.3127
AE	128.13	3	42.71	0.6409	0.5964
BC	9906.07	3	3302.02	49.55	< 0.0001
BD	128.68	1	128.68	1.93	0.1779
BE	279.62	1	279.62	4.20	0.0521
CD	416.73	3	138.91	2.08	0.1301
CE	79.44	3	26.48	0.3974	0.7561
DE	677.80	1	677.80	10.17	0.0041
<b>Residual</b>	1532.61	23	66.64		
<b>Cor Total</b>	47138.26	62			

The Model F-value of 17.55 implies the model is significant. There is only a 0.01% chance that an F-value this large could occur due to noise. P-values less than 0.0500 indicate model terms are significant. In this case A, B, C, E, BC, DE correspond to significant model terms. Values greater than 0.1000 indicate the model terms are not significant



## **CHAPTER THREE**

Development of a scalable production bioprocess for HIV-1 virus-like particles  
coupling continuous upstream with end-to-end downstream processing

---

Manuscript in preparation

## ABSTRACT

HIV-1 Gag virus-like particles (VLPs) have been drawing attention as vaccine platform for their non-infectivity, ability to induce robust immune responses and versatility. However, challenges in their production, purification, and preservation still hinder their application. The production process, often reliant on transient gene expression (TGE), faces scalability limitations. Moreover, the downstream processing (DSP) presents challenges, including separating VLPs from extracellular vesicles (EVs), scale-up, and the lack of analytical methods to monitor the entire process. A complete bioprocess for Gag VLPs production is presented here, combining perfusion-based upstream production with a three-step DSP. Perfusion-based continuous production of Gag VLPs demonstrated significant yield improvements, with a 2.4-fold increase in VLP volumetric productivity compared to previous methods. Subsequent DSP steps, including secondary clarification and anion exchange chromatography (AEC) capture, resulted in approximately 60% purity. This ensures its scalability potential and robustness. The post-purification lyophilization step maintained VLP integrity and stability. This study presents an intensification strategy to address critical challenges in Gag VLP production, purification, and preservation, offering insights into enhancing vaccine biomanufacturing and distribution.

## ABBREVIATIONS

**AEC:** Anion Exchange Chromatography, **ATF:** Alternating Tangential Flow, **CSPR:** Cell Specific Perfusion Rate, **Cryo-TEM:** Cryo-Transmission Electron Microscopy, **DBC:** Dynamic Binding Capacity, **DSP:** Downstream Processing, **dsDNA:** Double-Stranded DNA, **EVs:** Extracellular Vesicles, **FV:** Flow Virometry, **HEK293:** Human Embryonic Kidney 293 Cells, **HIV-1:** Human Immunodeficiency Virus Type 1, **IEC:** Ion Exchange Chromatography, **MR:** Medium Replacement, **NTA:** Nanoparticle Tracking Analysis, **PBS:** Phosphate-Buffered Saline, **Pdl:** Polydispersity Index, **RFU:** Relative Fluorescence Units, **RT:** Room Temperature, **SDS-PAGE:** Sodium Dodecyl Sulfate Polyacrylamide Gel Electrophoresis, **SE-HPLC:** Size Exclusion-High Pressure Liquid Chromatography, **TGE:** Transient Gene Expression, **VHU-1:** Viral Harvesting Unit, **VLPs:** Virus-Like Particles.

## **INTRODUCTION**

Vaccines based on HIV-1 Gag virus-like particles (VLPs) have received attention due to their safety profile together with their ability to elicit both humoral and cellular immune responses. Due to their non-infectivity, they also pose no threat during production and can be safely handled in research facilities or during administration [1], [2]. Gag VLPs offer great versatility for vaccine design. Their protein core, formed by repetitive subunits, is highly effective for eliciting an immune response [3], as well as acting as scaffold improving particle integrity [4]. Since they are enveloped particles, the membrane surface can be pseudotyped with different antigens, making them promising candidates for hybrid or chimeric vaccines against various diseases. VLPs harboring several viral antigens have already been reported, including H1N1 [5], H5N1 [6], west Nile virus, dengue [7], rabies [8], [9], equine herpes virus [10], human papilloma virus [11] and SARS-CoV-2 [12]. They have also been reported as promising vectors for targeted protein delivery and T-cell activation, expanding their application to cancer research [13]. The potential of Gag VLPs as a platform for novel vaccine designs and therapeutic uses is often limited by the challenges posed by their production process. The upstream production usually relies on transient gene expression (TGE) [14], presenting limited scalability for the conventional batch process used. Perfusion has been widely implemented in industry to intensify the manufacturing of biopharmaceuticals, increasing the cell density at which the process operates and enabling continuous product harvesting from the perfusion module permeate [15]. However, high cell density represents a limitation for TGE-based bioprocesses as transfection and infection provide the best cell-specific productivity when carried out at low cell densities [16]. This has slowed down the use of perfusion for TGE-based bioprocesses, where it has been limited to serve as a tool for medium replacement (MR) [17], [18], [19]. The subsequent VLP downstream processing and further preservation is also crucial to intensify their manufacturing and meet the necessary standards for their intended application [20], [21]. Currently, one of the main obstacles is presented by the separation of VLPs and naturally produced extracellular vesicles (EVs). Their similar physicochemical properties challenge the development of an efficient separation process [22]. Moreover, the absence of reliable methods to characterize both VLPs and EVs populations along the different steps of the process poses additional challenges to guarantee consistent quality and uniformity across batches [23].

An often-employed alternative for purification is density gradient ultracentrifugation, where nanoparticles are isolated based on their varying sedimentation rates in a dense medium like sucrose or calcium chloride. However, this method has significant drawbacks including limited scalability, particle disruption affecting its immunogenicity, time-consuming procedures, and labor-intensiveness [24]. In contrast, chromatography emerges as a preferred alternative due to its scalability and widespread use in bio-separation processes [25], [26], [27], [28]. Among chromatography techniques, ion-exchange chromatography (IEC) is the most prevalent for VLP purification, with nearly every industrial purification process incorporating at least one IEC step [12], [29], [30]. IEC separates molecules based on their surface charge and is typically classified into anion or cation exchange chromatography. Anion exchange chromatography (AEC) involves a resin with positively charged functional groups that attract negatively charged molecules. Since HIV-1 Gag VLPs possess an overall negative net charge [28], AEC, such as the HiScreen™ Capto™ Q ImpRes column, whose resin is composed of quaternary amine groups [31], could facilitate specific binding. This AEC capture step has been reported to achieve approximately 75% recovery [29].

Finally, maintaining the integrity of purified Gag VLPs in an appropriate formulation buffer continues to be a significant challenge in the field. Although cold chain storage is traditionally employed, the instability and lack of accessibility to products in regions where the cold chain cannot be assured can affect the effectiveness of the candidate [32]. Lyophilization, or freeze-drying, plays a crucial role in enhancing the stability and longevity of Gag VLPs based vaccines [33], [34].

In this study, a complete bioprocess for Gag VLPs production in HEK293 cells has been implemented. A perfusion-based upstream production was coupled with a three-step downstream purification process (DSP). The cell-free clarified VLP-containing harvest was obtained directly from the filter module used for cell retention in the perfusion process. This was followed by a depth filtration and AEC chromatography and concluded with a formulation step including lyophilization. The results from this comprehensive study on the production, purification and preservation of Gag VLPs aim to address the current challenges in the field and develop strategies to enhance their manufacturing and global distribution.

## **MATERIALS AND METHODS**

### **Cell Line and Culture Conditions**

The cell line used is a serum-free suspension-adapted Human Embryonic Kidney HEK293 (HEK293SF-3F6) cell line from the National Research Council of Canada (NRC) (Montreal, Canada), kindly provided by Dr. Amine Kamen. Cells were routinely cultured in disposable polycarbonate 125 mL vented shake flasks (Corning, New York, USA) and expanded in 250 mL and 1000 mL vented shake flasks (Corning) kept in a Kuhner shaker LT-X (Kuhner, Birsfelden, Switzerland) at 37°C, 5% CO<sub>2</sub> and 85% RH and 130 rpm. Cells were passaged every 2-3 days at densities of 0.3 – 0.5x10<sup>6</sup> cells/mL with viabilities over 95% to maintain them in exponential growth phase. Culture medium was HyCell TransFx-H from HyClone (GE Healthcare, Chicago, USA) supplemented with 4mM GlutaMAX (Gibco, ThermoFisher Scientific, San Jose, USA) and 0.1% Pluronic F-68 (Gibco). Cell concentration and cell viability were determined using a NucleoCounter NC-3000 automatic cell nuclei counter (Chemometec, Allerød, Denmark) following the manufacturer's instructions.

### **Transient Transfection and Protein Expression**

Standard transfection was performed at a cell density of 2x10<sup>6</sup> cells/mL using a DNA concentration of 1µg/mL. The cationic transfection reagent was PEIPro (PolyPlus, Illkirch-Graffenstaden, France). Briefly, the corresponding amount of DNA was added to fresh culture medium (10% of the culture volume to be transfected) and vortexed for 10 seconds. Then, PEI was mixed in a ratio of 2:1 (w/w) to DNA and was vortexed three times for 3 seconds followed by 15 minutes of incubation at RT. Finally, the appropriate volume of transfection mixture was added to the culture. The plasmid used in the transfection, encoded the HIV-1 Gag polyprotein linked in-frame with the eGFP under the same CMV enhancer and CMV promoter, hereafter noted as Gag::eGFP VLPs. More details were described by A. Venereo-Sanchez et al (2016) [35]. To measure the transfection efficiency, the percentage of GFP-positive cells was assessed using a BD FACS Canto II flow cytometer (BD Biosciences, San Jose, CA, USA).

### Bioreactor culture conditions and setup description

A BioStat B Plus bioreactor (Sartorius Stedim Biotech, Goettingen, Germany) was used for HEK293SF-3F6 cell cultivation. It was equipped with a 3-blade segment dual impeller with UP-DP configuration. The agitation and temperature were set to 200 rpm and 37 °C respectively. The pH was set at 7.1 and controlled with CO<sub>2</sub> and NaHCO<sub>3</sub> (7.5%w/v). The dissolved oxygen was controlled at 40% of air saturation by supplementing air by sparger at a constant flow of 0.1L/min and additional pure oxygen when needed. The bioreactor was seeded at 0.5x10<sup>6</sup> cells/mL in 1.5 L of working volume. Samples were taken every 24 h for cell counting and viability determination. Transfection was performed when cells reached 2x10<sup>6</sup> cells/mL. After transfection, VLP quantification was performed every 24h. Perfusion was performed using an alternating tangential flow (ATF) system (Repligen, Waltham, MA, USA) and a viral harvesting unit (VHU-1) of 10µm pore size and 0.05 m<sup>2</sup> of filtration area as cell retention device (Artemis Biosystems, Quincy, MA, USA). This filtration step is henceforth regarded as the primary clarification step. The ATF flow rate used was 0.8 L/min and the cell specific perfusion rate (CSPR) was set at 30 pL·cell<sup>-1</sup>·day<sup>-1</sup>. For transfection, perfusion was stopped for 2h to allow the DNA polyplexes to enter the cells [36]. The scale and pumps were set up as shown in **Figure 1A** and as described by Lavado-García et. al [18].

### Confocal microscopy visualization

The visualization of the viral harvest unit module was performed using a FluoView®FV1000 confocal microscope (Olympus, Tokyo, Japan) at sampling speed of 2 mm/pixel, excitation at 488 nm and detection at 500-600 nm. Step size was 2 mm/slice using XYZ scan mode. Longitudinal, transversal and luminal cuts were made from one of the tubular filters of the viral harvest module exposed to VLP-producing HEK293 cell cultures. Objective lens UPLAPO 10x, NA: 0.40 and optical zoom 1x were used.

### Secondary clarification of Gag::eGFP VLPs

Cell culture harvest from VHU-1 filter was pooled and then clarified with Supracap™ 50V100™ depth filter capsules (Pall Corporation, New York, NY, USA). The filter was preequilibrated with phosphate-buffered saline (PBS) 1X before filtration. The clarification was performed with a K2Ri pump (Repligen, Waltham, MA, USA) with MasterFlex 96410-13 silicon tubes (Cole-Parmer, Vernon Hills, IL, USA) connected to the

filter inlet and outlet; and a pressure sensor (Cole-Parmer, Vernon Hills, IL, USA) connected to the filter inlet. The turbidity of the clarified samples was measured using a portable Eutech TN-100 turbidimeter (Thermo Fisher Scientific, Waltham, MA, USA).

#### **Gag::eGFP VLPs capture step by AEC**

A Capto Q ImpRes (Cytiva, Uppsala, Sweden) automatically operated in an AKTA Pure 25 system (GE Healthcare) was used to capture the Gag::eGFP VLPs from the Supracap<sup>TM</sup> 50V100<sup>TM</sup> depth filter clarified media. Before loading, the column was pre-equilibrated with 5 column volumes (CV) of 6% buffer B (50 mM HEPES, 2M NaCl, pH = 7.2: Buffer B). The media was directly loaded into the column via the sample pump. After sample application, the column was washed with 5 CV of buffer B at 6%. Elution was achieved by a salt step gradient consisting of 20 CV of 15%, 35%, 45% and 65% of buffer B (300 mM NaCl, 700 mM NaCl, 900 mM NaCl and 1300 mM NaCl). Solutions were filtered using 0.22 µm filters. Chromatographic runs were performed with a flow rate of 1 mL/min. Fractions of 1 mL were collected and pooled according to the chromatograms. Both protocols mentioned above are deeply described in chapter one [29].

#### **Dynamic binding capacity (DBC) study for Capto Q ImpRes column**

In order to evaluate the DBC of 4.7mL prepacked HiScreen<sup>TM</sup> Capto Q<sup>TM</sup> ImpRes (Cytiva, Uppsala, Sweden) to capture Gag::eGFP VLPs, 460mL of Supracap<sup>TM</sup> 50V100<sup>TM</sup> depth filter clarified sample was loaded onto the column and the flow-through samples were collected and analysed by dot blot and flow virometry for the presence of Gag::eGFP VLPs. The purification process was performed as described above. The dynamic binding capacity was calculated using equation (1) according to Y.F. Tseng et al (2017) [37]:

$$Q_{B, 10\%} = V_A \cdot \frac{C_0}{V_C} \quad (1)$$

Where  $Q_{B, 10\%}$  is the dynamic binding capacity at 10% level [VLPs/mL],  $V_A$  is the volume of feed applied up to the break point [mL],  $C_0$  is the concentration of VLPs in the feed [VLPs/mL] and  $V_C$  is the total column bed volume [mL].

**Lyophilization of Gag::eGFP VLPs**

A volume of 1mL of purified Gag::eGFP VLPs was aliquoted in 1 mL glass vials (Scharlau, Sentmenat, Barcelona, Spain) for lyophilization. The purified Gag::eGFP VLPs were previously buffer exchanged into lyophilization formulation (500mM sucrose; 5% (w/v) arginine; 10mM Tris-HCL, 75mM sodium chloride and 0.02 % (w/v) polysorbate 80) using Zebaspin columns MWCO 7K, 0,5 ml (Life Technologies S.A, Thermo Fisher Scientific). Aliquots were frozen at -80°C and subsequently lyophilized at -60°C at 100 µbar for 48h in a Coolvacuum, Lyomicron (Granollers, Barcelona, Spain). Lyophilized samples were reconstituted in PBS 1X prior to analysis. Particle size and quality were assessed using Dynamic Light Scattering (DLS), Size exclusion-high performance liquid chromatography (SE-HPLC), and Cryo-transmission electron microscopy (Cryo-TEM). This methodology is deeply described in chapter two.

**SE-HPLC analysis**

HPLC analyses were conducted with an Agilent 1100 Series HPLC System (Agilent Technologies, Santa Clara, CA, USA) equipped with a SEC 300A 2.7µm (7.8x50mm) Guard and a SEC 300A 2.7µm (7.8x300mm) columns (Agilent Technologies) at Servei d'Anàlisi Química (SAQ) of UAB (Barcelona, Spain). The mobile phase was composed of 150 mM sodium phosphate (pH 7.0). The analyses were performed at a flow rate of 1 mL/min with UV detection at 220 nm. Samples were directly plunged (25µL) provided column equilibration. Recorded signal from formulation buffer was taken as blank.

**Total protein and dsDNA quantification**

Total protein concentration was determined using the Micro BCA protein assay kit (#23225, Thermo Fisher Scientific, Waltham, MA, USA), according to the manufacturer's instructions. Briefly, serial PBS-buffer dilutions (between 2-256-fold) of standard and samples were dispensed into the wells. After adding 150µL of the Micro BCA working reagent into each well, plates were incubated for one hour at 37°C. The bovine serum standard curve ranged from 1,5 to 200 µg/mL, and the absorbance was measured at 562 nm in the Victor 3 reader (Perkin Elmer, MA, USA). Protein concentration of the samples was determined using the standard curve.



DNA concentration was determined using the Quant-it™ PicoGreen dsDNA assay kit (#P11496, Thermo Fisher Scientific, Waltham, MA, USA), according to the manufacturer's instructions. Briefly, serial TE 1X-buffer dilutions (between 2-256-fold) of standard and the samples were dispensed into 96-well microplates. After adding 100 µL of the Quant-iT™ PicoGreen® reagent (dilution 1:1000) into each well, plates were incubated for 5 minutes at room temperature. The dsDNA standard curve ranged from 1,5 to 500 µg/mL, and the absorbance was measured on the Victor 3 (Perkin Elmer, MA, USA), prior and later to the Quant-iT™ PicoGreen® reagent addition since HIV-1 Gag-eGFP VLPs emit at the same range. The settings were  $\lambda_{excitation} = 480 \text{ nm}$  and  $\lambda_{emission} = 520 \text{ nm}$ . DNA concentration of the samples was determined using the standard curve and subtracting the native fluorescence.

### **Western Blot and SDS-PAGE**

40 µL of sample were mixed with 20 µL of 4x LDS Sample Buffer and 7 µL of 2M DTT, followed by 20 minutes incubation at 96°C. The prepared samples were stored at 4°C until applied. 20 µL of each sample were loaded onto precast NuPAGE Bis/Tris gels 4–12% (Invitrogen, Carlsbad, CA, USA). 5 µL of SeeBlue® Plus2 Pre-stained Protein Standard (Invitrogen, Carlsbad, CA, USA) was used as low molecular weight control. Gels were run at 200V, 400mA, 45 minutes, in MES-SDS running buffer. For SDS-PAGE gels, proteins were stained with Coomassie Brilliant Blue G-250 based EZBlue™ Gel Staining Reagent (Sigma Aldrich, St. Louis, MO, USA). For Western blot analysis, proteins were transferred onto 0,2 µm nitrocellulose membranes using the Trans-Blot® turbo system (Bio-Rad Laboratories, Hercules, CA, USA). Membranes were blocked with PBS 5% (w/v) non-fat dry milk for 30 minutes, washed with PBS 0.1% (w/v) Tween-20, and then incubated overnight at 4°C with the primary monoclonal antibody against HIV-1 p24 (dilution 1:2000 in PBS) (A2-851-500 Icosagen AS, Tartumaa, Estonia). After washing, product immunodetection was performed with an anti-mouse IgG antibody conjugated with a horseradish peroxidase (dilution 1:5000 in PBS 1X) (1706516, Bio-Rad Laboratories, Hercules, CA, USA), incubated two hours at room temperature, and washed with PBS 0,1% (w/v) Tween-20. Protein bands were visualized by incubating the membranes with a Clarity™ Western ECL Substrate solutions for 2–3 minutes and scans were taken in a ChemiDoc MP (Bio-Rad Laboratories, Hercules, CA, USA).

**Dot blot**

Samples were charged into Bio-Dot Apparatus (#1706545, Bio-Rad, Hercules, CA, USA) while a low vacuum was applied. Nitrocellulose membrane (#88018, Thermo Fisher Scientific, Waltham, MA, USA) was placed at the top of humidified filter paper. Once samples were transferred, membrane was incubated with the primary monoclonal antibody against HIV-1 p24 (dilution 1:2000 in PBS1X) (A2-851-500 Icosagen AS, Tartumaa, Estonia) and an anti-mouse IgG secondary antibody (dilution 1:5000 in PBS1X) (1706516, Bio-Rad Laboratories, Hercules, CA, USA) following the same procedure previously mentioned for Western blot.

**DLS analysis**

The DLS technique was used to determine the size of Gag::eGFP VLPs. The measurements were carried out at 25°C in a Zetasizer Nano ZS instrument (Malvern Instruments, Malvern, UK), equipped with a He/Ne 633 nm laser at 173°. 100 µL of the sample were placed in disposable plastic cuvettes. Three consecutive measurements of each sample with 10-15 scans of ten seconds were performed for each independent measurement. The hydrodynamic diameter (MHD), particle size distribution in volume, derived count rate, and polydispersity index (PDI) average results were automatically obtained.

**Gag::eGFP VLPs quantification by Fluorimetry**

The extracellular concentration of Gag::eGFP VLPs was assessed by fluorimetry using an ad hoc developed and validated quantification assay [38]. VLP-containing supernatants were recovered by cell culture centrifugation at 1,000xg for 5 min. Relative fluorescence unit values (RFU) were calculated by subtracting fluorescence unit (FU) values of non-transfected negative control samples.

**Gag::eGFP VLPs quantification by Nanoparticle Tracking Analysis (NTA)**

NTA was performed with a NanoSight® LM20 device (NanoSight Ltd., Amesbury, UK) equipped with a blue laser module (488 nm) to quantify Gag::eGFP VLPs and neutral density filter for total particle by light scattering. Data were analyzed with NanoSight® NTA 3.2 software. Briefly, samples were injected, and three technical replicate analyses were carried out. Subsequently, particles were identified and tracked by their Brownian motion at RT. Capture settings were recorded with a sCMOS camera (camera level of 8 for Gag::eGFP VLPs samples, and 11 for controls, viscosity: 0.9 cP) and analyzed with a detection threshold

of 4. For the bioreactor samples, supernatant was clarified by centrifugation 5 min at 1,000xg. For the samples coming from the harvest fraction, no clarification was needed. The data obtained from these analyses were also used to calculate the percentage of Gag::eGFP VLPs relative to the total nanoparticles in the measured samples

#### **Gag::eGFP VLPs quantification by Flow Virometry (FV)**

Concentration of Gag::eGFP fluorescent events was quantified using a CytoFLEX LX (Beckman Coulter, Brea, CA, USA), equipped with a 405 nm filter. The VLPs were detected based on violet side scatter (V-SSC) and FITC fluorescence signals. Laser gains were optimized with values set to 72 for forward scatter (FSC), 135 for side scatter (SSC), 9 for V-SSC, and 500 for FITC. Samples were diluted with PBS 1X until an abort rate value below 2% was achieved. A total of 300,000 events were analyzed at a flow rate of 10  $\mu$ L/min per sample. VSSC-H vs B525-FITC density plots were used to gate the different particle populations. Gating was adjusted manually for each channel. Events after 50 s were taken for analysis. The results were normalized employing an internal control quantified by NTA. The results were analyzed with CytExpert v.2.3 software (Beckman Coulter, Brea, CA, USA).

#### **Gag::eGFP VLPs visualization in Cryo-TEM**

The morphology and electron density of Gag::eGFP VLPs were investigated under cryogenic conditions. The samples were rapidly frozen by plunging them into liquid ethane at a temperature of -180°C. Approximately 2  $\mu$ L of the sample was then applied to holey carbon grids that had been pre-treated with glow discharge using a PELCO easiGlow discharger unit. The cryo-frozen samples were transferred to a Leica EM GP cryo workstation and subsequently examined using a JEM-2011 electron microscope (JEOL Ltd., Tokyo, Japan) operating at an acceleration voltage of 200kV. Throughout the imaging process, the temperature was maintained at -180°C by the continuous addition of liquid ethane. Images were captured using a CCD-multiscan camera (Gatan Inc., Pleasanton, CA, USA) for further analysis and characterization.

## RESULTS

### Perfusion-based continuous Gag::eGFP VLP harvest

To implement an efficient upstream process allowing for continuous harvest of VLPs, the VHU-1 filter module was employed in a perfusion process with the setup shown in **Figure 1A**. The CSPR was set at  $30 \text{ pL} \cdot \text{cell}^{-1} \cdot \text{day}^{-1}$  to maintain the cells at a retransfectable state at  $2 \cdot 10^6 \text{ cells/mL}$  while harvesting the produced VLPs. The perfusion process was implemented as described by Lavado-García et al [18]. HEK293 cells were transfected at  $2 \times 10^6 \text{ cells/mL}$  and re-transfected 24hpt following the optimization of the EGE protocol. Observed cell growth (**Figure 1B**) was consistent with the shake flask control and previously reported growth curves using the same set up [18]. Viable cell density (VCD) remained stable after 24hpt at around  $3 \cdot 4 \cdot 10^6 \text{ cells/mL}$  up to 168hpt when the process was stopped. The use of a filter module that allowed VLP filtration resulted in a gradual increase of VLP concentration in the harvest fraction, from around  $1 \cdot 10^9 \text{ VLP/mL}$  at 72hpt to more than  $2 \cdot 10^{10} \text{ VLP/mL}$  at 168hpt. VLP concentration measured in the bioreactor reached its maximum value at 120hpt with around  $4 \cdot 10^{10} \text{ VLP/mL}$  and then started decreasing (**Figure 1C**). In terms of daily-produced VLPs, the highest value was also achieved at 120hpt. The subsequent reduction in daily-produced VLPs led to the decrease in VLP concentration within the bioreactor (**Figure 1C-1D**). By the end of the process at 168hpt, and with the current CSPR of  $30 \text{ pL} \cdot \text{cell}^{-1} \cdot \text{day}^{-1}$ , 49.9% of the total produced VLPs were collected in the harvest fraction (**Figure 1D-1E**). This evidenced the potential for further optimization with the new implemented cell retention device. Interestingly, at 168hpt, the amount of daily-harvested VLPs exceeded for the first time the number of daily-produced VLPs (**Figure 1F-1G**). To be able to assess the daily filtration rate at the given CSPR, the theoretical amount of VLPs that could have been filtered, given the harvested volume in a day and the VLP concentration in the bioreactor, was compared to the actual VLP concentration measured in the harvested volume (**Figure 1H**). We could observe that the process gradually increased the filtration rate from 24 to 96hpt, where it reached >99% (**Figure 1I**). This suggested that the filter module presented some binding capacity, as it has been previously observed for other hollow fiber modules [18], [19], [39]. The quality of the VLP sample recovered in the harvest fraction was also verified, presenting non-significant changes compared to a VLP sample in the bioreactor in terms of particle size, total particle distribution and VLP-to-monomer ratio (**Figure 2**). At 168hpt, a total of  $2.1 \cdot 10^{14}$  VLPs were

produced (**Figure 1D**). This meant a 2.4-fold increase in volumetric productivity compared to the previously reported work for perfusion-based VLP production (**Table 1**).

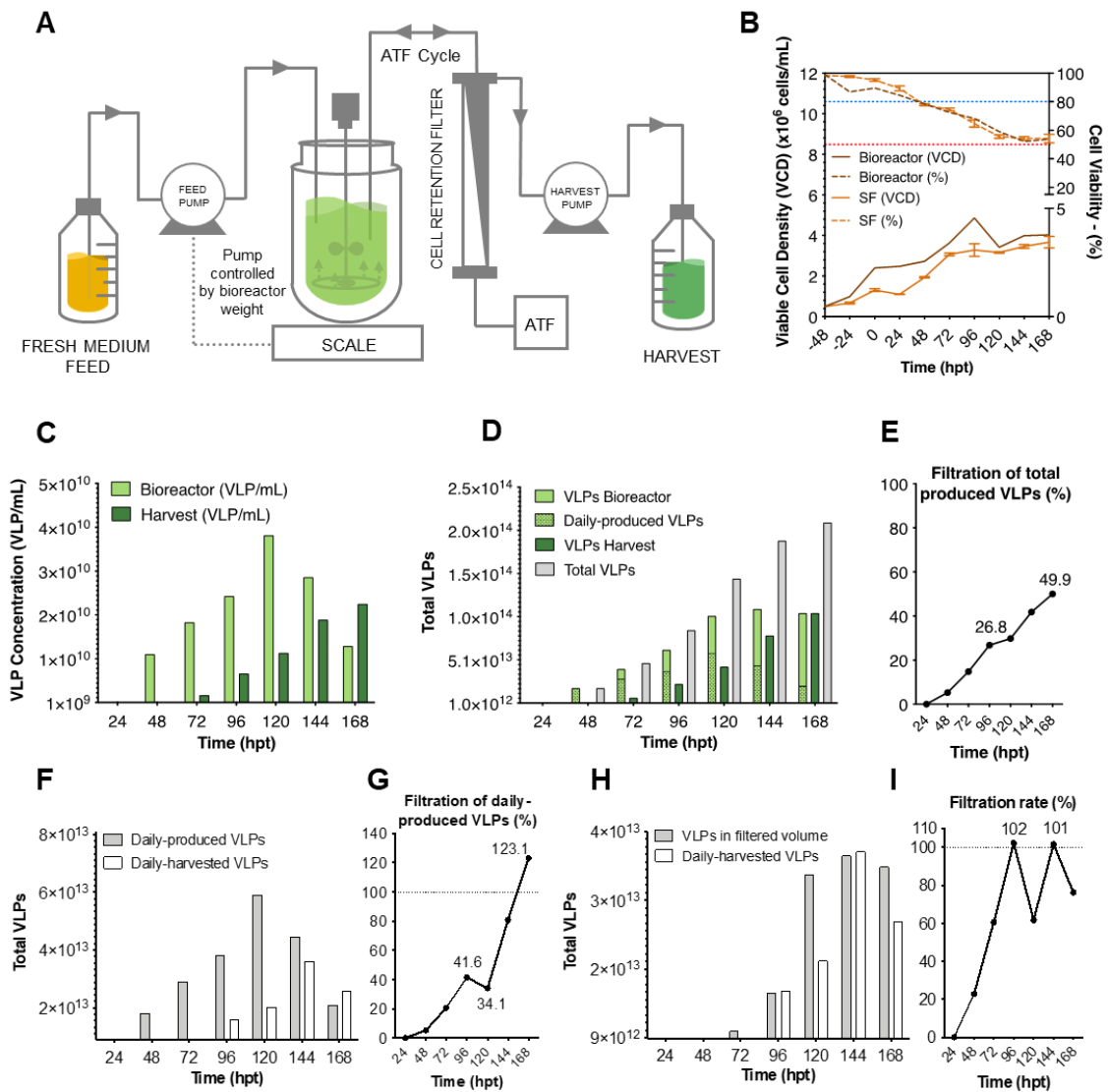


**Figure 1.** Production and filtration setup and parameters using VHU-1 filter module for VLP production. **A)** Schematic bioprocess diagram for the performed perfusion-based continuous VLP harvest. **B)** Viable cell density and cell viability along the process. The blue and red dotted line indicate 80 and 50% of cell viability, respectively. Cells were transfected at time point 0 and 24 hpt. Control shake flasks  $n=3$ , bioreactor  $n=1$ . **C)** VLP concentration measured in the bioreactor and harvest fraction along the process. **D)** Daily total VLP production in the bioreactor and harvest fractions along the process. **E)** Evolution of the filtration percentage to the harvest fraction of daily-produced total VLPs compared to total cumulative number of VLPs each day. **F)** Representation of the total daily-produced VLPs (grey) and total daily-harvested VLPs (blue) each day along the process. **G)** Evolution of the filtration percentage of daily-produced VLPs to the harvest fraction (blue in e) compared to the total number of daily-produced VLPs (grey in e). **H)** Representation of the total daily-harvested VLPs (blue) and the total VLPs quantified in the harvested volume (grey) each day along the process. **I)** Evolution of the filtration rate of each day comparing the number of daily-harvested VLPs (blue in g) to the theoretical number of VLPs that should have been filtered given the filtered volume at each day (grey in g). ATF: alternating tangential flow, SF: Shake flask, VCD: viable cell density, hpt: hours post-transfection

**Table 1.** Comparison of HFM and VHU cell retention devices

	HFM [18]	VHU
Material	PS, PES	PS, PP
Effective membrane surface area (m <sup>2</sup> )	0.13	0.01
Pore size (μm)	0.2 - 0.5	10
Length (cm)	60	23
Diameter (cm)	1.50	2.85
ATF flow rate (L/min)	0.6	0.8
Cell retention (%)	>99.9	>99.9
VLP retention (%)	>99.9	50
VLP concentration in bioreactor (VLP/mL)	$6.80 \cdot 10^{10}$	$6.97 \cdot 10^{10}$
VLP concentration in harvest (VLP/mL)	$1.29 \cdot 10^7$	$6.37 \cdot 10^{10}$
Total accumulated VLPs	$8.70 \cdot 10^{13}$	$2.10 \cdot 10^{14}$
Volumetric productivity (VLP · L <sup>-1</sup> · day <sup>-1</sup> )	$7.10 \cdot 10^{12}$	$1.71 \cdot 10^{13}$
Spent media / produced VLP (pL · VLP <sup>-1</sup> )	0.044	0.018

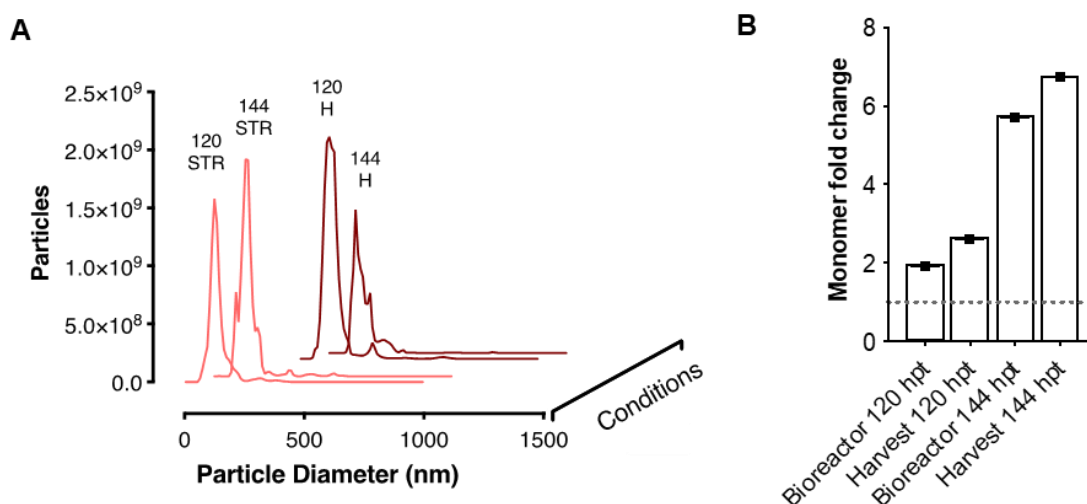


**Figure 2:** Quality of the produced VLPs **A)** Fluorescent total particle distribution measured by Nanoparticle tracking analysis (NTA) from samples coming the bioreactor (STR) and from the harvest fraction (H) at 120 and 144hpt. The peak in all conditions is located at around 140nm. **B)** Fold change ratio between the estimated particle concentration using fluorimetry and the detected actual particle concentration using NTA. This fold change shows the presence of unassembled free Gag monomers.

### Filter module characterization

Despite achieving a daily filtration rate of >99%, the gradual increase from 24 to 96hpt suggested some interaction between the VLPs and the fiber module. The fibers were analyzed by fluorescence confocal microscopy and showed some interaction in the luminal wall (**Figure 3A**). VLP-filter interaction was observed superficially in the luminal wall, reaching only ~200μm into the fiber wall of ~1.5 mm of total thickness

(**Figure 3B**). The transversal and longitudinal cuts of the fiber showed virtually no VLP interaction across the tube wall (**Figure 3B-3C**). This type of fiber showed significantly less particle retention compared to previously reported data on VLP production using other fiber modules [18] (**Table 1**).

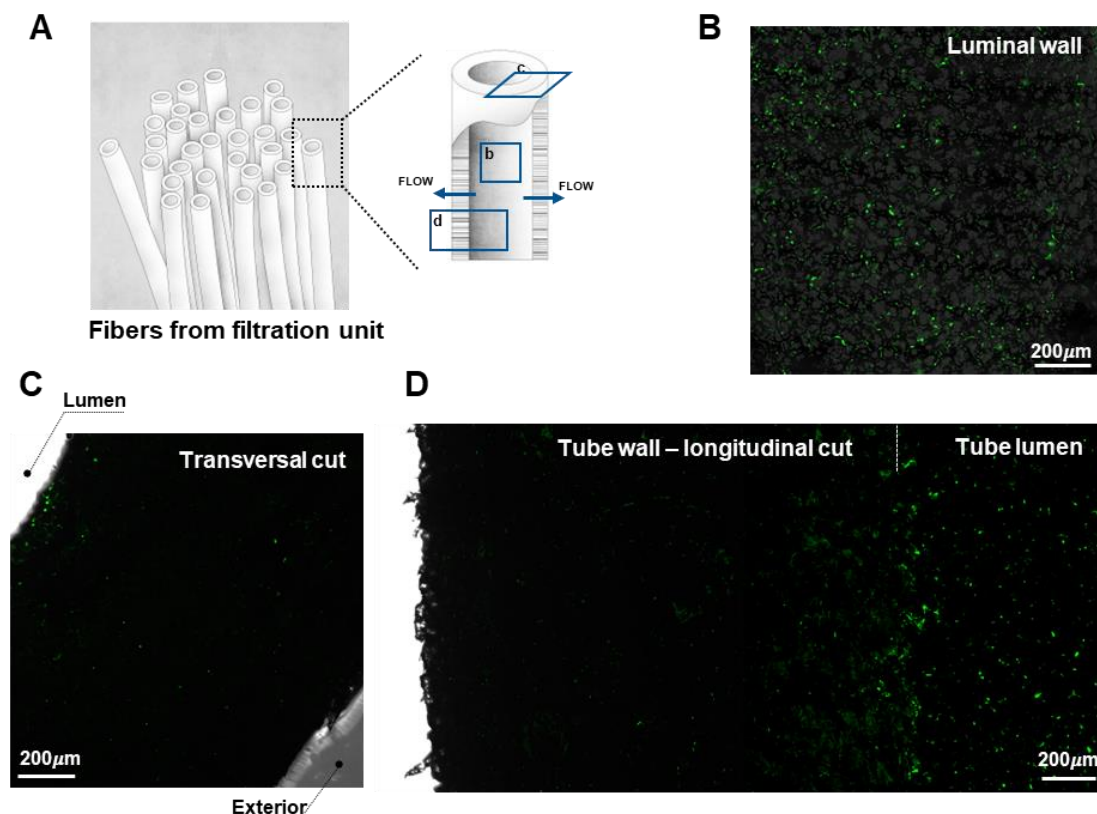


**Figure 3.** Confocal microscopy analysis of the viral harvest unit module. **A)** Schematic representation of the module fibers and the selected planes for imaging. **B)** Merge of reflected light and fluorescence emission for a cut of the luminal wall of the tube. **C)** Merge of transmitted light and fluorescent emission for a transversal cut of the filter wall. **D)** Merge of transmitted light and fluorescence emission of a longitudinal cut of the tube wall. Fluorescence is produced by the presence of retained GFP-containing VLPs.

At the end of the process, all the recovered harvest fractions were pooled before proceeding to DSP. The fact that VLPs were continuously harvested after VHU-1 filter as it allowed removal of >99% of cells (**Table 1**), allowed to integrate a primary clarification step in this initial phase, which presents a clear advantage over previously reported processes for VLP production [40]. This harvest pool fraction presented a concentration of  $8.66 \cdot 10^9$  Gag::eGFP VLPs/mL (**Table 2**) and was used as base material for the following DSP operations.

## Downstream process of the produced Gag::eGFP VLPs

### *Secondary clarification step*

The initial step in the downstream process consisted in the secondary clarification of the harvested product to further remove potential impurities such as cell debris, aggregates, and other contaminating particulate materials [25], [29], [41]. Turbidity was measured along the process to evaluate the efficiency of the secondary clarification step. The turbidity of the supernatant harvested from the primary clarification decreased from 20.6 NTU to 4.9 NTU following secondary clarification. 10 NTU was set as a critical value to proceed to the next chromatographic step. The feed pressure was maintained at 0 psi to avoid potential mechanical stress on the VLPs during clarification. As shown in **Table 2**, this process resulted in a 68% recovery of Gag::eGFP VLPs that corresponds to a concentration of  $5.87 \cdot 10^9$  Gag::eGFP VLPs/mL, and a 32% in purity with respect to the total nanoparticles of the sample from the primary clarification.

### *Capture step and dynamic binding capacity (DBC) study*

The capture step involved loading 115 mL, containing  $6.8 \cdot 10^{11}$  total Gag::GFP VLPs, from the secondary clarified sample directly into the Capto Q ImpRes AEC column (**Table 2**). The fractions obtained during the run were analysed considering the corresponding chromatogram (**Figure 4A**). The second step in the elution phase fraction (shown as P2) was considered the main product fraction due to the higher Gag::eGFP VLPs concentration and simultaneously lower total protein and dsDNA content (**Figure 4B and 4C**). Biochemical analyses showed Gag::eGFP polyprotein presence in samples coming from both primary and secondary clarification and eluted fractions P2, P3 and P4 (~87 kDa) by means of SDS-PAGE and Western blot anti-p24 (**Figure 4D and 4E**). However, the most intense signals were observed for the P2 sample, confirming the previous results. Therefore, the subsequent mass balance analyses were performed focusing on the P2 fraction. As shown in **Table 2**, P2 fraction contained  $8.18 \cdot 10^{10}$  Gag::eGFP VLPs/mL, accounting for 61% recovery relative to the loaded sample, with nearly 60% purity and a 25% enrichment of Gag::eGFP VLPs. This achievement indicates a 14-fold concentration increase and a 23-fold volume reduction in comparison to the secondary clarified sample.



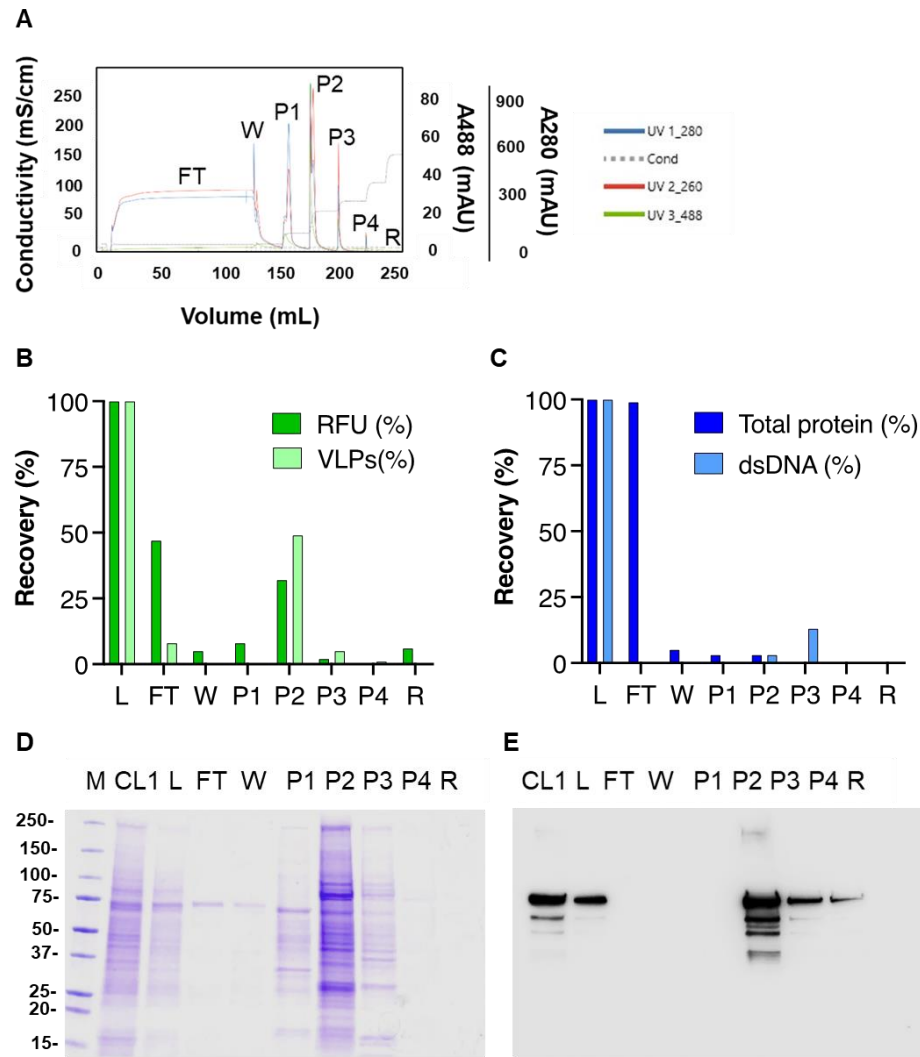


**Figure 4.** Purification data corresponding to a perfusion-based process for Gag::eGFP VLPs. **A)** Chromatogram of the step-gradient (15%, 35%, 45%, and 65%) purification; **B)** recovery of Gag::eGFP VLPs nanoparticle concentration measured by flow virometry (VLPs) and relative fluorescent units (RFU) measured by fluorimetry; **C)** total protein and dsDNA content measured by BCA and picogreen respectively; **D)** SDS-PAGE and **E)** anti-p24 Western Blot analysis for each fraction. The amount of protein loaded in the gel was normalized for each sample. *M*: molecular weight marker, *CL1*: primary clarified from VHU-1 filter, *L*: secondary clarified from Supracap 50V100 depth filter loaded into the Capto Q column, *F*: flow-through, *P1-P4*: elution peaks, *R*: regeneration peak, *Cond*: conductivity, *dsDNA*: double-stranded DNA, *SDS-PAGE*: sodium dodecyl sulfate-polyacrylamide gel electrophoresis.

Despite these are promising results in the field of DSP for VLPs, we have decided to study the DBC of this column with the objective of knowing the maximum amount of VLPs that can be loaded without loss of VLPs in the flow-through and to maximize recovery. Therefore, to determine the DBC,  $2.70 \cdot 10^{12}$  total Gag::eGFP VLPs from the secondary clarification step were applied to a 4.7-mL Capto Q ImpRes column. Samples from the flow-through were collected and analyzed by immunoblot (**Figure 5A**) and flow virometry for the presence of Gag::eGFP VLPs. It can be observed that approximately  $1.70 \cdot 10^{12}$  Gag::eGFP VLPs corresponding to 290 mL of secondary clarified sample were bound to the Capto Q ImpRes column before

breakthrough of 10% of Gag::eGFP VLP present in the feed occurred (**Figure 5B**). Based on this experiment, the DBC at 10% breakthrough was calculated to be approximately  $3.62 \cdot 10^{11}$  VLP per mL of column bed at the flow rate used (1mL/min).

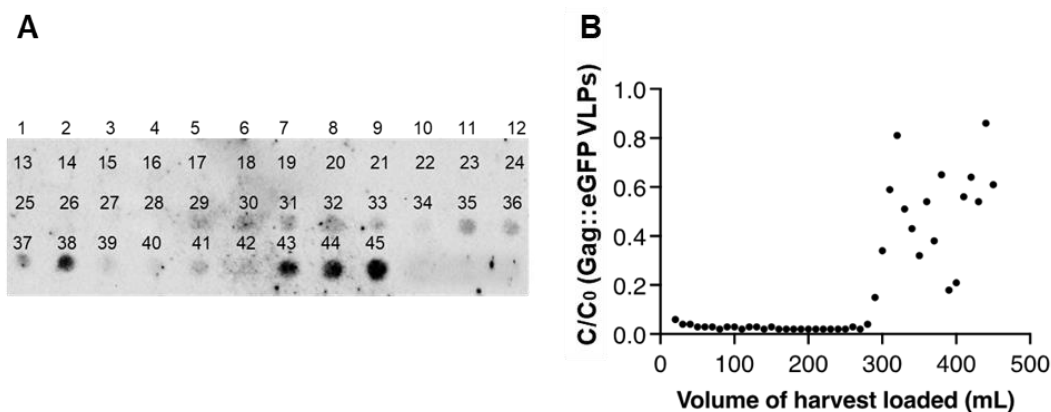


**Figure 5.** Investigation of the binding capacity of the 4.7mL HiScreen Capto Q ImpRes column. **A)** Immunoblot of the 46 flow-through (FT) fractions collected at every 10 mL during anion-exchange chromatography loading with 460 mL clarified harvest containing  $2.70 \cdot 10^{12}$  Gag::eGFP VLPs. **B)** Breakthrough curve to determine the dynamic binding capacity. The concentration (C) of Gag::eGFP VLPs leaking in the FT fractions was measured by flow virometry and normalized to the feed (Co) concentration.

### Characterization of purified and lyophilized Gag::eGFP VLPs

After elution from the capture step, Gag::eGFP VLPs were lyophilized under previously reported conditions. The quality of both purified and lyophilized Gag::eGFP VLPs was evaluated comparing size, SE-HPLC profile and shape. Analysis of the particle size distribution yielded an average hydrodynamic diameter of 130 nm for both experimental conditions, with a 95% confidence level. Furthermore, a low polydispersity index (Pdl) was observed, suggesting minimal variation in particle sizes within each condition. These findings underscored the uniformity and consistency of particle distribution (**Figure 6A**). The characterization conducted through the SE-HPLC enabled the evaluation of the quality of the lyophilized sample by comparing its profile with that of the purified sample. In this case, no significant differences were noted in the profiles, as all peaks aligned perfectly in terms of retention times and area [42] (**Figure 6B**). On the other hand, the morphology and shape of Gag::eGFP VLPs before and after lyophilization was confirmed by Cryo-TEM. **Figure 6C** shows electron-dense spherical nanoparticles surrounded by a lipid membrane under both conditions, consistent with previous reports for these VLPs [25], [29], [38]. Nanoparticle concentration of Gag::eGFP VLPs decreased from  $8.18 \cdot 10^{10}$  to  $5.24 \cdot 10^{10}$  Gag::eGFP VLPs/mL after lyophilization. After the

freeze-drying process, the obtained VLP titer remained within the same order of magnitude. Moreover, the purity level was maintained compared to the purified sample (Table 2).

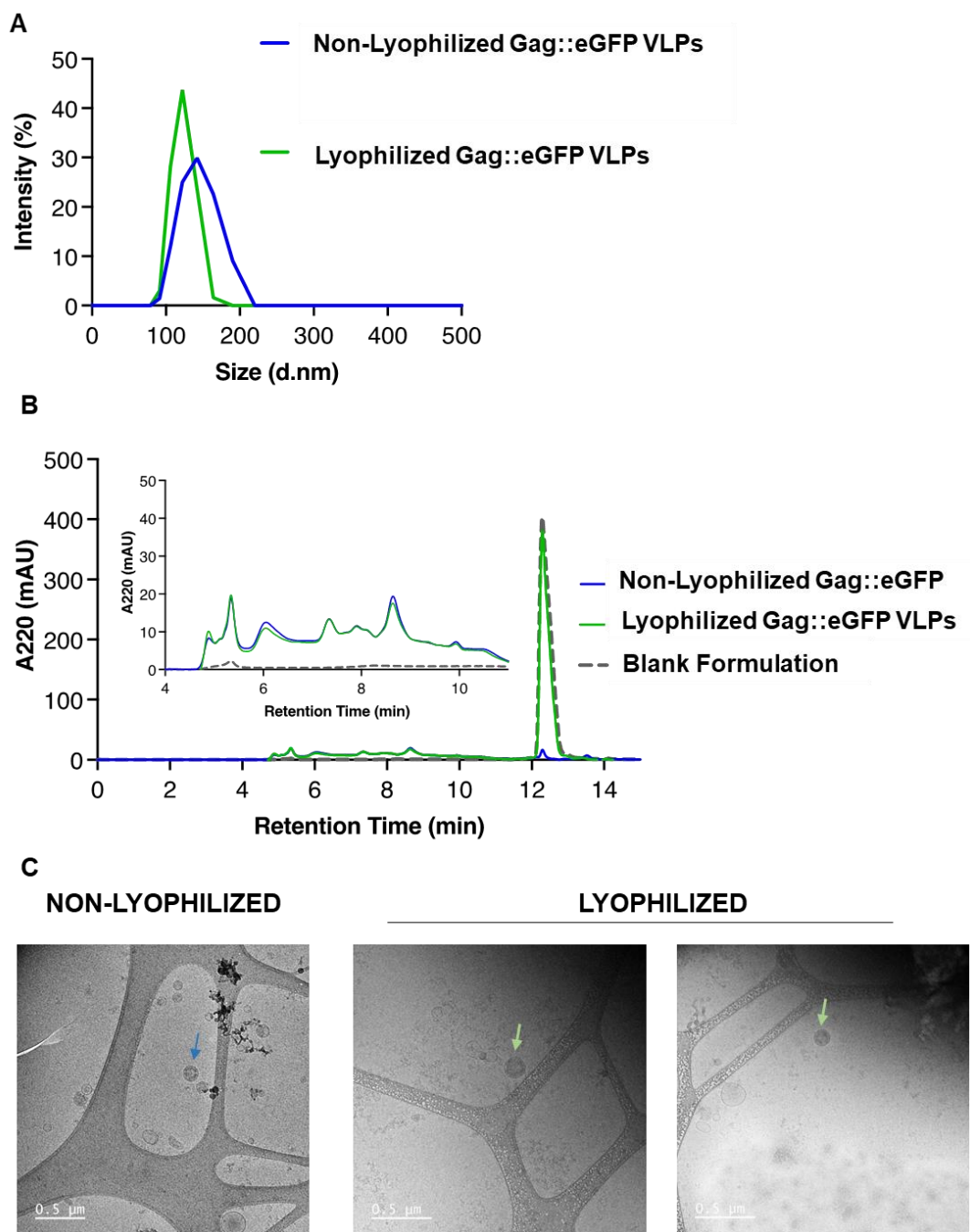


**Figure 6.** Biophysical characterization of purified and lyophilized Gag::eGFP VLPs. **A)** Particle size distribution analysis by DLS of Non-Lyophilized Gag::eGFP VLPs (Diameter size average:  $130 \pm 30$  d.nm, Pdl: 0.18) and Lyophilized Gag::eGFP VLPs (Diameter size average:  $130 \pm 20$  d.nm Pdl: 0.24). Two independent measurements were performed. **B)** SE-HPLC profile, normal and magnified view. **C)** Cryo-TEM micrographs. Narrows indicate Gag::eGFP VLPs. Abbreviations: DLS, Dynamic Light Scattering; Pdl, polydispersity index; SE-HPLC, Size exclusion-High pressure liquid chromatography; Cryo-TEM, Cryo-Transmission Electron Microscopy.

**Table 2:** Purification mass balance corresponding to a perfusion-based process for Gag::eGFP VLPs, total protein and dsDNA concentrations were measured by NTA, BCA and Picogreen assays respectively

Gag::eGFP VLPs recovery and purity							Total Protein and dsDNA Contaminant recovery			
Sample	Volume (mL)	Gag::eGFP VLPs/mL	Step Recovery* (%)	TP/mL	Purity (%) (VLPs/TPs)	Enrichment (%) (VLPs/TPs)	Total Protein (ug/mL)	Step Recovery* (%)	dsDNA (ng/mL)	Step Recovery* (%)
Primary Clarification	115	$8.66 \cdot 10^9$	-	$2.86 \cdot 10^{10}$	30	-	1096	-	4850.8	-
Secondary Clarification	115	$5.87 \cdot 10^9$	68	$1.82 \cdot 10^{10}$	32	2	479.8	44	1942.1	40
P2 Capto Q	5	$8.18 \cdot 10^{10}$	61	$1.44 \cdot 10^{11}$	57	25	315.6	3	1217.5	3
P2 Lyophilized	1	$5.24 \cdot 10^{10}$	64	$9.57 \cdot 10^{10}$	55	-	BLD	BLD	BLD	BLD

\*Recovery from previous step. *TP*: Total particles (Extracellular vesicles and Gag::eGFP VLPs mix); *P2 Capto Q*: elution peak from step 2 in Capto Q ImpRes chromatography; *dsDNA*: double stranded DNA, *BLD*: Below limit of detection.

## DISCUSSION

### The VHU-1 cell retention module allows continuous Gag VLP harvest

One of the main challenges for the implementation of a continuous process for Gag VLP production is the successful filtration of VLPs from the bioreactor in the upstream phase. VLPs present a bigger size than recombinant proteins for which conventional perfusion filter modules are designed. On the other side, production processes for viral particles, either via transfection or infection, are usually carried out transiently in batch or fed-batch [16]. Only recently, perfusion processes have begun to be applied in large-scale viral particle production [18], [19], [43], leading to new filter designs enabling successful VLP filtration and therefore harvesting in the membrane permeate rather than concentrating the produced VLPs in the bioreactor. In this work, we have implemented new VHU filter allowing continuous harvest to the permeate. The detected fluorescence in the inner walls of the filter coming from retained Gag::eGFP particles and monomers was 12-times lower in the VHU filter compared to previous observations [18]. While the same VLP concentration was achieved in the bioreactor, the total amount of VLP produced increased 2.4-fold (**Table 1**), allowing a subsequent increase in volumetric productivity. This further intensified the process, from requiring 0.044 pL of media per produced VLP to 0.018 pL/VLP (**Table 1**). This can be explained by the fact that removing produced particles and EVs from the extracellular medium has been reported to stimulate vesicle secretion in HEK293 cells [44]. Since naturally produced EVs share physicochemical properties with VLPs, allowing VLP filtration also led to EV filtration as observed by NTA measurements along the process (**Table 2**). Stimulation of vesicle secretion enhances Gag VLP budding, as VLPs can use

the endosomal pathway for exosome secretion as a secretion route [22], [45] . This finding indicates that implementing a continuous harvest of VLPs not only improves the process from a scalability perspective, but also contributes to improve VLP production from a cellular and metabolic level.

However, with the current setup and experimental procedure tested, at 168hpt only 49.9% of total produced VLPs are found in the harvest fraction. In order to increase the filtered VLPs, two strategies could be considered. The first strategy would be to reoptimize the CSPR. The CSPR used in this experiment was optimized to increase specific productivity while minimizing the spent media used in a pseudo-perfusion setup [18]. Using design of experiments to reoptimize this value using VLP concentration in the harvest as the response, could lead to a new CSPR value, expectedly higher than  $30 \text{ pL} \cdot \text{cell}^{-1} \cdot \text{day}^{-1}$ , that could allow recovery of more than 49.9% of VLPs in the harvest at 168hpt. The second strategy would be to maintain  $30 \text{ pL} \cdot \text{cell}^{-1} \cdot \text{day}^{-1}$  and switch off the feed at 168hpt, allowing the harvest pump to filter the remaining VLPs in the bioreactor. Nonetheless, this strategy would lead to higher cell concentration in the bioreactor, increasing the risk of filter clogging. Still, considering the cell concentrations used in transient transfection, this risk is considered potentially low. Optimizing the CSPR and the time to switch off the feed could also lead to a combination of both strategies.

A complementary approach to continue improving the integrated process would be to implement strategies that mitigate the cell density effect [16], allowing retransfections at higher cell densities. Engineering strategies such as optimizing the CSPR for transfection, the amount of DNA and the ATF filtration rate depending on cell concentration could not only improve VLP production, but also all TGE-based continuous bioprocess.

### **Purification yield and Gag VLP quality**

To purify and concentrate Gag::eGFP VLPs from the pooled perfusion-based continuous harvest, a DSP strategy was implemented. After the second clarification step, maintaining the turbidity below the critical value of 10 NTU assured that the subsequent chromatographic steps were initiated with a cleaner starting material, thereby enhancing the efficiency and yield of the purification process. This approach not only increases the likelihood of successful purification of the target VLPs but also minimizes the potential for

contamination, which is crucial for the scalability and robustness of the process. The observed 68% recovery of Gag::eGFP VLPs highlights the effectiveness of the secondary clarification step in retaining the target particles. Previous studies have shown that clarification of VLPs via depth filtration processes typically yields recovery rates of approximately 70%, in agreement with the results obtained here [12], [25] [46].

The Capto Q ImpRes column presented a viable option for large-scale VLP processing, striking a balance between recovery rates and purity that could significantly advance the field of VLP purification. This column was selected for the capture step due to its scalability, ease of handling, and effective performance in capturing large molecules and particles. This step facilitated a significant concentration of VLPs in the elution P2 fraction at conductivity values of 45-55 mS/cm. Similar elution conditions for VLPs have been reported [47], [48]. In this step Gag::eGFP VLPs purity levels of 60% were achieved, relative to total nanoparticles, aligning with results from previous research employing the same methodology (Chapter one [29] and two). The yield obtained was similar when using the same chromatography media for adenoviruses [49], or HIV-1 Gag VLPs [29], according to previous reports. The whole DSP also succeeded in the reduction of undesired residual cellular contaminants (**Table 2**), a crucial quality requirement for vaccines produced in cellular platforms [50]. These data support the use of strong quaternary amine ion exchangers to concentrate and purify HIV-1 Gag VLPs.

To further study the capture step, the DBC evaluation of the Capto Q ImpRes column was conducted by quantifying the amount of Gag VLP that can be loaded onto the column. The DBC value can vary based on several factors, including the type of column, the size of the VLPs, and the specific purification conditions employed. This critical parameter sheds light on the resin's ability to bind VLPs effectively during the chromatographic process, which is vital for designing efficient and scalable purification protocols and leveraging the robustness of the resins [51] [52].

Our findings suggest that a large-scale process could feasibly handle a VLP mass on the order of  $2.57 \cdot 10^{16}$  per cycle, assuming the DBC remains consistent in larger units as the column employed is available up to 71L. While higher DBCs have been observed for AEC using the Mustang Q membrane [25] and Monolith QA columns [28], the purity levels of VLPs relative to total nanoparticles in these cases fell below 50%,

Therefore, although alternative methods may offer higher DBC, the Capto Q ImpRes column presented a promising alternative.

The lyophilization process conducted post-purification produced nanoparticles with optimal characteristics in terms of size, quality, and morphology. DLS profiles for both purified and lyophilized Gag::eGFP VLPs samples indicated a homogeneous composition free from aggregates displaying the expected diameter size and morphology for Gag::eGFP VLPs [25], [27], [29], [38]. On the other hand, SE-HPLC provided a straightforward and rapid method for the quality control of VLP-based vaccines [53], [54]. The results from our study indicate no fluctuations in SE-HPLC profile between the purified and lyophilized samples, suggesting that lyophilization had not compromised the integrity of VLPs. Thus, their quality remained comparable to that of the pure sample. CryoTEM images further confirmed these results. Collectively, these findings highlighted VLP stability and integrity throughout the purification and lyophilization processes.

## **CONCLUSIONS**

In this work, we have shown that the implementation of a perfusion process coupled with a continuous VLP harvest improved 2.4-fold VLP volumetric productivity and allowed further intensification from the reported use of 0.044 to 0.018 pL of media per produced VLP. With the given parameters of the employed setup, 49.9% of the total produced VLPs were recovered in the harvest fraction where the cell retention device used for perfusion also allowed a first clarification step. Regarding the downstream processing, after the second clarification step 68% of the total produced VLPs were recovered. The capture step allowed 14-fold VLP concentration, 23-fold reduction in total volume and around 60% purity of VLPs. The final lyophilization step presented no significant loss when VLPs were resuspended after the freeze-drying process. Physicochemical characteristics of the produced VLPs were monitored throughout the whole production process, proving that the intensified bioprocess presented here is scalable and allows implementation for industrial VLP production.

## REFERENCES

- [1] J. Fuenmayor, F. Gòdia, and L. Cervera, "Production of virus-like particles for vaccines," *New Biotechnology*, vol. 39. Elsevier B.V., pp. 174–180, Oct. 25, 2017, doi: 10.1016/j.nbt.2017.07.010.
- [2] S. Nooraei *et al.*, "Virus-like particles: preparation, immunogenicity and their roles as nanovaccines and drug nanocarriers," *J. Nanobiotechnology*, vol. 19, no. 1, pp. 1–27, 2021, doi: 10.1186/s12951-021-00806-7.
- [3] R. Zuñiga *et al.*, "Relative Dominance of Gag p24-Specific Cytotoxic T Lymphocytes Is Associated with Human Immunodeficiency Virus Control," *J. Virol.*, vol. 80, no. 6, pp. 3122–3125, 2006, doi: 10.1128/jvi.80.6.3122-3125.2006.
- [4] C. Der Lee, Y. P. Yan, S. M. Liang, and T. F. Wang, "Production of FMDV virus-like particles by a SUMO fusion protein approach in *Escherichia coli*," *J. Biomed. Sci.*, vol. 16, no. 1, pp. 1–7, 2009, doi: 10.1186/1423-0127-16-69.
- [5] A. Venereo-Sánchez *et al.*, "Characterization of influenza H1N1 Gag virus-like particles and extracellular vesicles co-produced in HEK-293SF," *Vaccine*, vol. 37, no. 47, 2019, doi: 10.1016/j.vaccine.2019.07.057.
- [6] B. M. Giles and T. M. Ross, "A computationally optimized broadly reactive antigen (COBRA) based H5N1 VLP vaccine elicits broadly reactive antibodies in mice and ferrets," *Vaccine*, vol. 29, no. 16, pp. 3043–3054, 2011, doi: 10.1016/j.vaccine.2011.01.100.
- [7] A. J. Chua *et al.*, "A novel platform for virus-like particle-display of flaviviral envelope domain III: Induction of Dengue and West Nile virus neutralizing antibodies," *Virology*, vol. 10, pp. 1–18, 2013, doi: 10.1186/1743-422X-10-129.
- [8] L. Garnier *et al.*, "Incorporation of pseudorabies virus gD into human immunodeficiency virus type 1 Gag particles produced in baculovirus-infected cells," *J. Virol.*, vol. 69, no. 7, pp. 4060–4068, 1995, doi: 10.1128/jvi.69.7.4060-4068.1995.
- [9] D. Fontana, E. Garay, L. Cervera, R. Kratje, C. Prieto, and F. Gòdia, "Chimeric vlps based on hiv-1 gag and a fusion rabies glycoprotein induce specific antibodies against rabies and foot-and-mouth disease virus," *Vaccines*, vol. 9, no. 3, 2021, doi: 10.3390/vaccines9030251.
- [10] N. Osterrieder, R. Wagner, C. Brandmüller, P. Schmidt, and H. Wolf, "Protection against EHV-1 challenge infection in the murine model after vaccination with various formulations of recombinant glycoprotein gp14 (gB)," *Virology*, vol. 208, no. 2, pp. 500–510, 1995, doi: 10.1006/viro.1995.1181.
- [11] P. Di Bonito *et al.*, "Anti-tumor CD8+ T cell immunity elicited by HIV-1-based virus-like particles incorporating HPV-16 E7 protein," *Virology*, vol. 395, no. 1, pp. 45–55, 2009, doi: 10.1016/j.viro.2009.09.012.
- [12] A. Boix-Besora, E. Lorenzo, J. Lavado-García, F. Gòdia, and L. Cervera, "Optimization, Production, Purification and Characterization of HIV-1 GAG-Based Virus-like Particles Functionalized with SARS-CoV-2," *Vaccines*, vol. 10, no. 2, pp. 1–18, 2022, doi: 10.3390/vaccines10020250.
- [13] M. O. Mohsen, D. E. Speiser, A. Knuth, and M. F. Bachmann, "Virus-like particles for vaccination against cancer," *Wiley Interdiscip. Rev. Nanomedicine Nanobiotechnology*, vol. 12, no. 1, 2020, doi: 10.1002/wnan.1579.
- [14] S. Gutiérrez-Granados, L. Cervera, A. A. Kamen, and F. Gòdia, "Advancements in mammalian cell transient gene expression (TGE) technology for accelerated production of biologics," *Critical Reviews in Biotechnology*, vol. 38, no. 6. Taylor and Francis Ltd, pp. 918–940, Aug. 18, 2018, doi: 10.1080/07388551.2017.1419459.
- [15] J. M. Bielser, M. Wolf, J. Souquet, H. Broly, and M. Morbidelli, "Perfusion mammalian cell culture



- p for recombinant protein manufacturing – A critical review,”
- Biotechnol. Adv.*
- , vol. 36, no. 4, pp. 1328–1340, 2018, doi: 10.1016/j.biotechadv.2018.04.011.
- [16] J. Lavado-García, P. Pérez-Rubio, L. Cervera, and F. Gòdia, “The cell density effect in animal cell-based bioprocessing: Questions, insights and perspectives,” *Biotechnol. Adv.*, vol. 60, no. May, 2022, doi: 10.1016/j.biotechadv.2022.108017.
  - [17] J. Hong *et al.*, “Development of an alternating tangential flow (ATF) perfusion-based transient gene expression (TGE) bioprocess for universal influenza vaccine,” *Biotechnol. Prog.*, vol. 35, no. 5, 2019, doi: 10.1002/btpr.2831.
  - [18] J. Lavado-García, L. Cervera, and F. Gòdia, “An Alternative Perfusion Approach for the Intensification of Virus-Like Particle Production in HEK293 Cultures,” *Front. Bioeng. Biotechnol.*, vol. 8, no. June, pp. 1–16, 2020, doi: 10.3389/fbioe.2020.00617.
  - [19] M. D. Hein *et al.*, “Production of retroviral vectors in continuous high cell density culture,” *Appl. Microbiol. Biotechnol.*, vol. 107, no. 19, pp. 5947–5961, 2023, doi: 10.1007/s00253-023-12689-9.
  - [20] T. Vicente, A. Roldão, C. Peixoto, M. J. T. Carrondo, and P. M. Alves, “Large-scale production and purification of VLP-based vaccines,” *Journal of Invertebrate Pathology*, vol. 107, no. SUPPL. Jul. 2011, doi: 10.1016/j.jip.2011.05.004.
  - [21] M. Mittal, M. Banerjee, L. H. L. Lua, and A. S. Rathore, “Current status and future challenges in transitioning to continuous bioprocessing of virus-like particles,” *J. Chem. Technol. Biotechnol.*, vol. 97, no. 9, pp. 2376–2385, 2022, doi: 10.1002/jctb.6821.
  - [22] J. Lavado-García, I. González-Domínguez, L. Cervera, I. Jorge, J. Vázquez, and F. Gòdia, “Molecular Characterization of the Coproduced Extracellular Vesicles in HEK293 during Virus-Like Particle Production,” *J. Proteome Res.*, vol. 19, no. 11, pp. 4516–4532, 2020, doi: 10.1021/acs.jproteome.0c00581.
  - [23] Q. Zhao, S. Li, H. Yu, N. Xia, and Y. Modis, “Virus-like particle-based human vaccines: Quality assessment based on structural and functional properties,” *Trends Biotechnol.*, vol. 31, no. 11, pp. 654–663, 2013, doi: 10.1016/j.tibtech.2013.09.002.
  - [24] M. G. Moleirinho, R. J. S. Silva, P. M. Alves, M. J. T. Carrondo, and C. Peixoto, “Current challenges in biotherapeutic particles manufacturing,” *Expert Opinion on Biological Therapy*. 2019, doi: 10.1080/14712598.2020.1693541.
  - [25] I. González-Domínguez, E. Lorenzo, A. Bernier, L. Cervera, F. Gòdia, and A. Kamen, “A four-step purification process for gag vlps: From culture supernatant to high-purity lyophilized particles,” *Vaccines*, vol. 9, no. 10, pp. 1–19, 2021, doi: 10.3390/vaccines9101154.
  - [26] P. Pereira Aguilar *et al.*, “Capture and purification of Human Immunodeficiency Virus-1 virus-like particles: Convective media vs porous beads,” *J. Chromatogr. A*, vol. 1627, pp. 1–11, 2020, doi: 10.1016/j.chroma.2020.461378.
  - [27] P. Steppert *et al.*, “Separation of HIV-1 gag virus-like particles from vesicular particles impurities by hydroxyl-functionalized monoliths,” *J. Sep. Sci.*, vol. 40, no. 4, 2017, doi: 10.1002/jssc.201600765.
  - [28] P. Steppert *et al.*, “Purification of HIV-1 gag virus-like particles and separation of other extracellular particles,” *J. Chromatogr. A*, vol. 1455, pp. 93–101, Jul. 2016, doi: 10.1016/j.chroma.2016.05.053.
  - [29] E. Lorenzo, L. Miranda, F. Gòdia, and L. Cervera, “Downstream process design for Gag HIV - 1 based virus - like particles,” *Biotechnol. Bioeng.*, vol. 120, no. 9, pp. 2672–2684, 2023, doi: 10.1002/bit.28419.
  - [30] A. Roldão, M. C. M. Mellado, L. R. Castilho, M. J. T. Carrondo, and P. M. Alves, “Virus-like particles in vaccine development,” *Expert Review of Vaccines*, vol. 9, no. 10. pp. 1149–1176, Oct. 2010, doi: 10.1586/erv.10.115.

- [31] É. Szabó, L. Z. Baranyai, Z. Sütő, A. Salgó, and S. Gergely, "Attenuated total reflection fourier transform infrared spectroscopy based methods for identification of chromatography media formulations used in downstream processes," *J. Pharm. Biomed. Anal.*, vol. 180, 2020, doi: 10.1016/j.jpba.2019.113060.
- [32] O. S. Kumru, S. B. Joshi, D. E. Smith, C. R. Middaugh, T. Prusik, and D. B. Volkin, "Vaccine instability in the cold chain: Mechanisms, analysis and formulation strategies," *Biologicals*, vol. 42, no. 5, pp. 237–259, 2014, doi: 10.1016/j.biologicals.2014.05.007.
- [33] X. C. Tang and M. J. Pikal, "Design of Freeze-Drying Processes for Pharmaceuticals: Practical Advice," *Pharm. Res.*, vol. 21, no. 2, pp. 191–200, 2004, doi: 10.1023/b:pham.0000016234.73023.75.
- [34] F. Emami, A. Vatanara, E. J. Park, and D. H. Na, "Drying technologies for the stability and bioavailability of biopharmaceuticals," *Pharmaceutics*, vol. 10, no. 3, pp. 1–22, 2018, doi: 10.3390/pharmaceutics10030131.
- [35] A. Venereo-Sanchez *et al.*, "Hemagglutinin and neuraminidase containing virus-like particles produced in HEK-293 suspension culture: An effective influenza vaccine candidate," *Vaccine*, vol. 34, no. 29, pp. 3371–3380, Jun. 2016, doi: 10.1016/j.vaccine.2016.04.089.
- [36] L. Cervera, I. González-Domínguez, M. M. Segura, and F. Gòdia, "Intracellular characterization of Gag VLP production by transient transfection of HEK 293 cells," *Biotechnol. Bioeng.*, vol. 114, no. 11, pp. 2507–2517, 2017, doi: 10.1002/bit.26367.
- [37] Y. F. Tseng, T. C. Weng, C. C. Lai, P. L. Chen, M. S. Lee, and A. Y. C. Hu, "A fast and efficient purification platform for cell-based influenza viruses by flow-through chromatography," *Vaccine*, vol. 36, no. 22, pp. 3146–3152, 2018, doi: 10.1016/j.vaccine.2017.03.016.
- [38] J. Lavado-García, I. Jorge, A. Boix-Besora, J. Vázquez, F. Gòdia, and L. Cervera, "Characterization of HIV-1 virus-like particles and determination of Gag stoichiometry for different production platforms," *Biotechnol. Bioeng.*, vol. 118, no. 7, pp. 2660–2675, 2021, doi: 10.1002/bit.27786.
- [39] A. Nikolay, J. de Grooth, Y. Genzel, J. A. Wood, and U. Reichl, "Virus harvesting in perfusion culture: Choosing the right type of hollow fiber membrane," *Biotechnol. Bioeng.*, vol. 117, no. 10, pp. 3040–3052, 2020, doi: 10.1002/bit.27470.
- [40] S. Gutiérrez-Granados, F. Gòdia, and L. Cervera, "Continuous manufacturing of viral particles," *Current Opinion in Chemical Engineering*, vol. 22, 2018, doi: 10.1016/j.coche.2018.09.009.
- [41] S. B. Carvalho *et al.*, "Efficient filtration strategies for the clarification of influenza virus-like particles derived from insect cells," *Sep. Purif. Technol.*, vol. 218, pp. 81–88, Jul. 2019, doi: 10.1016/j.seppur.2019.02.040.
- [42] N. T. Lan *et al.*, "Stability of virus-like particles of red-spotted grouper nervous necrosis virus in the aqueous state, and the vaccine potential of lyophilized particles," *Biologicals*, vol. 51, no. October, pp. 25–31, 2018, doi: 10.1016/j.biologicals.2017.11.002.
- [43] M. D. Hein, A. Chawla, M. Cattaneo, S. Y. Kupke, Y. Genzel, and U. Reichl, "Cell culture-based production of defective interfering influenza A virus particles in perfusion mode using an alternating tangential flow filtration system," *Appl. Microbiol. Biotechnol.*, vol. 105, no. 19, pp. 7251–7264, 2021, doi: 10.1007/s00253-021-11561-y.
- [44] P. Pérez-Rubio, J. Lavado-García, L. Bosch-Molist, E. L. Romero, L. Cervera, and F. Gòdia, "Extracellular vesicle depletion and UGCG overexpression mitigate the cell density effect in HEK293 cell culture transfection," *Mol. Ther. Methods Clin. Dev.*, vol. 32, no. 1, p. 101190, 2024, doi: 10.1016/j.omtm.2024.101190.
- [45] J. Lavado-García, A. Díaz-Maneh, N. Canal-Paulí, P. Pérez-Rubio, F. Gòdia, and L. Cervera, "Metabolic engineering of HEK293 cells to improve transient transfection and cell budding of HIV-1

- virus-like particles," *Biotechnol. Bioeng.*, vol. 118, no. 4, pp. 1649–1663, 2021, doi: 10.1002/bit.27679.
- [46] S. B. Carvalho *et al.*, "Membrane-Based Approach for the Downstream Processing of Influenza Virus-Like Particles," *Biotechnol. J.*, vol. 14, no. 8, Aug. 2019, doi: 10.1002/biot.201800570.
- [47] K. Reiter, P. P. Aguilar, V. Wetter, P. Steppert, A. Tover, and A. Jungbauer, "Separation of virus-like particles and extracellular vesicles by flow-through and heparin affinity chromatography," *J. Chromatogr. A*, vol. 1588, pp. 77–84, Mar. 2019, doi: 10.1016/j.chroma.2018.12.035.
- [48] P. Pereira Aguilar *et al.*, "Polymer-grafted chromatography media for the purification of enveloped virus-like particles, exemplified with HIV-1 gag VLP," *Vaccine*, vol. 37, no. 47, pp. 7070–7080, 2019, doi: 10.1016/j.vaccine.2019.07.001.
- [49] M. G. Moleirinho *et al.*, "Clinical-Grade Oncolytic Adenovirus Purification Using Polysorbate 20 as an Alternative for Cell Lysis," *Curr. Gene Ther.*, vol. 18, no. 6, pp. 366–374, 2018, doi: 10.2174/1566523218666181109141257.
- [50] I. Knezevic, G. Stacey, and J. Petricciani, "WHO Study Group on cell substrates for production of biologicals, Geneva, Switzerland, 11-12 June 2007," *Biologicals*, vol. 36, no. 3, pp. 203–211, 2008, doi: 10.1016/j.biologicals.2007.11.005.
- [51] T. M. Lima, M. O. Souza, and L. R. Castilho, "Purification of flavivirus VLPs by a two-step chromatographic process," *Vaccine*, vol. 37, no. 47, pp. 7061–7069, 2019, doi: 10.1016/j.vaccine.2019.05.066.
- [52] P. L. Ferreira, H. Marie, T. Berger, B. Edelmann, O. Rammo, and F. Sousa, "Evaluation of novel chromatographic prototypes for supercoiled plasmid DNA polishing," *Front. Bioeng. Biotechnol.*, vol. 11, no. January, pp. 1–13, 2023, doi: 10.3389/fbioe.2023.1296444.
- [53] M. A. Al-ghobashy, M. M. Mostafa, H. S. Abed, F. A. Fathalla, and M. Y. Salem, "Correlation between Dynamic Light Scattering and Size Exclusion High Performance Liquid Chromatography for Monitoring the Effect of pH on Stability of Biopharmaceuticals Correspondence: Aggregate formation is a major problem affecting both safety and eff," *J. Chromatogr. B*, vol. 1060, pp. 1–9, 2017, doi: 10.1016/j.jchromb.2017.05.029.
- [54] Y. Yang *et al.*, "Size-exclusion HPLC provides a simple, rapid, and versatile alternative method for quality control of vaccines by characterizing the assembly of antigens," *Vaccine*, vol. 33, no. 9, pp. 1143–1150, 2015, doi: 10.1016/j.vaccine.2015.01.031.

## **CHAPTER FOUR**

Engineering of a CXCR4-targeted HIV-1 Gag VLP by T22 peptide functionalization

via copper-free click chemistry

## **ABSTRACT**

The use of VLPs as nanocarriers for biomolecules presents a promising alternative in drug delivery research. CXCR4 is a cell surface receptor marker associated with several types of cancer. T22 peptide is a known antagonist of this receptor that binds to and penetrates CXCR4 positive cells efficiently. In this work, Gag VLPs were produced in HEK293 cells and purified by anion exchange chromatography. The purification process allowed to obtain the Gag VLPs at a purity level of 60%. These VLPs were functionalized with the T22 peptide by click chemistry reactions. The ability of the Gag VLPs-T22 to penetrate CXCR4 positive cells were observed to be dose and time-dependent. CXCR4 positive cells exposed to  $8.0 \cdot 10^9$  functionalized Gag VLPs/mL were 30 times more fluorescent than those exposed to non-functionalized Gag VLPs after 24h of incubation. The non-entry of Gag VLPs-T22 into CXCR4 negative cells demonstrated the specificity of internalization via CXCR4 receptor. The functionalization of Gag VLPs with T22 ligand to target CXCR4 positive cells has been demonstrated and is crucial due to the receptor's significant role in the progression and metastasis of several types of cancer. By specifically targeting CXCR4, the VLPs can selectively deliver therapeutic biomolecules to cancer cells, thereby enhancing the efficacy of the treatment while minimizing off-target effects and reducing systemic toxicity.

## **ABBREVIATIONS**

**Cryo-TEM:** Cryogenic transmission electron microscopy, **CXCR4:** CXC chemokine receptor 4, **DBCO-sulfo-NHS:** Dibenzocyclooctyne-sulfo-N-hydroxysuccinimidyl ester, **DLS:** Dynamic Light Scattering, **GFP:** Green Fluorescent Protein, **HEK293:** Human Embryonic Kidney 293 cell line, **HIV-1:** Human Immunodeficiency Virus 1, **NTA:** Nanoparticle Tracking Analysis, **PBS:** Phosphate-buffered saline, **PDI:** Polydispersity index, **SEC-HPLC:** Size exclusion high-performance liquid chromatography, **SPAAC:** Strain-promoted alkyne-azide cycloaddition, **SDS-PAGE:** Sodium dodecyl sulfate-polyacrylamide gel electrophoresis, **SW1417:** Human colorectal adenocarcinoma cell line, **T22:** Tyr5,12, Lys7)-polyphemusin II peptide, **VLPs:** Virus-like particles.

## INTRODUCTION

The targeted delivery of genes and their products into cells or tissues encompasses various applications, including vaccine development, gene therapy, and diagnostic imaging, employing diverse techniques such as biological, chemical, and physical methods [1]. Recent years have seen the rise of nanocarriers like inorganic nanoparticles and lipid-nanoparticles for cargo delivery [2]. Among these, virus-like particles (VLPs) stand out as promising delivery vehicles, offering inherent biocompatibility, tunable surface properties, and targeted payload delivery [1], [3], [4], [5]. These nanoparticles mimic the structural conformation of native viruses but lack of viral genetic material, preventing any potential pathogenicity caused by infection or replication [6]. The three-dimensional structure and cell invasion property of VLPs also makes them an excellent candidate for intracellular delivery of biomolecules. VLPs have demonstrated advantages in drug delivery [7], including higher efficiency, consistent self-assembly, flexible functionalization, and low toxicity. Examples include targeted delivery of chemotherapeutic drugs, proteins/peptides, DNA, and siRNA, making VLPs versatile tools in biomedicine [8].

This work focuses specifically on the use of the immunodeficiency virus 1 (HIV-1) Gag VLPs fused to the Enhanced Green Fluorescent Protein (eGFP), hereinafter referred to as Gag::eGFP VLPs as a potential targeted drug nanocarrier. The cytoplasmic translation of the polyprotein Gag leads to self-assembly at the host cell membrane, facilitating the budding of Gag VLPs [9], [10]. During this process, VLPs acquire their outer envelope from the host cell's membrane, which can be engineered to express specific epitopes of interest. This engineering process involves genetic modifications and the co-expression of desired proteins, making VLPs versatile tools for diverse biomedical applications [11], [12], [13]. In recent years, chemical conjugation has emerged as an alternative approach to functionalize VLPs, gaining significant interest for its advantages over traditional methods and its substantial potential in biomedical applications [5], [14]. With the rapid advancement of click chemistry, a simple and efficient method, proteins and nucleic acids can be conjugated to azide or alkyne groups, and then directly linked to the VLP surface using either copper-catalyzed or copper-free click chemistry reactions [15], [16].

Strain-promoted alkyne-azide cycloaddition (SPAAC) copper-free conjugation has found extensive application in the functionalization of exosomes and VLPs across various fields. Its versatility has been

leveraged for applications ranging from synergistic cancer therapy and treatment of central nervous system injuries to drug delivery, antitumor vaccine development, tissue engineering, and *in vivo* cell imaging [17], [18], [19]. Functionalizing nanoparticles with SPAAC can essentially be accomplished through two methods. First, azides or alkynes can be introduced into biomolecules via metabolic incorporation of labeled metabolites, resulting in labeled nanoparticles. Alternatively, direct chemical conjugation to the nanoparticles enables orthogonal reactions with the partner molecules [20], [21].

This study presents a novel approach using a SPAAC reaction to functionalize Gag::eGFP VLPs with the T22 peptide. To the best of our knowledge, this is the first time this specific conjugation has been reported. The method employs a dual-reaction click chemistry approach previously optimized by Garcia-Trujillo et al (2024) [22], facilitating the expression of the T22 peptide on the surface of VLPs. Derived from horseshoe crab blood samples, the T22 peptide, also known as (Tyr5,12, Lys7)-polyphemusin II, has exhibited remarkable efficacy as a tag for intracellular targeting within CXC chemokine receptor 4 positive (CXCR4+) cells [23], effectively mediating the internalization of self-assembling protein-only nanoparticles [24], [25], [26], [27]. Notably, CXCR4 is a cell-surface receptor overexpressed in more than 20 cancer types, making it a prime target in cancer therapy [28], [29], [30], [31]. The objective of this study is to validate the targeted entry capability of T22-functionalized Gag::eGFP VLPs into CXCR4+ cells. This research holds significant promise as a potential tool for targeted drug delivery [32], particularly in cancer medicine [33], where specific targeting of tumor cells is of paramount importance.

## MATERIALS AND METHODS

### Cell line and culture conditions for nanoparticles production

The cell line used is a serum-free suspension-adapted Human Embryonic Kidney HEK293 (HEK293SF-3F6) cell line from the National Research Council of Canada (NRC) (Montreal, Canada), kindly provided by Dr. Amine Kamen. Cells were routinely cultured in disposable polycarbonate 125 mL vented shake flasks (Corning, New York, USA) and expanded in 250 mL and 1000 mL vented shake flasks (Corning) kept in a Kuhner shaker LT-X (Kuhner, Birsfelden, Switzerland) at 37°C, 5% CO<sub>2</sub> and 85% RH and 130 rpm. Cells were passaged every 2-3 days at densities of  $0.3 - 0.5 \cdot 10^6$  cells/mL with viabilities over 95% to maintain

them in exponential growth phase. Culture medium was HyCell TransFx-H from HyClone (GE Healthcare, Chicago, USA) supplemented with 4mM GlutaMAX (Gibco, ThermoFisher Scientific, San Jose, USA) and 0.1% Pluronic F-68 (Gibco). Cell concentration and cell viability were determined using a NucleoCounter NC-3000 automatic cell nuclei counter (Chemometec, Allerød, Denmark) following the manufacturer's instructions.

### **VLP production by transient transfection**

Cell transfection was performed at a cell density of  $2 \cdot 10^6$  cells/mL using a DNA concentration of 1  $\mu$ g/mL. The cationic transfection reagent was PEIPro (PolyPlus, Illkirch-Graffenstaden, France). Briefly, DNA was added to fresh culture medium (10% of the culture volume to be transfected) and vortexed for 10 seconds. Then, PEI was mixed in a ratio of 2:1 (w/w) to DNA and was vortexed three times for 3 seconds followed by 15 minutes of incubation at room temperature. Finally, the appropriate volume of transfection mixture was added to the cultures. The plasmid used encoded the HIV-1 Gag polyprotein fused in frame to the eGFP under the same CMV enhancer and CMV promoter. More details were described by A. Venereo-Sanchez et al (2016) [32]. To measure the transfection efficiency, the percentage of GFP-positive cells was assessed using a BD FACS Canto II flow cytometer (BD Biosciences, San Jose, CA, USA).

### **Gag::eGFP VLP purification process**

Cell culture supernatant (500 mL) was clarified with Supracap™ 50V100™ depth filter capsules (Pall Corporation, New York, NY, USA). Then, the clarified supernatant was loaded into a 4.7mL prepacked HiScreen™ Capto Q™ ImpRes (Cytiva, Uppsala, Sweden) automatically operated in an AKTA Pure system (Cytiva, Uppsala, Sweden). The purification has been described in detail previously in chapter one [34]. The purified Gag::eGFP VLPs were then buffer exchanged into PBS1X using Zebaspins columns MWCO 7K, 0.5 mL (Life Technologies S.A, Thermo Fisher Scientific).

### **Gag::eGFP VLP functionalization by click chemistry**

In this study, we performed bio-orthogonal strain-promoted azide-alkyne cycloaddition reactions using dibenzocyclooctyne-sulfo-N-hydroxysuccinimidyl ester (DBCO-sulfo-NHS) as a bifunctional crosslinker [20].



Initially, DBCO-sulfo-NHS reacted with primary amine-containing molecules on the envelope of Gag::eGFP VLPs. Subsequently, in the second reaction step, DBCO reacted with the azide containing T22 peptide, forming a triazole bond that facilitated the covalent attachment of T22 to the VLP surface. These reactions were conducted in PBS1X at pH 7.4 without any catalyst, under agitation at 37 °C. During the first reaction, 49.6 µM of DBCO-sulfo-NHS was added to  $3.7 \cdot 10^{11}$  VLPs/mL, resulting in a vast excess of DBCO relative to VLPs. This reaction was maintained for 24h. For the second reaction, 32.3 µM of T22 peptide was added in a molar ratio of 1:1.54 (T22: DBCO-sulfo-NHS) and the reaction was continued for 12h. To remove unconjugated reagents, an ultracentrifugation step at  $164000 \times g$  for 2h at 4°C was performed using a SW32-Ti rotor in an Optima L-100 XP ultracentrifuge (Beckman Coulter). The ultracentrifugation supernatants were discarded, and the functionalized nanoparticles were resuspended in pre-chilled PBS to the original reaction volume. The protocol performed here for functionalization is thoroughly described by García-Trujillo et al [22]. The T22 peptide (P-T22: RRWCYRKCYKGYCYRKCR) was chemically synthesized at the Institut de Química Avanzada de Catalunya (IQAC-CSIC, Barcelona, Spain), with a modified lysine containing an azide group added at the C-terminus of the peptide epitope. The N-terminus is acetylated, and the C-terminus contains an amide group.

### **Western Blot and SDS-PAGE**

40 µL of sample were mixed with 20 µL of 4x LDS Sample Buffer and 7 µL of 2M DTT, followed by 20 minutes incubation at 96°C. The prepared samples were stored at 4°C until applied. 20 µL of each sample were loaded onto precast NuPAGE Bis/Tris gels 4–12% (Invitrogen, Carlsbad, CA, USA). 5 µL of SeeBlue® Plus2 Pre-stained Protein Standard (Invitrogen, Carlsbad, CA, USA) was used as low molecular weight control. Gels were run at 200V, 400mA, 45 minutes, in MES-SDS running buffer. For SDS-PAGE gels, proteins were stained with Coomassie Brilliant Blue G-250 based EZBlue™ Gel Staining Reagent (Sigma Aldrich, St. Louis, MO, USA). For Western blot analysis, proteins were transferred onto 0.2 µm nitrocellulose membranes using the Trans-Blot® turbo system (Bio-Rad Laboratories, Hercules, CA, USA). Membranes were blocked with PBS1X 5% (w/v) non-fat dry milk for 30 minutes, washed with PBS1X 0.1% (w/v) Tween-20, and then incubated overnight at 4°C with the corresponding primary antibodies diluted 1:1000 in PBS1X. For detection of HIV-1 Gag VLPs was used the mouse monoclonal antibody anti-HIV-1 p24 (A2-851-500,

Icosagen, Tartu, Estonia), and for detection of T22 peptide was used the rat monoclonal antibody anti-T22 (developed in the Institut de Recerca Sant Pau, Barcelona, Spain). After primary incubation, membranes were incubated using anti-mouse IgG coupled with a horseradish peroxidase antibody produced in goat (1706516, Bio-Rad Laboratories, Hercules, CA, USA) or anti-rat IgG coupled with a horseradish peroxidase antibody produced in goat (31470, Thermo Fisher Scientific, Waltham, MA, USA), as required, in wash buffer for 1h at RT. Protein bands were visualized by incubating the membranes with a Clarity™ Western ECL Substrate solutions for 2–3 minutes and scans were taken in a ChemiDoc MP (Bio-Rad Laboratories, Hercules, CA, USA).

### **Dot blot**

Samples were charged into Bio-Dot Apparatus (#1706545, Bio-Rad Laboratories, Hercules, CA, USA) while a low vacuum was applied. Nitrocellulose membrane (#88018, Thermo Fisher Scientific, Waltham, MA, USA) was placed at the top of humidified filter paper. Once samples were transferred, membrane was incubated with the corresponding antibodies following the same procedure previously mentioned for Western blot.

### **DLS analysis**

The DLS technique was used to determine the size of Gag::eGFP VLPs. The measurements were carried out at 25°C in a Zetasizer Nano ZS instrument (Malvern Instruments, Malvern, UK), equipped with a He/Ne 633 nm laser at 173°. 100 µL of the sample were placed in disposable plastic cuvettes. Three consecutive measurements of each sample with 10-15 scans of ten seconds were performed for each independent measurement. The hydrodynamic diameter (MHD), particle size distribution in volume, derived count rate, and polydispersity index (PDI) average results were automatically obtained.

### **Gag::eGFP VLPs fluorescence emission by fluorimetry**

The fluorescence intensity was measured in a Cary Eclipse Fluorescence Spectrophotometer (Agilent Technologies, Santa Clara, CA, USA) to determine the concentration of Gag::eGFP VLPs. The settings were:  $\lambda_{\text{excitation}} = 488 \text{ nm}$  (slit = 5 nm) and  $\lambda_{\text{emission}} = 510 \text{ nm}$  (slit = 10 nm). The relative fluorescence unit (RFU) values were calculated by subtracting the obtained fluorescence intensity (FU) values from the

non-transfected negative control samples. An in-house developed and validated quantification assay was used to convert RFU values to Gag::eGFP concentration values [35].

#### **Gag::eGFP VLPs quantification by Nanoparticle Tracking Analysis (NTA)**

NTA was performed with a NanoSight® LM20 device (NanoSight Ltd., Amesbury, UK) equipped with a blue laser module (488 nm) to quantify Gag::eGFP VLPs and neutral density filter for total particle by light scattering. Data were analyzed with NanoSight® NTA 3.2 software. Briefly, samples were injected, and three technical replicate analyses were carried out. Subsequently, particles were identified and tracked by their Brownian motion at RT. Capture settings were recorded with a sCMOS camera (camera level of 8 for Gag::eGFP VLPs samples, and 11 for controls, viscosity: 0.9 cP) and analyzed with a detection threshold of 4. The data obtained from these analyses were also used to calculate the percentage of Gag::eGFP VLPs relative to the total nanoparticles in the measured samples

#### **Gag::eGFP VLPs quantification by Flow Virometry**

Concentration of Gag::eGFP fluorescent events was quantified using a CytoFLEX LX (Beckman Coulter, Brea, CA, USA), equipped with a 405 nm filter. The VLPs were detected based on violet side scatter (V-SSC) and FITC fluorescence signals. Laser gains were optimized with values set to 72 for forward scatter (FSC), 135 for side scatter (SSC), 9 for V-SSC, and 500 for FITC. Samples were diluted with PBS1X until an abort rate value below 2% was achieved. A total of 300,000 events were analysed at a flow rate of 10 µL/min per sample. VSSC-H vs B525-FITC density plots were used to gate the different particle populations. Gating was adjusted manually for each channel. Events after 50 s were taken for analysis. The results were normalized employing an internal control quantified by NTA. The results were analyzed with CytExpert v.2.3 software (Beckman Coulter, Brea, CA, USA).

#### **Gag::eGFP VLPs visualization in cryo-transmission electron microscopy (Cryo-TEM)**

The morphology and electron density of Gag::eGFP VLPs were investigated under cryogenic conditions. The samples were rapidly frozen by plunging them into liquid ethane at a temperature of -180°C. Approximately 2µL of the sample was then applied to holey carbon grids that had been pre-treated with glow discharge using a PELCO easiGlow discharger unit. The cryo-frozen samples were transferred to a

Leica EM GP cryo workstation and subsequently examined using a JEM-2011 electron microscope (JEOL Ltd., Tokyo, Japan) operating at an acceleration voltage of 200kV. Throughout the imaging process, the temperature was maintained at -180°C by the continuous addition of liquid ethane. Images were captured using a CCD-multiscan camera (Gatan Inc., Pleasanton, CA, USA) for further analysis and characterization. Nanoparticles diameter was analyzed using software ImageJ2 Fiji (National Institutes of Health, Bethesda, MD, USA).

### **SE-HPLC analysis**

High-pressure liquid chromatography (HPLC) analyses were conducted with an Agilent 1100 Series HPLC System (Agilent Technologies, Santa Clara, CA, USA) equipped with a 300A 2.7µm (7.8x300mm) (Agilent Technologies) Size Exclusion (SE) column at Servei d'Anàlisi Química (SAQ, UAB, Barcelona, Spain). The mobile phase was composed of 150 mM sodium phosphate (pH 7.0). The analytics were performed at a flow rate of 1 mL/min with UV detection at 220 nm. A volume of 25 µL of both Gag VLPs (functionalized and non-functionalized) was loaded onto the column. Protein-containing fraction of interest was collected and concentrated with a 30 kDa MWCO amicon ultra spin (Millipore, Billerica, MA). The concentrated fraction was analyzed by dot blot as previously described.

### **Cell culture conditions for *in vitro* experiments**

CXCR4+ HeLa (ATCC®CCL-2 TM) and CXCR4- SW1417 (ATCC®CCL-238 TM) cells were used for the functional characterization of Gag VLPs (functionalized and non-functionalized) *in vitro*. HeLa cells were maintained in MEM-α culture media supplemented with 10 % fetal bovine serum (Gibco, Thermo Fisher, Waltham, MA, USA). SW1417 cells were maintained in DMEM supplemented with 10 % fetal bovine serum. HeLa cells were cultured at 37 °C in a 5 % humidified atmosphere, while SW1417 were cultured at 37 °C in a 10 % humidified atmosphere. Before adding the nanoparticles to perform the different *in vitro* experiments, cells were previously cultured in 24-well plates (30000 cells/well) in the presence of Optipro medium (Gibco) with 100 U/mL penicillin/ streptomycin mix (Life Technologies) for 24h. For dose-response experiment, HeLa cells were incubated in presence of four different concentrations (8.4, 2.1, 0.4 and 0.2·10<sup>9</sup> VLPs/mL) of nanoparticles (T22-functionalized and non-functionalized) in a final volume of 250 µL for 24h. For time

course experiment, HeLa cells were incubated with  $2.1 \cdot 10^9$  VLPs/mL (T22-functionalized and non-functionalized) at 3 different times (1, 5 and 24h). The internalization experiment in SW1417 cells was performed similarly to the time course experiment but was limited to the time points of 1 and 24h. Cells were analyzed after treatment with 1 mg/mL trypsin (Gibco) for 15 minutes using a CytoFLEX (Beckman Coulter, Brea, CA, USA) flow cytometry with the CytExpert v.2.3 software (Beckman Coulter, Brea, CA, USA).

### **Confocal laser scanning microscopy**

For confocal analysis, CXCR4+ HeLa cells grown on MatTek culture dishes (MatTek Corporation, Ashland, MA, USA) were incubated with  $2.1 \cdot 10^9$  T22-conjugated nanoparticles per mL during 24h. Subsequently, the nuclei were labeled with 0.2 µg/mL Hoechst 33342 (Molecular Probes, Eugene, OR) and the plasma membranes with 2.5 µg/mL CellMask™ Deep Red (Molecular Probes) for 10 minutes in the dark. The cells were then washed with PBS1X. Live cells were recorded by TCS-SP5 confocal laser scanning microscopy (Leica Microsystems, Heidelberg, Germany) using a Plan Apo 63 × /1.4 (oil HC × PL APO lambda blue) objective as described elsewhere [36]. To determine particle localization inside the cell, stacks of 10–20 sections for every 0.5 µm of cell thickness were collected and three-dimensional models were generated using Imaris version 7.2.1. software (Bitplane, Zürich, Switzerland) as previously reported [37].

### **Statistical analysis**

Data was represented as mean ± Standard error (SEM). Statistical analyses were performed using the GraphPad Prism 5 software (GraphPad Software, San Diego, California USA). Results were analyzed by One-way ANOVA test. Differences were considered statistically significant when p-values < 0.05.

## **RESULTS**

### **Gag::eGFP VLPs functionalization with T22 peptide by click chemistry reactions**

The Gag::eGFP VLP material used for the functionalization experiments with the T22 peptide was obtained from a batch production of 500 mL by transient transfection, followed by its subsequent purification [34].

**Figure 1** shows a molecular characterization of the Gag::eGFP VLPs obtained in each step.

The expected elution peaks from Capto Q ImpRes AEC were observed in the chromatogram at 488 nm absorbance (**Figure 1A**). The fractions collected during the process were analysed. The second step in the elution phase fraction (named P2) was considered the main product fraction due to the higher Gag::eGFP VLP concentration, as indicated by flow virometry and fluorimetry results (**Figure 1B**). DLS was also utilized to characterize the sample at each step of the process. It was observed how the peak narrows with respect to the supernatant harvest as the sample becomes increasingly purified (**Figure 1C**). Additionally, as shown in the SDS-PAGE, as the process progresses, the sample corresponding to Gag::eGFP polyprotein is concentrated, and other contaminating proteins are eliminated. Moreover, the presence of Gag::eGFP was confirmed by Western blot (**Figure 1D**).

Subsequently, the concentrated and purified Gag::eGFP-VLPs from the P2 fraction were further processed by exchanging the buffer to PBS1X, resulting in 100% recovery of Gag::eGFP-VLPs. According to NTA measurements, the concentration of total particles and Gag::eGFP VLPs per mL in the final purified material was  $6.18 \cdot 10^{11}$  and  $3.7 \cdot 10^{11}$  respectively. This indicates a 60% purity of Gag::eGFP VLPs (**Table 1**).

**Table 1:** Data collection for the purification of Gag::eGFP VLPs for the functionalization experiments

Sample	Total particles/mL	Gag::eGFP VLPs/mL	Step Recovery (%)	Purity (%) (VLPs/Total Particle)
Harvest	$1.86 \cdot 10^{10}$	$9.19 \cdot 10^9$	-	49
Clarified	$7.50 \cdot 10^9$	$4.0 \cdot 10^9$	50	53
P2 (AEC)	$6.95 \cdot 10^{11}$	$4.15 \cdot 10^{11}$	50	60
P2 (PBS1X)	$6.18 \cdot 10^{11}$	$3.7 \cdot 10^{11}$	100	60

P2 (AEC): fraction P2 from Capto Q ImpRes anion exchange chromatography, P2 (PBS1X): fraction P2 after Zebaspin desalting step resuspended in PBS1X

The purified material was functionalized with T22 peptide using a two-step click chemistry strategy, specifically the bio-orthogonal copper-free strain-promoted azide-alkyne cyclo-addition (SPAAC) reaction. In the first reaction step, DBCO- sulfo-NHS, which can link to any primary amine-containing molecules on the envelope of Gag VLPs, was used as a bifunctional crosslinker. In the second reaction step, azide-containing T22 were covalently linked to nanoparticles' surface. Following this, an ultracentrifugation step

was included to remove unincorporated reagents (**Figure 1E**). This approach was based on the reaction optimization previously reported by Garcia-Trujillo et al., (2024) [22].

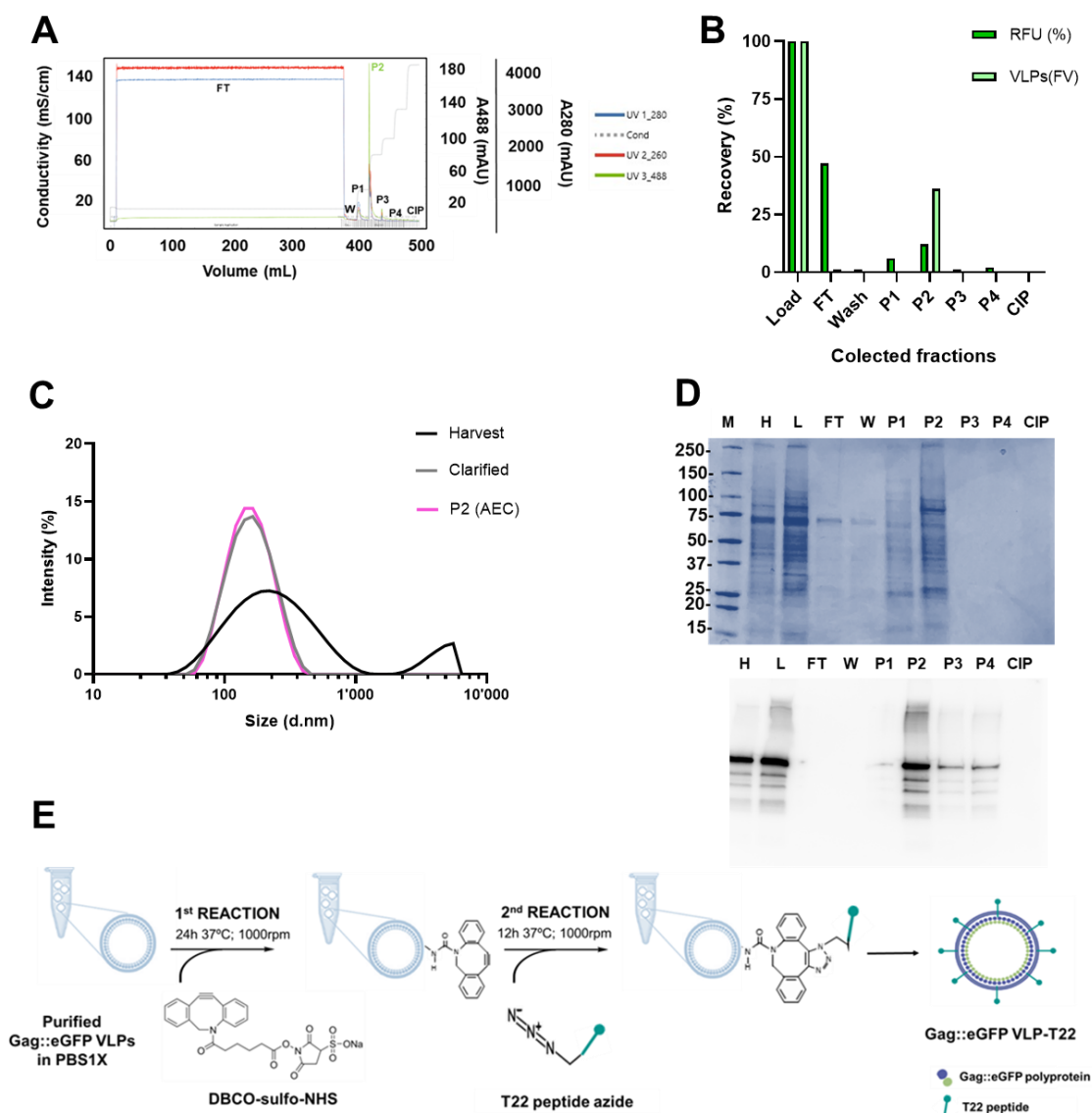


**Figure 1:** Purification data corresponding to Gag::eGFP VLPs. **A**) Chromatogram of the step-gradient (15%, 35%, 45%, and 65%) purification of Gag::eGFP VLPs clarified supernatant by Capto Q ImpRes column; **B**) Gag::eGFP VLPs quantified through flow virometry (VLP) and relative fluorescent units (RFU) by fluorimetry, recovery percentages (%); **C**) Particle size distribution analysis by DLS (Harvest: MHD=204,6 and Pdl =0.490, Clarified: MHD=128,9 and Pdl =0.238, P2 (AEC): MHD=142,2 and Pdl =0.151, P2(Desalting): MHD=136,3 and Pdl =0.193; **D**) SDS-PAGE and p24 Western blot of purification run. **E**) Schematic representation of the proposed reaction pathway to conjugate the T22 peptide to the surface of Gag::eGFP VLPs by the two-step click chemistry reaction (Adapted from [22]). *M*, molecular weight standard; *H*, harvest supernatant; *L*, sample loaded to the column (clarified harvest supernatant); *FT*: flowthrough; *W*: wash peak; *P1-P4*: pooled fractions for elution peaks 1–4; *CIP*: cleaning in place; *DLS*, Dynamic Light Scattering; *Pdl*, polydispersity index; *MHD*, mean hydrodynamic diameter; *P2 (AEC)*: fraction P2 from Capto Q ImpRes anion exchange chromatography; *SDS-PAGE*, sodium dodecyl sulfate polyacrylamide gel electrophoresis. *DBCO-sulfo-NHS*, dibenzocyclooctyne-sulfo-N-hydroxysuccinimidyl ester

In this study, a comprehensive analysis was conducted to validate the covalent binding and to assess the properties of T22- functionalized Gag::eGFP VLPs (hereafter noted as Gag::eGFP VLPs-T22). The analysis included DLS, CryoTEM, immunoblotting with specific antibodies, and SE-HPLC. The results were consistently compared with those obtained from purified material, non-functionalized Gag::eGFP VLPs.

Based on DLS profile evidence, it is observed that Gag::eGFP VLPs-T22 have a larger diameter (266.6nm) compared to non-functionalized Gag VLPs (136.3nm) (**Figure 2A**). The increase in diameter could be due to the bonded T22 epitopes on the surface of the Gag VLPs, which contribute to the larger size observed during DLS analysis. Furthermore, Cryo-TEM analysis revealed that T22-functionalized Gag::eGFP VLPs maintained their characteristic morphology when compared to non-functionalized counterparts, suggesting that the functionalization process did not affect the integrity of the Gag VLPs (**Figure 2B**).

Although the diameter measurements for the T22-functionalized and non-functionalized Gag VLPs were approximately 160 nm and 100 nm, respectively, which were lower than those obtained through DLS analysis, the same trend was observed. Specifically, the functionalized VLPs had a larger diameter compared to the non-functionalized VLPs in both measurement techniques.

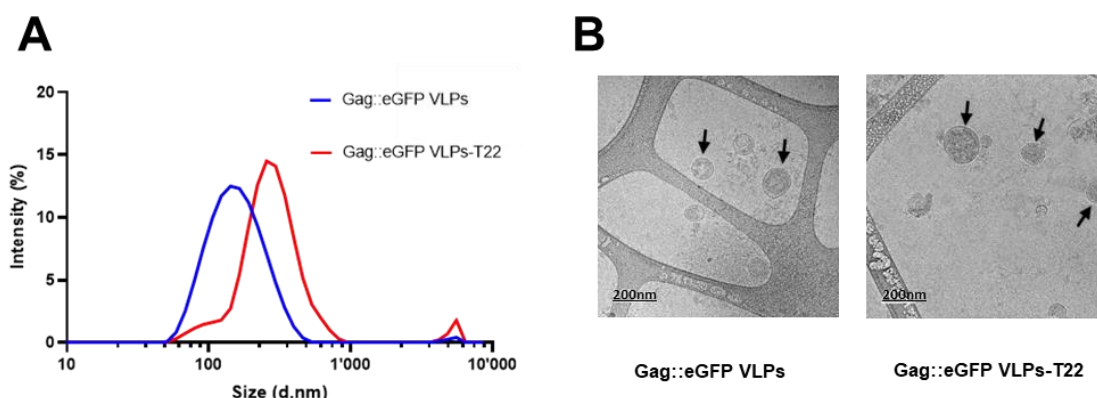


**Figure 2** Size characterization of T22- functionalized Gag::eGFP VLPs: **A**) Particle size distribution analysis by DLS (Gag::eGFP VLPs: MHD=136,3 and Pdl =0.193, Gag::eGFP VLPs-T22: MHD=266,6 and Pdl =0.378. **B**) Cryo-TEM micrographs of Gag::eGFP VLPs and Gag::eGFP VLPs-T22. Black narrows indicate Gag::eGFP VLPs in both samples. Scale bar = 200nm. *DLS*, Dynamic Light Scattering; *Pdl*, polydispersity index; *MHD*, mean hydrodynamic diameter; *Cryo-TEM*, Cryo-Transmission Electron Microscopy.

To verify the presence of the T22 peptide conjugated to the Gag::eGFP VLPs, a Western blot under denaturing conditions was performed. Both, T22-functionalized and non-functionalized VLPs showed HIV-1 Gag bands, while only T22-functionalized VLPs and a T22 containing positive control protein (T22GFPH6)



showed signal corresponding to T22 (**Figure 3A**). Notably, for the T22-functionalized Gag VLPs, a smear-like signal was observed. This suggests that the T22 peptide may have cross-linked or covalently bound to various proteins or protein fragments on the surface of the Gag VLPs.

Additionally, SE-HPLC analysis revealed a single peak for both types of VLPs, eluting at an early retention time (~4.2 minutes). This retention time is consistent with the expected elution behaviour for nanoparticles of this size (**Figure 3B**). To confirm the presence of both VLPs and the T22 peptide, we collected and analysed the fraction corresponding to Gag::eGFP VLPs-T22 by Dot blot. The analysis revealed signals of both anti-HIV-1 Gag and anti-T22 antibodies, confirming the elution of functionalized Gag::eGFP VLPs-T22 in this fraction.

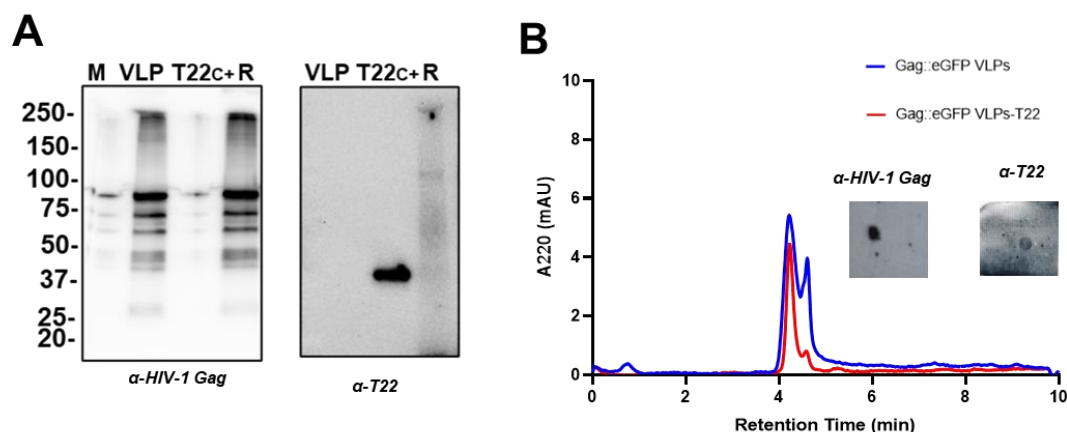


**Figure 3:** Molecular characterization of T22- functionalized Gag::eGFP VLPs. **A)** Western blot of T22- functionalized Gag::eGFP VLPs and two respective controls (left: anti-HIV-1 Gag monoclonal antibody; right: anti-T22 monoclonal antibody). **B)** SE-HPLC profile of Gag::eGFP VLPs and Gag::eGFP VLPs-T22. Gag and T22 presence in the collected fraction corresponding to retention time of 4.2 min of the Gag::eGFP VLPs-T22 is also shown using the anti-HIV-1 Gag monoclonal antibody and anti-T22 monoclonal antibody by Dot blot. *M*, molecular weight standard; *VLP*, Gag::eGFP VLPs; *T22c+*, protein T22GFPH6 as positive control of T22 signal; *R*, Gag::eGFP VLPs-T22.

### CXCR4-dependent cell uptake of Gag::eGFP VLPs-T22

After having corroborated the functionalization of Gag::eGFP VLPs-T22 nanoparticles, their ability to enter cells expressing the CXCR4 receptor was evaluated. First, the dose-response dynamics of T22-functionalized nanoparticles in HeLa (CXCR4<sup>+</sup>) cells was investigated by exposing the cells to four concentrations of nanoparticles, comparing both non-functionalized and T22-functionalized Gag VLPs. Following a 24h incubation period, nanoparticle uptake via fluorescence intensity, was assessed. When

these nanoparticles were added to the culture medium, HeLa (CXCR4+) cells exposed to  $8.40 \cdot 10^9$  and  $2.1 \cdot 10^9$  Gag::eGFP VLP-T22 showed higher fluorescence values than those exposed to Gag::eGFP VLPs (**Figure 4A**). Since the specific fluorescence of both nanoparticles is similar (**Figure 4B**), the fluorescent emission intensity can be interpreted as a valid parameter to comparatively assess the intracellular GFP accumulation. Based on these insights, the concentration of  $2.1 \cdot 10^9$  Gag::eGFP VLPs-T22/mL was selected for subsequent experiments as it provides substantial fluorescence enhancement while saving material for the rest of the assays.

Time course monitoring assay was also performed to further understand the dynamics of nanoparticle uptake by cells. One hour after exposure to Gag::eGFP VLPs-T22, the uptake of nanoparticles was already evident, and the amount of intracellular fluorescence progressively increased for the following 24h at least, reaching a maximum signal 5h after exposure (**Figure 4C**). As expected, non-functionalized Gag::GFP VLPs showed significantly lower fluorescence values, which were considered background nonspecific uptake [38].

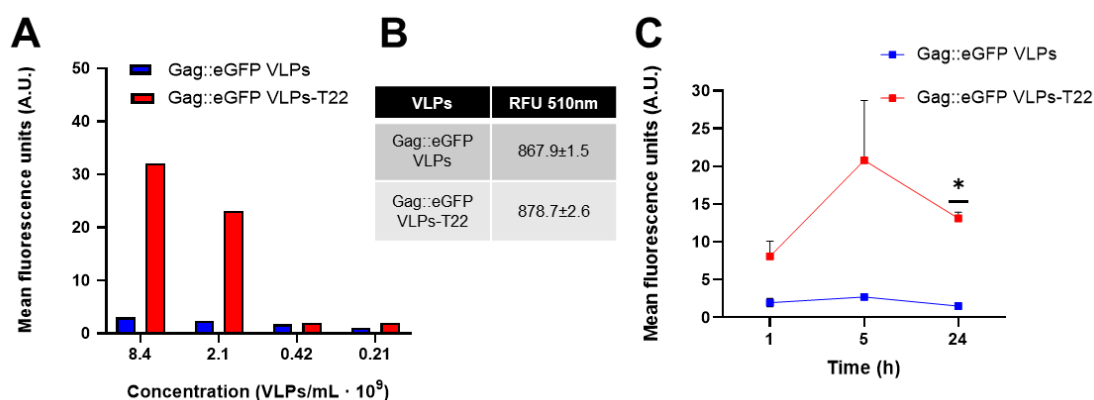


**Figure 4.** Internalization of Gag::eGFP VLPs and Gag::eGFP VLPs-T22 in HeLa cells. **A)** Dose-response of Gag::eGFP VLPs and Gag::eGFP VLPs-T22 assessed by flow cytometry after 24h of incubation. **B)** Intrinsic fluorescent emission of Gag::eGFP VLPs and Gag::eGFP VLPs-T22, exciting at 488 nm and detecting at 510 nm. **C)** Time course monitoring by flow cytometry of  $2.1 \cdot 10^9$  Gag::eGFP VLPs and Gag::eGFP VLPs-T22 per mL. In A) and C) fluorescence values are referred to those of background cells. Color blue indicate Gag::eGFP VLPs and color red Gag::eGFP VLPs-T22. In C) data are shown as mean  $\pm$  standard error. Significant statistical differences between data pairs (Gag::eGFP VLPs vs. Gag::eGFP VLPs-T22 at a respective time) are represented by \* at  $p < 0.05$ ;  $n = 2$  per group. Statistical analysis performed by Student t-test.

The high cell penetrability of Gag::eGFP VLPs-T22 was further confirmed by confocal microscopy of treated HeLa cell cultures (**Figure 5**). Three-dimensional reconstructions of individual cells exposed to Gag::eGFP VLPs-T22 indicated perinuclear and membrane localization of fluorescence in the form of nanoparticles. No signal was observed in the untreated control HeLa cells.

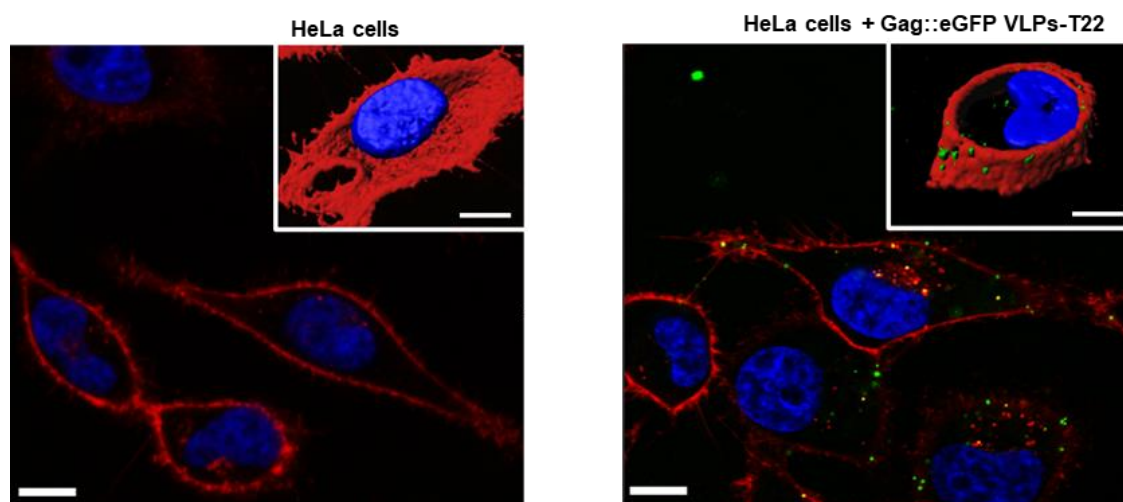


**Figure 5:** Confocal images of HeLa cells (**left**) and HeLa cells exposed to  $2.1 \cdot 10^9$  Gag::eGFP VLPs-T22 (**right**) for 24h. Nuclei are labeled in blue and cell membranes in red. Bar indicates 10  $\mu$ m. Detail of a HeLa cell and HeLa cell exposed to Gag::eGFP VLPs-T22, showing the intracellular localization of nanostructured, fluorescent entities, in an isosurface representation within a three-dimensional volumetric x-y-z data field are represented in the upper white square.

To confirm whether the cellular uptake of Gag::eGFP VLP-T22 was mediated by its binding and internalization through the cell surface receptor CXCR4 and its ligand T22, we exposed SW1417 cells, which do not express CXCR4 (CXCR4<sup>-</sup> cells) and compared them with HeLa cells (CXCR4<sup>+</sup>). As demonstrated in **Figure 6**, the entry of Gag::eGFP VLPs-T22 nanoparticles into cells depends on the presence of the CXCR4 receptor. Notably, the fluorescence signal in SW1417 cells was significantly lower than that in HeLa cells after exposure to the T22 nanoconjugate at both 1h and 24h. Additionally, no differences were observed in the nonspecific entry of non-functionalized VLPs.

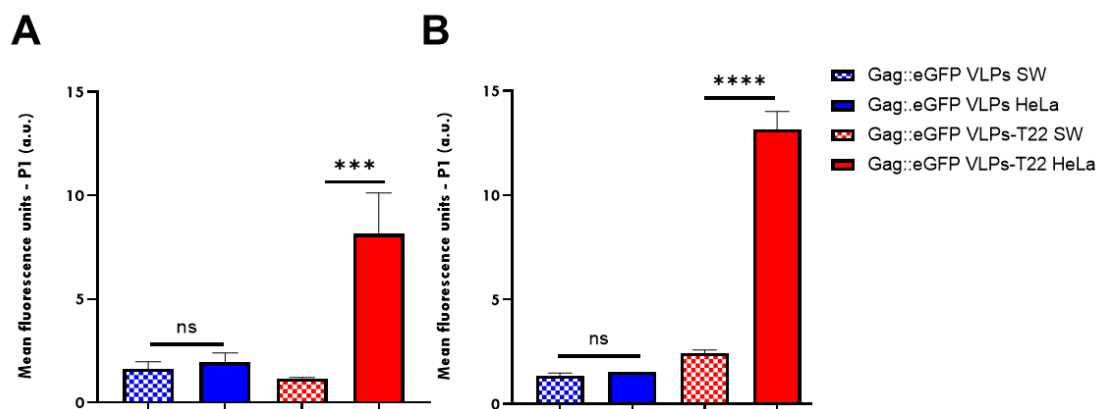


**Figure 6.** Internalization of Gag::eGFP VLPs and Gag::eGFP VLPs-T22 in SW1417 and HeLa cells for 1 hour **A)** and 24 hours **B).** Data are shown as mean  $\pm$  standard error. Fluorescence values are referred to those of background cells. Significant statistical differences between data pairs (Gag::eGFP VLPs-T22 in HeLa cells and Gag::eGFP VLPs-T22 in SW cells) are represented by \*\*\*  $p < 0.001$ ; \*\*\*\*  $p < 0.0001$ ;  $n = 2$  per group. Statistical analysis performed by One-way ANOVA test.

## DISCUSSION

### Functionalization efficiency and characterization

VLPs have emerged as promising delivery vehicles in biology and biomedicine, with potential in enhancing drug delivery efficiency. Specifically, attaching targeting ligands to VLPs can significantly improve their precision and efficiency in delivering drugs to specific cells and tissues [7], [24], [39]. Indeed, controlling cell targeting and drug penetrability is crucial in modern medicine. The successful development of intracellular targeting agents can lead to substantial enhancement in drug stability and efficacy, while also reducing toxicity. Here Gag::eGFP VLPs are first produced [40], purified and functionalized with the T22 peptide through chemical conjugation. The purification method performed involved clarification, capture, and desalting, as reported in previous studies [34]. This approach achieved Gag VLPs with 60% purity and the appropriate concentration and morphological characteristics for subsequent functionalization steps. The use of this DSP method for generating VLPs intended for chemical conjugation reactions is rarely reported. Generally, in these cases, the starting VLP material is purified by ultracentrifugation using a sucrose or cesium chloride gradient, as reported by K. G. Patel and J. R. Swartz (2011) for bacteriophage MS2 and bacteriophage Q $\beta$  VLPs [17] and by C. C. Chen et al (2018) for cowpea mosaic virus (CPMV) and tobacco mosaic virus lysine mutant (TMVlys) [41], [42]. However, this purification method is time-consuming, labor-intensive, and not scalable. The purification method performed in this work offers a more efficient and

scalable alternative, significantly streamlining the production process for VLPs intended for chemical conjugation. Chemical linking is a simple and efficient approach for biomolecule coupling [43]. The click chemistry procedure performed in this study has been previously optimized and allows to functionalize nanoparticles in an easy and quick approach. This process can be completed within just two days, significantly reducing the time required to evaluate peptides or epitopes of interest. Additionally, the presence of abundant lysines on the surfaces of the VLPs allows high-density functionalization of the target ligands [14], [17]. Also, chemical conjugation offers a superior alternative to gene transfection methodologies for modifying the surface of VLPs. This advantage is exemplified by M. Peacy et al (2007) [44] who reported a tenfold increase in peptide association with Rabbit haemorrhagic disease virus (RHDV)-like particles when using chemical conjugation, compared to the incorporation of a single peptide per VLP achieved through genetic engineering. However, the main disadvantages of functionalizing VLPs through chemical reactions include the high expense associated with large-scale manufacturing and the necessity of a final polishing step to remove excess reagents that are not incorporated into the VLPs. In this work, the polishing step was performed by ultracentrifugation according to previous optimization studies [22]. However, Patel and Swartz (2011) [17] and Park et al (2020) [45] have reported promising results using a SEC by Supelco GFC500 column and a Zeba spin filter, respectively. Therefore, for large-scale manufacturing, it is recommended to replace the ultracentrifugation step with SEC or a diafiltration method, using TFF, for instance [46]. Although some VLP vaccines have been approved by the Food and Drug Administration (FDA) for human use, functionalizing a VLP with a new epitope produces an unknown particle that requires thorough characterization. Various versions of a VLP vaccine can be created based on its size and the nature or length of the displayed epitope. Consequently, analysing their molecular properties becomes crucial, necessitating appropriate methods to confirm their structural integrity. The most utilized methods for VLP characterization include analytic ultracentrifugation, high-performance chromatography, cryo-electron microscopy, atomic force microscopy, transmission electron microscopy, dynamic light scattering, and immunoblot assays. These techniques verify the VLP's integrity for epitope display [47]. In this work, we performed a DLS analysis to determine the diameter size and the presence of fragments or aggregates [48]. In both cases studied (T22-functionalized and non-functionalized Gag::eGFP VLPs), stable dispersion of nanoparticles was shown with no signs of aggregation. As illustrated in **Figure 2A** the functionalized

particles exhibited a larger diameter size compared to the non-functionalized ones, as expected. This enlargement is attributed to the addition of molecular layers or coatings during nanoparticle functionalization, resulting in an overall increase in diameter particle size. In addition to size, cryo-TEM was able to show that overall structure, and morphology of the T22-functionalized Gag VLPs were also maintained after functionalization procedure. Cryo-TEM has been widely used to characterize the morphology of Gag VLPs obtained in different production platforms. Compared to TEM, it induces fewer structural changes due to rapid freezing during sample preparation [48], [49]. The Cryo-TEM images showed both Gag::eGFP VLPs and Gag::eGFP VLPs-T22 as regular nanoparticles measuring ~100-200 nm in diameter as expected while aggregates or broken particles were scarcely detectable [34], [50]. The difference between the nanoparticle sizes reported by cryoTEM and DLS are explained by the different methods used. In the DLS method, a water layer is included around the particle and calculated into the hydrodynamic radius, typically leading to an apparent diameter increase when compared to other methods [48], [51], [52]. On the other hand, although cryo-TEM is a direct observation method that allows visualization of individual nanoparticles, sampling is a concern since a finite number of particles is typically measured. Similar results, regarding this differences, have been reported for influenza virions lipid bilayer vesicles and other lipid-based nanoparticles [53]. Even though the estimated average particle size differed between the techniques, both methods indicates that the T22-functionalized Gag VLP is larger than non-functionalized Gag VLPs. We further confirmed the conjugation of the T22 peptide to de Gag::eGFP VLPs using western blot. Notably, the smear-like signal and the appearance of multiple high molecular weight bands may indicate that multiple coat proteins were conjugated. J Park et al (2020) [45] demonstrate similar results regarding DLS, western blot and TEM analysis when conjugate antibodies to different VLPs using the SPAAC reaction. L.L Huang et al (2013) [54] also employ TEM for morphological characterization of conjugated enveloped Virus. Regarding SE-HPLC, this technique provides a straightforward, rapid, and flexible method for evaluating the quality of VLPs. This analysis is crucial for monitoring the stability and degradation patterns of biopharmaceuticals [55]. The SE-HPLC profiles obtained reveal a single peak at the same early retention time for both VLPs under study. These results are consistent with the DLS profile discuss above, confirming no presence of aggregates. Moreover, elution at early retention times indicates the presence of large molecules, like VLPs, which is consistent with our results. Overall, these findings underscore the integrity of the Gag::eGFP VLPs-T22

throughout the functionalization process. Additional confirmation analyses of the functionalization could be conducted to provide a more comprehensive evaluation. For example, immunogold labeling with an anti-T22 primary antibody and a gold-labeled secondary antibody could be used to visualize the localization of the T22 peptide on the surface of the functionalized VLPs. Boix-Besora et.al (2022) [11] have reported the use of this immunodetection technique to analyze chimeric Gag VLPs expressing the SARS-CoV-2 spike protein in their superfcies.

### **Cellular uptake studies**

The surface of VLPs can be extensively modified with various biomolecules. These ligands can enable specific cellular targeting, and potentially facilitate extravasation [56]. M. J. Rohovie et al. (2016) [43] reported several examples of surface ligands displayed on different types of VLPs. These chemical modifications, involving peptides and proteins, are more common than those involving nucleic acids, lipids, and glycans [57]. In this context, M. L. Hovlid et al (2012) [58] reported a chemically functionalized Cowpea mosaic virus (CPMV) coat protein displaying an RGD oligopeptide sequence that showed strong and selective affinity for several different cancer cell lines expressing RGD-binding integrin receptors. Another example is reported by D. Banerjee et al. (2010) [59], who described transferrin conjugation to Q $\beta$  VLPs, allowing specific recognition by transferrin receptors, which are upregulated in a variety of cancers. In our work, we demonstrate through various in vitro assays [60] the effective CXCR4<sup>+</sup> cell targeting capacity of Gag::eGFP VLPs functionalized with the T22. Notably, the function of this peptide as a cell-receptor specific ligand is associated with its N-terminal [24], [61], [62]. Therefore, functionalization by the C-terminal, maintaining the N-terminal biologically active group free, is mandatory, as we performed in this case. T22 had been previously identified as ligand [24], [63], [64] for CXCR4 receptor which is a relevant molecular marker of cancer stem cells [65]. In this context, several researchers have explored CXCR4-targeting by using self-assembling protein nanoparticles that show multivalent display of the T22 peptide (T22-GFP-H6). Based on this nanocarrier, M.V Céspedes et al (2018) [66] assessed the antimetastatic activity of a nanoconjugate (T22-GFP-H6-FdU) that selectively delivers Oligo- Floxuridine to CXCR4<sup>+</sup> cells. This targeted drug delivery approach yields potent antimetastatic effect, through selective depletion of metastatic CXCR4<sup>+</sup> cancer cells, and validates metastatic stem cells (MetSCs) as targets for clinical therapy. R. Díaz

et al (2018) [67] demonstrated in animal models of acute myeloid leukemia, that T22-empowered ricin toxin containing nanoparticles (T22-mRTA-H6) showed an impressive and highly selective therapeutic effect, dramatically reducing the leukemia cells affectation of clinically relevant organs. Additionally, E. Rioja-Blanco et al (2022) [68] used CXCR4-targeted self-assembling protein nanoparticles based on two potent microbial toxins: de-immunized catalytic domain of *Pseudomonas aeruginosa* (PE24) exotoxin A and the diphtheria exotoxin (DITOX) domain. Both nanotoxins contained the T22 peptide ligand to specifically target CXCR4-overexpressing head and neck squamous cell carcinoma (HNSCC) cells. The toxins, were stable and effectively internalized by target cells, displaying a potent antitumor effect in the absence of systemic toxicity in a CXCR4+ subcutaneous HNSCC mouse model. However, although self-assembling T22-enhanced nanoparticles have been widely studied, this work presents a different approach that combines the advantages of Gag VLPs as a targeted drug delivery platform, including its easily modifiable envelope, with the promising results obtained from the T22 peptide. The results obtained from cellular uptake studies indicate that functionalized Gag::eGFP VLPs-T22 exhibit superior penetration capacity into CXCR4+ cells compared to the parental Gag::eGFP VLPs, and this is observed in a dose-dependent (**Figure 4A**) and time-dependent (**Figure 4C**) manner. Considering both types of analyses and the similarity of the specific fluorescence of both VLPs, the amount of intracellular material differed comparing functionalized and non-functionalized nanoparticles, highlighting the enhanced uptake of Gag::eGFP VLPs-T22 by CXCR4+ cells. The results shown here are similar to those previously reported by U. Unzueta et al (2012) [24] and R. Díaz et al (2018) [67] using T22-GFP-H6 nanoparticles. Gag::eGFP VLPs-T22 accumulation was also assessed by confocal microscopy. The images confirmed the presence of Gag::eGFP VLPs-T22 confirming the results achieved by flow cytometry. While an important part of this nanoconjugate was found intimately associated to the cell membrane, 3D confocal reconstructions revealed an intracellular localization of this VLPs. Similar results were reported by E. Voltà-Durán et al [26] and U. Unzueta et al [24] when analysing T22-self-assembled nanoparticles distribution in CXCR4+ cells using confocal techniques. Additionally, it is important to confirm that the entry of conjugated Gag::eGFP VLPs-T22 into cells is specific through binding to the CXCR4 receptor and not random. To demonstrate this, several researchers have reported different experiments using specific competitors that bind to the receptor, thereby blocking the entry of the nanoparticles [24] [26], [66], [69]. Alternatively, cell lines with minimal presence of the receptor on their



surface have been used. This includes the SW1417 cell line used in this work, which has previously been reported as a CXCR4 negative cell line [27], [69]. The results confirm the specificity of Gag::eGFP VLPs-T22, as no evidence of cellular entry is observed in the SW1417 cell line. This observation is notable and significant, as it prevents internalization and toxicity in normal cells with low or negligible CXCR4 receptor levels [67], [70]. Moreover, ensuring the specificity of entry for the functionalized nanoparticles avoid the severe side effects that appeared on previous clinical trials testing ricin anticancer effect as reported by N. Tyagi et al (2015) [71]. In general, our study highlights the effective targeting and cellular uptake of Gag::eGFP VLPs functionalized with the T22 peptide, demonstrating a significant potential for specific drug delivery to CXCR4+ cancer cells. Future work could explore the *in vivo* efficacy of these functionalized VLPs in animal models, investigate the therapeutic potential of different drug payloads.

## CONCLUSIONS

Overall, the results from the T22-specific functionalization of Gag::eGFP VLPs and *in vitro* assays emphasize the potential of this nanoconjugate for developing drug delivery vehicles utilizing target peptides presented by these nanoparticles. Additionally, cellular internalization studies have revealed the selective entry of the functionalized nanoparticles into CXCR4+ cells. To summarize, this study underscores the promise of the optimized SPAAC click chemistry reaction for functionalizing Gag::eGFP VLPs, thereby facilitating their application in nanoparticle-based drug delivery therapies. Future investigations, such as *in vivo* studies to assess therapeutic efficacy and biodistribution of T22-functionalized Gag::eGFP VLPs, would be valuable for advancing this research area.

## REFERENCES

- [1] T. Ramqvist, K. Andreasson, and T. Dalianis, "Vaccination, immune and gene therapy based on virus-like particles against viral infections and cancer," *Expert Opin. Biol. Ther.*, vol. 7, no. 7, pp. 997–1007, 2007, doi: 10.1517/14712598.7.7.997.
- [2] L. Duan *et al.*, "Nanoparticle-Based Drug Delivery Systems: An Inspiring Therapeutic Strategy for Neurodegenerative Diseases," *Polymers (Basel)*, vol. 15, no. 9, pp. 1–19, 2023, doi: 10.3390/polym15092196.
- [3] A. Raguram, S. Banskota, and D. R. Liu, "Therapeutic *in vivo* delivery of gene editing agents," *Cell*, vol. 185, no. 15, pp. 2806–2827, 2022, doi: 10.1016/j.cell.2022.03.045.

- [4] M. An *et al.*, "Engineered virus-like particles for transient delivery of prime editor ribonucleoprotein complexes in vivo," *Nat. Biotechnol.*, 2024, doi: 10.1038/s41587-023-02078-y.
- [5] J. He *et al.*, "Virus-like Particles as Nanocarriers for Intracellular Delivery of Biomolecules and Compounds," 2022.
- [6] B. Donaldson, Z. Lateef, G. F. Walker, S. L. Young, and V. K. Ward, "Virus-like particle vaccines: immunology and formulation for clinical translation," *Expert Rev. Vaccines*, vol. 17, no. 9, pp. 833–849, 2018, doi: 10.1080/14760584.2018.1516552.
- [7] Izzat F.B.M Suffian and Khuloud T. Al-Jamal, "Bioengineering of virus-like particles as dynamic nanocarriers for in vivo delivery and targeting to solid tumours," *Adv. Drug Deliv. Rev.*, vol. 180, p. 114030, 2022, doi: <https://doi.org/10.1016/j.addr.2021.114030>.
- [8] X. Ding, D. Liu, G. Booth, W. Gao, and Y. Lu, "Virus-Like Particle Engineering: From Rational Design to Versatile Applications," *Biotechnol. J.*, vol. 13, no. 5, pp. 1–19, 2018, doi: 10.1002/biot.201700324.
- [9] L. Cervera *et al.*, "Production of HIV-1-based virus-like particles for vaccination: achievements and limits," *Appl. Microbiol. Biotechnol.*, vol. 103, no. 18, pp. 7367–7384, 2019, doi: 10.1007/s00253-019-10038-3.
- [10] Christopher Sumner and Akira Ono, "Relationship between HIV-1 Gag Multimerization and Membrane Binding," vol. 14, no. 3, p. 622, 2022, doi: 10.3390/v14030622.
- [11] A. Boix-Besora, E. Lorenzo, J. Lavado-García, F. Gòdia, and L. Cervera, "Optimization, Production, Purification and Characterization of HIV-1 GAG-Based Virus-like Particles Functionalized with SARS-CoV-2," *Vaccines*, vol. 10, no. 2, pp. 1–18, 2022, doi: 10.3390/vaccines10020250.
- [12] A. Boix-Besora, F. Gòdia, and L. Cervera, "Gag Virus-like Particles Functionalized with SARS-CoV-2 Variants: Generation, Characterization and Recognition by COVID-19 Convalescent Patients' Sera," *Vaccines*, vol. 11, no. 11, 2023, doi: 10.3390/vaccines11111641.
- [13] D. Fontana, E. Garay, L. Cervera, R. Kratje, C. Prieto, and F. Gòdia, "Chimeric vlps based on hiv-1 gag and a fusion rabies glycoprotein induce specific antibodies against rabies and foot-and-mouth disease virus," *Vaccines*, vol. 9, no. 3, 2021, doi: 10.3390/vaccines9030251.
- [14] M. T. Smith, A. K. Hawes, and B. C. Bundy, "Reengineering viruses and virus-like particles through chemical functionalization strategies," *Curr. Opin. Biotechnol.*, vol. 24, no. 4, pp. 620–626, 2013, doi: 10.1016/j.copbio.2013.01.011.
- [15] D. D. Hein, Christopher. Liu, Xin-Ming. Wang, "Click Chemistry, a Powerful Tool for Pharmaceutical Sciences," *Natl. Inst. Heal. J.*, vol. 25, no. 10, pp. 1–7, 2008, doi: 10.1007/s11095-008-9616-1.Click.
- [16] "Recent trends in click chemistry as a promising technology for virus-related research," no. January, 2020.
- [17] K. G. Patel and J. R. Swartz, "Surface Functionalization of Virus-Like Particles by Direct Conjugation Using Azide - Alkyne Click Chemistry," pp. 376–387, 2011.
- [18] H. Hu and N. F. Steinmetz, "Development of a virus-like particle-based Anti-HER2 breast cancer vaccine," *Cancers (Basel)*, vol. 13, no. 12, pp. 1–14, 2021, doi: 10.3390/cancers13122909.
- [19] M. O. Mohsen *et al.*, "Vaccination with nanoparticles combined with micro-adjuvants protects against cancer," *J. Immunother. Cancer*, vol. 7, no. 1, pp. 1–13, 2019, doi: 10.1186/s40425-019-0587-z.

- [20] T. Tian *et al.*, "Surface functionalized exosomes as targeted drug delivery vehicles for cerebral ischemia therapy," *Biomaterials*, vol. 150, pp. 137–149, 2018, doi: 10.1016/j.biomaterials.2017.10.012.
- [21] N. Winssinger, "Bioorthogonal chemistry," *Chimia (Aarau)*, vol. 72, no. 11, p. A755, 2018, doi: 10.1038/s43586-021-00028-z.Bioorthogonal.
- [22] M. García-Trujillo, J. Lavado-García, A. Boix-Besora, L. Cervera, and Francesc Gòdia, "Optimizing Strain-Promoted Azide-Alkyne Cycloaddition to Functionalize Gag HIV-1 Virus-Like Particles and Extracellular Vesicles with Spike Epitopes against SARS-CoV-2," *Vaccines*, vol. Submitted, 2024.
- [23] T. Murakami *et al.*, "Inhibitory Mechanism of the CXCR4 Antagonist T22 against Human Immunodeficiency Virus Type 1 Infection," *J. Virol.*, vol. 76, no. 2, pp. 933–933, 2002, doi: 10.1128/jvi.76.2.933.2002.
- [24] U. Unzueta, N. Ferrer-miralles, I. Casanova, J. Cedano, and A. Villaverde, "Intracellular CXCR4 + cell targeting with T22-empowered protein-only nanoparticles," 2012.
- [25] Y. Núñez *et al.*, "T22-PE24-H6 Nanotoxin Selectively Kills CXCR4-High Expressing AML Patient Cells In Vitro and Potently Blocks Dissemination In Vivo," *Pharmaceutics*, vol. 15, no. 3, 2023, doi: 10.3390/pharmaceutics15030727.
- [26] E. Voltà-Durán *et al.*, "The Diphtheria Toxin Translocation Domain Impairs Receptor Selectivity in Cancer Cell-Targeted Protein Nanoparticles," *Pharmaceutics*, vol. 14, no. 12, pp. 1–13, 2022, doi: 10.3390/pharmaceutics14122644.
- [27] E. Voltà-Durán *et al.*, "Design and engineering of tumor-targeted, dual-acting cytotoxic nanoparticles," *Acta Biomater.*, vol. 119, no. xxxx, pp. 312–322, 2021, doi: 10.1016/j.actbio.2020.11.018.
- [28] A. Zlotnik, "Chemokines and cancer," *Int. J. Cancer*, vol. 119, no. 9, pp. 2026–2029, 2006, doi: 10.1002/ijc.22024.
- [29] P. Liu, P. Long, Y. Huang, F. Sun, and Z. Wang, "CXCL12/CXCR4 axis induces proliferation and invasion in human endometrial cancer," *Am. J. Transl. Res.*, vol. 8, no. 4, pp. 1719–1729, 2016.
- [30] H. Kulbe, N. R. Levinson, F. Balkwill, and J. L. Wilson, "The chemokine network in cancer - Much more than directing cell movement," *Int. J. Dev. Biol.*, vol. 48, no. 5–6, pp. 489–496, 2004, doi: 10.1387/ijdb.041814hk.
- [31] F. Balkwill, "The significance of cancer cell expression of the chemokine receptor CXCR4," *Semin. Cancer Biol.*, vol. 14, no. 3, pp. 171–179, 2004, doi: 10.1016/j.semcancer.2003.10.003.
- [32] M. Pautler and S. Brenner, "Nanomedicine : promises and challenges for the future of public health," pp. 803–809, 2010, doi: 10.2147/IJN.S13816.
- [33] E. Medina-Gutiérrez *et al.*, "Potent Anticancer Activity of CXCR4-Targeted Nanostructured Toxins in Aggressive Endometrial Cancer Models," *Cancers (Basel)*, vol. 15, no. 1, 2023, doi: 10.3390/cancers15010085.
- [34] E. Lorenzo, L. Miranda, F. Gòdia, and L. Cervera, "Downstream process design for Gag HIV - 1 based virus - like particles," *Biotechnol. Bioeng.*, vol. 120, no. 9, pp. 2672–2684, 2023, doi: 10.1002/bit.28419.
- [35] J. Lavado-García, I. Jorge, A. Boix-Besora, J. Vázquez, F. Gòdia, and L. Cervera, "Characterization of HIV-1 virus-like particles and determination of Gag stoichiometry for different production

- platforms," *Biotechnol. Bioeng.*, vol. 118, no. 7, pp. 2660–2675, 2021, doi: 10.1002/bit.27786.
- [36] E. Vazquez *et al.*, "Protein nanodisk assembling and intracellular trafficking powered by an arginine-rich (R9) peptide," *Nanomedicine*, vol. 5, no. 2, pp. 259–268, 2010, doi: 10.2217/nnm.09.98.
- [37] E. Vázquez *et al.*, "Internalization and kinetics of nuclear migration of protein-only, arginine-rich nanoparticles," *Biomaterials*, vol. 31, no. 35, pp. 9333–9339, 2010, doi: 10.1016/j.biomaterials.2010.08.065.
- [38] E. Voltà-Durán *et al.*, "High-precision targeting and destruction of cancer-associated PDGFR- $\beta$ + stromal fibroblasts through self-assembling, protein-only nanoparticles," *Acta Biomater.*, vol. 170, no. October, pp. 543–555, 2023, doi: 10.1016/j.actbio.2023.09.001.
- [39] S. J. Kaczmarczyk, K. Sitaraman, H. A. Young, S. H. Hughes, and D. K. Chatterjee, "Protein delivery using engineered virus-like particles," 2011, doi: 10.1073/pnas.1101874108/-/DCSupplemental.www.pnas.org/cgi/doi/10.1073/pnas.1101874108.
- [40] L. Cervera, I. Gonz Alez-Dom Inquez, M. Ia, M. Segura, and F. G. Odia, "Intracellular Characterization of Gag VLP Production by Transient Transfection of HEK 293 Cells," doi: 10.1002/bit.26367/abstract.
- [41] C. C. Chen, M. Stark, M. Baikoghli, and R. H. Cheng, "Surface functionalization of hepatitis E virus nanoparticles using chemical conjugation methods," *J. Vis. Exp.*, vol. 2018, no. 135, pp. 1–8, 2018, doi: 10.3791/57020.
- [42] D. E. Prasuhn, P. Singh, E. Strable, S. Brown, M. Manchester, and M. G. Finn, "Plasma clearance of bacteriophage Q $\beta$  particles as a function of surface charge," *J. Am. Chem. Soc.*, vol. 130, no. 4, pp. 1328–1334, 2008, doi: 10.1021/ja075937f.
- [43] M. J. Rohovie, M. Nagasawa, and J. R. Swartz, "Virus-like particles: Next-generation nanoparticles for targeted therapeutic delivery," *Bioeng. Transl. Med.*, vol. 2, no. 1, pp. 43–57, 2017, doi: 10.1002/btm2.10049.
- [44] M. Peacey, S. Wilson, and V. K. Baird, Margaret A.Ward, "Versatile RHDV Virus-Like Particles: Incorporation of Antigens by Genetic Modification and Chemical Conjugation," *Biotechnol. Bioeng.*, vol. 98, pp. 968–977, 2007, doi: 10.1002/bit.
- [45] J. Park, P. L. Chariou, and N. F. Steinmetz, "Site-Specific Antibody Conjugation Strategy to Functionalize Virus-Based Nanoparticles," *Bioconjug. Chem.*, vol. 31, no. 5, pp. 1408–1416, 2020, doi: 10.1021/acs.bioconjchem.0c00118.
- [46] S. B. Carvalho *et al.*, "Membrane-Based Approach for the Downstream Processing of Influenza Virus-Like Particles," *Biotechnol. J.*, vol. 14, no. 8, Aug. 2019, doi: 10.1002/biot.201800570.
- [47] F. P. and F. C. Jerri C. Caldeira , Michael Perrine, "Virus-Like Particles as an Immunogenic Platform for Cancer Vaccines," *Viruses*, vol. 12, p. 488, 2020, doi: doi:10.3390/v12050488.
- [48] I. González-Domínguez, E. Puente-Massaguer, L. Cervera, and F. Gòdia, "Quality assessment of virus-like particles at single particle level: A comparative study," *Viruses*, vol. 12, no. 2, 2020, doi: 10.3390/v12020223.
- [49] M. Adrian, J. Dubochet, J. Lepault, and A. W. McDowell, "Cryo-electron microscopy of viruses," *Nature*, vol. 308, no. 5954, pp. 32–36, 1984, doi: 10.1038/308032a0.
- [50] I. González-Domínguez, E. Lorenzo, A. Bernier, L. Cervera, F. Gòdia, and A. Kamen, "A four-step purification process for gag vlps: From culture supernatant to high-purity lyophilized particles,"

- Vaccines*, vol. 9, no. 10, pp. 1–19, 2021, doi: 10.3390/vaccines9101154.
- [51] T. Koho *et al.*, “Purification of norovirus-like particles (VLPs) by ion exchange chromatography,” *J. Virol. Methods*, vol. 181, no. 1, pp. 6–11, 2012, doi: 10.1016/j.jviromet.2012.01.003.
  - [52] E. Puente-Massaguer, M. Lecina, and F. Gòdia, “Application of advanced quantification techniques in nanoparticle-based vaccine development with the Sf9 cell baculovirus expression system,” *Vaccine*, vol. 38, no. 7, pp. 1849–1859, Feb. 2020, doi: 10.1016/j.vaccine.2019.11.087.
  - [53] B. J. Lindsay *et al.*, “Morphological characterization of a plant-made virus-like particle vaccine bearing influenza virus hemagglutinins by electron microscopy,” *Vaccine*, vol. 36, no. 16, pp. 2147–2154, 2018, doi: 10.1016/j.vaccine.2018.02.106.
  - [54] L. L. Huang, G. H. Lu, J. Hao, H. Wang, D. L. Yin, and H. Y. Xie, “Enveloped virus labeling via both intrinsic biosynthesis and metabolic incorporation of phospholipids in host cells,” *Anal. Chem.*, vol. 85, no. 10, pp. 5263–5270, 2013, doi: 10.1021/ac4008144.
  - [55] Y. Yang *et al.*, “Size-exclusion HPLC provides a simple, rapid, and versatile alternative method for quality control of vaccines by characterizing the assembly of antigens,” *Vaccine*, vol. 33, no. 9, pp. 1143–1150, 2015, doi: 10.1016/j.vaccine.2015.01.031.
  - [56] D. T. Le and K. M. Müller, “In vitro assembly of virus-like particles and their applications,” *Life*, vol. 11, no. 4, 2021, doi: 10.3390/life11040334.
  - [57] Craig S. McKay and M.G. Finn, “Click Chemistry in Complex Mixtures: Bioorthogonal Bioconjugation,” *Chem Biol*, vol. 21, no. 9, pp. 1075–1101, 2014, doi: 10.1016/j.chembiol.2014.09.002.
  - [58] Marisa L. Hovlid *et al.*, “Guiding Plant Virus Particles to Integrin-Displaying Cells,” *Jama*, vol. 4, no. 12, pp. 3698–3705, 2012, doi: 10.1039/c2nr30571b. Guiding.
  - [59] D. Banerjee, A. P. Liu, N. Voss, S. L. Schmid, and M. G. Finn, “Multivalent Display and Receptor-Mediated Endocytosis of Transferrin on Virus-Like Particles,” *Jama*, vol. 11, no. 9, pp. 1273–1279, 2010, doi: 10.1002/cbic.201000125.
  - [60] N. Serna *et al.*, “Nanostructured toxins for the selective destruction of drug resistant human CXCR4+ colorectal cancer stem cells,” *J. Control. Release*, vol. 320, pp. 96–104, 2020, doi: 10.1016/j.jconrel.2020.01.019.
  - [61] M. V. Céspedes *et al.*, “In vivo architectonic stability of fully de novo designed protein-only nanoparticles,” *ACS Nano*, vol. 8, no. 5, pp. 4166–4176, 2014, doi: 10.1021/nn4055732.
  - [62] U. Unzueta *et al.*, “Non-amyloidogenic peptide tags for the regulatable self-assembling of protein-only nanoparticles,” *Biomaterials*, vol. 33, no. 33, pp. 8714–8722, 2012, doi: 10.1016/j.biomaterials.2012.08.033.
  - [63] H. Tamamura *et al.*, “Pharmacophore identification of a chemokine receptor (CXCR4) antagonist, T22 ([Tyr5,12, Lys7]-polyphemusin II), which specifically blocks T cell-line-tropic HIV-1 infection,” *Bioorganic Med. Chem.*, vol. 6, no. 7, pp. 1033–1041, 1998, doi: 10.1016/S0968-0896(98)00061-3.
  - [64] H. Tamamura *et al.*, “Effective lowly cytotoxic analogs of an HIV-cell fusion inhibitor, T22 ([Tyr5,12, Lys7]-polyphemusin II),” *Bioorganic Med. Chem.*, vol. 6, no. 2, pp. 231–238, 1998, doi: 10.1016/S0968-0896(97)10037-2.
  - [65] S. Cabrero-De Las Heras and E. Martínez-Balibrea, “CXC family of chemokines as prognostic or predictive biomarkers and possible drug targets in colorectal cancer,” *World J. Gastroenterol.*, vol.

- 24, no. 42, pp. 4738–4749, 2018, doi: 10.3748/wjg.v24.i42.4738.
- [66] M. V. Céspedes *et al.*, “Selective depletion of metastatic stem cells as therapy for human colorectal cancer,” *EMBO Mol. Med.*, vol. 10, no. 10, pp. 1–22, 2018, doi: 10.15252/emmm.201708772.
- [67] R. Díaz *et al.*, “Selective CXCR4 + Cancer Cell Targeting and Potent Antineoplastic Effect by a Nanostructured Version of Recombinant Ricin,” vol. 1800665, pp. 1–12, 2018, doi: 10.1002/smll.201800665.
- [68] E. R. Blanco *et al.*, “CXCR4-targeted nanotoxins induce GSDME- dependent pyroptosis in head and neck squamous cell carcinoma,” *J. Exp. Clin. Cancer Res.*, pp. 1–17, 2022, doi: 10.1186/s13046-022-02267-8.
- [69] O. Cano-Garrido *et al.*, “Biparatopic protein nanoparticles for the precision therapy of cxcr4+ cancers,” *Cancers (Basel)*, vol. 13, no. 12, pp. 1–17, 2021, doi: 10.3390/cancers13122929.
- [70] U. Unzueta, M. V. Céspedes, E. Vázquez, N. Ferrer-Mirallès, R. Mangues, and A. Villaverde, “Towards protein-based viral mimetics for cancer therapies,” *Trends Biotechnol.*, vol. 33, no. 5, pp. 253–258, 2015, doi: 10.1016/j.tibtech.2015.02.007.
- [71] N. Tyagi, M. Tyagi, M. Pachauri, and P. C. Ghosh, “Potential therapeutic applications of plant toxin-ricin in cancer : challenges and advances,” 2015, doi: 10.1007/s13277-015-4028-4.

## **GENERAL DISCUSSION**

---

The growing interest in the use of enveloped virus like particles (eVLPs) as novel vaccines, vectors for gene and cancer therapy, or nanocarriers for drug delivery applications lead to an increase demand for efficient and scalable production platforms [1], [2], [3]. The purification of VLPs, and the removal of contaminants, mainly extracellular vesicles, host cell protein and host cell DNA, can only be achieved through a combination of different steps [4], [5]. In this context, the first contribution of this thesis (**Chapter One**) focuses on designing a scalable purification process for enveloped HIV-1 Gag VLPs fused to eGFP (Gag::eGFP VLPs) that can be also applied to other enveloped VLP-based products. The process proposed includes four steps: clarification, concentration and intermediate purification, capture, and polishing. For each step, a trade-off between different technologies has enabled to select the best performance DSP configuration.

For the clarification step, depth filtration through a membrane is the proposed technique. One of its main advantages is that it is a scalable technique, however, careful selection of pore size and membrane material are key to ensure maximum product recovery [6]. Venereo-Sanchez et al. (2017) [7] used a two-step depth filtration for the clarification of Gag-based VLPs. Including a first filtration step with a wider pore size can help avoid the generation of a significant cake where the VLPs can be retained, and results in higher recoveries. Since HIV-1 Gag VLPs are covered with the lipid envelope, they are usually negatively charged; therefore, electrostatic interactions can occur in membrane processes. For this reason, selection of inert membranes is recommended, instead of positively charged membranes where the VLPs can be retained. Depth filtration has been also used for clarification of Influenza, Hepatitis C, and rotavirus VLPs, produced using insect cells [8], [9], [10]. Moreover, Human Influenza A virus have been clarified directly from the culture broth with HA recovery yields ranging from 85–93% with depth filtration [11], which is consistent with the results presented here.

Regarding secondary clarification, long-term storage at -80 °C followed by primary clarification is often necessary for large-scale processes when sometimes holding points are needed. Consequently, a second clarification step can be then required to eliminate precipitates and/or aggregates formed during thawing. Notably, studies addressing this specific approach are not common in the literature. However, the obtained



results show that implementing this technique successfully reduce the contaminant dsDNA content and maintained the VLP concentration without any losses.

The following steps usually include a concentration technique, and/ or a chromatography [12] [13]. Indeed, filtration and chromatography have become the pillars for downstream processing of biological particles [4]. When capture steps are employed, a prior concentration step using tangential flow filtration (TFF) is often unnecessary. However, for large sample volumes, concentration by TFF can be of interest [14], [15], [16]. Reducing the initial volume through TFF concentration can decrease the time and load required in the capture step [17]. Using TFF with a 300 kDa PES membrane, Gag::eGFP VLPs preparation can be concentrated tenfold with 100% VLP recovery in the retentate fraction, and more than 85% of dsDNA and total protein content removal. These results were superior to those reported by Venereo-Sanchez et al. (2016) [18] and P.E. Cruz et al (2000) [19] using 1000 kDa and 300 kDa PES membrane for Gag VLPs respectively. Moreover, the use of hollow fibers has been reported as another alternative unit operation in virus concentration and purification due to their open channels and lot-to-lot consistency [5], [10], [17]. Also, the use of Hollow-fibers devices can result in lower shear rates when compared with membrane cassette devices and have been used in the manufacturing of several viral particles [8], [11].

On the other hand, the advantages of including a Multimodal Chromatography (MC) as intermediate purification step, is that impurities which could interact with the resins/membranes, can be eliminated [12]. This improves the capture efficiency of the molecule of interest in subsequent bind-elution steps. The results obtained in terms of contaminating protein reduction and VLP recovery were lower than those reported in the literature using the Capto Core 700 column [20], [21]. Given the potential of using this type of chromatography as an intermediate step, one possible approach to improve these results is to study the dynamic binding capacity (DBC) of the column [22]. Additionally, testing different flow rates and buffer conditions during the runs could further enhance performance. Furthermore, according to Tseng Y-F et al. (2017) [23], better contaminant removal can be obtained using the Capto Core 700 column after an anionic exchange chromatography.

Different chromatographic modes can be applied for the capture step in the DSP of the Gag VLPs. This is also a scalable technology, and not only allows reducing the volume, but also to further purify the

nanoparticles [24]. The separation principle in chromatography relies on physicochemical interactions between solutes in the mobile phase and the surface functional groups of the stationary phase (chromatography resin). The type of interaction mainly depends on the type of ligand in the chromatography resin.

Ion-exchange chromatography is one of the most widely used chromatographic techniques for purification of large particles such as VLPs [25]. The performance obtained in recovery and purity enrichment with Capto Q ImpRes resin was particularly notable, demonstrating significant DNA removal efficiency, achieving an 87% reduction in host cell DNA. This promising result eliminates the need for DNase treatment, presenting a notable advantage in large-scale processes [26]. On the other hand, a 37% enrichment of VLPs respect to total nanoparticles was obtained. This performance was superior compared to the other two ion-exchange chromatography methods tested, making it the most effective option for this purpose. This type of resin has also been used in the purification of oncolytic adenovirus [17] and influenza viruses [22], [23], yielding results comparable to those observed here. These data support the use of strong quaternary amine ion bound to a high-flow agarose base matrix to capture and purify eVLPs.

On the other hand, monolithic columns offer distinct advantages over conventional resin beads due to their unique structural and functional properties. In comparison to conventional resin beads, monoliths are produced *in situ* by a polymerization process that creates a continuous homogeneous block with network of flow channels with open pores. This results in very high porosity of up to 90%, allowing high flow rates with low pressure drops and high binding capacity for the efficient separation of large biomolecules or bio-nanoparticles [27], [28], [29]. Different ligands for chromatographic separation can easily be coupled to the polymer network [30]. In this work, two different types of functionalized monoliths were tested, Monolith QA for IEC and Monolith OH<sup>-</sup> for HIC. The best results were obtained with the Monolith QA, which suggests that the ion exchange principle provided by the QA ligand allows a better recovery of the Gag VLPs, compared to the hydrophobic exchanges provided by the OH ligand. The results obtained here are consistent with those reported by other authors using the same types of monolith resins [13], [27], [29]. Although this type of chromatography has advantageous characteristics, such as a high convective flow, which maintain a low pressure drop resulting in high adsorption kinetics for large biomolecules or bio-nanoparticles [31], one of

the reported problems is flow dependent entrapment of large particles. Particles or large molecules can be trapped in narrow channels or small pores. When the upstream diffusion is higher than the downstream convective flow this effect can be reversed, but ultimately leads to pressure increase or loss of binding capacity [32]. Another reported issue is that the monolith bed is not fully rigid. High flow rates or pressure drops can lead to a structural change and a compression leading to increased process pressures after several process cycles, especially when working with crude feed stocks [33].

Although affinity chromatography has recently gained more importance in biotherapeutic product manufacturing due to its unique selectivity [34], recovery percentages for VLPs or similar particles are generally around 50% as reported M.W. Wolff et al. (2010) [35] for Vaccinia Ankara Virus and M.M. Segura et al. (2007) [36] for lentiviral vectors, both using heparin-based affinity chromatography. The results obtained in this thesis using this type of chromatography showed a Gag VLPs recovery of 23% and 42% for Capto Heparin and POROS Heparin respectively. However, these outcomes were superior to those reported by K. Reiter et al. (2018) [20] which achieved only a 15% recovery of Gag VLPs using heparin-based affinity chromatography. Furthermore, it is noteworthy the high purity level (over 70%) for Gag VLPs relative to the total nanoparticle was obtained.

Polishing is a critical step when clinical-grade material is required. Residual host-cell protein and host-cell DNA must be reduced to acceptable threshold values set by regulatory agencies [2]. Additionally, this step can be used to introduce the correct formulation buffer. Despite the limitations of size exclusion chromatography, such as low capacity and product dilution, it remains one of the most commonly used techniques for polishing, removing low molecular weight impurities, and facilitating buffer exchange in the final formulation [5], [37]. High recovery levels of Gag VLPs (74%) and an almost complete reduction of contaminants were achieved in our work using the size-exclusion medium Sepharose 4 Fast Flow during the polishing step. These results represent an improvement respect to those report for oncolytic adenovirus [17] and also for Gag VLPs [38]. However, despite these results and considering the limitations of size exclusion chromatography (SEC), flow-through chromatographic separation has become an important step for polishing purposes. Resins such as Capto Core 700 and various membrane adsorbers have been used in a negative mode for the polishing of biotherapeutic particles [39], [40], [41], [42]. Additionally,

ultrafiltration/diafiltration (UF/DF) can serve as an alternative polishing step, allowing for simultaneous purification and exchange into the final formulation buffer [6], [26].

Overall, a complete purification train for Gag VLPs, consisting of clarification with the Supracap depth filter, without benzonase treatment, capture by IEC with the Capto Q ImpRes and polishing by SEC with the Sepharose 4 FF resulted in the obtention of Gag VLPs with a purity of 64% relative to total nanoparticles. The final recovery of the entire process, relative to the initial crude supernatant, was 38%, and the contaminant content met regulatory requirements. The VLP recovery results obtained in this work are comparable to those reported by Y. F. Tseng et al. (2017) [23], C. Peixoto et al. (2006) [8], and I. González-Domínguez (2021) [38], who achieved recoveries of 33%, 37%, and 23%, respectively. The DSP unit operations studied in this thesis are suitable for large-scale manufacturing due to their scalability, supporting their potential use as a platform for Gag VLP purification and might be suitable for other VLPs as well [43]. Furthermore, the use of SEC not only for polishing to achieve high purity, but also for performing buffer exchange to obtain the product of interest in the final buffer selected for further processing and formulation has been demonstrated.

A second relevant step to consider in the development of VLP is their preservation. Specifically relevant for their use as vaccines is the need for preservation methods that do not require cold storage. For this reason, the formulation buffer for the lyophilization (or freeze-drying) of Gag VLPs has been explored (**Chapter Two**). Despite the obvious advantages of lyophilized material in comparison to cold chain storage, the process of freeze-drying is still challenging in viral-based vaccines, especially for enveloped viruses [44]. For that reason, optimization of the formulation buffer is crucial to minimize the negative effects of this process. The lyophilization process depends on multiple variables, and it is important to systematically optimize them to obtain the most suitable conditions for freeze-drying.

A specific fractional factorial DoE was used to achieve the best formulation buffer for lyophilization through the evaluation of different characteristics of Gag VLPs [45], [46], [47]. This approach allowed to efficiently evaluate multiple variables and their interactions while minimizing the number of experiments runs in order to save time and in reducing material costs [48]. The DoE helped to understand the interaction between the excipients and their effects on Gag VLPs characteristics, such as particle size, concentration, and quality.

Although this experimental design has helped us optimize the formulation buffer, it can also be applied in future work aimed at optimizing the lyophilization process parameters like freezing rate, and primary, and secondary drying temperatures [44]. To achieve this, it is essential to evaluate not only the characteristics of the Gag VLPs but also factors more specifically related to the process. These include assessing the moisture content, conducting thermal analysis of the dried VLP formulations, and examining the morphology of the lyophilized products [49] [50]. A similar approach to optimize VLP-based vaccine formulations has been reported by R. Lang et al (2009) [51], S. Saboo et al (2016) [45] and Y. Liu (2024) [52]. These studies focused on vaccines against nicotine addiction based on VLPs of the RNA phage Q $\beta$ , VLP vaccines against Human Papillomavirus, and Live Recombinant Pseudorabies Virus Vaccines, respectively. However, there is limited evidence of studies of this kind on for Gag VLP-based vaccines.

The characterization of the Gag VLPs is an issue of high relevance in the development of production bioprocesses. Indeed, nanoparticle characterization methods including NTA, DLS, flow virometry, SE-HPLC and cryo-TEM, have been widely reported in the literature [53], [54], [55] and have been instrumental in identifying and selecting the optimal formulation for lyophilization, ensuring the preservation of the desired VLP properties. It is worth highlighting that other methods, such as Structured Illumination Microscopy (SRFM), have also been used to the characterize and quantify of HIV-1 Gag VLPs present in crude supernatants [56]. On the other hand, the application of Atomic Force Microscopy (AFM) in viral-based product characterization can provide relevant information in the study of their composition and structure. Different studies have been performed on virus characterization using AFM, where the external and internal structure or its nucleic acid content has been observed [57]. Therefore, these methodologies could also be considered in future work, along with additional techniques related to the specific biological functions of the VLPs, to obtain a more comprehensive and exhaustive characterization of the lyophilized nanoparticles.

The optimized multicomponent excipient formulation for the lyophilization of Gag VLPs includes sucrose (Cryo-lyo protectant), arginine (bulking agent) Tris-HCl (buffer) sodium chloride (tonicity modifier), and polysorbate 80 (surfactant). Each excipient contributes with specific properties to achieve Gag VLPs with the desired characteristics post-lyophilization. Incorporation of sucrose as stabilizer helps in protection against chemical and physical instability, aggregation and fusion of the VLPs during lyophilization [58].

Comparison of sucrose to other stabilizer like trehalose shows that sucrose can provide more benefits. Sucrose is cheaper, and due to its more predictive transformation behaviour, it is more effective as a stabiliser, especially in terms of conservation of the tertiary structure of a protein [59], [60]. The use of sucrose in VLP formulations has been reported by I. González-Domínguez et al (2021) [38] and R.K Jamil (2014) [61] for Gag VLPs and RS-12 strain live-attenuated mumps, respectively. Arginine has been used in formulations not only as bulking agent but also as a stabilizer [62], [63]. It is commonly included in several parenteral formulations for solutions, suspensions, and lyophilized drug products [64]. Furthermore, a mixture of arginine, glutamic acid, and isoleucine has been demonstrated to provide stability to a tested protein during lyophilization and storage [60], [65]. TrisHCl is a commonly used buffer in parenteral formulations, along with acetate, citrate, tartrate, and phosphate [60] [64]. One example of its use was reported by S. Zhai et al (2004) who included TrisHCl in the formulation for lyophilization of Herpes Simplex Virus 2 (HSV-2) vaccine, achieving high recoveries [66]. Regarding tonicity modifiers excipients, previous studies have shown that glycerol can lead to complete hemolysis of human erythrocytes due to its ability to pass freely through cell membranes [67]. As a result, using glycerol as the sole tonicity modifier would create a hypotonic formulation, potentially causing local muscle damage and pain upon intramuscular injection. To avoid these disadvantages, the use of NaCl [38], [51] or dextrose [49] provides a better alternative to adjust the osmolarity of the formulations, ensuring they are isotonic and compatible with parenteral administration. Consequently, the final formulation buffer contained NaCl as the tonicity modifier excipient. A small percentage of surfactant Polysorbate 80 was included as well to prevent aggregation through the protein surfaces, by surfactant adsorption to the hydrophobic regions on the protein surface, or to the interfaces between ice/ air and water. Surfactants increase the free energy required for protein unfolding and reduce the surface tension of interfaces formed during lyophilisation and reconstitution [62], [67].

Ensuring the stability of these formulations is critical for maintaining their effectiveness and safety over time. Therefore, studying its thermostability under various conditions is of significant importance. According to the results obtained in the stability study, the optimal temperature for preserving Gag::eGFP VLPs after lyophilization for a period of up to 4 weeks, whether in lyophilized or reconstituted form, is at 4°C. Although these results are promising for the lyophilization of enveloped VLPs, future work should focus on developing

and optimizing lyophilization methods and formulations to increase the stability of the nanoparticles for longer periods of time. This will facilitate their use and transportation worldwide, with the ultimate goal of eliminating the need for cold-chain storage for VLP vaccines.

The study of the production of complex nanoparticles like VLPs should be addressed in a comprehensive approach including all the different steps studied, from upstream, to downstream and final product preservation. To this end, and based on the previous findings, a perfusion-based upstream production followed by a three-step downstream purification process is proposed in **Chapter Three**. While viral particle production is typically done transiently in batch or fed-batch processes [68], recent advancements have enabled the use of perfusion processes [69], [70], [71]. In the perfusion approach selecting a filtration membrane enabling cell retention and continuous harvest of VLPs in the membrane is crucial to improve production efficiency. The improvement achieved in this work can be attributed to the removal of extracellular particles and EVs, which stimulates vesicle secretion in HEK293 cells, as VLPs utilize the endosomal pathway for exosome secretion [72]. This removal minimizes potential inhibitory effects on transfection since EVs and other extracellular particles can compete with transfection agents or interfere with the uptake of genetic material by the cells. Therefore, their removal creates a cleaner environment, which can enhance the efficiency of transfection [68], [72].

Consequently, implementing continuous VLP harvest not only improved scalability but also enhanced production at the cellular and metabolic levels by ensuring a consistent supply of nutrients, efficient waste removal, stable culture conditions, reduced cellular stress and the removal of inhibitory substances. These factors collectively enhance cellular metabolism, leading to improved VLP production efficiency [68].

However, only 49.9% of total produced VLPs are harvested in this perfusion process strategy and the remaining 50% is retained in the bioreactor. To increase this, two strategies could be explored: reoptimizing the CSPR and switching off the feed at the end of the perfusion period to allow the harvest pump to filter the remaining supernatant in the bioreactor. The latter, however, risks of filter clogging due to increased cell concentration. Further improvements could involve strategies to mitigate the cell density effect [68], allowing re-transfections at higher cell densities. Optimizing CSPR for transfection, DNA amount, and ATF filtration rate based on cell concentration could enhance VLP production in perfusion and TFG based bioprocesses.

For downstream processing, the proposed process includes a second clarification step to ensure clean starting material for chromatographic steps, enhancing purification efficiency and yield. The Capto Q ImpRes column can operate at large-scale, balancing recovery rates and purity, with VLP purity levels of 60% post-capture. With the lyophilization process post-purification nanoparticles with optimal characteristics, maintaining size, quality, and morphology are obtained.

Finally, the potential applications of VLPs are not reduced to vaccine development but also as versatile nanocarriers for various approaches, including drug delivery, gene therapy, and cancer treatment [73]. Engineered VLPs are promising delivery vehicles combining the advantages of viral and nonviral methods. VLPs, formed by the assembly and budding of retroviral polyproteins, can encapsulate cargo molecules and can transduce mammalian cells without carrying a packaged genome. This avoids the risk of viral genetic material integrating into host genomes. For example, VLPs have been used to deliver Cas9 nucleases, and recent advancements have achieved efficient *in vivo* delivery of adenine base editor with single guide RNA ribonucleoproteins (RNPs) using engineered VLPs [74]. These VLPs overcome molecular bottlenecks in cargo packaging, release, and localization, and offer several advantages: they do not have stringent cargo size limitations, can package transient RNPs to minimize off-target effects, and can be pseudotyped with different glycoproteins for specific cell targeting [74]. The potential of functionalizing Gag VLPs with the T22 peptide, through chemical conjugation, to target and penetrate CXCR4<sup>+</sup> cells have been explored in **Chapter Four**. T22 peptide had been previously identified as ligand for CXCR4 receptor [75] [76] [77] which is a relevant molecular marker for anti-cancer drug targeting [78]. In this context, several researchers have studied CXCR4-targeted self-assembling protein nanoparticles using T22-GFP-H6 conjugates. For instance, E. Voltà-Durán et al (2020) [79] introduce CXCR4-targeted self-assembling protein nanoparticles conjugated with microbial toxins and antitumor drugs, demonstrating stability and internalization in target cells, and promising for treating drug-resistant cancers. Moreover, M Virtudes Céspedes et al (2018) [80] highlight the selective elimination of metastatic stem cells in colorectal cancer using a Floxuridine-delivering nanoconjugate, which significantly prevents and regresses metastases with minimal toxicity to normal tissues. Another example is reported by R Días et al (2018) [81], who present a recombinant plant toxin engineered into CXCR4-targeted nanoparticles, which exhibit potent cytotoxicity against CXCR4<sup>+</sup> cancer



cells and demonstrate significant therapeutic effects in acute myeloid leukemia models. Collectively, these studies underscore the potential of targeted nanoparticle-based approaches in enhancing the precision and effectiveness of cancer therapies.

In addition to its use in this work, click chemistry methodology can be applied in process development to adapt quantification methods for pre-clinical and clinical preparations. In this regard S.B. Carvalho et al (2016) [82], developed a functionalized influenza VLP through the alkyne-azide cycloaddition reaction allowing for the specific incorporation of a reporter during process development, facilitating precise tracking and optimization. Importantly, it also ensures the seamless translation of non-tagged candidates for manufacturing purposes, maintaining the integrity and suitability of the final product for clinical applications. On the other hand, click chemistry offers several advantages over other modification approaches such as gene transfection. Genetic insertion sometimes fails to yield a VLP because of improper recombinant protein folding. Chemical cross-linking of a synthetic peptide to a preformed VLP avoids this problem [83]. However, despite the limitation, genetic fusions can yield a more uniform product and can be produced biosynthetically in a single step and often in very high yields [84]. Furthermore, in the case of MS2 VLP reported by B. Chackerian et al (2011) [85], the genetic insertion has the added advantage of enabling epitope identification in a process akin to phage display by affinity-selection on antibody targets from complex random-sequence or antigen fragment libraries. Similar approaches have been reported by several researchers [86], [87], [88]. Another notable example is the work reported by S J. Kaczmarczyk et al (2011) [89] which describe a VLP derived from an avian retrovirus, that can deliver proteins either to the surface or the interior of cells. They have demonstrated the effectiveness of this technology by delivering a number of biologically active proteins, including GFP, Cre recombinase, cytotoxic enzymes Fcy::Fur (cytosine deaminase and uracil phosphoribosyl-transferase fusion protein), and human Caspase 8, to the inside of cells. In addition to intracellular delivery of proteins, they have shown that protein ligands, such as TRAIL and IFN- $\gamma$ , can be displayed on the surface of VLPs and can cause appropriate signalling in cell. Therefore, in future studies, it could be interesting to test a genetic modification strategy to obtain VLPs conjugated with the T22 peptide.

The successful functionalization process was evaluated through *in vitro* cellular uptake experiments. The presence of eGFP fused to the Gag polyprotein, which forms the VLPs, allowed tracking them within the

cells. This GFP reporter fusion facilitated the analysis of the *in vitro* experiments [90]. Cellular uptake studies revealed that Gag::eGFP VLPs-T22 exhibit superior penetration into CXCR4+ cells compared to nonfunctionalized Gag VLPs, in a dose- and time-dependent manner. Confocal microscopy confirmed intracellular localization, emphasizing the specificity of entry via CXCR4 receptors. This specificity prevents internalization in CXCR4-negative cells, reducing potential toxicity. Similar results have been obtained by other researchers [75], [81], [91] conducting the same experimental analyses, supporting our findings. This study underscores the potential of Gag::eGFP VLPs-T22 for targeted drug delivery to CXCR4+ cancer cells. Based on the results of this work, future strategies should focus on developing Gag VLPs-T22 engineered to transport molecules of biomedical interest, replacing the GFP reporter. Additionally, the *in vivo* efficacy of these drug payloads should be studied in animal models.

Overall, the work presented in this thesis, provides significant progress in the scalable purification, formulation, and functionalization of HIV-1 Gag VLPs. The proposed downstream process enables high recovery and purity levels suitable for scale-up. Furthermore, the optimized lyophilization formulation enhanced the stability and quality of the Gag VLPs, offering a potential solution to the challenges associated with cold chain storage. Finally, the successful functionalization of Gag VLPs with the T22 peptide highlights their potential as targeted drug delivery vehicles, particularly for cancer therapy. Future research should continue to explore and optimize these processes, expanding their applicability to other VLPs and therapeutic applications.

## REFERENCES

- [1] S. H. Wong, A. Jassey, J. Y. Wang, W. C. Wang, C. H. Liu, and L. T. Lin, "Virus-like particle systems for vaccine development against viruses in the flaviviridae family," *Vaccines*, vol. 7, no. 4, pp. 1–20, 2019, doi: 10.3390/vaccines7040123.
- [2] L. Cervera *et al.*, "Production of HIV-1-based virus-like particles for vaccination: achievements and limits," *Appl. Microbiol. Biotechnol.*, vol. 103, no. 18, pp. 7367–7384, 2019, doi: 10.1007/s00253-019-10038-3.
- [3] M. O. Mohsen, L. Zha, G. Cabral-Miranda, and M. F. Bachmann, "Major findings and recent advances in virus-like particle (VLP)-based vaccines," *Semin. Immunol.*, vol. 34, no. August, pp. 123–132, 2017, doi: 10.1016/j.smim.2017.08.014.
- [4] M. W. Wolf and U. Reichl, "Downstream processing of cell culture-derived virus particles," *Expert Rev. Vaccines*, vol. 10, no. 10, pp. 1451–1475, 2011, doi: 10.1586/erv.11.111.
- [5] P. Nestola, C. Peixoto, R. R. J. S. Silva, P. M. Alves, J. P. B. Mota, and M. J. T. Carrondo, "Improved virus purification processes for vaccines and gene therapy," *Biotechnol. Bioeng.*, vol. 112, no. 5, pp. 843–857, 2015, doi: 10.1002/bit.25545.
- [6] S. B. Carvalho *et al.*, "Membrane-Based Approach for the Downstream Processing of Influenza Virus-Like Particles," *Biotechnol. J.*, vol. 14, no. 8, Aug. 2019, doi: 10.1002/biot.201800570.
- [7] A. Venereo-Sanchez *et al.*, "Process intensification for high yield production of influenza H1N1 Gag virus-like particles using an inducible HEK-293 stable cell line," *Vaccine*, vol. 35, no. 33, pp. 4220–4228, Jul. 2017, doi: 10.1016/j.vaccine.2017.06.024.
- [8] C. Peixoto, M. F. Q. Sousa, A. C. Silva, M. J. T. Carrondo, and P. M. Alves, "Downstream processing of triple layered rotavirus like particles," *J. Biotechnol.*, vol. 127, no. 3, pp. 452–461, 2007, doi: 10.1016/j.jbiotec.2006.08.002.
- [9] S. B. Carvalho *et al.*, "Efficient filtration strategies for the clarification of influenza virus-like particles derived from insect cells," *Sep. Purif. Technol.*, vol. 218, pp. 81–88, Jul. 2019, doi: 10.1016/j.seppur.2019.02.040.
- [10] L. Besnard *et al.*, "Clarification of vaccines: An overview of filter based technology trends and best practices," *Biotechnol. Adv.*, vol. 34, no. 1, pp. 1–13, Jan. 2016, doi: 10.1016/j.biotechadv.2015.11.005.
- [11] B. Kalbfuss, Y. Genzel, M. Wolff, A. Zimmermann, R. Morenweiser, and U. Reichl, "Harvesting and Concentration of Human Influenza A Virus Produced in Serum-Free Mammalian Cell Culture for the Production of Vaccines," *Biotechnol. Bioeng.*, vol. 97, no. 1, pp. 73–85, 2006, doi: 10.1002/bit.21139.
- [12] T. M. Lima, M. O. Souza, and L. R. Castilho, "Purification of flavivirus VLPs by a two-step chromatographic process," *Vaccine*, vol. 37, no. 47, pp. 7061–7069, 2019, doi: 10.1016/j.vaccine.2019.05.066.
- [13] P. Pereira Aguilar *et al.*, "Capture and purification of Human Immunodeficiency Virus-1 virus-like particles: Convective media vs porous beads," *J. Chromatogr. A*, vol. 1627, pp. 1–11, 2020, doi: 10.1016/j.chroma.2020.461378.
- [14] A. Negrete, A. Pai, and J. Shiloach, "Use of hollow fiber tangential flow filtration for the recovery and concentration of HIV virus-like particles produced in insect cells," *J. Virol. Methods*, vol. 195, pp. 240–246, 2014, doi: 10.1016/j.jviromet.2013.10.017.
- [15] D. L. Grzenia, J. O. Carlson, P. Czermak, B. Han, R. K. Specht, and S. R. Wickramasinghe, "Purification of densonucleosis virus by tangential flow ultrafiltration," *Biotechnol. Prog.*, vol. 22, no.

- 5, pp. 1346–1353, 2006, doi: 10.1021/bp060077c.
- [16] S. R. Wickramasinghe, B. Kalbfuß, A. Zimmermann, V. Thorn, and U. Reichl, “Tangential flow microfiltration and ultrafiltration for human influenza A virus concentration and purification,” *Biotechnol. Bioeng.*, vol. 92, no. 2, pp. 199–208, 2005, doi: 10.1002/bit.20599.
  - [17] M. G. Moleirinho *et al.*, “Clinical-Grade Oncolytic Adenovirus Purification Using Polysorbate 20 as an Alternative for Cell Lysis,” *Curr. Gene Ther.*, vol. 18, no. 6, pp. 366–374, 2018, doi: 10.2174/1566523218666181109141257.
  - [18] A. Venereo-Sanchez *et al.*, “Hemagglutinin and neuraminidase containing virus-like particles produced in HEK-293 suspension culture: An effective influenza vaccine candidate,” *Vaccine*, vol. 34, no. 29, pp. 3371–3380, Jun. 2016, doi: 10.1016/j.vaccine.2016.04.089.
  - [19] P. E. Cruz, C. C. Peixoto, K. Devos, J. L. Moreira, E. Saman, and M. J. T. Carrondo, “Characterization and downstream processing of HIV-1 core and virus-like- particles produced in serum free medium,” *Enzyme Microb. Technol.*, vol. 26, no. 1, pp. 61–70, 2000, doi: 10.1016/S0141-0229(99)00128-3.
  - [20] K. Reiter, P. P. Aguilar, V. Wetter, P. Steppert, A. Tover, and A. Jungbauer, “Separation of virus-like particles and extracellular vesicles by flow-through and heparin affinity chromatography,” *J. Chromatogr. A*, vol. 1588, pp. 77–84, Mar. 2019, doi: 10.1016/j.chroma.2018.12.035.
  - [21] P. Lagoutte *et al.*, “Scalable chromatography-based purification of virus-like particle carrier for epitope based influenza A vaccine produced in *Escherichia coli*,” *J. Virol. Methods*, vol. 232, pp. 8–11, 2016, doi: 10.1016/j.jviromet.2016.02.011.
  - [22] T. Weigel, T. Solomaier, A. Peuker, T. Pathapati, M. W. Wolff, and U. Reichl, “A flow-through chromatography process for influenza A and B virus purification,” *J. Virol. Methods*, vol. 207, pp. 45–53, 2014, doi: 10.1016/j.jviromet.2014.06.019.
  - [23] Y. F. Tseng, T. C. Weng, C. C. Lai, P. L. Chen, M. S. Lee, and A. Y. C. Hu, “A fast and efficient purification platform for cell-based influenza viruses by flow-through chromatography,” *Vaccine*, vol. 36, no. 22, pp. 3146–3152, 2018, doi: 10.1016/j.vaccine.2017.03.016.
  - [24] M. G. Moleirinho, R. J. S. Silva, P. M. Alves, M. J. T. Carrondo, and C. Peixoto, “Current challenges in biotherapeutic particles manufacturing,” *Expert Opin. Biol. Ther.*, vol. 20, no. 5, pp. 451–465, 2019, doi: 10.1080/14712598.2020.1693541.
  - [25] P. Kramberger, L. Urbas, and A. Štrancar, “Downstream processing and chromatography based analytical methods for production of vaccines, gene therapy vectors, and bacteriophages,” *Hum. Vaccines Immunother.*, vol. 11, no. 4, pp. 1010–1021, 2015, doi: 10.1080/21645515.2015.1009817.
  - [26] T. Vicente, A. Roldão, C. Peixoto, M. J. T. Carrondo, and P. M. Alves, “Large-scale production and purification of VLP-based vaccines,” *Journal of Invertebrate Pathology*, vol. 107, no. SUPPL. Jul. 2011, doi: 10.1016/j.jip.2011.05.004.
  - [27] P. Steppert *et al.*, “Separation of HIV-1 gag virus-like particles from vesicular particles impurities by hydroxyl-functionalized monoliths,” *J. Sep. Sci.*, vol. 40, no. 4, pp. 979–990, 2017, doi: 10.1002/jssc.201600765.
  - [28] P. Gerster *et al.*, “Purification of infective baculoviruses by monoliths,” *J. Chromatogr. A*, vol. 1290, pp. 36–45, 2013, doi: 10.1016/j.chroma.2013.03.047.
  - [29] P. Steppert *et al.*, “Purification of HIV-1 gag virus-like particles and separation of other extracellular particles,” *J. Chromatogr. A*, vol. 1455, pp. 93–101, 2016, doi: 10.1016/j.chroma.2016.05.053.
  - [30] A. Jungbauer and R. Hahn, “Monoliths for fast bioseparation and bioconversion and their applications in biotechnology,” *J. Sep. Sci.*, vol. 27, no. 10–11, pp. 767–778, 2004, doi: 10.1002/jssc.200401812.

- [31] A. Jungbauer and R. Hahn, "Polymethacrylate monoliths for preparative and industrial separation of biomolecular assemblies," *J. Chromatogr. A*, vol. 1184, no. 1–2, pp. 62–79, 2008, doi: 10.1016/j.chroma.2007.12.087.
- [32] E. I. Trilisky and A. M. Lenhoff, "Flow-Dependent Entrapment of Large Bioparticles in Porous Process Media," *Biotechnol. Bioeng.*, vol. 104, no. 1, pp. 127–133, 2009, doi: 10.1002/bit.22370.
- [33] A. Podgornik, A. Savnik, J. Jančar, and N. L. Krajnc, "Design of monoliths through their mechanical properties," *J. Chromatogr. A*, vol. 1333, pp. 9–17, 2014, doi: 10.1016/j.chroma.2014.01.038.
- [34] M. Zhao, M. Vandersluis, J. Stout, U. Haupts, M. Sanders, and R. Jacquemart, "Affinity chromatography for vaccines manufacturing: Finally ready for prime time?," *Vaccine*, vol. 37, no. 36, pp. 5491–5503, 2019, doi: 10.1016/j.vaccine.2018.02.090.
- [35] M. W. Wolff *et al.*, "Capturing of cell culture-derived modified vaccinia ankara virus by ion exchange and pseudo-affinity membrane adsorbers," *Biotechnol. Bioeng.*, vol. 105, no. 4, pp. 761–769, 2010, doi: 10.1002/bit.22595.
- [36] M. M. Segura, A. Garnier, Y. Durocher, H. Coelho, and A. Kamen, "Production of lentiviral vectors by large-scale transient transfection of suspension cultures and affinity chromatography purification," *Biotechnol. Bioeng.*, vol. 98, no. 4, pp. 789–799, 2007, doi: 10.1002/bit.21467.
- [37] R. Morenweiser, "Downstream processing of viral vectors and vaccines," *Gene Ther.*, vol. 12, pp. S103–S110, 2005, doi: 10.1038/sj.gt.3302624.
- [38] I. González-Domínguez, E. Lorenzo, A. Bernier, L. Cervera, F. Gòdia, and A. Kamen, "A four-step purification process for gag vlps: From culture supernatant to high-purity lyophilized particles," *Vaccines*, vol. 9, no. 10, pp. 1–19, 2021, doi: 10.3390/vaccines9101154.
- [39] C. F. Shen *et al.*, "Optimization and scale-up of cell culture and purification processes for production of an adenovirus-vectored tuberculosis vaccine candidate," *Vaccine*, vol. 34, no. 29, pp. 3381–3387, 2016, doi: 10.1016/j.vaccine.2016.04.090.
- [40] T. Weigel, T. Solomaier, S. Wehmeyer, A. Peuker, M. W. Wolff, and U. Reichl, "A membrane-based purification process for cell culture-derived influenza A virus," *J. Biotechnol.*, vol. 220, pp. 12–20, 2016, doi: 10.1016/j.jbiotec.2015.12.022.
- [41] P. Fernandes, C. Peixoto, V. M. Santiago, E. J. Kremer, A. S. Coroadinha, and P. M. Alves, "Bioprocess development for canine adenovirus type 2 vectors," *Gene Ther.*, vol. 20, no. 4, pp. 353–360, 2013, doi: 10.1038/gt.2012.52.
- [42] G. Iyer *et al.*, "Reduced surface area chromatography for flow-through purification of viruses and virus like particles," *J. Chromatogr. A*, vol. 1218, no. 26, pp. 3973–3981, 2011, doi: 10.1016/j.chroma.2011.04.086.
- [43] C. L. Effio and J. Hubbuch, "Next generation vaccines and vectors: Designing downstream processes for recombinant protein-based virus-like particles," *Biotechnology Journal*, vol. 10, no. 5. Wiley-VCH Verlag, pp. 715–727, May 01, 2015, doi: 10.1002/biot.201400392.
- [44] L. J. J. Hansen, R. Daoussi, C. Vervaet, J. P. Remon, and T. R. M. De Beer, "Freeze-drying of live virus vaccines: A review," *Vaccine*, vol. 33, no. 42. Elsevier Ltd, pp. 5507–5519, Oct. 13, 2015, doi: 10.1016/j.vaccine.2015.08.085.
- [45] S. Saboo *et al.*, "Optimized Formulation of a Thermostable Spray-Dried Virus-Like Particle Vaccine against Human Papillomavirus," *Mol. Pharm.*, vol. 13, no. 5, pp. 1646–1655, 2016, doi: 10.1021/acs.molpharmaceut.6b00072.
- [46] S. Shi and A. J. Hickey, "PLGA microparticles in respirable sizes enhance an in vitro T cell response to recombinant mycobacterium tuberculosis antigen TB10.4-Ag85B," *Pharm. Res.*, vol. 27, no. 2, pp. 350–360, 2010, doi: 10.1007/s11095-009-0028-7.

- [47] M. I. Amaro, L. Tajber, O. I. Corrigan, and A. M. Healy, "Optimisation of spray drying process conditions for sugar nanoporous microparticles (NPMPs) intended for inhalation," *Int. J. Pharm.*, vol. 421, no. 1, pp. 99–109, 2011, doi: 10.1016/j.ijpharm.2011.09.021.
- [48] C. A. Rezende, B. W. Atta, M. C. Breitzkreitz, R. Simister, L. D. Gomez, and S. J. McQueen-Mason, "Optimization of biomass pretreatments using fractional factorial experimental design," *Biotechnol. Biofuels*, vol. 11, no. 1, pp. 1–15, 2018, doi: 10.1186/s13068-018-1200-2.
- [49] F. Susa *et al.*, "Comparative Studies of Different Preservation Methods and Relative Freeze-Drying Formulations for Extracellular Vesicle Pharmaceutical Applications," *ACS Biomater. Sci. Eng.*, vol. 9, no. 10, pp. 5871–5885, 2023, doi: 10.1021/acsbiomaterials.3c00678.
- [50] B. S. Bhatnagar, R. H. Bogner, and M. J. Pikal, "Protein stability during freezing: Separation of stresses and mechanisms of protein stabilization," *Pharm. Dev. Technol.*, vol. 12, no. 5, pp. 505–523, 2007, doi: 10.1080/10837450701481157.
- [51] R. Lang, G. Winter, L. Vogt, A. Zürcher, B. Dorigo, and B. Schimmele, "Rational design of a stable, freeze-dried virus-like particle-based vaccine formulation," *Drug Dev. Ind. Pharm.*, vol. 35, no. 1, pp. 83–97, 2009, doi: 10.1080/03639040802192806.
- [52] Y. Liu *et al.*, "Screening and Stability Evaluation of Freeze-Dried Protective Agents for a Live Recombinant Pseudorabies Virus Vaccine," vol. 12(1), p. 65, 2024, doi: 10.3390/vaccines12010065.
- [53] L. H. L. Lua, N. K. Connors, F. Sainsbury, Y. P. Chuan, N. Wibowo, and A. P. J. Middelberg, "Bioengineering Virus-Like Particles as Vaccines," *Biotechnol. Bioeng.*, vol. 111, pp. 425–440, 2014, doi: 10.1002/bit.25159/abstract.
- [54] I. González-Domínguez, E. Puente-Massaguer, L. Cervera, and F. Gòdia, "Quality assessment of virus-like particles at single particle level: A comparative study," *Viruses*, vol. 12, no. 2, 2020, doi: 10.3390/v12020223.
- [55] S. Gutiérrez-Granados, L. Cervera, F. Gòdia, J. Carrillo, and M. M. Segura, "Development and validation of a quantitation assay for fluorescently tagged HIV-1 virus-like particles," *J. Virol. Methods*, vol. 193, no. 1, pp. 85–95, 2013, doi: 10.1016/j.jviromet.2013.05.010.
- [56] I. González-Domínguez, E. Puente-Massaguer, L. Cervera, and F. Gòdia, "Quantification of the HIV-1 virus-like particle production process by super-resolution imaging: From VLP budding to nanoparticle analysis," *Biotechnol. Bioeng.*, vol. 117, no. 7, pp. 1929–1945, 2020, doi: 10.1002/bit.27345.
- [57] P. J. de Pablo, "Atomic force microscopy of virus shells," *Semin. Cell Dev. Biol.*, vol. 73, pp. 199–208, 2018, doi: 10.1016/j.semcdb.2017.08.039.
- [58] M. Bjelošević, A. Zvonar Pobirk, O. Planinšek, and P. Ahlin Grabnar, "Excipients in freeze-dried biopharmaceuticals: Contributions toward formulation stability and lyophilisation cycle optimisation," *Int. J. Pharm.*, vol. 576, p. 119029, 2020, doi: 10.1016/j.ijpharm.2020.119029.
- [59] N. Jovanović, A. Bouchard, G. W. Hofland, G. J. Witkamp, D. J. A. Crommelin, and W. Jiskoot, "Distinct effects of sucrose and trehalose on protein stability during supercritical fluid drying and freeze-drying," *Eur. J. Pharm. Sci.*, vol. 27, no. 4, pp. 336–345, 2006, doi: 10.1016/j.ejps.2005.11.003.
- [60] V. Gervasi, R. Dall Agnol, S. Cullen, T. McCoy, S. Vucen, and A. Crean, "Parenteral protein formulations: An overview of approved products within the European Union," *Eur. J. Pharm. Biopharm.*, vol. 131, pp. 8–24, 2018, doi: 10.1016/j.ejpb.2018.07.011.
- [61] R. K. Jamil *et al.*, "Evaluation of the thermal stability of a novel strain of live-attenuated mumps vaccine (RS-12 strain) lyophilized in different stabilizers," *J. Virol. Methods*, vol. 199, pp. 35–38, 2014, doi: 10.1016/j.jviromet.2013.12.020.

- [62] B. M. Rayaprolu, J. J. Strawser, and G. Anyarambhatla, "Excipients in parenteral formulations: selection considerations and effective utilization with small molecules and biologics," *Drug Dev. Ind. Pharm.*, vol. 44, no. 10, pp. 1565–1571, 2018, doi: 10.1080/03639045.2018.1483392.
- [63] B. M. Baynes, D. I. C. Wang, and B. L. Trout, "Role of arginine in the stabilization of proteins against aggregation," *Biochemistry*, vol. 44, no. 12, pp. 4919–4925, 2005, doi: 10.1021/bi047528r.
- [64] S. Pramanick, D. Singodia, and V. Chandel, "Excipient selection in parenteral formulation development," *Pharma Times*, vol. 45, no. 3, pp. 65–77, 2013, doi: 10.1080/03639045.2018.1483392.
- [65] S. H. Paik, Y. J. Kim, S. K. Han, J. M. Kim, J. W. Huh, and Y. I. Park, "Mixture of three amino acids as stabilizers replacing albumin in lyophilization of new third generation recombinant factor VIII GreenGene F," *Biotechnol. Prog.*, vol. 28, no. 6, pp. 1517–1525, 2012, doi: 10.1002/btpr.1640.
- [66] S. Zhai, R. K. Hansen, R. Taylor, J. N. Skepper, R. Sanches, and N. K. H. Slater, "Effect of freezing rates and excipients on the infectivity of a live viral vaccine during lyophilization," *Biotechnol. Prog.*, vol. 20, no. 4, pp. 1113–1120, 2004, doi: 10.1021/bp034362x.
- [67] R. K. Evans *et al.*, "Development of Stable Liquid Formulations for Adenovirus-Based Vaccines," vol. 93, no. 10, pp. 2458–2475, 2004, doi: 10.1002/jps.20157.
- [68] J. Lavado-García, P. Pérez-Rubio, L. Cervera, and F. Gòdia, "The cell density effect in animal cell-based bioprocessing: Questions, insights and perspectives," *Biotechnol. Adv.*, vol. 60, no. May, 2022, doi: 10.1016/j.biotechadv.2022.108017.
- [69] J. Lavado-García, L. Cervera, and F. Gòdia, "An Alternative Perfusion Approach for the Intensification of Virus-Like Particle Production in HEK293 Cultures," *Front. Bioeng. Biotechnol.*, vol. 8, no. June, pp. 1–16, 2020, doi: 10.3389/fbioe.2020.00617.
- [70] M. D. Hein *et al.*, "Production of retroviral vectors in continuous high cell density culture," *Appl. Microbiol. Biotechnol.*, vol. 107, no. 19, pp. 5947–5961, 2023, doi: 10.1007/s00253-023-12689-9.
- [71] M. D. Hein, A. Chawla, M. Cattaneo, S. Y. Kupke, Y. Genzel, and U. Reichl, "Cell culture-based production of defective interfering influenza A virus particles in perfusion mode using an alternating tangential flow filtration system," *Appl. Microbiol. Biotechnol.*, vol. 105, no. 19, pp. 7251–7264, 2021, doi: 10.1007/s00253-021-11561-y.
- [72] P. Pérez-Rubio, J. Lavado-García, L. Bosch-Molist, E. L. Romero, L. Cervera, and F. Gòdia, "Extracellular vesicle depletion and UGCG overexpression mitigate the cell density effect in HEK293 cell culture transfection," *Mol. Ther. Methods Clin. Dev.*, vol. 32, no. 1, p. 101190, 2024, doi: 10.1016/j.omtm.2024.101190.
- [73] M. Zdanowicz and J. Chroboczek, "Virus-like particles as drug delivery vectors," *Acta Biochim. Pol.*, vol. 63, no. 3, pp. 469–473, 2016, doi: 10.18388/abp.2016\_1275.
- [74] M. An *et al.*, "Engineered virus-like particles for transient delivery of prime editor ribonucleoprotein complexes in vivo," *Nat. Biotechnol.*, 2024, doi: 10.1038/s41587-023-02078-y.
- [75] U. Unzueta, N. Ferrer-miralles, I. Casanova, J. Cedano, and A. Villaverde, "Intracellular CXCR4 + cell targeting with T22-empowered protein-only nanoparticles," 2012.
- [76] H. Tamamura *et al.*, "Pharmacophore identification of a chemokine receptor (CXCR4) antagonist, T22 ([Tyr5,12, Lys7]-polyphemusin II), which specifically blocks T cell-line-tropic HIV-1 infection," *Bioorganic Med. Chem.*, vol. 6, no. 7, pp. 1033–1041, 1998, doi: 10.1016/S0968-0896(98)00061-3.
- [77] H. Tamamura *et al.*, "Effective lowly cytotoxic analogs of an HIV-cell fusion inhibitor, T22 ([Tyr5,12, Lys7]-polyphemusin II)," *Bioorganic Med. Chem.*, vol. 6, no. 2, pp. 231–238, 1998, doi: 10.1016/S0968-0896(97)10037-2.
- [78] S. Cabrero-De Las Heras and E. Martínez-Balibrea, "CXC family of chemokines as prognostic or

- predictive biomarkers and possible drug targets in colorectal cancer," *World J. Gastroenterol.*, vol. 24, no. 42, pp. 4738–4749, 2018, doi: 10.3748/wjg.v24.i42.4738.
- [79] E. Voltà-Durán *et al.*, "Design and engineering of tumor-targeted, dual-acting cytotoxic nanoparticles," *Acta Biomater.*, vol. 119, no. xxxx, pp. 312–322, 2021, doi: 10.1016/j.actbio.2020.11.018.
- [80] M. V. Céspedes *et al.*, "Selective depletion of metastatic stem cells as therapy for human colorectal cancer," *EMBO Mol. Med.*, vol. 10, no. 10, pp. 1–22, 2018, doi: 10.15252/emmm.201708772.
- [81] R. Díaz *et al.*, "Selective CXCR4 + Cancer Cell Targeting and Potent Antineoplastic Effect by a Nanostructured Version of Recombinant Ricin," vol. 1800665, pp. 1–12, 2018, doi: 10.1002/sml.201800665.
- [82] S. B. Carvalho *et al.*, "Bioorthogonal Strategy for Bioprocessing of Specific-Site-Functionalized Enveloped Influenza-Virus-Like Particles," *Bioconjug. Chem.*, vol. 27, no. 10, pp. 2386–2399, 2016, doi: 10.1021/acs.bioconjchem.6b00372.
- [83] M. J. Rohovie, M. Nagasawa, and J. R. Swartz, "Virus-like particles: Next-generation nanoparticles for targeted therapeutic delivery," *Bioeng. Transl. Med.*, vol. 2, no. 1, pp. 43–57, 2017, doi: 10.1002/btm2.10049.
- [84] F. P. and F. C. Jerri C. Caldeira, Michael Perrine, "Virus-Like Particles as an Immunogenic Platform for Cancer Vaccines," *Viruses*, vol. 12, p. 488, 2020, doi: doi:10.3390/v12050488.
- [85] A. Manuscript, P. Epitope, and I. By, "Peptide Epitope Identification By Affinity-Selection On Bacteriophage MS2 Virus-like Particles," vol. 409, no. 2, pp. 225–237, 2011, doi: 10.1016/j.jmb.2011.03.072.Peptide.
- [86] A. Boix-Besora, E. Lorenzo, J. Lavado-García, F. Gòdia, and L. Cervera, "Optimization, Production, Purification and Characterization of HIV-1 GAG-Based Virus-like Particles Functionalized with SARS-CoV-2," *Vaccines*, vol. 10, no. 2, pp. 1–18, 2022, doi: 10.3390/vaccines10020250.
- [87] A. Boix-Besora, F. Gòdia, and L. Cervera, "Gag Virus-like Particles Functionalized with SARS-CoV-2 Variants: Generation, Characterization and Recognition by COVID-19 Convalescent Patients' Sera," *Vaccines*, vol. 11, no. 11, 2023, doi: 10.3390/vaccines11111641.
- [88] D. Fontana, E. Garay, L. Cervera, R. Kratje, C. Prieto, and F. Gòdia, "Chimeric vlps based on hiv-1 gag and a fusion rabies glycoprotein induce specific antibodies against rabies and foot-and-mouth disease virus," *Vaccines*, vol. 9, no. 3, 2021, doi: 10.3390/vaccines9030251.
- [89] S. J. Kaczmarczyk, K. Sitaraman, H. A. Young, S. H. Hughes, and D. K. Chatterjee, "Protein delivery using engineered virus-like particles," 2011, doi: 10.1073/pnas.1101874108/-/DCSupplemental.www.pnas.org/cgi/doi/10.1073/pnas.1101874108.
- [90] L. Cervera, S. Gutiérrez-Granados, M. Martínez, J. Blanco, F. Gòdia, and M. M. Segura, "Generation of HIV-1 Gag VLPs by transient transfection of HEK 293 suspension cell cultures using an optimized animal-derived component free medium," *J. Biotechnol.*, vol. 166, no. 4, pp. 152–165, Jul. 2013, doi: 10.1016/j.jbiotec.2013.05.001.
- [91] E. Voltà-Durán *et al.*, "The Diphtheria Toxin Translocation Domain Impairs Receptor Selectivity in Cancer Cell-Targeted Protein Nanoparticles," *Pharmaceutics*, vol. 14, no. 12, pp. 1–13, 2022, doi: 10.3390/pharmaceutics14122644.



## **CONCLUSIONS**

---

## CONCLUSIONS

From the results obtained in this thesis, the following conclusions can be highlighted:

1. The design of the HIV-1 Gag::eGFP VLPs purification process, combining clarification, concentration/intermediate purification, capture, and polishing, was performed by evaluating different operational units for each step. Clarification effectively separated most cell aggregates and debris from the HIV-1 Gag::eGFP VLPs in the supernatant using depth filtration without significant loss of VLPs. This was refined by secondary clarification, reducing dsDNA content. Tangential flow filtration enabled further concentration, removing more than 85% of dsDNA and total protein content. Capto Q ImpRes IEC showed the best results among all chromatographic methods tested for capturing and purifying VLPs. Finally, higher purity, desalting, and buffer exchange were achieved using S4FF SEC. The downstream process design achieved a total recovery of 38% of Gag::eGFP VLPs, with nearly 100% removal of total protein and dsDNA from the crude supernatant. Of note, the technologies selected in each step are suitable for large-scale manufacturing.
2. A buffer formulation for a lyophilization process of HIV-1 Gag::eGFP VLPs, composed of sucrose, arginine, TrisHCl, sodium chloride, and polysorbate 80, was optimized and validated using a design of experiments approach. The VLPs obtained after the lyophilization process presented size, concentration, and quality characteristics remarkably similar to the non-lyophilized VLPs. Additionally, VLPs stored at 4°C for 4 weeks, either in lyophilized or reconstituted form, preserved their integrity and stability. The formulation design in enhancing the properties and usability of VLPs for vaccine development, improving their transportation, distribution, and accessibility is very relevant.
3. A complete bioprocess for Gag::eGFP VLP production was implemented in this work, combining perfusion-based upstream with a three-step purification process. In this study, it was demonstrated

that coupling a perfusion process with continuous VLP harvest enhanced VLP volumetric productivity by 2.4 times and significantly reduced media usage compared to the previously reported work for perfusion-based VLP production. The process achieved a 49.9% VLP recovery in the harvest fraction and around 60% of purity after downstream processing. Additionally, the capture step concentrated VLPs 14-fold and reduced the total volume 23-fold, with no significant loss observed after lyophilization.

4. The Gag::eGFP VLPs produced in HEK293 cells and purified by the designed DSP to a 60% of purity, were successfully functionalized with the T22 peptide using a click chemistry reaction. The functionalization was confirmed by DLS analysis and western blot followed by SE-HPLC studies. *In vitro* experiments demonstrated that these functionalized nanoparticles could efficiently penetrate CXCR4 positive cells in a dose and time-dependent manner and could not penetrate CXCR4 negative cells, indicating high specificity. This targeted approach using nanoparticles such functionalized VLPs could provide an approach to enhance therapeutic efficacy by selectively delivering drugs to cancer cells, reducing off-target effects and systemic toxicity. The findings underscore the potential of T22-functionalized Gag::eGFP VLPs as a nanoconjugate for drug delivery.

